Mechanical and Microstructural Behavior Evolution of Lead Free Solder Materials Under Different Thermal Exposures

by

S M Kamrul Hasan

A dissertation submitted to the Graduate Faculty of
Auburn University
in partial fulfillment of the
requirements for the Degree of
Doctor of Philosophy

Auburn, Alabama
May 6, 2023

Keywords: microelectronics reliability, lead-free solder, harsh environment applications, high temperature aging, thermal cycling, nanoindentation, microstructural evolution

Approved by

Jeffrey C. Suhling, Chair, Quina Distinguished Professor of Mechanical Engineering
Hareesh V. Tippur, McWane Professor of Mechanical Engineering
Michael J. Bozack, Professor Emeritus of Physics
James S. Davidson, Gottlieb Professor of Civil Engineering

Abstract

With the growth of electronic packaging industries, ranging from automobile to hand-held products, reliability is a major concern. Also, to keep pace with the increasing demand of end users for integration, miniaturization, light weight, high speed, and multi-functionality of portable electronic devices such as mobile phones, digital cameras, as well as personal digital assistant (PDA), electronic packaging industries are intended to manufacture packages of high density and smaller dimension. These packages consist of smaller solder joint interconnects with solder balls in each area and short distance between the solder balls. The reliability of smaller electronic packages is greatly affected by environment and application where it is being used, compared to the traditional one. Solder joints provide mechanical support, electrical and thermal interconnection between packaging levels in microelectronics assembly systems. Proper functioning of these interconnections and the reliability of the electronic packages depend largely on the mechanical properties of the solder joints. Lead free solders are common as interconnects in electronic packaging due to their relatively high melting point, attractive mechanical properties, thermal cycling reliability, and environment friendly chemical properties. However, Lead free electronic assemblies are often subjected to thermal cycling during qualification testing or during actual use. During the dwells at the constant high temperature extreme, the lead free solders joints will experience thermal aging phenomena, resulting in microstructural evolution and material property degradation. Additional aging effects can also occur in the ramp periods from low to high temperature. In real scenario, CTE mismatch occurs between die and PCB causes shear fatigue on solder joints and

affects the reliability of the entire package. Many studies were conducted to investigate the effect of aging on lead free solder alloy properties and the reliability of assemblies in thermal cycling. In addition, the effect of thermal cycling on mechanical properties evolution of lead free solder joints was also observed. However, no study has focused on how thermal cycling with different profiles (ramp and dwell times) affects the mechanical property evolution in lead free solders. This research involves several projects to create a database of mechanical properties of bulk and real solder joints, and the associated mechanical and microstructural evolution under different thermal exposures.

In the first project, mechanical behavior evolution of SAC305 lead free solder material was investigated under different thermal exposures. Uniaxial test specimens were prepared by reflowing solder in rectangular cross-section glass tubes with a controlled temperature profile. After reflow solidification, the samples were placed into the environmental chamber and thermally cycled from -40 C to +125 C under a stress-free condition (no load). Several thermal cycling profiles were examined including: (1) 150 minute cycles with 45 minutes ramps and 30 minutes dwells, (2) air-to-air thermal shock exposures with 30 minutes dwells and near instantaneous ramps, and (3) 90 minute cycles with 45 minutes ramps and 0 minutes dwells (thermal ramp only), (4) no cycling (simple aging at high temperature extreme). After the preconditioning, mechanical properties including stress-strain and creep response were explored at room temperature. Stress-strain behavior under different thermal exposures has been compared in terms of exposure time. Creep tests were performed at three different stress levels (σ = 10, 12, and 15 MPa). Creep response recorded measuring secondary creep strain rate. The creep response of SAC305 solder material under different thermal exposures has been compared in terms of stress

levels. Mechanical behavior under different thermal exposures has been compared to explore the most detrimental thermal exposures.

In the second project, the mechanical behavior evolution of SAC+3% (SAC_Q) lead free solder material under different thermal exposures has been investigated. At the first phase, tensile testing, and creep testing were conducted to extract the mechanical properties including effective elastic modulus, ultimate tensile strength (UTS), yield strength (YS), and secondary creep strain rate. For tensile testing, 8-10 samples were tested at room temperature at a strain rate of 0.001(sec^{-1}) to extract the stress-strain properties. Creep testing was also conducted at room temperature at three different stress levels (10, 12, and 15 MPa). Creep properties were evaluated in terms of secondary creep strain rate. At the second phase, tensile properties evolution of both SAC305 and SAC+3%Bi were compared for different thermal exposures in terms of exposure time to understand the reliability performance of both lead free solder alloy under harsh environment. Also, secondary creep strain rate of both SAC305 and SAC+3%Bi under different thermal exposures has been compared with stress levels.

In the third project, the evolution of mechanical properties of both SAC305 and SAC+3%Bi solder joints under different thermal exposures have been explored. Mechanical properties were recorded as modulus, hardness, and yield strength. The size of the solder joints were 30 mils. Mechanical properties were extracted using nanoindentation technique. For nanoindentation, samples were prepared by attaching the package on epoxy mold using glue followed by grinding, polishing, and finally optical microscopy (OM) to find out single grain joint for avoiding grain orientation effect on mechanical properties. After the sample preparation, all samples were preconditioned and

then tested at room temperature to measure the mechanical properties. For each exposure time, 10 indents were made in a row and average was taken to extract the mechanical properties. Mechanical properties were compared under different thermal exposures with exposure time for each solder alloy. Also, mechanical properties evolution under different thermal exposures for both bulk solder and solder joint of SAC305 and SAC+3%Bi were compared to observe the effect of thermal exposures on small scale and large scale specimen.

In the final project, the microstructural evolution of SAC305 (96.5Sn-3.0Ag-0.5Cu) and SAC+3%Bi (Sn-4.0Ag-0.5Cu-3.0Bi-0.05Ni-0.007Ge) bulk solder have been investigated for different thermal exposures including isothermal aging, slow thermal ramping, and slow thermal cycling utilizing Scanning Electron Microscopy (SEM). Particularly, microstructural changes occurring under different thermal exposures within fixed regions have been monitored in selected lead free bulk solder material to create time-lapse imagery of the microstructure evolution. For the microstructural study, a slot was made on an epoxy mold and the sample was inserted into the slot followed by grinding, polishing, and exposed in a thermal chamber for 0, 1, 5, and 20 days. Finally, the topography of the microstructure of a fixed region was captured using the SEM system. This process generated several images of the microstructure as the thermal exposures progressed containing the visual and quantitative information of Bi diffusion in β-Sn matrix and the evolution of Ag_3Sn IMC particles as a function of exposure time during different thermal exposures.

Acknowledgments

I would like to express my deepest appreciation to my advisor Dr. Jeffrey C. Suhling for his continuous supervision and untiring support throughout my PhD study at Auburn University. I am grateful for getting the opportunity to work with a mentor like him. He is one of my role models and a source of inspiration. He continuously and convincingly conveys a spirit of pursuit of excellence and perfection in research. I am really grateful that I had the opportunity to work with an exceptional mentor who taught me beyond what is expected in academia. I am also grateful to my advisory committee members including Dr. Hareesh V. Tippur, Dr. Michael J. Bozack, and Dr. James Davidson for their insightful discussion about this research work. Special thanks are extended to my friends and co-workers Dr. Abdullah Fahim, Dr. KM Rafidh Hassan, Dr.Jing Wu, Dr. Jun Chen, Dr. Aminul Hoque, Dr. Ashraful Haq, Dr. Promod Chowdhury, Dr. Md Mahmudur Rahman Chowdhury, Mohammad Al Ahsan, Debabrata Mondal, Golam Rakib Mojumder, Shouvik Chakroborty, Jason Smith, and John Marcell for their support.

I am heartily grateful to my parents Md Noor Hossain, Lutfa Hossain for their support to my study and life in the United States. I am grateful to my beautiful daughter Sharnaz Irza Eyana to come in my life and make me more focused. Finally, I solemnly dedicate this dissertation and all achievements in pursuit of doctoral degree to my wife, Farihatun Naima, for her perseverance and support, and her understanding during my busy time at graduate school have been priceless to me.

Table of Contents

Abstract…………………… ii

Acknowledgments………… vi

Table of Contents……… vii

List of Figures……… xiv

List of Tables………… xx

CHAPTER 1………… 1

INTRODUCTION……… 1

1.1 Overview of Solders in Microelectronics 1

1.2 Lead Free Solders Choices 3

1.3 Candidates for Alternative Lead-Free Solders 5

1.3.1 Tin 6

1.3.2 Chromium (Cr) 7

1.3.3 Nickel (Ni) 8

1.3.4 Zinc (Zn) 8

1.3.5 Cobalt (Co) 9

1.3.6 Bismuth (Bi) 9

1.3.7 Antimony (Sb) 9

1.3.8 Germanium (Ge) 10

1.3.9 Sn-Ag-Cu System 10

1.3.10 Sn-Ag-Cu + X System 13

1.4 Characteristics and Applications of Sn-Ag-Cu Solder Material 14

1.5 Mechanical Properties of Lead Free Solders 14
1.5.1 Tensile Properties (Stress-Strain Behavior)... 15
1.5.2 Creep Properties... 18
1.5.3 Mechanisms of Creep Deformation 21
1.6 Nanoindentation...23
1.7 Harsh Environment applications of Electronics 24
1.8 Objectives of This Research 25
1.9 Organization of the Dissertation 26
CHAPTER 2 28
LITERATURE REVIEW 28
2.1 Introduction...28
2.2 Aging Effects on Tensile Properties 29
2.2.1 Aging Effects on Bulk Solders 30
2.2.2 Aging Effects on Solders Joints.. 31
2.3 Aging Effects on Creep Properties 35
2.4 Effects of Thermal Cycling on Solder Joints...36
2.5 Constitutive Modeling for Stress-Strain Tests...37
2.6 Constitutive Modeling for Creep 38
2.7 Reduction of Aging and Thermal Cycling Effect by Dopant 41
2.8 Nanoindentation on SAC Solder Joints 46
2.9 Effect of Aging and Thermal Cycling on the Microstructure of Solder 47
2.10 Summary...55
CHAPTER 3 57

EXPERIMENTAL PROCEDURE ... 57
3.1 Introduction ... 57
3.2 Uniaxial Test Sample Preparation ... 58
3.3 Thermal Chambers and Thermal Cycling Profiles ... 62
3.4 Uniaxial Tensile Testing System ... 66
3.5 Typical Testing Data and Data Processing ... 67
3.5.1 Typical Test Data ... 67
3.5.2 Stress-Strain and Creep Data Processing ... 68
3.6 Microstructure Study ... 70
3.6.1 Sample Preparation and Image Capturing Using Scanning Electron Microscopy (SEM) ... 70
3.6.2 Measurement of Area and Number of IMC Particles Using Image Processing ... 74
3.6.3 Measurement of IMC Particle Diameter ... 76
3.6.4 Tracking the Changes in IMC Particle Diameter during Isothermal Aging ... 78
3.7 Nanoindentation Method and Test Procedures ... 79
3.7.1 Sample Preparation for Nanoindentation ... 79
3.7.2 Measurement of Elastic Modulus and Hardness ... 82
3.8 Summary and Discussion ... 87
CHAPTER 4 88
MECHANICAL CHARACTERIZATION OF SAC305 SOLDER MATERIAL UNDER DIFFERENT THERMAL EXPOSURES ... 88

4.1 Introduction.....88

4.2 Alloy Composition and Experimental Test Matrix.....89

4.3 Stress vs. Strain Data of SAC305 Solder Under Different Thermal Exposures.....91

4.4 Comparison Between Aging and Different Thermal Exposures.....95

4.5 Effective Elastic Modulus, UTS, and YS Evolution with Exposure Times.....99

4.6 Creep Test Matrix of SAC305 Solder Under Different Thermal Exposures.....101

4.7 Creep Response Under Different Thermal Exposures.....102

4.8 Comparison Between Aging and Different Thermal Exposures with Elapsed Time.....109

4.9 Evolution of Creep Response Under Different Exposures with Stress Level.....110

4.10 Summary and Discussion.....113

CHAPTER 5 116

INVESTIGATION ON MECHANICAL PROPERTIES OF.....116

SAC+X SOLDER MATERIAL AND COMPARISON WITH SAC305 SOLDER MATERIAL UNDER DIFFERENT THERMAL EXPOSURES.....116

5.1 Introduction.....116

5.2 Alloy Composition and Experimental Test Matrix.....118

5.3 Stress vs. Strain Data of SAC+X Solder Under Different Thermal Exposures.....119

5.4 Comparison Between Aging and Different Thermal Exposures.....123

5.5 E, UTS, and YS Evolution of SAC+Bi Solder with Exposure Time.....127

5.6 Creep Test Matrix of SAC305 Solder Under Different Thermal Exposures.....129

5.7 Creep Response of SAC+Bi Solder Under Different Thermal Exposures.....130

5.8 Comparison Between Aging and Different Thermal Exposures with Elapsed Time 137
5.9 Evolution of Creep Response of SAC+Bi Solder Under Different Exposures with Stress Level 138
5.10 Comparison of Modulus, UTS, and YS Between SAC305 and SAC+Bi Solder Material Under Different Thermal Exposures 141
5.11 Comparison of Creep Response Between SAC305 and SAC+Bi Solder Material Under Different Thermal Exposures 148
5.12 Summary and Discussion 155
CHAPTER 6 156
INVESTIGATION ON MECHANICAL PROPERTIES EVOLUTION OF SAC305 AND SAC+Bi SOLDER JOINT BY NANOINDENTATION TECHNIQUE 156
6.1 Introduction 156
6.2 Sample Preparation for Nanoindentation Technique 158
6.3 Room Temperature Nanoindentation System and Test Procedure 158
6.4 Factors Influence in Nanoindentation Test Results 160
6.4.1 Influence of Holding Time on Modulus and Hardness 160
6.4.2 Influence of Surface Effect on Modulus and Hardness 164
6.5 Modulus, Hardness, and Yield Strength Measurement of SAC305 Solder Joints Under Different Thermal Exposures 166
6.6 Evolution of Modulus, Hardness, and Yield Strength of AC305 Solder Joints with Elapsed Time 171

6.7 Modulus, Hardness, and Yield Strength Measurement of SAC+Bi Solder Joints Under Different Thermal Exposures 174
6.8 Evolution of Modulus, Hardness, and Yield Strength of SAC+Bi Solder Joints with Elapsed Time 177
6.9 Comparison of Modulus Between Bulk Solder and Solder Joint 179
6.10 Comparison of Yield Strength Between Bulk Solder and Solder Joint 182
6.11 Summary and Discussion 184
CHAPTER 7 186
MICROSTRUCTURAL EVOLUTION OF SAC305 AND SAC+Bi SOLDER UNDER DIFFERENT THERMAL EXPOSURES 186
7.1 Introduction 186
7.2 Microstructural Evolution of SAC305 Solder 187
7.3 Sample Preparation and Experimental Procedure 190
7.4 Thermal Cycling Chamber for Preconditioning 193
7.5 Scanning Electron Microscopy (SEM) Imaging of SAC305 Solder 195
7.6 Effect of Thermal Exposure on Microstructure of SAC305 Solder 196
7.6.1 Effect of Aging 196
7.6.2 Effect of Slow Thermal Ramping (No Dwell) 199
7.6.3 Effect of Slow Thermal Cycling (Ramp+Dwell) 202
7.7 Measurement of Area and Number of IMC 205
7.8 Measurement of Particle Diameter and Evolution with Exposure Time 207
7.9 Comparison of Normalized Average Particle Diameter Evolution 209
7.10 Correlation Between Mechanical and Microstructural Evolution 210

7.11 Microstructure Analysis of SAC+Bi Solder Alloy 214
7.12 Comparison of Normalized Average Particle Diameter Evolution 228
7.13 Correlation Between Mechanical and Microstructural Evolution 229
7.14 Microstructural Evolution of SAC305 and SAC+Bi Solder Under Different Thermal Exposures with Exposure Time..230
7.15 Summary and Discussion...231
CHAPTER 8 233
SUMMARY AND CONCLUSIONS 233
8.1 Literature Review..233
8.2 Experimental Procedures 234
8.3 Mechanical Behavior Evolution of SAC305 Solder Under Different Thermal Exposure 235
8.4 Response of SAC+Bi Solder Alloy Under Different Thermal Exposure 237
8.5 Nanoindentation Characterization of SAC305 and SAC+Bi Solder Joint 238
8.6 Microstructure Study of SAC305 and SAC+Bi Solder Under Different Thermal Exposure 239
8.7 Summary 240
8.8 Future Work 243
REFERENCES 244

List of Figures

Figure 1.1 Lead Free Solder Market Share 5

Figure 1.2 Elastic Modulus and Coefficient of Thermal Expansion (CTE) of Tin as a Function of Crystal Orientation [1] 7

Figure 1.3 Typical 3-D Ternary Phase Diagram 11

Figure 1.4 Sn-Ag-Cu Ternary Phase Diagram 11

Figure 1.5 Schematic Overview of Mechanical Behavior of a) Ceramics, Polymers below their Glass Transition Temperature (Tg) and Non Ductile Material b) Ductile Materials c) Polymers above Tg 16

Figure 1.6 Typical Stress-Strain Curve. 18

Figure 1.7 Typical Creep Curve. 20

Figure 1.8 A Typical Creep Deformation Map. 22

Figure 1.9 Berkovich Tip. 24

Figure 1.10 Temperature Cycling of Electronic Packages 25

Figure 3.1 Equipment used for Specimen Preparation 59

Figure 3.2 Water Quenched (WQ) Cooling Profiles 59

Figure 3.3 Heller 1800EXL Reflow Oven 60

Figure 3.4 Reflow (RF) Cooling Profiles 60

Figure 3.5 Solder Uniaxial Test Specimens 61

Figure 3.6 X-Ray Inspection of Solder Test Specimens (Good and Bad Samples) 62

Figure 3.7 (a) Thermal Cycling Chamber, and (b) Thermal Shock Chamber 63

Figure 3.8 (a) Slow Thermal Cycling, (b) Slow Thermal Ramping, and (c) Thermal Shock 65
Figure 3.9 Mechanical Test System with Uniaxial Sample 67
Figure 3.10 SAC Stress-Strain Curve and Material Properties 68
Figure 3.11 Empirical Model Fit to Solder Stress-Strain Curves 69
Figure 3.12 Grinding and Polishing Machine 70
Figure 3.13 Autopolisher 71
Figure 3.14 OLYMPUS BX60 Optical Microscope 71
Figure 3.15 Zeiss Polarized Light Microscope 72
Figure 3.16 Zeiss Cross Beam 550 SEM 72
Figure 3.17 Hysitron TI950 Triboindenter 73
Figure 3.18 Typical Fixed Region with Indentation Marks 74
Figure 3.19 Image Processing Steps for IMC Particle Area Calculations (a) After Outlining All the Particles (b) Binary Image 75
Figure 3.20 Schematic Representation of an IMC with Several Possible Exposed Area above the Surface Layer 76
Figure 3.21 Side and Top View of an Ideal Spherical IMC Particle Showing Actual and Apparent Diameters 77
Figure 3.22 3x3 BGA Specimen Sample 79
Figure 3.23 Sample Preparation Procedure for Nanoindentation Testing 81
Figure 3.24 (a) SAC305 Single Grain, (b) SAC305 Multiple Grain, (c) SAC+3%Bi Single Grain, (d) SAC+ 3%Bi Multiple Grain Solder Joint 82

Figure 3.25 Representative SAC305 Solder Joint after Nanoindentation Testing 83

Figure 3.26 An Example of The Loading Profile Used During Nanoindentation Testing 84

Figure 3.27 An Example of Load-Displacement Curve Obtained.................................. 85

After Nanoindentation Test.. 85

Figure 4.1 Stress-Strain Behavior of SAC305 Alloy Under Different Thermal Exposures 93

Figure 4.2 Stress-Strain Behavior Comparison Under Different Thermal Exposure 98

Figure 4.3 Stress-Strain Behavior Evolution Under Different Thermal Exposures 100

Figure 4.4 Creep Data of SAC305 Solder at Different Stress Levels Under Aging....... 104

Figure 4.5 Creep Data of SAC305 Solder Under Slow Thermal Ramping 106

Figure 4.6 Creep Data of SAC305 Solder at Under Slow Thermal Cycling 107

Figure 4.7 Representative Strain vs. Time Plot at Stress level 10 MPa......................... 109

Figure 4.8 Creep Rate Evolution Under Different Thermal Exposures with Stress Levels 112

Figure 5.1 Stress-Strain Behavior of SAC+Bi Under Different Thermal Exposures..... 121

Figure 5.2 Comparison of Stress-Strain Behavior of SAC+Bi 126

Figure 5.3 Tensile Properties Evolution Under Different Thermal Exposure 128

Figure 5.4 Creep Data of SAC+Bi Under Isothermal Aging... 132

Figure 5.5 Creep Data of SAC+Bi Solder Under Slow Thermal Ramping 134

Figure 5.6 Creep Data of SAC+Bi Under Slow Thermal cycling 135

Figure 5.7 Representative Strain vs. Time Plot Under Different Thermal Exposures at Stress level 15 MPa.. 137

Figure 5.8 Creep Rate vs. stress plot of SAC+Bi Under Different Thermal Exposures 140

Figure 5.9 Comparison of Effective Elastic Modulus Evolution Between SAC305 and SAC+Bi Solder Material Under Different Thermal Exposures............. 143

Figure 5.9 Comparison of Ultimate Tensile Strength Evolution Between SAC305 and SAC+Bi Solder Material Under Different Thermal Exposures............. 145

Figure 5.10 Comparison of Yield Tensile Strength Evolution Between SAC305 and SAC+Bi Solder Material Under Different Thermal Exposures............. 147

Figure 5.12 Creep Rate Evolution of SAC305 and SAC+Bi Under STR 152

Figure 5.13 Creep Rate Evolution of SAC305 and SAC+Bi Under STC 154

Figure 6.1 Nanoindentation System for Room Temperature Testing............................ 159

Figure 6.2 Permanent Indentation After Nanoindentation Testing................................ 160

Figure 6.1 Load –Displacement Curve (a) Standard Polycarbonate and (b) Solder...... 162

Figure 6.2 Load –Displacement Curve (a) Standard Quartz and (b) IMCs................. 163

Figure 6.3 Variation of (a) Modulus and (b) Hardness with Different Holding Time .. 164

Figure 6.4 Multiple Load-unload Load Function 165

Figure 6.5 Variation of Modulus and Hardness of Solder Joint 165

Figure 6.8 Indentation Marks on SAC+Bi Solder Joint For Property Extraction........... 167

Figure 6.9 Representative Normalized Modulus vs. Time Pot for SAC305 Alloy 168

Figure 6.10 Representative Load vs. Displacement curve of SAC305 Solder Joint for Different Thermal Profiles with Exposure Time 171

Figure 6.11 Evolution of Mechanical Properties of SAC305 Solder Joints under Aging and Different Thermal Exposures... 173

Figure 6.12 Indentation Marks on SAC+Bi Solder Joint For Property Extraction......... 174

Figure 6.13 Evolution of Mechanical Properties of SAC+Bi Solder Joints under Different Thermal Exposures 178

Figure 6.14 Normalized Modulus Evolution Under Different Thermal Exposures 181

Figure 6.15 Normalized Yield Strength Evolution Under Different Thermal Exposures 184

Figure 7.1 Microstructure of SAC305 Solder (a) Before Aging and (b) After Aging... 188

Figure 7.2 Location Based Variation in the Microstructure of SAC305 Solder............ 190

Figure 7.3 IsoMet 1000 Precision Cutter 191

Figure 7.4 Flow Chart of Experimental Procedure (a) Slot Cutting, (b) Sample Insertion, (c) Grinding, (d) Autopolishing, (e) Nanoindentation, (f) Zeiss Cross Beam 500 SEM, (g) Image Processing 192

Figure 7.5 (a) Thermal cycling chamber (b) Thermal Profiler 194

Figure 7.6 Example Region of Interest and Nanoindentation Markers 195

Figure 7.7 Microstructure Evolution of SAC305 Solder Under Isothermal Aging........ 198

Figure 7.8 Microstructure Evolution of SAC305 Solder Under STR............................ 201

Figure 7.9 Microstructure Evolution of SAC305 Solder Under STC............................ 204

Figure 7.10 Image Processing Steps for IMC Particle Area Calculations (a) After Outlining All the Particles (b) Binary Image and (c) Final Image from ImageJ 206

Figure 7.11 Changes in IMC Particle Diameter with Exposure Time Under Different Thermal Exposure 209

Figure 7.12 Comparison of Normalized Average Particle Diameter Evolution Under Different Thermal Exposure with Exposure Time................................ 210

Figure 7.13 Correlation Between Microstructure and Mechanical Properties of SAC305 Solder Alloy 211

Figure 7.14 Change of Normalized Ultimate Tensile Strength with Normalized Average Particle Diameter 212

Figure 7.15 Relationship Between UTS and IMC Particle Diameter 213

Figure 7.16 Change of Normalized Creep Rate with Normalized Average Particle Diameter 214

Figure 7.17 Relationship Between Creep Rate and IMC Particle Diameter.................. 214

Figure 7.18 Sn-Bi Phase Diagram (http://www.metallurgy.nist.gov/) 216

Figure 7.19 Microstructure Evolution of SAC+Bi Solder Under Aging 220

Figure 7.20 Microstructure Evolution of SAC+Bi Under Slow Thermal Ramping....... 224

Figure 7.21 Microstructure Evolution of SAC+Bi Solder Under Slow Thermal Cycling 227

Figure 7.22 Comparison of Normalized Average Particle Diameter Evolution of SAC+Bi Alloy Under Different Thermal Exposure with Exposure Time 228

Figure 7.23 Correlation Between Microstructure and Mechanical Properties of SAC+Bi 229

Figure 7.24 Normalized Particle Diameter Evolution with Time for SAC305 and SAC+Bi Under Different Thermal Exposure 231

List of Tables

List of Tables xx

Table 3.1 Conversion Table of Cycles to Time for the Various Profiles 65

Table 4.1 Vendor Specified Compositions of SAC305 Solder Material 90

Table 4.2 Test Matrix of Tensile Testing Under Different Thermal Exposures............... 90

Table 4.2 Mechanical Property of SAC305 Solder Under Different Thermal Exposures 94

Table 4.4 Creep Test Matrix of SAC305 Solder Material 101

Table 4.5 Increase Ratio of Creep Rate at Different Stress Levels and Time 108

Table 5.1 Vendor Specified Compositions of SAC305 and SAC+X Solder Material ... 118

Table 5.2 Test Matrix of Tensile Testing Under Different Thermal Exposures............. 118

Table 5.3 Mechanical Property of SAC+Bi Solder Under Different Thermal Exposures 122

Table 5.4 Creep Test Matrix of SAC+Bi Solder Material 129

Table 5.5 Increase Ratio of Creep Rate at Different Stress Levels and Time 136

Table 6.1 Modulus of SAC305 Solder Joints Under Different Thermal Exposures 169

Table 6.2 Hardness of SAC305 Solder Joints Under Different Thermal Exposures...... 170

Table 6.3 Modulus of SAC+Bi Solder Joints Under Different Thermal Exposures 175

Table 6.4 Hardness of SAC+Bi Solder Joints Under Different Thermal Exposures...... 176

Table 7.1 IMC Particle Diameter of Different Locations Under Different Thermal Exposure with Different Exposure Time 207

CHAPTER 1

INTRODUCTION

1.1 Overview of Solders in Microelectronics

Lead free solders provide excellent thermo-mechanical properties and commonly used as interconnections in electronic packages. As a joining material, in electronic assemblies, Solder joints provide mechanical support, electrical and thermal interconnection between packaging levels in microelectronics assembly systems. It also helps to dissipate the heat generated from the Si-chip [1].

With the emergence of the modern electronic packaging technology over the last few decades, solder alloys have been the primary interconnect material used in electronic packaging. In the past, eutectic 63Sn-37Pb has been the most extensively used soldering alloy in the packaging industries. The eutectic Sn-Pb solders were very attractive due to their relatively low melting temperature (183 °C) and excellent ductility and good reliability and for their superior wettability and compatibility with most substrates and devices [2].

There is a general trend towards products that minimize harmful effects on the environment and human health. This trend is further reinforced by the RoHS ban on harmful substances and WEEE regulations on recycling and minimizing of electronic wastes. In June 2000, the EU adopted two directives, the Waste of Electrical and Electronic

Equipment (WEEE) and the Directive of the Restriction of the Use of Certain Hazardous Substances (RoHS) [3]. The WEEE directive requires that lead has to be removed from any end-of-life electrical or electronic components. The RoHS specifically bans lead from electrical and electronic components manufactured after July 1, 2006. As a result of the enforcement of the directives, all electrical or electronic equipment and devices produced in or imported to E.U. member states must comply with these lead-free standards except those items that are exempted from the bans. In addition to legislation enforcement there are emerging detection technologies to enforce compliance. So due to the general push towards the eco-efficiency and green electronics, manufacturers are motivated for the adoption of lead free electronics. Therefore, the conversion to lead free solders in the global electronic market appears imminent [4].

In the United States, as soon as lead-free solder legislation was proposed, the lead-free solder project headed by the NCMS initiated research and development of lead-free solder in a program lasting 4 years [5]. The results of the project have been made available in a database and offer information on such matters as modifying equipment and processes for selecting alternative materials. The project initially selected for study 79 types of alloys considered at the time to be potential candidates for use in lead-free solder. Basic attributes considered included toxicity, resource availability, economic feasibility, and wetting characteristics. The selection process narrowed the field down to the final seven alloys, and these received secondary evaluation for reliability and ease of mounting manufacturing. Evaluation of the individual alloys did not result in the final selection of a single candidate, but three alloys, Sn–58Bi, Sn–3.5Ag–4.8Bi, and Sn–3.5Ag, were recommended as candidates. Screening comments indicated that the Sn–58Bi eutectic alloy

was not suitable for use as standard solder due to the scarcity of Bi resources. However, since this material can be used for mounting at less than 200 °C, and has chalked up a 20-year plus record of use in mainframe computers, this solder was deemed suitable for special applications. These results were used to construct a database on lead-free solder that includes the information in these tables along with other items such as (1) recommended applications for lead-free solder, (2) alloy composition guidelines reflecting price and availability, (3) database of the 7 selected alloys and comparison with Sn–Pb eutectic alloy, (4) data on the characteristics of the other 70 eliminated alloys, (5) optimal process conditions using various test PWBs, (6) strength evaluation and metallurgical reaction analysis for the selected alloys and various surface mounting process reactions, (7) predicted life (using NCMS Project proprietary life prediction software) and thermal fatigue evaluation for 4 of the selected alloys, and (8) assessment of nontoxicity and alloy composition.

1.2 Lead Free Solders Choices

In selecting suitable alternative of Sn-Pb soldering materials, it is important to take into consideration that the properties of the alternative solders are comparable or superior to Sn-Pb solders. Compatible candidates of the Sn-Pb solders must have the following behaviors [6]:

- melting temperature similar to eutectic Sn-Pb for a similar reflow profile
- sufficient wettability for good metallization process
- good electrical properties for transmitting electrical signals
- strong mechanical properties for good fatigue resistance and reliability

- inexpensive and easier manufacturability

Among various alloy systems that are considered as lead-free solder candidates, Sn-Ag-Cu alloys have been recognized as the most promising because of their relatively low melting temperature (compared with the Sn-Ag binary eutectic lead free solder), superior mechanical properties, and good compatibility with other components [7-9]. Sn-Ag-Cu alloys are widely used as lead-free solutions for ball-grid-array (BGA) interconnection in the microelectronic packaging industry as solder balls and pastes. Although no "drop in" replacement has been identified that is suitable for all applications, Sn-Ag, Sn-Ag-Cu (SAC), and other alloys involving elements such as Sn, Ag, Cu, Bi, In, and Zn have been identified as promising replacements for standard 63Sn-37Pb eutectic solder. Industries have proposed several SAC alloys which include 96.5Sn-3.0Ag-0.5Cu (SAC 305) in Japan, 95.5Sn-3.8Ag-0.7Cu (SAC 387) in the EU, and 95.5Sn-3.9Ag-0.6Cu (SAC 396) in the USA. The International Printed Circuit Association has suggested that 96.5Sn-3.0Ag-0.5Cu (SAC305) and Sn-3.9Ag- 0.6Cu (two near-eutectic alloys) will be the most widely used alloys in the future [10]. This prediction is attributed to their good mechanical properties, acceptable wetting properties, and suitable melting points [8, 11, 12].

A relatively large number of lead-free solder alloys have been proposed so far, including binary, ternary and even quaternary alloys. More than 70 alloys have been identified in the literature. Among them, the majority of the alloys are Sn-based alloys, that is, Sn is the preferred major constituent. In fact, Sn-rich lead-free alloys have occupied more than 80% in the wave solder market share and more than 90% in the reflow solder market share (Figure 1.1). The main benefits of the various SAC alloy systems are their

relatively low melting temperatures compared with the 96.5Sn–3.5Ag binary eutectic alloy, as well as their superior mechanical and solderability properties when compared to other lead-free solders. There are some major challenges for the current series of lead-free solders. SAC series alloys have a higher melting temperature, around 217 °C, compared to 183 °C for the eutectic Sn-Pb solders. They thus require higher reflow temperature during the manufacturing process, which can lead to reliability problems. The excessive buildup of intermetallic formed at the interface between the solder joints and the copper pad can also cause reliability problems. High costs are another issue for lead-free solders.

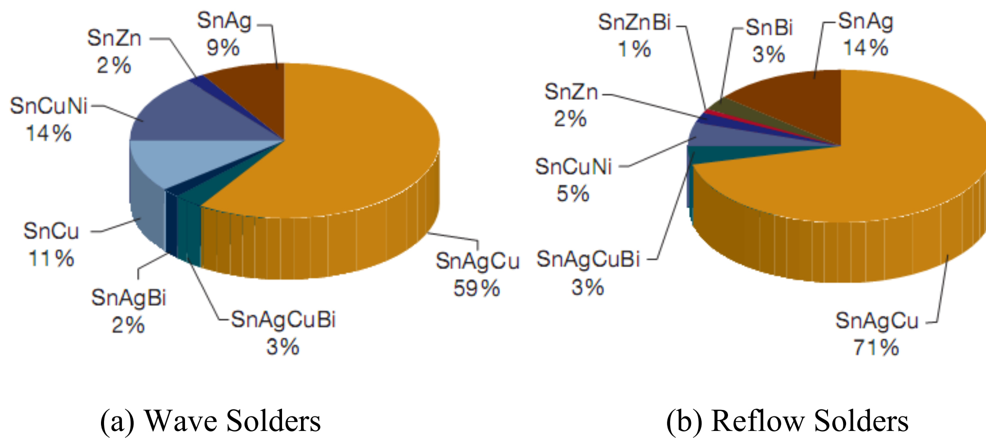

(a) Wave Solders (b) Reflow Solders

Figure 1.1 Lead Free Solder Market Share

1.3 Candidates for Alternative Lead-Free Solders

About 70 different alloys were proposed as an alternative to the Sn-Pb solder. Most of these are Sn based solder where Sn is the main constituent along with one, two or even three other minor elements. These minor elements are added mainly to 1) decrease the melting temperature and 2) improve wetting and reliability of the solder [1]. The properties

of Sn and the effects of different alloying elements on the Sn based solder alloys are described below:

1.3.1 Tin

The melting temperature of elemental Sn is 231 °C. One of the main reasons of choosing Sn as the principle component in the lead free solder for electronic applications is its ability to spread and wet a number of various different substrates. In the solid state, tin can have two different phases or crystal structures 1) white or β-Sn with tetragonal crystal structure and 2) gray or α-Sn with diamond cubic crystal structure. At the room temperature the thermodynamically stable phase is β-Sn. Upon cooling, when the temperature goes below 13 °C (allotropic transformation temperature), α-Sn becomes the thermodynamically stable phase. The allotropic transformation of β-Sn to α-Sn, results a significant volume change (around 27%) causing blistering of the tin surface, cracking or disintegration. This phenomenon is mainly a surface event and often referred as 'tin pest'. The low ductility of α-Sn is another reason of causing blistering and cracking of the tin after the transformation [1, 13, 14]. Although the equilibrium temperature for β-Sn to α-Sn is 13 °C, the transformation occurs only after a significant undercooling and an extensive incubation period as long as several years. For example, no 'tin pest' was found on a SAC387 bulk sample after storing at -40 °C for 5 years [14]. Presence of heterogeneous nuclei, also known as seeding, can considerably accelerate the kinetics of the transformation. The possibility of $\beta \rightarrow \alpha$ transformation in a actual solder joint is even limited due to the constraints (component and substrate) on the both side of the joint [13, 14].

Addition of other elements, as an impurity, can affect the allotropic transformation. For example, the presence of Pb, Bi, Sb, Cu, Ge and Si inhibit $\beta \rightarrow \alpha$ transformation while the presence of As, Zn, Al and Mg promote the transformation [13, 14].

Sn has a body centered tetragonal crystal structure (β-Sn), at room temperature, which is anisotropic. Hence, tin shows an anisotropic thermal (e.g., CTE) and mechanical (e.g. elastic modulus) properties as shown in Figure 1.2. As a result, during thermal cycling experiment, cracking occurs along the grain boundaries [1].

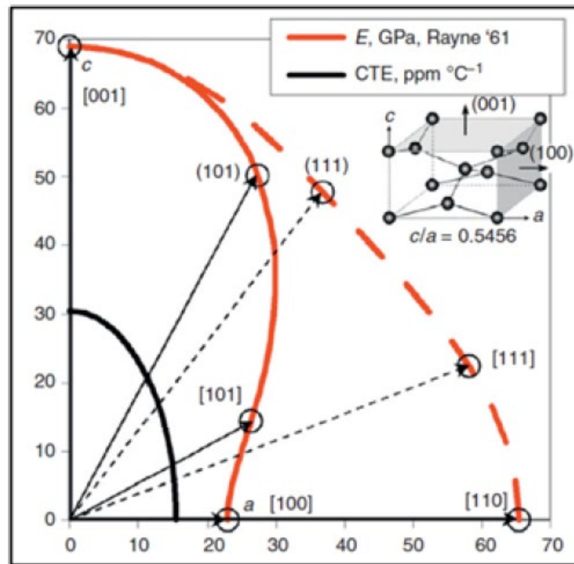

Figure 1.2 Elastic Modulus and Coefficient of Thermal Expansion (CTE) of Tin as a Function of Crystal Orientation [1]

1.3.2 Chromium (Cr)

Cr helps to improve shear ductility after long term aging. Besides, it also suppress kirkendall void formation in the solder joints [15].

1.3.3 Nickel (Ni)

Among all the micro-alloy additives, Ni is one of the most common elements. Addition of Ni improves fluidity of SAC solders. Ni also improves the high strain rate properties of solder joints. For example, the drop strength of SAC alloys can be significantly improved by Ni addition. Although Ni does not have any significant influence on the creep properties of the solder, it inhibits Cu diffusion and thus reduce the thickness of Cu_3Sn intermetallic compound (IMC). The Ni addition greater than 0.01 wt% could suppress the growth of Cu_3Sn IMC even after long term (2000 hours) aging. Since Cu_3Sn IMC is very brittle, the growth of Cu_3Sn layer is very critical for the brittle failure of the solder joints. Addition of Ni on SAC solder causes to form more stable $(Cu, Ni)_6Sn_5$ IMC which act as a barrier layer and suppress the growth of Cu_3Sn layer. Therefore, by reducing the thickness of brittle Cu_3Sn layer, Ni helps to improve strength of the solder joints. Ni also helps to improve strength by refining solder microstructure [16].

1.3.4 Zinc (Zn)

While Ni reduces only the formation Cu_3Sn, Zn doping can retard both Cu_3Sn and Cu6Sn5 IMC's in SAC solders. Zn also helps to improve the interface quality after multiple reflow and high temperature aging. Addition of 1.5% Zn in SAC207 solder could refine Ag_3Sn and Cu6Sn5 IMC's and hence increase strength by dispersion strengthening [15].

1.3.5 Cobalt (Co)

Co helps to reduce the growth of Cu_3Sn layer during high temperature aging. Addition of small amount of Co (<0.1 wt.%) can improve the properties of SAC solders. Co increases the number of nucleation sites and hence significantly refine the grains of SAC305 solder. Thus it helps to improve shear strength of the solder joints [15].

1.3.6 Bismuth (Bi)

If added in small amount, Bi can improve the wetting ability and reduce melting temperature of lead free solder alloys. It also increases strength of the bulk solder and inhibit the large Ag_3Sn formation in the bulk solder. It is recommended to avoid Pb contamination in the solder before using Bi as an additive. Because Bi can react with Pb to form a brittle IMC at the grain boundary and reduce strength significantly. If present in excess amount, Bi can cause solidification crack due to the increase in the gap between solidus and liquidus temperature [15].

1.3.7 Antimony (Sb)

Sb improves mechanical properties of lead-free solders but it is toxic in nature. A small percentage (0.5 wt%) of Sb can improve drop test reliability of SAC solder joints [16]. Besides, Sb also helps to enhance strength of the solder by solid solution strengthening [17].

1.3.8 Germanium (Ge)

Ge doped solders shows low Cu dissolution from the Cu pad and hence suitable for the wave soldering process. Ge significantly improve wetting properties of the lead free solders and refine the solder microstructure. As a result, Ge addition improves the strength and ductility of the lead free solder [16].

1.3.9 Sn-Ag-Cu System

As shown in Figure 1.1, Sn-Ag-Cu (SAC) has been the most popular, widely used lead free solder in today's market. Although they are still not identified as the "drop in" replacement for all applications, a variety of SAC alloys with different chemical compositions have been the proposed by various user groups and industry experts. These include: SAC105 (98.5Sn-1.0Ag-0.5Cu), SAC205 (97.5Sn-2.0Ag-0.5Cu), SAC305 (96.5Sn-3.0Ag-0.5Cu), and SAC405 (95.5Sn-4.0Ag-0.5Cu), known as the SACN05 series; SAC387 (95.5Sn-3.8Ag-0.7Cu), SAC396 (95.5Sn-3.9Ag-0.6Cu), and SAC357 (95.2Sn-3.5Ag-0.7Cu), identified as near eutectic SAC choices; SAC3810 (95.2Sn-3.8Ag-1.0Cu), SAC3595 (95.55Sn-3.5Ag-0.95Cu), SAC0307 (9Sn-0.3Ag-0.7Cu), and SAC107 (98.3Sn-1.0Ag-0.7Cu), designed for special needs such as high temperature application, drop and shock optimization, thermal cycling reliability etc. The main benefits of the various SAC alloy systems are their relatively low melting temperatures compared with the 96.5Sn-3.5Ag binary eutectic alloy, as well as their superior mechanical and manufacturability properties when compared to other lead free solders [18].

Figure 1.3 shows a typical 3-D ternary phase diagram. The contours on the top surfaces of the figure represent the isothermal lines. Each of the 3 sectors represents the

binary phase diagram of two of the three elements. The center of the diagram, where the isothermal lines reach the common, lowest point, is the eutectic point of the ternary system. Figure 1.4 is the top view (2-D) of the ternary phase diagram of Sn-Ag-Cu.

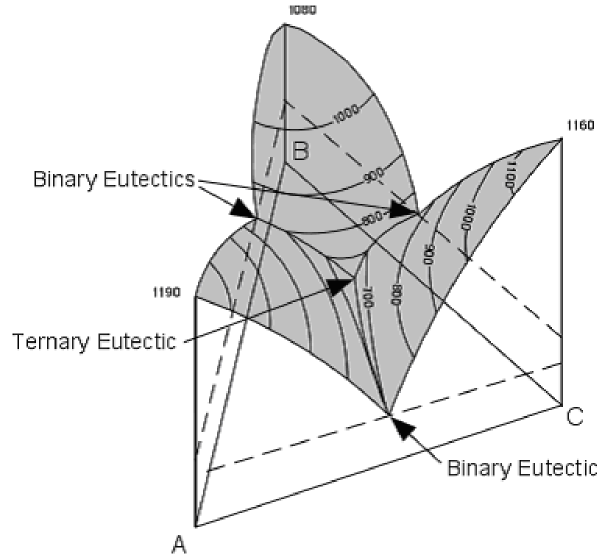

Figure 1.3 Typical 3-D Ternary Phase Diagram

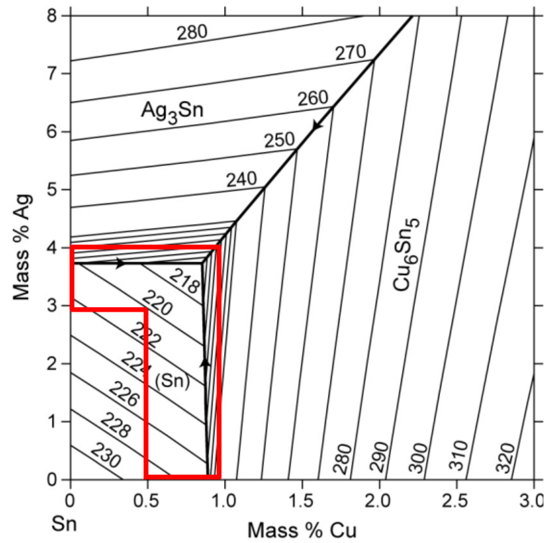

Figure 1.4 Sn-Ag-Cu Ternary Phase Diagram

The area indicated in the red box is the near eutectic region. Most of the SAC alloy compositions currently on the market are within this region. The eutectic and near eutectic melting temperature has been determined to be 217 °C, although the precise eutectic point is not known [19].

In SAC alloys, the formation of intermetallic compounds between the primary elements Sn and Ag, and Cu affect all the properties of the alloys. There are three possible intermetallic compounds that may be formed: Ag_3Sn forms due to the reaction between Sn and Ag (Figure 1.5) and Cu6Sn5 forms due to the Sn and Cu reaction. The compound Cu_3Sn will not form at the eutectic point unless the Cu content is high enough for the formation of Cu_3Sn at higher temperatures, so in bulk specimens Cu_3Sn is not presented. There is no reaction between Ag and Cu to form any kind of intermetallic compounds. The particles of intermetallic compounds possess much higher strength than the bulk material. Fine intermetallic particles in the Sn matrix can therefore strengthen the alloys. The intermetallic compounds can also improve the fatigue life of the solders, as SAC alloys are reported to be 3-4 times better fatigue properties than the Sn-Pb eutectic solders. The higher fatigue resistance is believed to be contributed by the interspersed Ag_3Sn and Cu6Sn5 particles, which pin and block the movement of dislocations. The many patents that have been granted for SAC systems have limited their use and hindered research on several of the SAC alloys. However, many familiar alloy such as SAC305 and SAC405 are not patented to avoid excessive licensing and fees [18].

Despite the benefits mentioned above, SAC family solders sometimes are still questionable as complete substitutes for eutectic Sn-Pb because of costs, some patent issues

(particularly outside Europe), aesthetic consideration (dross problem of SAC solders), and relatively high melting temperature (217 °C vs. 183 °C).

1.3.10 Sn-Ag-Cu + X System

Sn-Ag-Cu alloys have shown potential to be successful substitutes for eutectic Sn-Pb, however, the industry is still looking for a "perfect" solution. According to the results of many recent studies, performance characteristics of solder alloys are able to be optimized by doping, that is, by adding a small amount of other alloying elements into the SAC solder alloys.

The proposed doping element candidates include Bi, Ni, Co, Ge, Zn, La, Mg, Mn, Ce, Ti, Fe, In, B, etc. For example, adding 0.05% (wt.) Ni can successfully stabilize the microstructure, inhibit the excessive consumption of metal base and thus increase the reliability of the solder joints [20-22]. In addition, doping rear earth (RE) elements can significantly enhance wettability, refine microstructure and improve ductility of SAC alloys [23-26].

Even though dopants can greatly alter the mechanical, electrical and physical behavior of SAC solders, the effect on melting temperature, however, is found to be negligible. This is another advantage for doped solder alloys because manufacturers can still use the same processing conditions as conventional SAC alloys.

Meanwhile, the known issues for SAC-X solders are also apparent. For instance, the material properties and interfacial behavior of solder alloys have been demonstrated to be very sensitive to the quantity of the X-additive. As a result, it takes much more time and cost to figure out the optimal composition levels for the dopants.

1.4 Characteristics and Applications of Sn-Ag-Cu Solder Material

The advantages of SAC series over other Pb-free systems include relatively low melting temperatures, superior mechanical and solderability properties, and good tolerance for Pb contamination. These characteristics give SAC alloys good compatibility with existing electronics packaging infrastructure. In fact, there is a long history of using 95.5Sn–4.0Ag–0.5Cu (SAC405) to form solder joints for BGA packages. The high market share (≈ 70%) by SAC series alloys on a global scale provides strong evidence of its world-wide acceptance. Also, nanoscale lead-free solders ("nano-solders") have been proposed and investigated in the development of nano-soldering technique for nanoscale assembly and integration. Tin (Sn)-based and indium (In)-based lead-free nano-solders have been synthesized directly onto multisegmented nanowires using electro deposition method in nanoporous templates. Furthermore, high temperature lead free solders are being used in medical industries today where a variety of intrusive procedures used requiring tools, instruments, sensors and components in materials that are inert with respect to reactions with the body [27]. Also, new surgical techniques have been developed to improve the quality of operations, reduce the risk to patients and reduce the pain experienced by patients. Environmental concerns and the concern about toxicity and health hazards indicate that there is a drive to develop and use lead-free solders.

1.5 Mechanical Properties of Lead Free Solders

In an electronic device, a number of different types of engineering materials exists in a close proximity. For example, a printed circuit board (PCB) is typically a glass fiber reinforced polymer (composite material), a die is a semiconductor material which is often

encapsulated in a plastic or a ceramic, and the tracking and the solder joints are metallic materials. Solder joints are used to create an electrical circuit by mounting chips and components on the PCB. Hence an ideal solder joint should have a good conductivity to transmit electrical signals and at the same time, adequate strength to provide mechanical support and connection. Hence, mechanical properties of solder joints are critically important to ensure reliability of the electronic products. Among all the mechanical properties, tensile, fatigue, and creep performance of the solder are critically important. Thus an accurate measurement of mechanical properties and development of constitutive equations for solder materials are required in mechanical design, process optimization and reliability assessment.

1.5.1 Tensile Properties (Stress-Strain Behavior)

Under the action of an increasing stress, metals usually exhibit elasticity, plasticity, and a maximum in stress is followed by necking and fracture. The slope of the linear elastic portion of the stress vs. strain plot is the modulus, and the stress at termination of elastic behavior is the yield stress. The extent of deformation prior to fracture is known as ductility. Ceramics display only elastic behavior until fracture, which is associated with cracking and very limited deformation (brittleness). Polymers may exhibit both characteristics above according to the temperature. Above the glass transition temperature, T_g, extensive deformation due to mechanisms quite unlike those in metals may follow a small degree of elasticity. Below this temperature, polymers exhibit ceramic-like behavior. In all material categories, the maximum stress attained is the tensile/compressive/shear strength according to the mode of stressing employed. Composites are physical mixtures

and exhibit the average properties of their components, taking into account the proportions of each. These characteristic features of monotonic behavior are summarized in Figure 1.5. The fracture strains of brittle materials and the yield strains of metals are generally less than 1% (the yield strain of solders is around 0.1–0.2%). The amount of deformation prior to the attainment of maximum strength is between about 3% and 7% for common solder alloys.

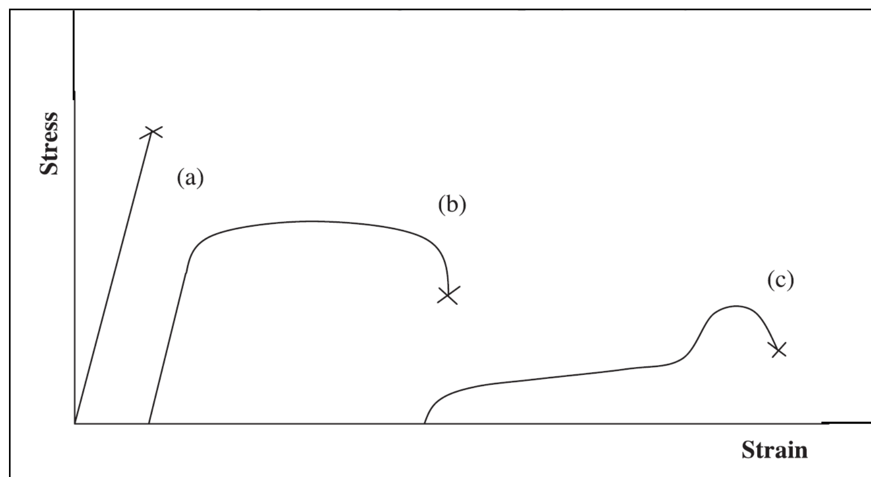

Figure 1.5 Schematic Overview of Mechanical Behavior of a) Ceramics, Polymers below their Glass Transition Temperature (Tg) and Non Ductile Material b) Ductile Materials c) Polymers above Tg

Tensile properties indicate how the material will react to forces being applied in tension. Although solder joints are rarely under pure tensile/compressive loading, tensile properties are still crucial indicators for design purposes. Through tensile tests, several material properties can be determined, such as effective modulus, yield stress (YS), ultimate tensile strength (UTS), elongation, etc. In most of the cases that engineering stress-strain curves are employed by neglecting the change in cross sectional area.

Tensile properties are generally described by stress-strain curves. Figure 1.6 shows a typical engineering stress strain curve. A typical engineering stress-strain curve for solder alloys consists of an elastic region and a plastic region. In the elastic region, when the stress is reduced, the material will return to its original shape. In this linear region, the material obeys the relationship defined by Hooke's Law. However, since the effective modulus includes small inelastic deformations or time-dependent deformations such as creep, it is usually smaller than the dynamic modulus measured by the acoustic or ultrasonic wave method, which largely eliminates the inelastic deformation due to rapid wave propagation [28-30]. Also, Ralls, et al. showed that the elastic modulus of metal will decrease with increasing temperature [31]. The underlying reason for this is because the distance between adjacent atoms increases at higher temperatures which in turns decrease the elastic modulus.

When the load is high enough to exceed the elastic limits the material will experience plastic deformation, which is permanent. At this stage the material is undergoing a rearrangement of its internal molecular or microscopic structure, in which atoms are being moved to new equilibrium positions. Specimens subject to plastic deformation will simultaneously elongate and decrease in diameter. The Yield Stress (YS) is defined as just enough stress to cause the onset of plastic deformation. However, YS is difficult to determine. In engineering practice, a specified small amount of plastic deformation is used, with 0.2% being the widely accepted value [32]. This is determined by a parallel line drawn at 0.2% of the strain to the elastic slope (Figure 1.6). When the load is removed at a point above the yield stress, the stress-strain curve will be approximately parallel to the initial modulus.

The ultimate tensile strength (UTS) is the maximum engineering stress level reached in a stress-strain test. In ductile materials similar to solders, the UTS are usually well outside of the elastic portion and the elastic strain is very small comparing to the plastic strain. When necking occurs, the engineering stress decreases and the specimen eventually fail.

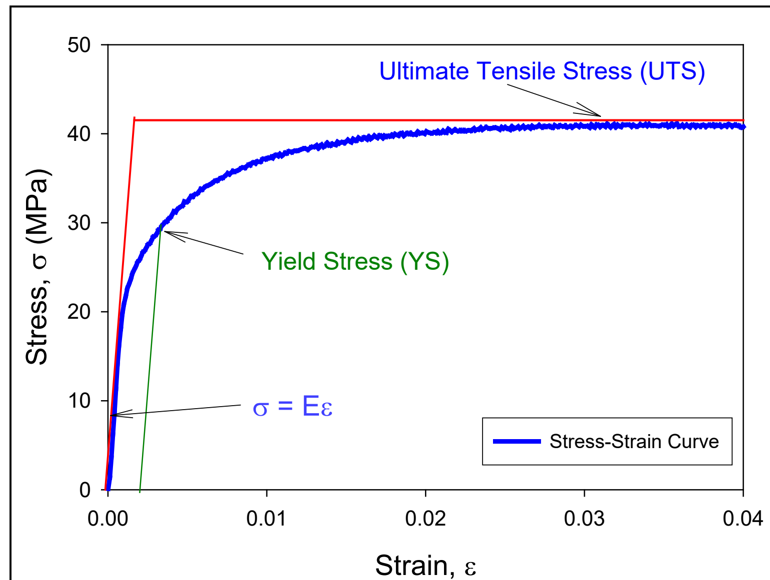

Figure 1.6 Typical Stress-Strain Curve.

1.5.2 Creep Properties

Creep deformation refers to the time dependent plastic flow or deformation of a material that occurs when the material is exposed to a constant load, typically below yield stress, for a long period of time. Creep deformation becomes significant when the material operates at a high homologous temperature (T_h), which is defined by the ratio of operating temperature (T) and the melting temperature (T_m) of the material.

$$T_h = \frac{T}{T_m} \tag{1.4}$$

Creep deformation becomes the dominant failure mode in a metallic material if T_h is greater than $0.5T_m$ [33]. The melting temperature of lead free SAC solder is around 217 °C (490 K) causing T_h for the alloys, for room temperature (298 K) operating conditions, is $0.61T_m$. As a result, lead free SAC solder alloys display creep deformation even in room temperature operating condition. Due to the mismatches of the coefficient of thermal expansion (CTE) of silicon chip and other assembly materials used in an electronic package, solder joints are remain under mechanical stress. These mechanical stresses can cause time dependent creep deformation of solder materials. In microelectronic packaging, creep deformation is regarded as one of the major failure mechanisms of solder joints [34].

Creep test is typically conducted by applying a constant uniaxial load on the test specimen at a particular temperature. During the test, deformation of the test specimen is recorded as a function of test time and the result of the creep test is presented as a 'creep strain' vs. 'time' plot. The extent of creep deformation significantly depends on the applied stress level and the test temperature. Figure 1.7 represents a typical creep curve which consists of three distinct regions, after the initial jump, namely, primary, secondary, and tertiary regions.

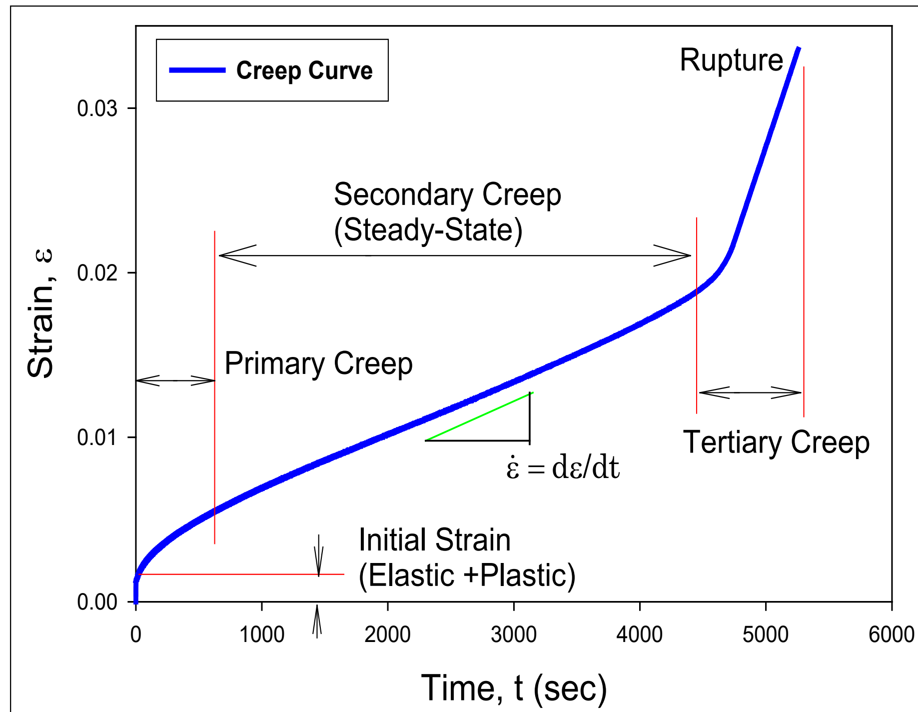

Figure 1.7 Typical Creep Curve.

Every creep test begins with an initial strain which corresponds to the instantaneous response (mostly elastic) of the material due to the applied force/load. In the primary creep stage, the material starts to deform with at a high strain rate (high slope at the beginning of the primary region) and then the strain rate decrease gradually with increasing time. This is due to the work hardening of the material which resists deformation. Eventually, with increasing test time, the creep strain rate reaches to a steady state stage which is known as steady state creep or secondary creep region. The constant creep rate, in the secondary stage, is due to the dynamic balance between strain hardening and recrystallization [32]. The strain rate in the secondary stage is very important since very often researchers use this parameter in the finite element simulations to predict reliability of the solder joints under different test conditions. After secondary creep, the material enter into the tertiary

creep region followed by an immediate rupture. Tertiary region begins when the strain rate start increasing abruptly from the constant value.

1.5.3 Mechanisms of Creep Deformation

Several creep mechanisms have been proposed such as dislocation glide, dislocation creep, grain boundary diffusion, and lattice diffusion which can be summarized in a creep deformation map, as shown in Figure 1.8 [35, 36]. The deformation diagram was first introduced by Ashby in 1972 [36], and has been widely accepted and studied by other researchers in the area. In the deformation map show in Figure 1.8, the abscissa is the homologous temperature and the ordinate is normalized tensile or shear stress. The top of the map is bounded to the theoretical or ideal stress, below which is the onset of dislocation glide. *Dislocation glide* occurs at high stress levels over the entire homologous temperature range. In this case, the dislocation moves along the slip planes [37]. Dislocation creep is characterized by a high-temperature deformation mechanism with homologous temperatures greater than $0.5T_m$ and requiring intermediate high stress. The deformation results from diffusion controlled dislocation movement, with dislocations climbing away from barriers.

Coble proposed a *grain boundary based diffusion* mechanism, which involves the atomic or ionic diffusion along the grain boundaries [38]. The deformation occurs at intermediate low stress levels over an intermediate to low temperature range. Nabarro-Herring Creep or *lattice or bulk diffusion* occurs at low stress level and high temperature. In this case, interstitial atoms and lattice vacancies along the gradient of a grain boundary migrate in reversed directions in the presence of tension or compression pressure. Lattice

or bulk diffusion becomes the primary deformation mechanism under this circumstance [39]. If there is no pressure, interstitial atoms and lattice vacancies will migrate in proportion to the gradient of their concentrations. Under pressure, the lattice defects tend to move in directions to relieve the imbalance of pressure. The movement will eventually cause creep deformation.

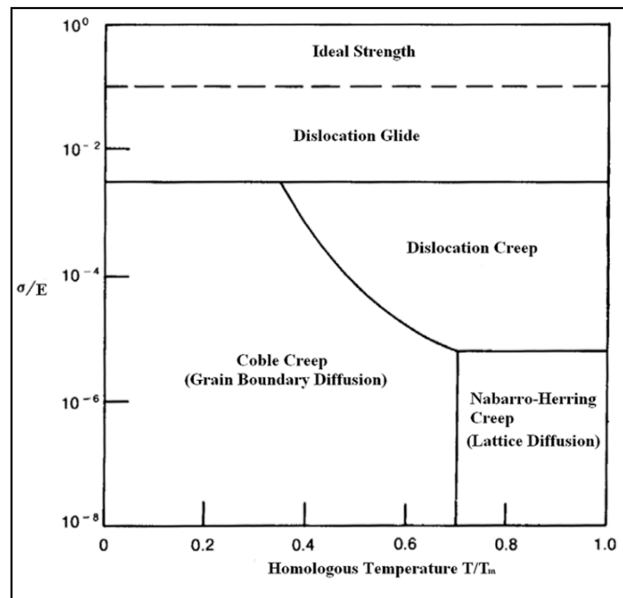

Figure 1.8 A Typical Creep Deformation Map.

Grain-boundary sliding may also be involved in the creep deformation at high temperatures [30] where the displacement of grains can be induced by stress at high temperatures. However, this is not an independent deformation mechanism, but may accompany one or more of the above deformation mechanisms.

Due to the high homologous temperature (> $0.5T_m$) of most solder alloys under normal operating conditions, the stress level determines the creep deformation mechanism. At low stress levels, the controlling mechanism is lattice diffusion and grain-boundary diffusion. As the stress rises to intermediate levels, dislocation creep takes over, and at

high stress level, dislocation gliding becomes dominant. Additionally, the contribution of grain boundary gliding to creep deformation should be taken in account at all stress levels.

1.6 Nanoindentation

Indentation testing is a technique where a hard tip, with known mechanical properties, is pressed into the surface of a test sample to extract the test sample's properties. The load applied on the indenter tip caused it to penetrate into the test sample surface. When the applied load reaches to the user specified value, it can be held for a certain period of time (for creep properties) or remove instantaneously (for hardness and elastic modulus). Removal of the applied load leaves an impression or indent on the sample surface.

Nanoindentation (NI) is a kind of indentation testing where the penetration length is measured in nanometer. The development of the NI technique has been motivated by the miniaturization of the engineering materials as well as the development of the nanostructured materials. Since the area of the indenter tip is well defined (known geometry), the indent area can be easily determined from the tip penetration depth from the sample surface. Elastic modulus, hardness and creep properties of a material can be obtained from indentation load displacement data [40].

Because of having very high hardness and elastic modulus, diamond is typically used to make indenter tip. Indenter tips are available in different shape and the choice of indenter tip shape depends on the type of required information from a NI test. Berkovich tip is used in this study (Figure 1.9).

This is the most common indenter tip and used to measure mechanical properties using a NI technique. The shape of a Berkovich tip is similar to a three-sided pyramid

where the faces meet at a single point (Figure 1.5). The tip can maintain its self-similar geometry to a significantly small scale. The center to face angle of the tip is 65.3°.

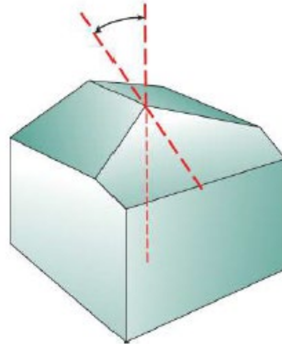

Figure 1.9 Berkovich Tip.

1.7 Harsh Environment applications of Electronics

The reliability of electronics used in various devices depends on the environmental conditions experienced during field use. In oil and gas exploration, avionics, automotive, and defense applications, electronics typically experience very harsh environments compared to consumer electronics [41, 42]. The electronic systems used in under-the-hood automotive applications can be operated at temperatures over 150 °C [43, 44]. For example, engine control modules mounted directly onto the engine experiences high-temperature excursions while in operation. In vehicles, when the engine is turned on, it continues to ramp up to the maximum operating temperature from the ambient temperature while the engine continues to be in operational state. Electronics experience extremely high temperatures during this period, and there can be fluctuation in the temperature conditions.

The electronic systems used in daily applications, also experiences ambient temperatures above 100 °C, and temperature changes [45]. During this application, specifically in winter countries, the temperature fluctuates from negative to high temperature up to 125 °C. The reliability of electronics is an important concern here since temperature changes causes CTE mismatch happens between various components in electronic packages. CTE mismatch between die and PCB causes shear fatigue on solder joints and causes crack initiation, propagation and failure of the components.

Electronics used in commercial and defense aircrafts and ground military vehicles also experience high temperatures and thermal cycling environment.

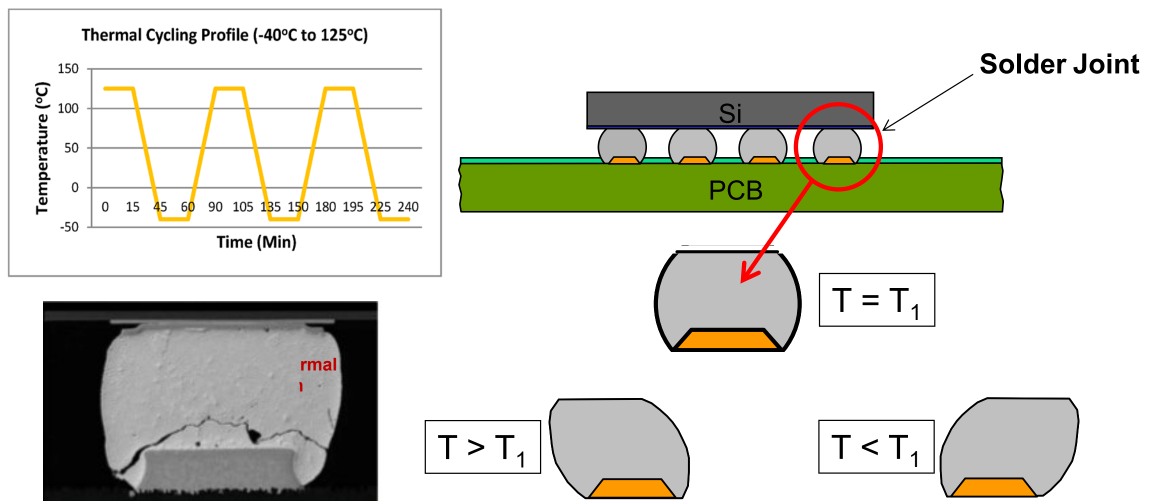

Figure 1.10 Temperature Cycling of Electronic Packages

1.8 Objectives of This Research

The motivation of this research is to explore the mechanical behavior evolution of lead-free solder alloys under harsh environment applications like aging and thermal cycling

to predict solder joint reliability in microelectronic packaging. The Primary objectives of this research involve:

(1) Investigate the Stress-Strain and Creep Behavior Evolution of Bulk SAC305 Solder Material under Different Thermal Exposures such as Isothermal Aging, Slow Thermal Ramping, Thermal Shock, and Slow Thermal Cycling

(2) Understand the Stress-Strain and Creep Behavior Evolution of SAC+Bi Solder Material under Different Thermal Exposures

(3) Compare the Evolutions of the Mechanical Properties (Stress-Strain, Creep) of SAC+Bi and SAC305 Solder Materials for Various Thermal Exposures

(4) Investigate the Mechanical Behavior (Modulus, Hardness, Yield Strength) Evolution of SAC305 and SAC+Bi Solder Joints (Balls) for Different Thermal Exposures by Nanoindentation Technique

(5) Compare the Mechanical Behavior Evolutions of Bulk Solder and Solder Joints of Both SAC305 and SAC+Bi Alloys

(6) Understand the Microstructural Evolution of Bulk SAC305 and SAC+Bi Solder Alloy when Exposed to Different Thermal Exposures

1.9 Organization of the Dissertation

This dissertation mainly focuses on investigating the mechanical and microstructural behavior evolution of lead-free Solder alloys under different thermal exposures and is presented in the following chapters:

Chapter 1: Introduction to lead free solders alloys and mechanical properties of solder materials.

Chapter 2: Literature Review on Different Thermal Exposures Effects, Mechanical Properties, Nanoindentation on SAC Solder Joints, and Microstructural Evolution During Different Thermal Exposures of SAC Alloys

Chapter 3: Description of Experimental Procedure, Sample Preparation, Uniaxial Tensile Tests, Creep Tests, Nanoindentation Modulus And Hardness Test, And Data Processing.

Chapter 4: Mechanical Characterization of SAC Solder Material for Different Thermal Cycling Exposures

Chapter 5: Comparison on Mechanical Behavior Evolution of SAC Solder Materials for Different Thermal Exposures

Chapter 6: Investigation on Evolution of Mechanical Properties of SAC Solder Joints by Nanoindentation Technique

Chapter 7: Microstructural Evolution of SAC Solders for Different Thermal Cycling Exposures

Chapter 8: Summary and conclusions of the dissertation

CHAPTER 2

LITERATURE REVIEW

2.1 Introduction

As the electronic industries transition to lead free soldering by the motivation of environmental concerns, legislative mandates, and market differentiation, great efforts have been undertaken to develop desirable lead free solders and establish a corresponding database of material properties. Many researchers have attempted to measure the key mechanical properties of lead free solders. However, large discrepancies have been found in the published data from various groups. There are several reasons for these discrepancies. Firstly, the differences in specimen preparation methods among the researchers cause different microstructures in the specimens that directly affect the experimental results significantly. Secondly, the testing methods and the test conditions may also be different which will again affect the results. Thirdly, mechanical properties obtained from the bulk solders might be different from the measured properties of solder joints. Finally, the lack of standardization in the data acquisition and processing of mechanical properties makes it difficult to obtain good laboratory-to-laboratory comparisons.

Apart from the above-mentioned reasons for the discrepancies in solder material properties, another critical factor is aging effects. Aging is mostly neglected in the majority

of prior studies, which will further exacerbate these problems. It has been observed from recent studies that isothermal aging leads to large reductions (up to 50%) in several key material properties for lead free solders including stiffness (modulus), yield stress, ultimate strength, and strain to failure [33]. Even more dramatic evolution has been observed in the creep response of aged lead free solders, where up to 100X increases were found in the steady state (secondary) creep strain rate (creep compliance) of SAC solders that were simply aged at room temperature [46, 47]. For elevated temperature aging at 125 °C [48], the creep strain rate was observed to change even more dramatically (up to 10,000X increase for SAC105).

In real applications, solder joints are continuously exposed to aging/thermal cycling during service. It has been well documented that the microstructure, mechanical response, and failure behavior of solder materials are constantly evolving under such circumstances [49-84]. It has also been demonstrated that aging effects are universally detrimental to reliability and cause reductions in stiffness, yield stress, ultimate strength, and strain to failure, as well as highly accelerated creep. Solder joints with highly degraded microstructure and material properties are so vulnerable that the service life of the package is often severely shortened.

2.2 Aging Effects on Tensile Properties

Studies on the effects of aging on solder material properties are primarily divided into two groups, which are aging effects on bulk solders and aging effects on solder joints. These are described in subsequent sub-sections.

2.2.1 Aging Effects on Bulk Solders

Evolution of mechanical properties with aging in both Sn-Pb and lead free solders has been reported in recent years. Researchers have done numerous studies on the effects of aging on bulk solder properties as well as some studies on solder joints in actual components. Most studies show aging has significant effects on the mechanical properties of solder materials. In 1956, Medvedev [62] reported a 30% loss of tensile strength for bulk Sn-Pb solder after 450 days of room temperature (RT) aging, and a 23% loss in tensile strength for solder joints under a similar exposure. Room temperature aging effects on solder alloys has been presented by Lampe [60]. He showed that after 30 days of room temperature aging, the shear strength and the hardness of Sn-Pb and Sn-Pb-Sb solders reduced by approximately 20%. Miyazawa [77] reported reduction of hardness and microstructural coarsening for Sn-Pb solders aged at 25 and 100 °C for 1000 hours.

Xiao, et al. [66] investigated the stress-strain behavior of SAC396 solder alloy which were subjected to aging at 25 and 180 °C for various amount of time. They have shown that the strength reduces by 25% for aging at room temperature for 35 days and a 33% reduction for aging at 180 C for 9 days. Ding, et al. investigated the influence of aging on fracture behavior of Sn-Ag solder in tensile tests [56]. They have shown that the solder samples tensile strength reduce very quickly for isothermal aging at 180 °C for 120 hours. Ma, et al. [85] studied the evolution of Young's modulus, yield stress, and ultimate tensile strength of SAC305 and SAC405 solder alloys under various aging conditions. A linear-exponential model was developed to describe the material property evolution. They have shown that the material properties decreased dramatically in the first 20 days for both

room temperature aging as well as elevated temperature aging. After 20 days of aging, the properties change slowly and linearly and it continues for longer aging time.

Zhang, et al. [86] also studied the aging effects on tensile properties of SACN05 (N = 1%, 2%, 3% and 4% silver) series solders for different amount of aging at temperatures 25-125 °C. They have demonstrated that the mechanical properties degraded more dramatically when the aging temperature was increased. The data also shows that the degradation becomes linear with longer aging time. Cai, et al. [51] have also shown that the aging effects are significant for lead free solders (SAC105, SAC205, SAC305 and SAC405) for room temperature aging as well as elevated temperature aging. They have also shown that the aging effects can be reduced by using certain dopants to (e.g. Bi, In, Ni, La, Mg, Mn, Ce, Co, Ti, Zn, etc.) SAC solder alloys to enhance the reliability of lead free solders. Finally, Mustafa, et al. [78] have demonstrated that the hysteresis loop area in cyclic (tension/compression) loading of various SAC solder alloys changes significantly with aging. For strain controlled tests, the hysteresis loop area decreases and for the stress controlled tests, the loop area increases with aging time.

2.2.2 Aging Effects on Solders Joints

Isothermal aging effects have also been reported to lower the strength and to reduce reliability of solder joints. The mechanical response of solder joints to external loading can be different from the bulk solders due to fine microstructure, grain orientation (single grain/ multigrain), and the presence of intermetallic compounds at joint boundaries.

Coyle, et al. [87] reported 20% shearing strength reduction of BGA solder joints after 240 hours of aging at room temperature. A 10% shearing strength reduction has been

reported by Lee, et al. [88] for the BGA packages just after 3 days room temperature aging. Chilton, et al. [89] reported a 15% fatigue strength reduction of Sn-Pb solder joints of a SMD test package which were aged for 60 days at room temperature. Li, et al. [90] studied the elevated temperature aging effects on flip-chip packages with SAC solders. They have shown that the shear strength of solder bumps subjected to aging at 80 °C decreased gradually with aging. Also for the aging temperatures 150 and 175 °C, the degradation of shear strength of the bumps were much faster. They also reported that the fracture of the solder bumps occurred at the bulk solder. Koo, et al. [91] found that 63Sn-37Pb solder joint strength on electroplated Ni/Au BGA substrate was significantly affected by aging at 170 °C for up to 21 days, while the deterioration of shear properties of Sn-3.5Ag was much smaller. Darveaux [92] indicated that after 24 hours of aging at 125 °C, all alloys showed a 10% to 30% reduction in solder joint strength. All of the solder joints failed within the bulk solder and exhibited high ductility. In addition, the ductility of all of the Pb-free solder joints decreased with increased aging [66]. Oliver et al. [93] reported that the joint strength of Sn-3.5Ag and SAC325 solder on both Ni/Au and Sn/Pb pad metallizations were unchanged after aging at room temperature as well as elevated temperature for 1000 hours. However they found reduction in shear strength of solder joint in Sn-Pb solders.

Pang, et al. [94] studied the aging effects on the mechanical properties and fatigue life of Sn-Pb solder joint specimens that were subjected to thermal cycling conditions from -40 to 125 °C. They have shown that the shear strength reduces significantly for specimens that were subjected to 1000 thermal cycles. They have also shown that the fatigue life of the specimens dropped by 6 times compared to non-cycled specimens. Zhou, et al. compared the joint strengths of SAC387 on both Cu and Ag substrates at an aging

temperature of 170 °C, and concluded that aging had little effect on the SAC/Ag interface, but dramatically softened the SAC/Cu joint. The softening difference was said to be due to lower residual stresses at the SAC/Ag joint interface. Chen, et al. [73] studied the effects of aging on the solder bump shear strength for both Sn-Pb and Sn-3.5Ag solders. They reported that shear strength for both solder materials decreases after aging at 150 °C for 1500 hours, 8.9% for Sn-Pb solder bumps and 5.3% for Sn-3.5Ag. Kim, et al. [59] also reported similar results in which they reported an average 5% decrease in joint strength in stud bump samples for aging at 150 °C for 300 hours.

The degradations of the stiffness, strength, and creep compliance with aging are expected to be universally detrimental to reliability of solder joints in lead free assemblies. This has been demonstrated explicitly in the recent investigation of Lee and coworkers [88], where aging has been shown to degrade the Thermal Cycling Reliability (TCR) of lead free Plastic Ball Grid Array (PBGA) assemblies subjected to Accelerated Life Testing (ALT). They have shown dramatic degradation in fatigue life of BGA components with SAC 305 solders, which were subjected to thermal cycling from 0 to 100 °C with prior aging at either 100 or 150 °C. The amount of life degradation was found to be dependent on the surface finish of the PCB substrates, with 44% degradation observed for ENIG surface finish and 20% degradation observed for OSP surface finish under the most severe aging conditions (1000 hours at 150 °C) prior to thermal cycling accelerated life testing.

In a similar study, Lee, et al. [95] showed that the lifetime of wafer-level chip scale packages with SAC305 solder interconnects was reduced by 29% for 500 hours of aging at 150 °C. Zhang, et al. [81] have investigated the correlation between the effects of isothermal aging on the reliability of PBGA components. They have shown that for 6

months aging at 125 °C that the reliability of SAC105 components dropped by 53%. Smetana, et al. [96] have performed an extensive study on the effects of prior isothermal preconditioning (aging) on the thermal cycling lifetime for a variety of components. Similar to the investigations discussed above, it was observed that prior aging reduced the thermal cycling characteristic life of SAC BGA assemblies subjected to 0 to 100 °C cycling. It was also found that changes occurred in the Weibull slope, suggesting other failure modes were created by aging. They also found that prior aging increased the thermal cycling reliability of certain components (e.g. 2512 chip resistors and certain QFNs). Similar results of improved reliability with aging were found for components subjected to a smaller thermal cycling range of 20 to 80 °C. This led them to conclude that aging does not universally reduce solder joint fatigue life.

The effects of aging on the degradation of the thermal cycling reliability of lead free BGA assemblies have been studied recently by Zhang, et al. [81]. In their studies, PBGA daisy chain test assemblies were subjected to up to 2 years of aging (25, 55, 85, and 125 °C), followed by thermal cycling from -40 to 125 °C or -40 to 85 °C to failure. They have shown that for all component sizes and lead free solder alloys, the solder joint thermal cycling reliabilities of the BGA components were severely reduced by prior aging. For up to 12 months prior aging for the components with Im-Ag PCB surface finish and thermal cycling from -40 to 125 °C, they have observed clear degradation in life for aged components relative to non-aged components and the amount of degradation was exacerbated with higher aging temperatures. Using the 63.2% Weibull characteristic life (η) as a failure metric, the reliability was observed to decrease by 37% (6 months aging)

and 53% (12 months aging) for the 19 mm BGA components subjected to aging at 125 °C prior to thermal cycling.

Gradual aging also occurs during thermal cycling tests due to the high temperature dwells at the top of each thermal cycle. Several recent studies [97-101] have demonstrated that there is a strong dwell time effect on thermal cycling reliability for lead free electronics; with longer dwell times leading to reductions in the thermal cycling life.

2.3 Aging Effects on Creep Properties

It has been found in the literature that aging at room temperature as well as elevated temperatures have significant effects on creep deformation of lead free solder alloys. Darveaux, et al. [92] reported a faster creep rate for aged solder specimens than non-aged specimens. For both SAC305 and SAC405 solders and for aging at 125 °C for 1 day, they found 20 times increase in the creep rate for aged specimens. Xiao, et al. [66] found that SAC396 showed much lower absolute creep rates compared with eutectic Sn-Pb and ascribed this increase in creep resistance to the finely dispersed intermetallic compound (IMC) precipitates in the Sn matrix. Wiese, et al. [65, 102] investigated the creep behavior of SAC 387 solder with short (1 day at 125 °C) and long (49 days at 125 °C) thermal storage times. They found that the creep rate of solder increase significantly for short time aging at 125 C but relatively smaller changes occurred for longer aging times.

Ma, et al. [103] studied the evolution of secondary creep rate with aging for SAC305 and SAC405 solders. They showed that the secondary creep rates for SAC solders increase with aging at either room temperature or elevated temperature. Also, for both SAC solders exposed to elevated temperature aging, the effects were much higher than

those for room temperature aging. A more detailed investigation was conducted by Zhang, et al. [86] on aging effects on the creep behavior of lead free solders. They reported that for 6 months aging at 125 °C, the secondary or steady state creep rate of SAC105 solder increased by about 10000 times. Also, for other aging temperatures (25 to 125 °C), they found that the both the primary and secondary creep rates increase with 6 months aging. Finally, Cai, et al. [51] demonstrated that by using certain types of dopants in SAC solders, the aging effects on steady state creep rate can be reduced. They showed that for no aging the creep rates of doped solders were higher than SAC105 and SAC205 due to lower silver contents of the doped solders compared to SAC105. However, with 6 months aging at temperatures 25 to 125 °C, the secondary creep rates of the doped solders were smaller than the creep rates of SAC105.

2.4 Effects of Thermal Cycling on Solder Joints

In microelectronics packaging, complex stresses and strains are usually generated in the components due to the CTE mismatch of different materials. Coefficient of Thermal Expansion (CTE) mismatch between the package and the board during the cycles was considered as the dominant factor that affects the reliability of board-level solder interconnections [54, 55]. Due to the miniaturization of electronic devices along with the adoption of lead-free solder alloys [57], solder interconnection reliability has received an increasing attention during the recent years. Numerous studies have been carried out to find out the root causes of failures in electronic devices under various operation conditions. Researchers have found that the CTE mismatch between the Printed Circuit Board (PCB) which is composed of FR4 material and polymer; and the package, which is composed of

substrate, die, and mold compound, results in a thermomechanical fatigue damage of solder joints when the board- level package subjected to thermal cycling. In many cases, failure occurs due to thermomechanical shear fatigue where cracks initiate and then propagate through the bulk solder joint [61, 64-65].

2.5 Constitutive Modeling for Stress-Strain Tests

The linear elastic region in a uniaxial stress-strain curve can be modeled by Hooke's law where stress and strain are related by an elastic modulus (E). The plastic strain hardening region can be modeled by a time-independent non-linear stress-strain relationship based on either isotropic or kinematic strain hardening. Isotropic hardening assumes that the origin of the von Mises yield surface remains stationary in the stress space and the size of its yield surface expands resulting from strain hardening. In kinematic hardening, the von Mises yield surface does not change in size, but the origin of the yield surface is allowed to translate in the stress space to model strain hardening effects of increasing plastic flow stress. For solder materials, the tensile stress and strain curves are dependent on the test temperature and strain rate. The elastic modulus (E), yield stress (YS) and the tensile strength (UTS) properties vary with temperature and strain rate.

For a typical thermal cycling temperature range from -40 to 125 ^{o}C, these mechanical properties reduce with the increase in temperature. The solder material has a homologous temperature from 0.5 to 0.8 for this temperature range. Also, the creep deformation in a solder material is highly dependent on the stress and temperature state. Thus, a time-dependent elastic-plastic-creep constitutive model, or viscoplastic constitutive model, is needed to facilitate finite element modeling for simulation of solder

joint reliability during thermal cycling tests. High temperatures induce transitions in macroscopic fracture, and these transitions parallel the changes in the strength and ductility of materials [104]. Materials lose strength at higher temperatures. Hertzberg stated that the material strength increases with the testing strain rate, following a form similar to Holloman's Equation [104], where stress is related to strain rate through some strain hardening exponent.

Solder alloys possess very high homologous temperatures. The properties of solder alloys are strongly dependent on both the temperature and strain rate. Jones, et al. [105, 106] have observed an approximately linear relationship between the strength and temperature. Pang, Shi and co-workers [107] have observed similar experimental results, with a near linear relationship with temperature and a power law relation with the strain rate. Several other studies have also observed similar material behavior for both Sn-Pb eutectic and lead-free solder alloys [108-123].

The Ramberg-Osgood model describes the elastic-plastic behavior of materials, and can be used to describe to describe the stress-strain curve of solder materials [112]. In prior work, the Ramberg-Osgood model hardening exponent n and the stress coefficient σ_o were modified to be temperature and strain rate dependent. The temperature and strain-rate dependent modified Ramberg-Osgood model was also applied by Pang, et al. [112].

2.6 Constitutive Modeling for Creep

In general, the creep behavior of materials consists of three different stages: primary creep, secondary creep, and tertiary creep. In the primary creep regime, the material undergoes strain hardening, resulting in a decreasing strain rate with time. In the secondary

stage, also known as steady-state creep regime, the creep strain rate is essentially constant, showing a very slow decrease. In tertiary stage, strain rate increases with time and ultimately results in failure of the material. Solder alloys are often subjected to steady-state creep regime under typical thermo-mechanical loading conditions. Constitutive modeling of creep deformation is needed to predict the end-of-life of electronic components by using finite element analysis. A constitutive creep model is established by conducting creep tests at different temperatures and stress levels. The materials constants are important in determining the accuracy of end-of–life predictions for solder joints using finite element analysis. Large discrepancies between the creep model and experimental data would degrade the accuracy of these predictions.

The minimum creep rate may be linked with the applied stress, σ, by a series of equations according to the dominant creep mode. There are mainly three types of creep modes, namely, power law creep, exponential creep, and combination creep. Creep is highly sensitive to both applied stress level and to test temperature. As a thermally activated process, the creep rates increase exponentially with temperature. The effect of stress is dependent upon the controlling creep mechanism. The two widely used creep models are the Dorn power law model [113], and the Garofalo hyperbolic sine model [114]. In logarithmic coordinates, the Dorn power law model yields a linear relationship between the creep strain rate and applied stress for a specified temperature. Nonlinear experimental curves for creep, however, have been found over the entire stress range. The high stress regime exhibits the largest stress exponent n, and the low stress regime exhibits the smallest n value for any given temperature. This phenomenon is referred to as "power law break

down" and indicates that the Dorn model is not suitable for fitting data obtained over large stress ranges.

The Garofalo model was established for matching creep behavior at both low and high stresses. At low and medium stresses, the creep strain rate depends on stress to the power n. At high stresses, the creep strain rate is an exponential function of stress. The model is able to predict the creep deformation over intermediate temperature regimes for the entire stress range, but it underestimates the creep deformation at both low (-40 °C) and high (125 and 150 °C) temperatures.

Ma and Suhling [33] have evaluated the creep parameters in the two models for various Pb-containing and Pb-free solder alloys and found large discrepancies in the creep data for solder alloys of the same chemical composition. There are several reasons that could explain the differences, including the specimen design, variations in testing method and test conditions used by different researchers, and storage time and temperature before the creep test. Moreover, it is important to recognize that the creep behavior of bulk solder significantly differs from solder in a joint due to the effects of microstructure evolution, intermetallic compound formation, and constraint due to different methods of assembly. Since creep modeling is often to be incorporated in finite element analysis to predict the end-of-life of electronic package, the discrepancies in material constants will directly affect the accuracy of prediction.

A third widely used creep constitutive model was proposed by Weise, et al. [102], and is often referred to as the double power law. They identified two mechanisms for steady state creep deformation for the bulk and PCB samples. They attributed them to climb controlled (low stress process) and combined gliding/climbing (high stress process)

behavior and represented steady state creep behavior using two power law terms. In electronic packages, thermal mismatch induced stresses can result in extensive plastic deformation at solder joints, which is responsible for the low cycle thermal fatigue failure of solder materials. An expression for the strain was proposed by Yang, et al. [100] where total strain was divided into elastic, plastic, and creep strains.

Apart from these models, several other creep constitutive models have been proposed by researchers. Shi, et al. [101] established a unified dislocation-controlled creep constitutive model that described the creep deformation of solder alloy over a wide temperature range (-40 to 150 °C) and explained the temperature dependencies of the stress exponent n and activation energy Q. For creep strain rates at very low stress levels, they further developed a unified diffusion-controlled creep constitutive model to describe low temperature Coble creep and high temperature Nabarro-Herring creep. Clech [99] established obstacle-controlled creep models for both Pb-containing and Pb-free solder alloys. Creep deformation is impeded by discrete obstacles (phases, precipitates, grain boundaries, and other defects) distributed throughout the Sn-matrix in Sn-based solders. By taking these impeding elements into consideration, the rate-dependent obstacle-controlled creep models are able to resolve the anomalies observed in the classical analysis of creep data including stress and/or temperature dependences of activation energies and stress exponents in the Power Law or Hyperbolic Sine models.

2.7 Reduction of Aging and Thermal Cycling Effect by Dopant

Addition of 4th element in the SAC solder is known as doped SAC alloy. Dopants play an important role to control microstructure and mechanical properties of the alloy.

Dopants have been found to strongly influence the properties and behaviors of lead free solders. For example, addition of Bismuth (Bi) as a dopant has been demonstrated to have several beneficial effects. Bi helps to reduce solidification temperature, increases strength by means of precipitation hardening, and also helps to reduce IMC (Intermetallic Compound) layer thickness in lead free solder materials [123]. The Effect of Bi on the mechanical properties of a SAC (Sn3.5Ag0.9Cu) alloy was investigated by Matahir and coworkers [124]. They reported that the shear strength increased with increasing Bi addition up to 2 wt%. Beyond that point, the shear strength decreased with increasing Bi%. Improved shear strength might attribute to the role of Bi on the morphology of microstructure and distribution of dominant IMC (Ag_3Sn). Reduction of strength at higher Bi content was due to the evolution of Bi rich phase and fragmentation of the IMC. Pandher, et al. [125] also reported that addition of 2% Bi in SAC alloys improves wetting and alloy spreading.

Zhao, et al. [126] found that addition of 0.02% Ni to SAC105 increased the formation of NiCuSn IMC and reduced the localized grain size at solder/NiAu pad interface. In addition, the effects using various doped elements (i.e. Co, Fe, In, Ni, Zn and Cu) in SAC305 BGA solder joints on Cu pads were studied by Sousa, et al. [127]. They concluded that addition of low levels of Zn had a significant beneficial effect on the interfacial IMC. Lee and coworkers [128] found that micro-alloying SAC alloys with Ni and Bi improved thermal fatigue life and drop impact resistance. Yeung, et al. [129] studied a novel lead-free solder SAC_Q. Based on drop test, thermal cycling, and finite element simulation, they conclude that the doped alloy has improved board level reliability

when compared to SAC105. Additional literature publications on the effects of dopants have been reviewed in reference [51].

Sun et al. [130] reviewed the effects of different alloying elements (Mn, Fe, Bi, Ni, In, Zn, Ga, Sb, Mg), Rear Earth (RE) Elements (Ce, La, Y, Er, Pr, Nd, Yb), and nanoparticles (Al_2O_3, Al, TiO_2, ZnO, ZrO_2, CNT, Graphene, CeO_2, TiB_2, Ni-Coated CNT, Mo, SiC, $SrTiO_3$, Co) on melting temperature, wettability, mechanical properties, microstructure, interfacial reaction and Sn whiskers.

For SAC305 solder, average width of eutectic region was found as 6.8±2.8 μm and grain size of β-Sn was 24.8±5.9 μm. Indium (In), helps to refine IMC and Sn-rich phase as well as makes the microstructure more uniform. Titanium (Ti) can significantly reduce Sn grain size and width of eutectic region by heterogeneous nucleation of IMC's. Iron (Fe) forms large $FeSn_2$ IMC which has a weak interface with β-Sn matrix. Magnesium (Mg) helps to coarsen eutectic region. Addition of Al in SAC105 refines β-Sn dendrites and enlarge eutectic regions. Besides, it also prevent Ag_3Sn and Cu6Sn5 and forms two new IMC Ag_3Al and Al_2Cu. Zn also helps to refine β-Sn dendrites significantly. Ni was found to reduce the size of Sn-rich phase and refine the microstructure. Since Antimony (Sb) has higher affinity towards Sn, presence of Sb reduces the driving force to form Cu-Sn IMC's resulting a narrow IMC layer in the solder joint. Sb also helps to refine IMC grain size.

RE elements can significantly refine the microstructure of SAC solders. Er can reduces the particle size of Ag_3Sn and Cu6Sn5 whereas Pr and Nd refine β-Sn dendrites and IMC particle size by forming uniformly dispersed fine $RESn_3$. These fine particles act as heterogeneous nucleation sites during solidification. However, excessive amount of RE

elements will cause to form bulk $RESn_3$ phase which has a negative effect on mechanical properties. La, Ce, and Y also have a similar effect on solder microstructure.

Al and Ni nanoparticle was found to reduce IMC particle size, spacing and IMC layer thickness by forming very fine and uniformly dispersed Sn-Ni-Cu and Sn-Sg-Al IMCs. Addition of small amount of Fe nanoparticles refine the microstructure and forms $FeSn_2$ phase. Al_2O_3 nanoparticles increase the size of eutectic region and reduce Ag_3Sn particle size. TiO_2 and SiC nanoparticle reduces the size and spacing between Ag_3Sn particles. $SrTiO_3$ nanoparticle reduces the size of Ag_3Sn and Cu6Sn5 particles by promoting the rate of nucleation during solidification. ZnO suppresses Ag_3Sn and Cu6Sn5 IMC formation and reduces β-Sn grain size by 22%.

The effect of dopants on the aging induced changes in microstructure was also studies by a number of scientists. Sadiq et al. [131] worked with different Lanthanum (La) doped SAC305 alloys and recorded the changes in microstructure and mechanical properties during isothermal aging at 150 °C for 6 different aging conditions (i.e. 0 , 10, 25, 50, 100 and 200 hours). They reported that La drastically reduces the IMC particle size and also significantly inhibit the growth of IMC particles during isothermal aging. Based on polarized light image they found that in as cast condition, grain size of SAC305 was ~8 mm and was significantly reduced (~1 mm) after La addition. From the graph presented in that paper, it is also clear that aging doesn't have any significant influence in average grain size.

In another study, Lee et al. [132] studied the effect of Lanthanum (La) addition and high temperature storage on the microstructure and microhardness of Sn-3.5Ag solder joints. Their experimental results confirms that addition of La refine the solder

microstructure. They explained that during solidification of the solder, $LaSn_3$ compounds form at the beginning and provide extra nucleation sites for Ag_3Sn IMC to grow resulting a refine microstructure. Addition of La was also found to reduce the thickness of IMC layer after soldering as well as isothermal aging. They also reported that La addition helps to improve microhardness and thermal resistance of solder joints.

Hao et al. [133] studied the effects rare earth element Er addition on the evolution of microstructure of lead free eutectic SAC (Sn-3.8Ag-0.7Cu) solder joints during isothermal aging. Aging was conducted at 170 °C for 4 different holding periods (i.e. 0, 200, 500 and 1000 hours). The authors measured the thickness of IMC layer of Sn-3.8Ag-0.7Cu and Sn-3.8Ag-0.7Cu-0.15Er alloy after different aging duration. They found that Er addition reduces the thickness of IMC layer in as reflowed condition and also significantly reduces the growth during aging. They argued that Er combines with Sn to form $ErSn_3$ IMC and reduces the activity of Sn which subsequently suppress the formation of Cu_6Sn_5 IMC layer. They also observed that $ErSn_3$ IMCs formed during solidification of solder act as a heterogeneous nucleation site for Ag_3Sn and Cu_6Sn_5 precipitates. The increase in nucleation sites results a refinement of Ag_3Sn and Cu_6Sn_5 particles. Addition of Er also found to make the microstructure more uniform and reduce the coarsening rate of the IMCs during isothermal aging.

Witkin [134] and Delhaise et al. [135] studied the effect of aging of Bi doped SAC alloys. In both study, the authors reported an elimination or at least reduction of aging induced degradation in SAC-Bi alloys.

2.8 Nanoindentation on SAC Solder Joints

Most prior work on solder mechanical behavior and aging effects has involved tension, compression, and shear testing of miniature bulk solder specimens. Sample geometries have included traditional uniaxial tensile specimens, small cylinders in compression, lap shear specimens, and Iosipescu shear specimens. A more limited number of researchers have examined aging effects by mechanical loading of solder joints [57, 64, 65, 92]. These studies have involved shearing of custom fabricated solder ball arrays [64, 65, 92], as well as impression creep experiments [57].

Nanoindentation techniques [40] have recently become popular for measuring mechanical properties and creep deformation behavior of extremely small material samples, and several investigators [75, 136-148] have applied them to lead free solders. Early solder nanoindentation studies included room temperature measurements of the elastic modulus E and hardness H of β-Sn dendrites, eutectic phases, and individual Ag_3Sn and Cu6Sn5 intermetallic compounds [136, 137, 146, 148]. Hasnine et al. [75, 140-142], have examined aging effects in SAC solder joints extracted from PBGA assemblies using nanoindentation. Their results showed that the aging induced degradations of the room temperature mechanical properties (modulus, hardness) of single grain SAC joints were of similar magnitudes to those seen previously by testing of larger "bulk" solder specimens with hundreds of grains. However, the degradation of the creep response, while still significant (15-100X increase), was less in the solder joints relative to larger uniaxial tensile specimens (200-7500X increase). This was due to the single grain nature of the joints considered, and the lack of the grain boundary sliding creep mechanism. They also

tested very small tensile specimens (10 mm long) with 10-20 grains, and the creep degradation results were similar to the single joint specimens.

Knowledge of elevated temperature behavior, especially creep behavior, is critical to understanding solder joint reliability in thermal cycling and accelerated life testing. Elevated temperature nanoindentation measurements of modulus and hardness of bulk SAC305 and SAC357 solder samples were performed by Gao, et al. [138], and Han and coworkers [139]. In addition, the latter authors also examined the sensitivity of the creep response of lead free solder to temperature. Sadiq, et al. [147] have investigated the nanoindentation elastic modulus and hardness of β-Sn and eutectic phases within a SAC305 solder joint at temperatures ranging from 45-85 °C. Another solder nanoindentation study over a larger temperature range (25-150 °C) was performed by Lotfian, et al. [143], where they reported the mechanical properties of the constituent phases of SAC397 solder joints. Marques, et al. [144, 145] used nanoindentation to study mechanical properties and creep behavior of SAC305 solder joints over a wide temperature range (25-175 °C). Based on finite element simulations, they also developed a method to correlate nanoindentation creep results with uniaxial creep data.

2.9 Effect of Aging and Thermal Cycling on the Microstructure of Solder

Due to their low melting temperatures, solders are exposed to high homologous temperatures in most product applications. Thus, there is a continuous state of active diffusion processes in the solder alloys, and their microstructures are inherently unstable and will continually evolve during normal operating temperature conditions of electronic packaging assemblies. High temperature storage, which is also known as isothermal aging,

of the solder alloys causes a significant change in the microstructure leading to a degradation of mechanical properties. Chou [149] studied the effect of isothermal aging on microstructure of Sn-Pb and lead free SAC solder joints. He reported a significant phase coalescence of eutectic Sn-Pb solder joint after aging. Xu et al. [61] measured the thickness of IMC layer of different Sn-Pb alloys with different surface finishes after isothermal and thermal cycling aging. Based on their experimental results they had proposed an integrated model to predict the IMC layer growth under different isothermal aging and thermal cycling environment.

Ubachs et al. [150] developed a model to predict microstructural evolution during isothermal aging of Sn-Pb alloy by numerical simulation. They focused their study on a fixed region and compared experimental observation of phase growth during isothermal aging at 150 °C, for 0 to 15 hours, with the predicted phase growth by simulation.

In recent days, electronic industries are moving towards lead free solders due to the growing concern about environment. Effect of aging in lead free solder is even more significant. Sahaym et al. [151] examined the evolution of microstructure of bulk SAC105 and SAC305 solder during isothermal aging at 150 °C. They observed the changes of identical region after 4 different aging durations (0, 110, 194, and 310 hours). In as reflowed condition, they found that the microstructure is consisted of several pro-eutectic colonies of β-Sn grains surrounded by eutectic regions. Most of the grains in a pro-eutectic colony has low angle (<15°) boundaries with the neighboring grains. They reported that after 310 hours of aging, the average size of IMC precipitates has increased from 0.35 μm to 2.5 μm and the average grain size has increase from 4.5 μm to 7.5 μm.

The authors also observed that a small percentage (~10%) of β-Sn grains, especially those near the eutectic region, has went through recrystallization during isothermal aging. They claimed the stress on the β-Sn grains, due to the growth of IMC particle, is responsible for the recrystallization. The extent of recrystallization was less in SAC105 than in SAC305 due to the relative difference in IMC volume fraction. Although not mentioned clearly in the text, it is evident from their graph that the number of high angle grain boundary has been reduced and low angle grain boundary has been increased after aging for 100 hours.

Maleki et al. [152] studied the evolution of microstructure of SAC405 and pure Sn during isothermal aging at 150 °C after 144 hours and 296 hours. They also performed Mechanical testing (shear test) to correlate changes in microstructure and mechanical properties. Sample size was approximately 1 × 0.3 × 0.3 mm and it was attached to Cu-pad. They reported that in as-reflowed condition, the microstructure of SAC405 was consisted of ~70 vol% of eutectic phase and ~30 vol% of β-Sn dendrite, whereas the mean diameter of IMC particles and interparticle distance was ~250nm and ~630 nm, respectively. Average particle size increases with aging time due to Ostwald ripening. During IMC growth, they attributed bulk diffusion to be the main rate controlling mechanism. On the other hand, aspect ratio decreases and interparticle spacing increases with aging due to the driving force to reduce surface energy. Electron backscatter diffraction (EBSD) analysis confirmed the presence of large grains (~200 μm) in SAC405 solder before aging. After 296 hours of aging at 150 °C they didn't find any significant change in grain size and orientation. On the other hand, pure tin has a fine grain (~10 μm) microstructure before aging which grows significantly during aging and become ~200 μm

after aging. They attributed the reduction of mechanical properties during aging for SAC 405 to the IMC's coarsening whereas for pure Sn to the grain coarsening.

Telang et al. [153] worked on the effects of aging at 150 °C on microstructure, especially grain size and grain-boundary misorientation, of several alloys including Pure Sn (ingot and reflowed), Eutectic Sn-3.5Ag (ingot), Eutectic Sn-3.8Ag-0.7Cu (ingot), Sn-1.6Ag (solder ball), Sn-3.0Ag (solder ball), and Sn-3.0Ag-0.6Cu (solder ball). For Sn-3.5Ag alloy they studied three different aging conditions (i.e. 0, 200, and 400 hours.) whereas for rest of the alloys they studied two different aging conditions (i.e. 0. and 200 hours). Before aging, grain size of pure Sn ingot and Reflowed Pure Sn was 50-150 μm (equiaxed) and 100-250 μm (equiaxed), respectively. After aging for 200 hours, the grain size of pure Sn for both condition was >500 μm with irregular shape. They found ledges, in SEM image, along the grain boundary (confirmed by polarized light microscopy) of sample after aging. According to the authors, these ledges were formed due to anisotropic nature of thermal expansion coefficient (CTE) of Sn grain. After aging, when the sample was taken out from the oven, different grains contracted with different magnitudes leading to the ledges. They also argued that the extent of contraction depends on the size and the orientation of the grain. Before aging, the sample had smaller grain size. As a result, when the sample was kept inside the oven, difference in expansion of different grains was relatively small. This resulted small ledges along the grains of as reflowed sample. Although the grain boundaries moved during the aging process, these ledges were retained throughout the experiment.

After comparing the microstructure of eutectic Sn-Ag (3.5% Ag) ingot with pure Sn ingot, they found that Sn-Ag alloy has a much finer (10-30 μm) grain size, which was

very stable. Aging of Ag-Sn alloy did not cause any significant grain growth due to the pinning effect of Ag_3Sn IMC particles. On the other hand, the grain size of SAC (Sn-3.8Ag-0.7Cu) ingot was similar to that of Sn-Ag ingot (10-30 μm). But, aging for 200 hours caused a significant growth in the grain size (~120 μm) of the alloy. Although not stated clearly in the text, it is evident from the misorientation histogram that the extent of misorientation, among the grains, for the both alloys decrease with increasing aging time. From their experimental observations the authors also have discussed the effect of Ag and Cu on preferred grain orientation and grain size.

Allen et al. [70] studied two near eutectic lead free SAC solders (bulk Sn-3.5Ag-0.9Cu and SAC405 joint). They used 3 different aging temperatures (152, 177, and 201 °C) and 5 different aging durations (0, 1, 2, 4, and 8 weeks). They measured the density of IMC particle after different aging conditions and based on their experimental results they conclude that the rate controlling mechanism for coarsening is volume diffusion ($n=3$). They also reported that the coarsening kinetics of eutectic SAC solder is slower than that of eutectic Sn-Pb solders.

Kumar et al. [154] worked with SAC105 and SAC305 alloys. For isothermal aging experiments, they polished a bulk reflowed solder samples and then aged the samples at 150 °C in high vacuum (to prevent oxidation). After different aging intervals (i.e. 0, 110, 194, 220, and 330 hours) they captured the SEM image of the same region, of any particular sample, to quantify the coarsening behavior of the IMC's. They found that the growth rate of Cu_6Sn_5 particles are much faster than Ag_3Sn particles, due to the higher diffusivity of Cu than Ag in Sn matrix. Besides, the fraction of Ag_3Sn particles was significantly higher than Cu_6Sn_5 particles. Hence, they decided to focus their study on the coarsening of Ag_3Sn

particles only. The authors introduced a new parameter named as explicit parameter '$C_{Ag}D_{Ag}t/T$', where C_{Ag} and D_{Ag} are solubility and diffusivity of Ag in Sn matrix, respectively, to capture the thermomechanical history of a lead free solder during isothermal aging. Utilizing this parameter, they predicted coarsening rate of Ag_3Sn particles, during isothermal aging, and then compared with the experimental observations. They conclude that the model could efficiently measure thermomechanical history during isothermal aging and thermomechanical cycling (TMC) below 200 cycles. After 200 cycles the IMC particles undergo dissolution and re-precipitation/redistribution which can't be captured properly by this model. In addition to coarsening, during isothermal aging, they also had observed recrystallization near the eutectic region. They explained that the growth of IMC particles might play an important role in recrystallization.

Besides bulk solder samples, researchers have also explored the effect of aging on the actual solder joints. Chauhan et al. [155] monitored the effect of isothermal aging at 100 °C on phase coarsening and evolution of SAC305 solder joint. They used image processing software to quantify size, interparticle spacing and volume fraction of Ag_3Sn and Cu_6Sn_5 IMC's. Impact of these changes on secondary creep response was modeled using multiscale creep model. The authors performed their experiments in 4 different aging conditions (0, 24, 600, and 1000 hours.) and presented average results of 3 samples (solder joint) for each aging condition. They found that the size of Ag_3Sn increases monotonically with increasing aging time whereas the size of Cu_6Sn_5 decreased after 600 hours of aging. They didn't find any significant change in Sn grain morphology after 1000 hours (41 days) of aging.

Yang et al. [156] prepared solder joints using 2 different soldering methods (laser and infrared soldering) and captured the evolution of microstructure during aging up to 190 ºC for times up to 300 days. They reported that the evolution is consisted of the growth of IMC's and the Cu-Sn layer near the interface. Although they had studied two different initial microstructure, obtained from 2 different soldering methods, aging at 190 ºC caused the final microstructures to be the same.

Chiu et al. [157] examined the effect of aging time and temperature on the board level reliability during the drop test of lead free SAC solder joints. They reported that kirkendall void formation, at the interface of Cu pad and Cu_3Sn IMC, is the main reason for getting lower drop reliability during drop test.

Fix et al. [79] explored the effect of aging time (0 to 1000 hours) and temperatures (125 to 175 °C) on the microstructure of SAC405 solder joint. They have confirmed a significant growth of Ag_3Sn and Cu_6Sn_5 IMCs with aging time. The authors modeled phase growth based on Ostwald ripening mechanism. They conclude that a growth exponent n = 3, which indicated volume diffusion as the growth rate controlling mechanism, matches very well with the experimental growth rate data.

The effect of aging at 150 °C on the evolution of eutectic Sn-Ag solder joint for up to 800 hours was studied by Ahat et al. [158]. From experimental results, they conclude that the thickness of IMC layer increases linearly with square root of aging time. Choi et al. [159] investigated the effect of different soldering and aging time on the interface layer of Sn-3.5Ag solder and Cu substrate. They used the same solder joint to age at 130 °C for different time duration up to 800 hours They found that thickness of IMC layer continue

to grow with increasing aging duration. However, the growth behavior of IMC layer during aging strongly depends on the initial morphology and hence on the soldering time.

Akhtar et al. [160] studied the evolution of microstructure near the interface of a solder joint during isothermal aging at 150 °C, for four different aging duration (0, 250, 500, and 1000 hours). They used SAC305 solder joint (ball diameter 500 μm) with two different surface finish (Immersion Gold (ImAu) and Immersion Tin (Sn)). Image analysis software ImageJ was used to measure the thickness of the IMC layer. They also calculated the activation energy based on the measured thickness data. They found that the thickness of the IMC layer increases with increasing aging time. Besides, the morphology of the IMC layer, for both surface finishes, change from scallop type to layer type after the aging treatment. Based on their calculations they found that the activation energy of SAC305/ImSn system was less than SAC305/ImAu system resulting a higher IMC layer growth rate in SAC305/ImSn system.

A comparative study was performed by Berthou et al. [161] where the authors compared the failure mechanism of BGA packages with SAC305 solder joints subjected to two different conditions: (a) accelerated thermal cycling (ATC) between -55 to 125 °C and (b) thermal storage at 80, 125, and 150 °C for 1000 hours. During ATC, they found recrystallization of big Sn grains to small grains in the regions of high stress accumulation. Cracks initiates and grows at interface of the new recrystallized grains. On the other hand, thermal storage for 1000 hours caused a significant growth of IMC layer near the interface as well as the IMCs in the bulk. They didn't report any recrystallization after thermal storage.

2.10 Summary

In this chapter, the existing literature on the effects of aging and thermal cycling on the mechanical properties and the microstructure of lead free solder and various materials in PBGA packages was extensively discussed. The mechanical properties of a solder are strongly influenced by its microstructure, which is controlled by its thermal history including its solidification rate and thermal exposures after solidification. Aging and thermal cycling of lead free solders leads to degradations in their mechanical and failure behaviors. For example, research in the literature has shown that aging and thermal cycling leads to large reductions in solder material properties including shear strength, elastic modulus, nanoindentation joint modulus and hardness, high strain rate mechanical behavior, creep response. Other studies have shown that aging causes severe degradations in uniaxial cyclic stress-strain curves and fatigue life, shear cyclic stress-strain curves and fatigue life, fracture behavior, drop reliability, and thermal cycling reliability.

Dopants have been found to strongly influence the properties and behaviors of lead free solders. For example, Bi helps to reduce solidification temperature, increases strength by means of precipitation hardening, helps to reduce IMC (Intermetallic Compound) layer thickness, and also reduce aging and thermal cycling induced degradation of mechanical properties in lead free solder materials. Ni helps to improve thermal fatigue life and drop test performance by refining Sn grain size and reducing the IMC layer formation near the Cu pad. The effects of rear earth (RE) elements and nanoparticle addition on the properties of lead free solder was also discussed in this chapter.

Nanoindentation methods have shown great potential for characterizing solder materials and its individual phases to observe temperature, aging and temperature cycling

effects at the joint scale. Nanoindentation is mainly used to extract elastic modulus and hardness of solder joints. Many of the prior works have also used nanoindentation technique to characterize the creep properties although most of the nanoindentation experiments, on solder joints, were conducted at room temperature.

The changes in solder mechanical behavior are a result of the evolution of the SAC solder microstructure that occurs during aging. The most well-known and widely observed changes are coarsening of the Ag_3Sn and Cu_6Sn_5 intermetallic compounds (IMCs) present in the eutectic regions between beta-Sn dendrites. Several researchers have proposed empirical models to describe the growth of these secondary phase particles as a function of aging temperature and aging time, and related this growth to mechanical property changes.

CHAPTER 3

EXPERIMENTAL PROCEDURE

3.1 Introduction

The specimen preparation and testing techniques are presented in this chapter. Micro-scale uniaxial tensile specimens were prepared in a rectangular shaped hollow glass tube using a vacuum suction method. The test specimens were then cooled either by a water quenched profile or an industry standard reflow profile. Typical dimension of the uniaxial tensile specimens were 80 (length) ☓ 3 (width) ☓ 0.5 (height) mm. Uniaxial tensile tests were performed using a micro tension torsion testing system.

For this study, SAC305 (96.5Sn-3.0Ag-0.5Cu) and SAC_Q (92.7Sn-3.4Ag-0.5Cu3.3Bi) lead free solder joints were tested. The joints had a diameter of about 30 mils (762 µm). The samples consisted of a 3 x 3 Ball Grid Array (BGA) of the lead free alloys to be tested. The substrates used in the specimens were FR-4 PCBs. Samples which had an Immersion Silver (ImAg) surface finish on the copper pads were chosen. Flux was deposited on the pads using a stencil. A reflow profile with a maximum temperature of 245 °C was obtained with the help of a Vitonics-Soltec convection oven. The profile also ensured that the assembly was kept above the liquidus temperature for about 45-60 seconds. The samples were then cleaned, dried and stored in a freezer at -40 °C to hinder any aging effects.

Samples were mounted on an epoxy mold by glue followed by autopolishing to make the solder joints suitable for nanoindentation tests. Since the properties of SAC solder joints are highly dependent on crystal orientation, polarized light microscopy techniques was utilized to determine the orientation of the tested joints. For all the experiments, only single grain solder joints were used to avoid introducing any unintentional variation from changes in the crystal orientation across the joint cross-section.

3.2 Uniaxial Test Sample Preparation

Initially, bulk solder material is melted in a quartz crucible using circular heating elements (see Figure 3.1). The heater in the melting process is excited using a digital controller, which uses feedback from a thermocouple attached on the crucible. The solder is drawn into the glass tube by inserting one end into the molten solder in the crucible, and then applying suction to the other end using a rubber tube connected to a vacuum source. The amount of solder drawn into the tube is controlled using a regulator on the vacuum line. After the desired amount of solder fills the tube, it is solidified by quenching in a room temperature water bath.

Tensile specimens were prepared using two different solidification profiles.

1) Water quenched (WQ) solidification profile, leading to fine microstructures and the upper limits of the mechanical properties for each alloy.

Reflowed (RF) solidification profile, leading to a coarse microstructure very similar to an actual solder joints. The solder test specimens were passed through a controlled heating and cooling chamber using a SMT (surface mount technology) reflow oven. The

temperature vs. time variations for the WQ profile is shown in Figure 3.2. For the samples with reflowed profile, test specimens were initially prepared using WQ profile and then the samples within the glass tubes were sent through a 9 zone Heller 1800EXL reflow oven (Figure 3.3).

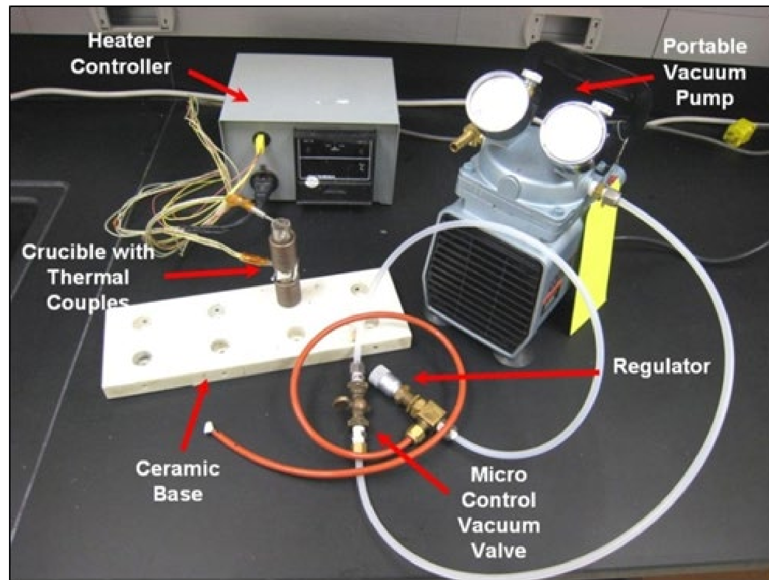

Figure 3.1 Equipment used for Specimen Preparation

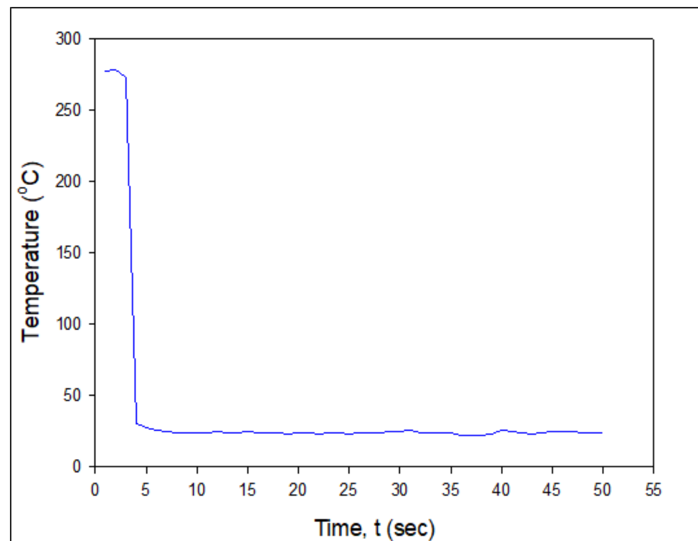

Figure 3.2 Water Quenched (WQ) Cooling Profiles

Figure 3.3 Heller 1800EXL Reflow Oven

Inside the oven, solder samples were re-melted and experienced to a pre-set temperature profile which is very similar to that used for the actual solder joints. The reflow temperature profile used in this study is presented in Figure 3.4.

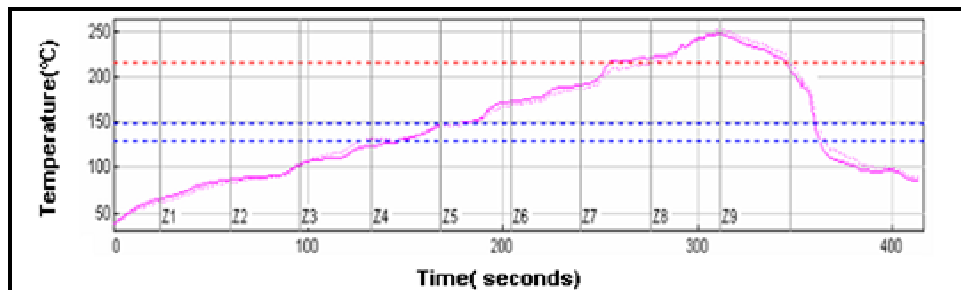

Figure 3.4 Reflow (RF) Cooling Profiles

A typical glass tubes filled with solder and final solder samples after extraction from the glass tubes are shown in Figure 3.5. Glass has lower coefficient of thermal expansion (CTE) compared to solder. As a result, for some solder alloy and cooling rate combinations, solidified solder samples were easily pulled out from the glass tube due to the difference is the CTE of glass and solder. Another way followed to extract the solder

sample from the glass tube is by carefully breaking the glass. The tubes in this work had a length of 120 mm, and a cross-sectional area of 3.0 x 0.5 mm. A thickness of 0.5 mm was chosen since it matches the height of typical BGA solder joints. The nominal dimensions of the final test samples were 80 x 3 x 0.5 mm. The specimens were stored in a low temperature freezer after the water quenched/reflow process to minimize any aging effects. The solder microstructure has been verified to be consistent throughout a specimen volume, and from specimen to specimen by cross-sectioning. A micro-focus x-ray system was used to inspect the samples for the presence of flaws (e.g. notches and external indentations) and/or internal voids (non-visible). Specimens with no flaws and voids were generated using proper experimental techniques, and Figure 3.6 illustrates x-rays scans for good and poor specimens.

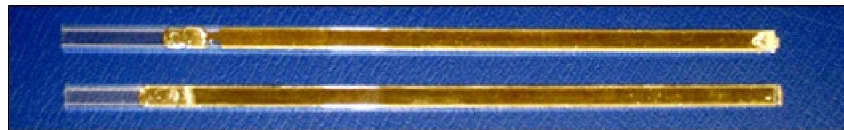

(a) Within Glass Tubes

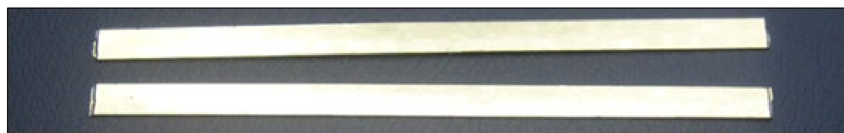

(b) After Extraction

(c) Cross-Section

Figure 3.5 Solder Uniaxial Test Specimens

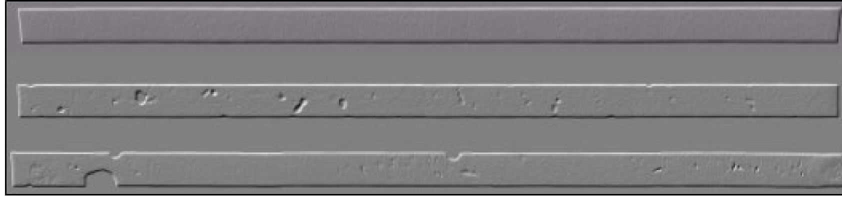

Figure 3.6 X-Ray Inspection of Solder Test Specimens (Good and Bad Samples)

3.3 Thermal Chambers and Thermal Cycling Profiles

After sample fabrication process, all the samples were preconditioned in either thermal cycling chamber (Fig. 3.7 (a)), or thermal shock chamber (Fig. 3.7(b)) for various durations (i.e. 1, 2, 5, 20, 50, and 100 days). Thermal cycling chamber was used for different thermal exposures such as slow thermal ramping, and slow thermal cycling. On the other hand, thermal shock chamber was used for thermal shock profile. Thermal shock chamber has two different chambers. Top one is called "hot chamber", and bottom one is called "cold chamber". There is a basket which can move instantaneously between these two chambers.

Different thermal profiles were considered in this study were: (1) isothermal aging at 125 C, (2) slow thermal cycling from -40 C to +125 C with 45 minutes ramps and 30 minutes dwells (Fig. 3,8 (a)), (3) thermal ramping with 45 minutes ramps and no dwells (Fig. 3,8 (b)), (4) thermal shock with 30 minutes dwell and instantaneous ramping between hot and cold temperatures (Fig. 3,8 (c)). The number of cycles exhibited for same exposure time by each thermal exposures are shown in Table 1. It depends on the total time spent for each cycle by each thermal exposures.

(a)

(b)

Figure 3.7 (a) Thermal Cycling Chamber, and (b) Thermal Shock Chamber

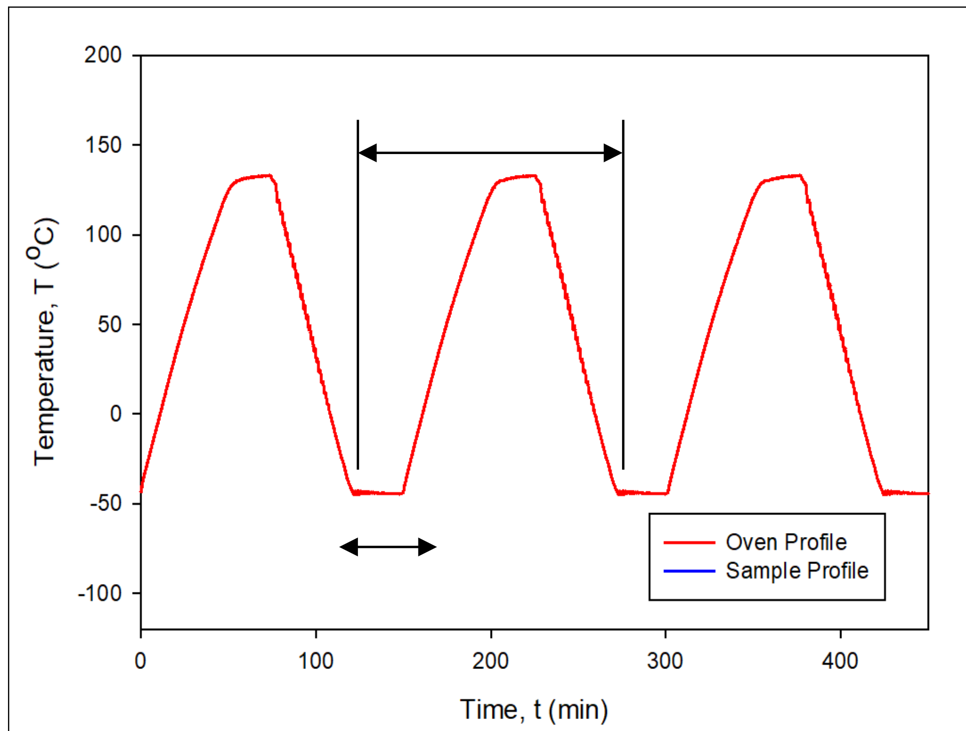

(a)

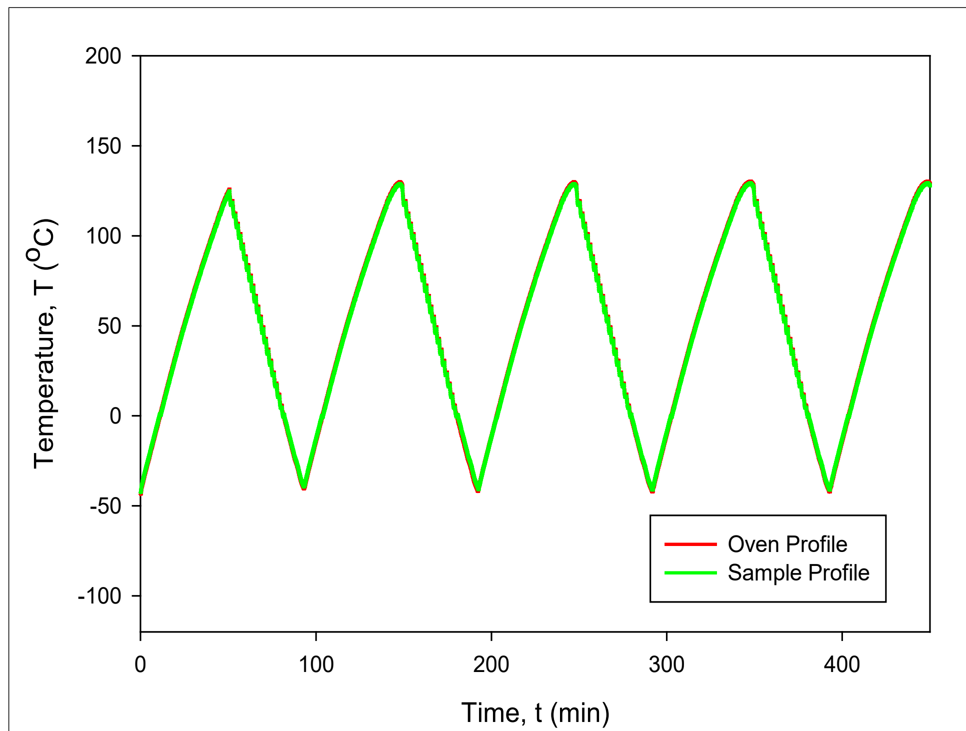

(b)

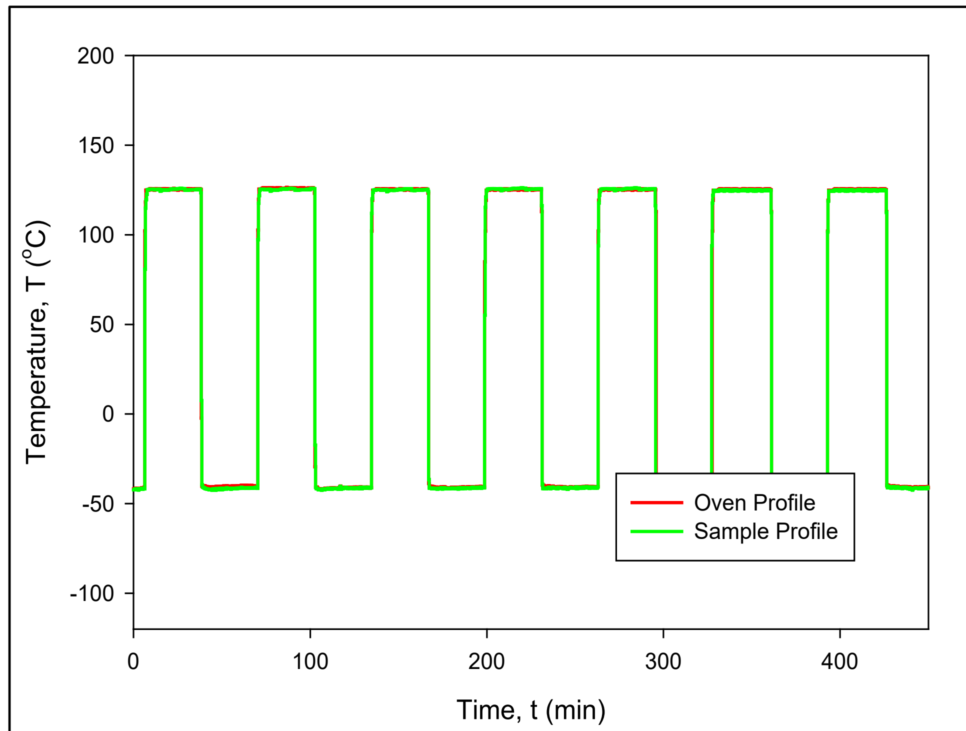

(c)

Figure 3.8 (a) Slow Thermal Cycling, (b) Slow Thermal Ramping, and (c) Thermal Shock

Table 3.1 Conversion Table of Cycles to Time for the Various Profiles

Exposure Time (Days)	Aging (Days)	Slow Thermal Cycling	Slow Thermal Ramping	Thermal Shock
		Number of cycles		
0	0	0	0	0
1	1	10	~15	24
2	2	19	~30	48
5	5	48	~75	120
20	20	192	~300	480
50	50	480	~750	1200
100	100	960	~1500	2400

3.4 Uniaxial Tensile Testing System

The tension/torsion thermo-mechanical test system (Wisdom Technology MT-200) used to perform the stress-strain tests in this study is presented in Figure 3.7. This instrument is optimized for loading small specimens such as thin films, solder joints, gold wire, fibers, etc. It provides an axial displacement resolution of 0.1 micron. Samples can be tested over a temperature range of -185 to +300 °C using supplemental environmental chambers added to the system. However, the high temperature system has been calibrated to accurately control the specimen temperature. Appendix A.1 represents the variation in set temperatures and specimen temperatures. The calibrated temperature table has also been included in Appendix A.1.

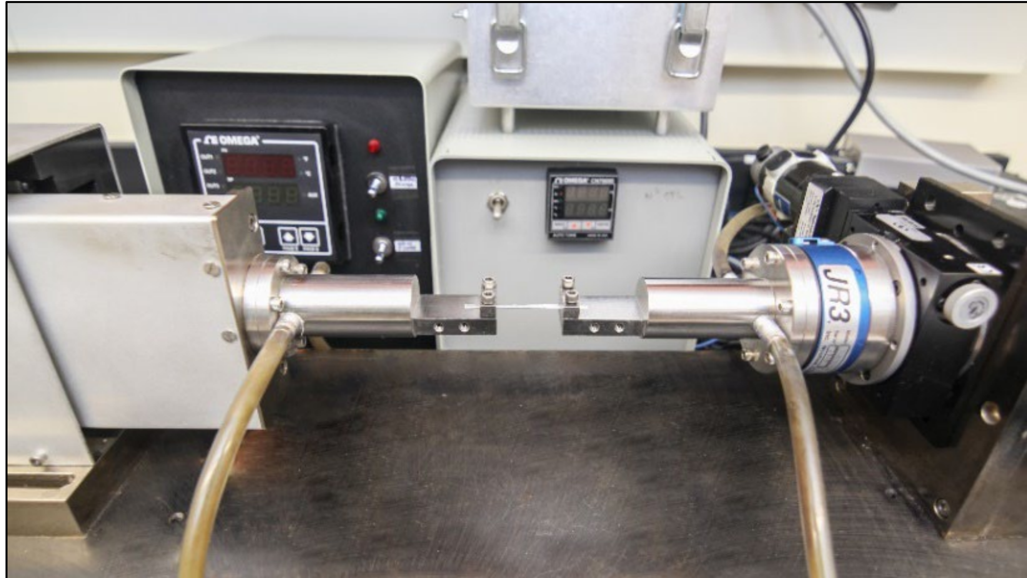

(a)

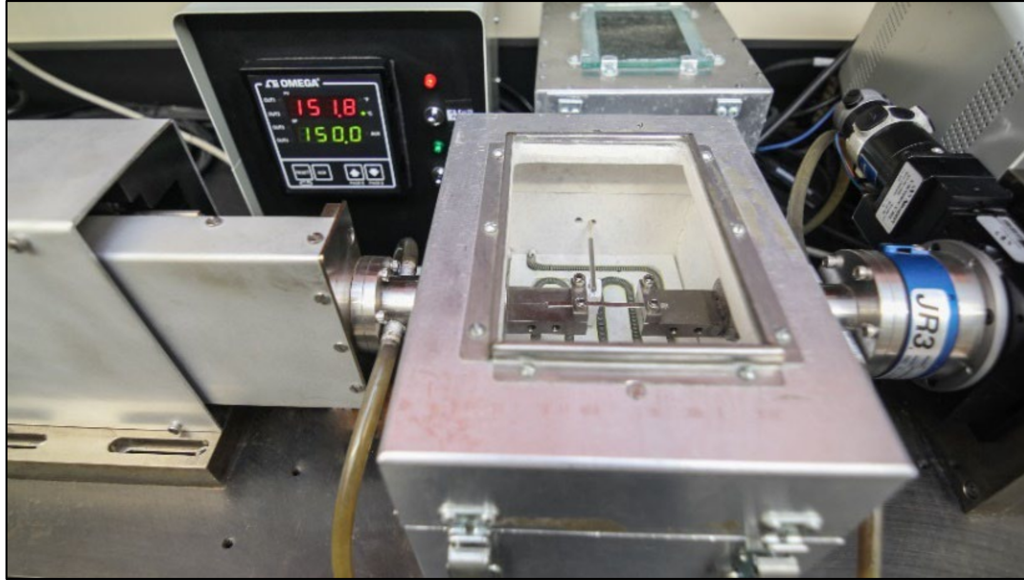

(b)

Figure 3.9 Mechanical Test System with Uniaxial Sample

Forces and displacements were measured in the uniaxial tests, and the axial stress and axial strain were calculated using

$$\sigma = \frac{F}{A} \qquad \varepsilon = \frac{\Delta L}{L} = \frac{\delta}{L} \tag{3.1}$$

Where, F is the measured uniaxial force, δ is the measured crosshead displacement, σ is the uniaxial stress, ε is the uniaxial strain, A is the original cross-sectional area, and L is the chosen specimen gage length (initial length between the grips). The gage length of the specimen was kept as 60 mm (thus the length to width ratio was 20 to 1).

3.5 Typical Testing Data and Data Processing

3.5.1 Typical Test Data

A typical SAC solder tensile stress strain curve is illustrated in Figure 3.8. The standard material properties are labelled on the graph including the effective elastic

modulus E (initial slope of the stress-strain curve). This effective modulus is rate dependent since solder behavior is viscoplastic. The value of the effective modulus will become the true elastic modulus as the testing speed is increased to the limit of infinite strain rate. The yield stress σ_Y (YS) is defined using the typical definition of the stress level that results in a permanent strain of $\varepsilon = .002 = 0.2\%$ upon unloading. The maximum (saturation) stress on the stress-strain curve is the ultimate tensile strength σ_u (UTS). As shown the figure, the stress-strain curve for the solder material has an elastic region at the beginning, a small transition region followed by a plastic region. As the strain becomes significantly high, localized deformation takes place which is also known as necking. Necking causes a visible reduction in cross-sectional area and a drop in the applied load, near the end of the stress strain curve, leading towards a rupture.

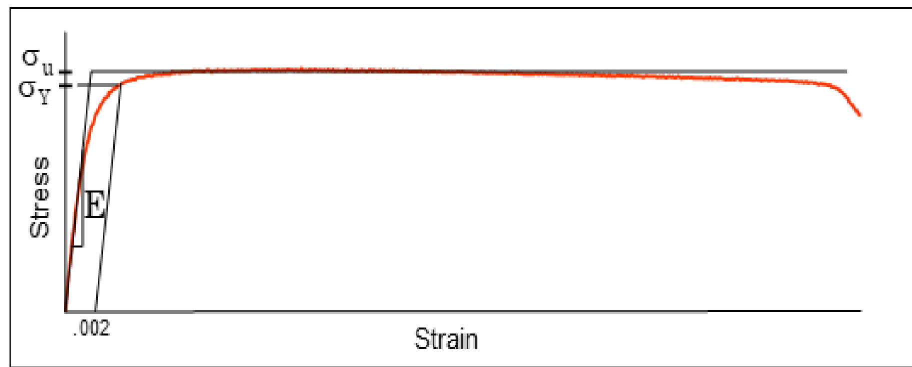

Figure 3.10 SAC Stress-Strain Curve and Material Properties

3.5.2 Stress-Strain and Creep Data Processing

Figure 3.9 illustrates a typical set of 5 solder stress strain curves measured for the same alloy under similar environmental and aging conditions. In this work, a four parameter hyperbolic tangent empirical model

$$\sigma = C_1 \tanh(C_2\varepsilon) + C_3 \tanh(C_4\varepsilon) \quad (3.2)$$

has been used to represent the "average" stress-strain curve through a set of experimental data (red curve in Figure 3.9). Material constants C_1, C_2, C_3, and C_4 are determined through regression fitting of the model to experimental data. The effective elastic modulus E at zero strain is calculated from the model constants using

$$E = \sigma'(0) = C_1C_2 + C_3C_4 \quad (3.3)$$

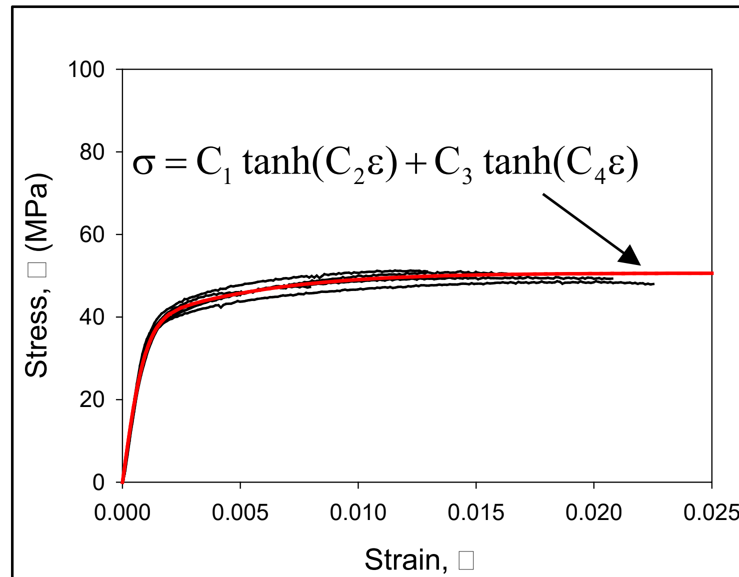

Figure 3.11 Empirical Model Fit to Solder Stress-Strain Curves

For the creep testing, 5 constant load/stress tests were performed for each leg of the test matrix. The four parameter Burger's (spring-dashpot) model given by

$$\varepsilon = C_0 + C_1 t + C_2(1 - e^{-C_3 t}) \quad (3.4)$$

was used to fit the average raw experimental data, where C_0, C_1, C_2, and C_3 are fitting constants. Constant C_1 represents the "steady state" creep strain rate.

3.6 Microstructure Study

3.6.1 Sample Preparation and Image Capturing Using Scanning Electron Microscopy (SEM)

For microstructure analysis, a slot was made on an epoxy mold. Then fabricated solder samples were cut into small pieces and inserted into the slot. Details of the preparation process included mechanical grinding with several SiC papers (#320 to #400, #600, #800 and #1200) in a rotating metallographic disc as shown in Figure 3.12. The final polishing was conducted with 0.02 μm colloidal silica suspensions (BUEHLER MasterMet 2) and BUEHLER ChemoMet polishing cloth in both manual and autopolisher. This procedure resulted in mirror finish samples suitable for optical microscopy, Scanning Electron Microscopy (SEM), as well as nanoindentation. Microstructure analysis of the solder alloys was performed on the mounted and polished testing coupons by using an OLYMPUS BX60 Optical Microscope (Figure 3.14), Zeiss Polarized Light Microscope (Figure 3.15), and a Zeiss Cross Beam 550 SEM (Figure 3.16). In addition, EDS (Energy-Dispersive X-ray Spectroscopy) was employed to explore the chemical composition of different phases in the microstructure.

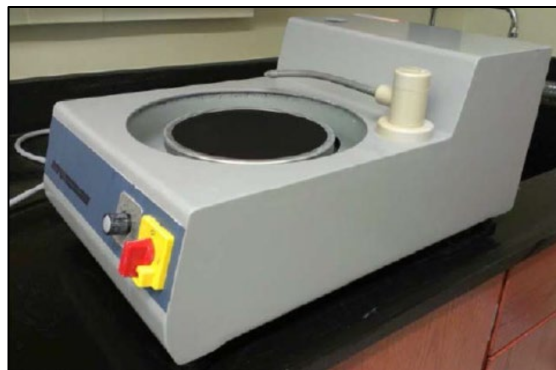

Figure 3.12 Grinding and Polishing Machine

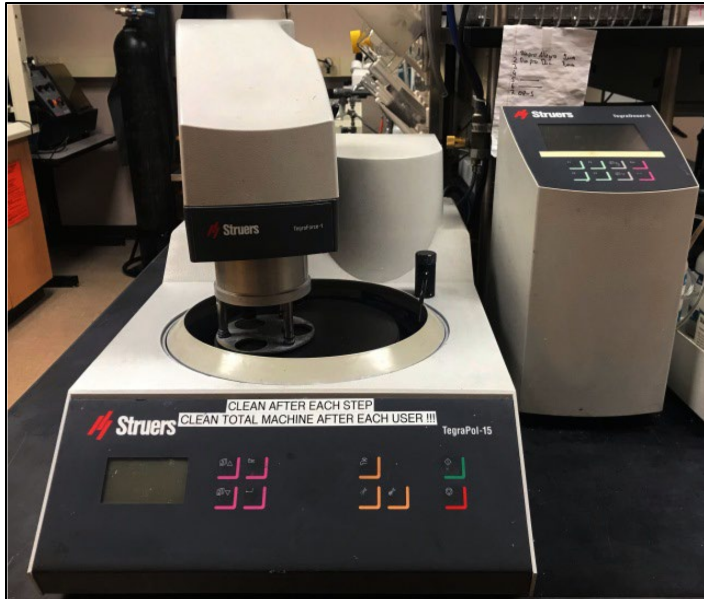

Figure 3.13 Autopolisher

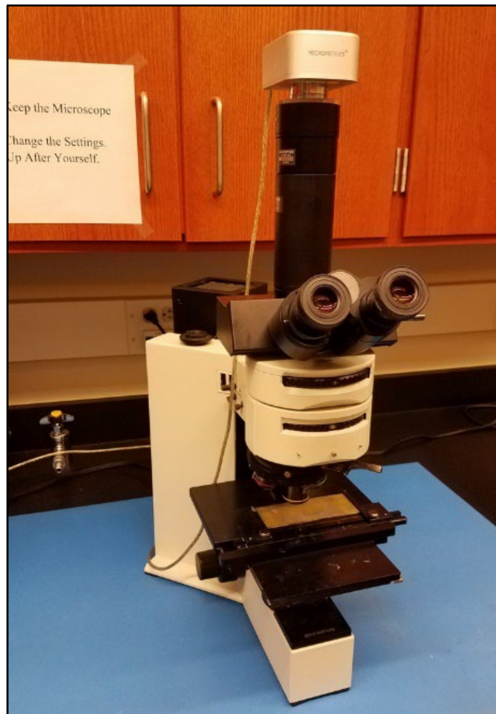

Figure 3.14 OLYMPUS BX60 Optical Microscope

Figure 3.15 Zeiss Polarized Light Microscope

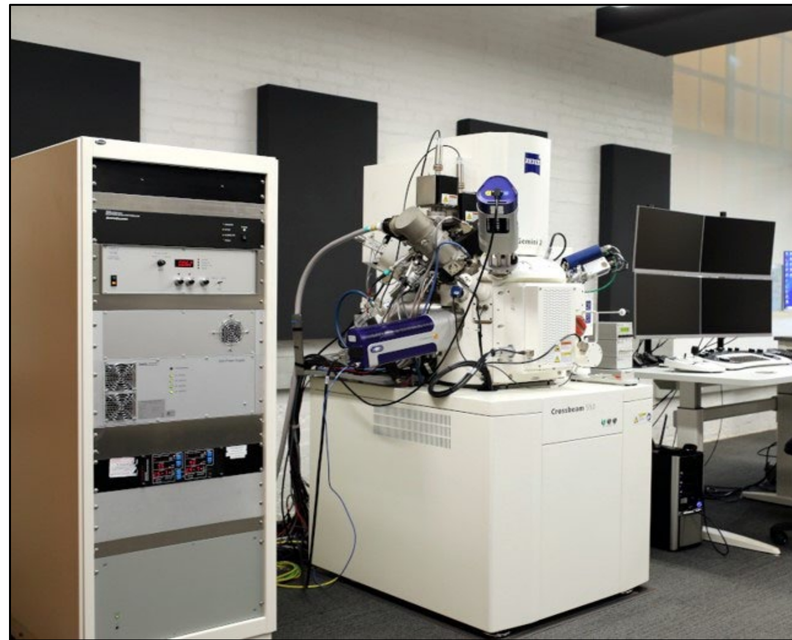

Figure 3.16 Zeiss Cross Beam 550 SEM

The prepared samples were then placed within the nanoindentation system (Figure 3.17), and several fixed square regions with dimensions of approximately 90 x 90 µm were then selected in the polished region of each sample for subsequent SEM observations. To

locate and track the selected fixed regions, they were demarcated using four nanoindentation marks placed at their corners using a Hysitron TI 950 nanoindentation system as shown in Figure 3.18. After polishing and applying the nanoindentation marks, the specimens were carefully removed from the temporary carriers. The indentation marks were positioned close enough to enable region identification, but far enough away from the region to avoid influencing the microstructure evolution. Lastly, a field emission SEM was used to study the changes of solder microstructure caused by both thermal cycling and aging.

Figure 3.17 Hysitron TI950 Triboindenter

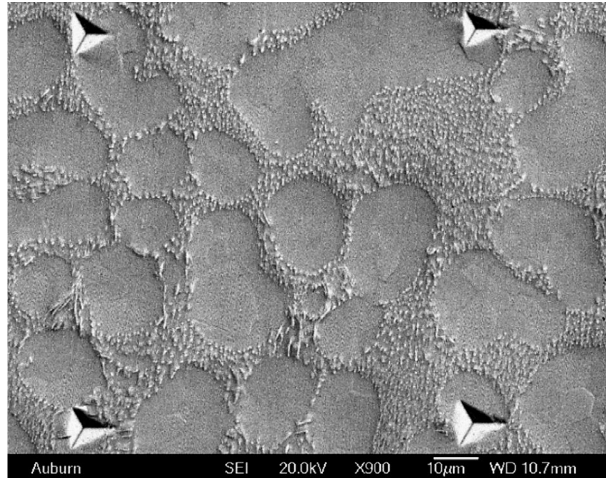

Figure 3.18 Typical Fixed Region with Indentation Marks

3.6.2 Measurement of Area and Number of IMC Particles Using Image Processing

After capturing the images for different durations under isothermal aging, slow therma ramping, thermal shock, and slow thermal cycling quantitative analyses of the size metrics of the IMC particles were performed with all of the SEM images to study the evolution of IMC particles. The analyzed regions were typically chosen intentionally to be interdendritic regions with a rich concentration of IMC particles. The area of each particle, the total area of all of the particles, and the total number of particles in each selected region and aging time were determined using image analysis software (Adobe Photoshop) and MATLAB.

The particle size measurement process involves 3 major steps. In first step, all the IMC particles were outlined in Adobe Photoshop. After that, the gray scale images were converted into a binary image. Finally, the average area of the particles (White spots), in the binary image, and the number of particles were calculated using MATLAB. Figure

3.19 shows an example of image processing. The particles were outlined very carefully so that all the individual particles in the field were identified and counted for analysis.

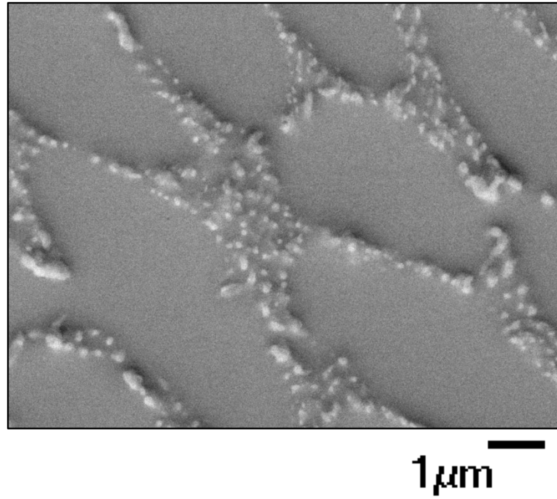

(a)

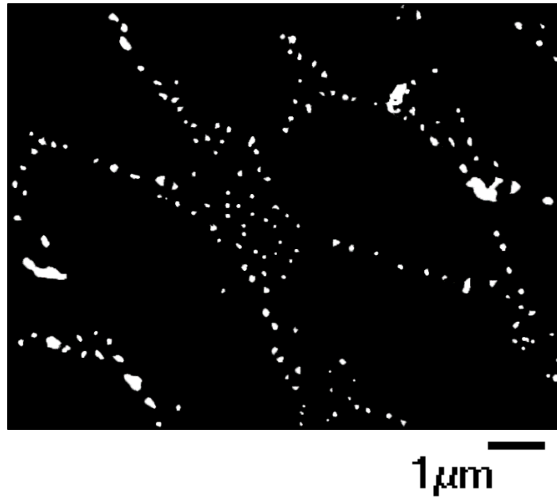

(b)

Figure 3.19 Image Processing Steps for IMC Particle Area Calculations (a) After Outlining All the Particles (b) Binary Image

3.6.3 Measurement of IMC Particle Diameter

For an ideal spherical IMC particle, the amount of the particle that is visible on the polished cross-sectional surface is actually unknown as shown in Figure 3.20. In this case, the black portion of the particle represents the portion on IMC exposed on the polished surface, while the gray shaded portion is the portion of the IMC below the surface. As indicated in Figures 3.20 and 3.21, the observed particle diameter (apparent diameter) for a particle is actually less than or equal to the actual particle diameter. Thus, the measured (apparent) average particle diameter must be adjusted to calculate the actual average particle diameter.

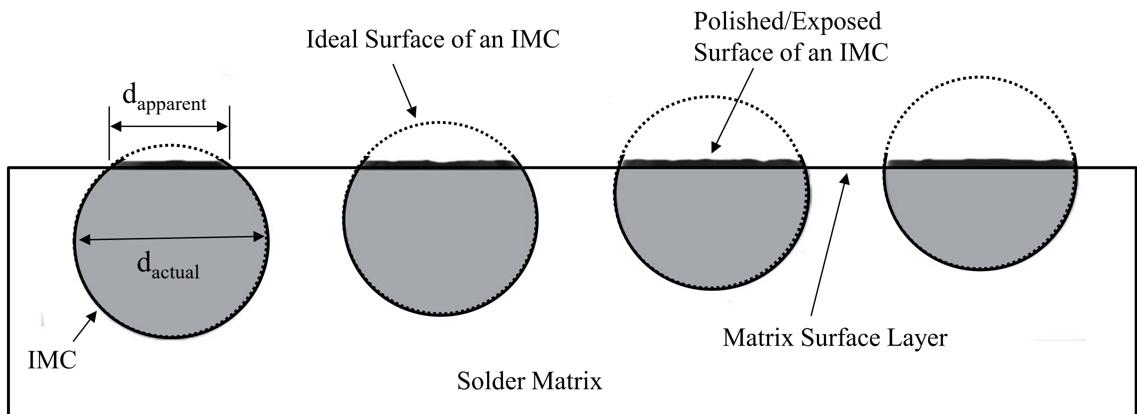

Figure 3.20 Schematic Representation of an IMC with Several Possible Exposed Area above the Surface Layer

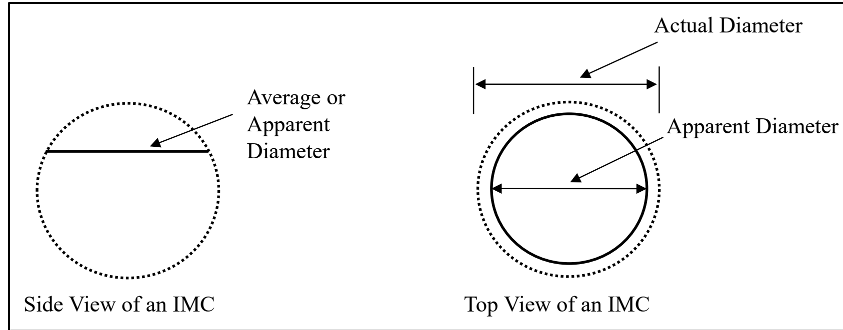

Figure 3.21 Side and Top View of an Ideal Spherical IMC Particle Showing Actual and Apparent Diameters

For a fixed particle with diameter d, the apparent/measured particle diameter $d_{apparent}$ can be several different values based on the vertical position of the particle (Figure 3.20). The average value of $d_{apparent}$ can be found mathematically by averaging all possible values obtained from all possible vertical positions for the particle:

$$(d_{apparent})_{ave} = 2 \times (R_{apparent})_{ave} = \frac{2}{R}\int_{0}^{R}\sqrt{(R^2 - x^2)}dx \qquad (3.5)$$

$$(d_{apparent})_{ave} = \frac{2}{R} \times \frac{\pi R^2}{4} = \frac{\pi}{4} d_{actual} \qquad (3.6)$$

$$d_{actual} = \frac{4}{\pi}(d_{apparent})_{ave} \qquad (3.7)$$

Equation 3.26 was used to estimate the actual diameter of each particle by adjusting the measured (apparent) diameter.

If the particles are spherical, the apparent diameter of the exposed surface of each particle can be calculated by assuming a circular relation between particle surface area and apparent diameter:

$$A_{apparent} = \pi R^2 = \frac{\pi}{4}(d_{apparent})^2 \quad (3.8)$$

$$d_{apparent} = \frac{2}{\sqrt{\pi}}\sqrt{A_{apparent}} \quad (3.9)$$

Combining of Equations (3.7, 3.9) yields the relation for the particle diameter in terms of the measured/particle surface area:

$$d_{actual} = \frac{4}{\pi}(d_{apparent})_{ave} = \frac{8}{\pi^{3/2}}\sqrt{(A_{apparent})_{ave}} \quad (3.10)$$

Additionally, this analysis also assumes that the particle does not move vertically during any thermal exposures.

3.6.4 Tracking the Changes in IMC Particle Diameter during Isothermal Aging

For very durations of isothermal aging at a particular temperature, three regions similar to that shown in Figure 3.19 were processes and analyzed. The evolution of the average diameter of the IMC particles and the total number of particles data were gathered for all three regions and then the data were fitted using a two term exponential relation

$$\frac{d}{d_o} = k_1 e^{k_2 t} + k_3 e^{k_4 t} \quad (3.11)$$

where d is the average diameter of all particles at time t, d_o is the average diameter of all particles at time t = 0, and K_1, K_2, K_3, and K_4 are fitting constants.

3.7 Nanoindentation Method and Test Procedures

3.7.1 Sample Preparation for Nanoindentation

For this study, SAC305 (96.5Sn-3.0Ag-0.5Cu) and SAC_Q (92.7Sn-3.4Ag-0.5Cu-3.3Bi) lead free solder joints were tested. The joints had a diameter of about 30mils (762 μm). Figure 3.22 shows an example of the test joints used for the experiments. The samples consisted of a 3 x 3 Ball Grid Array (BGA) of the lead free alloys to be tested. The substrates used in the specimens were FR-4 PCBs. Samples which had an Immersion Silver (ImAg) surface finish on the copper pads were chosen. Flux was deposited on the pads using a stencil. A reflow profile with a maximum temperature of 245 °C was obtained with the help of a Vitonics-Soltec convection oven. The profile also ensured that the assembly was kept above the liquidus temperature for about 45-60 seconds. The samples were then cleaned, dried and stored in a freezer at -40 °C to hinder any aging effects. double-sided tape to facilitate polishing.

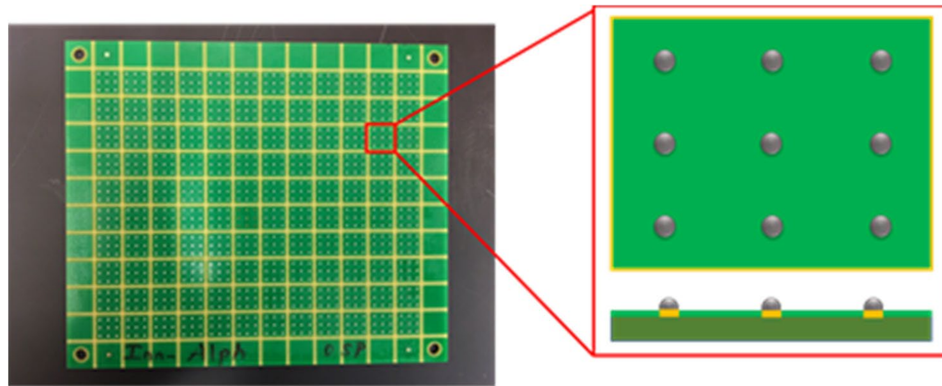

Figure 3.22 3x3 BGA Specimen Sample

Samples were covered with a tape and then confined in epoxy resin. The tape was used to prevent epoxy from entering the space between the individual joints which allows the cycling of each joint separately. Another purpose is to avoid thermal mismatch during

thermal exposure between solder joint and epoxy. The tape from these samples were removed by coarse grinding using a 320 grit SiC paper. Grinding papers up to 1200 grit were then used to reduce the scratches on the samples. The samples were then finally polished using a 0.02 μm colloidal silica suspension to flatten the top surface of the solder joints and making the joints suitable for nanoindentation tests (Figure 3.23). All the polished joints were viewed under a Polarized Light Microscope to verify that all experiments were conducted on single grain joints (Figure 3.24).

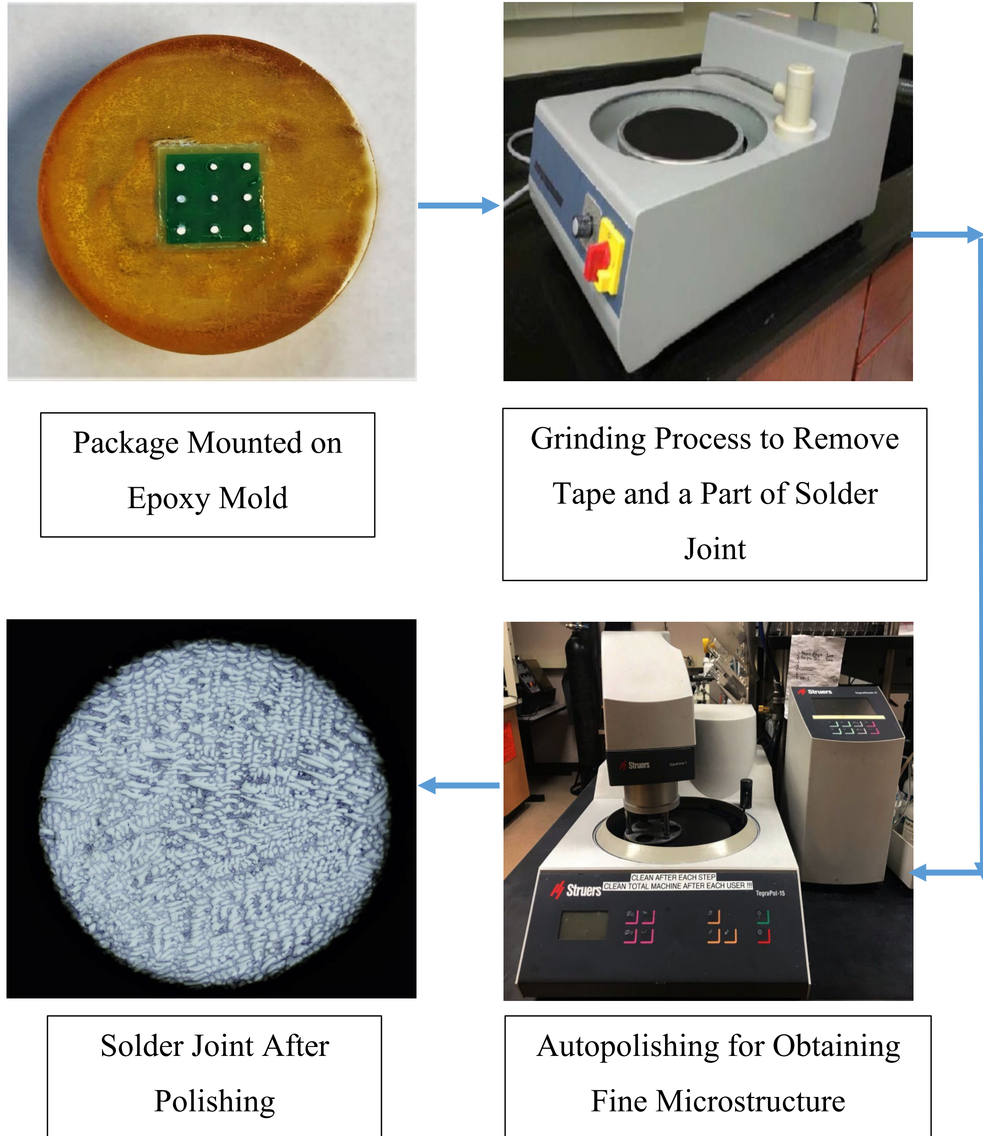

Figure 3.23 Sample Preparation Procedure for Nanoindentation Testing

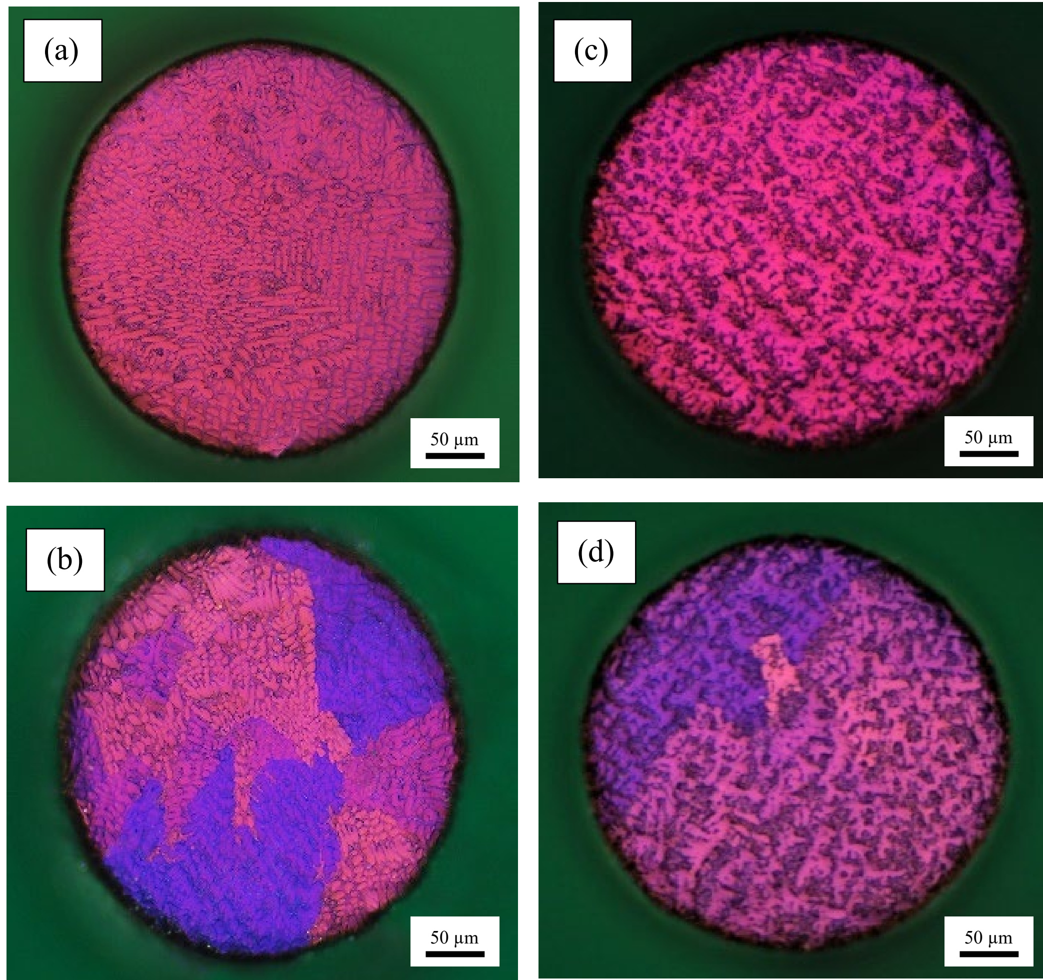

Figure 3.24 (a) SAC305 Single Grain, (b) SAC305 Multiple Grain, (c) SAC+3%Bi Single Grain, (d) SAC+ 3%Bi Multiple Grain Solder Joint

3.7.2 Measurement of Elastic Modulus and Hardness

The nanoindentation tests in this work were performed using an instrumented Hysitron TI 950 nanoindentation system (Figure 3.17) and a Berkovich indenter tip. During each indentation experiment, load versus indentation displacement response of the test samples in the direction normal to the cross-sectional surface was measured.

Figure 3.25 shows a cross-section of a SAC305 lead free solder joint sample after nanoindentation testing. In this study, for each thermal exposures, 10 indentations were made in a row. The measured test data were averaged to obtain statistically relevant results and consistency of inspection. The indents in a set were positioned at least 3b apart, where b is the width of a single indent, to avoid interactions between the plastic zones created by the indentations. Figure 3.26 shows a typical example of loading profile used during nanoindentation, for hardness and modulus testing. The loading profile has three segments 1) loading from 0 mN to peak force, 2) holding at peak force, and 3) unloading from peak force to 0 mN. Depending on the type of the test material, the different parameters in the loading profile was adjusted to get an accurate measurement.

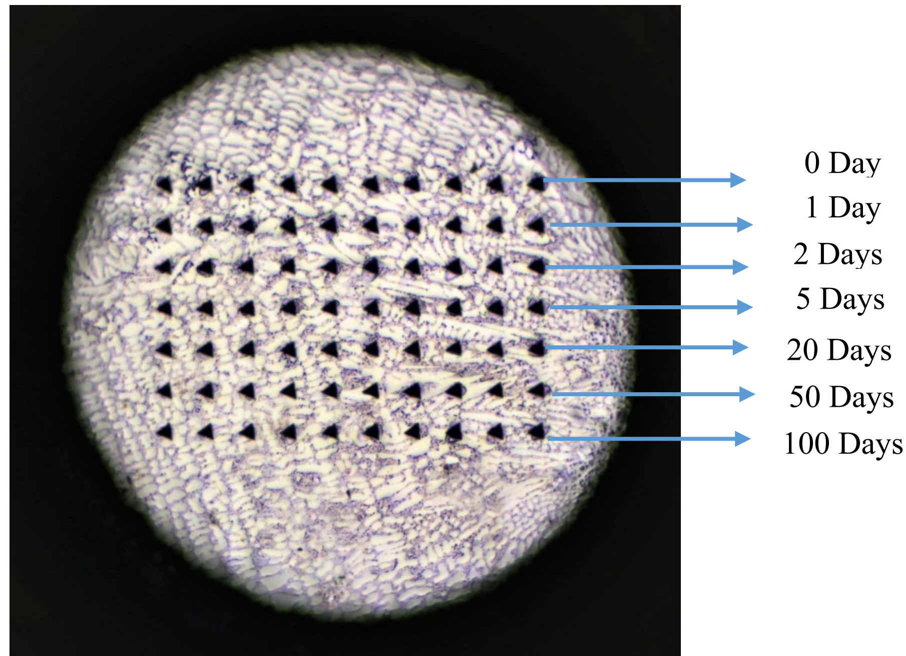

Figure 3.25 Representative SAC305 Solder Joint after Nanoindentation Testing

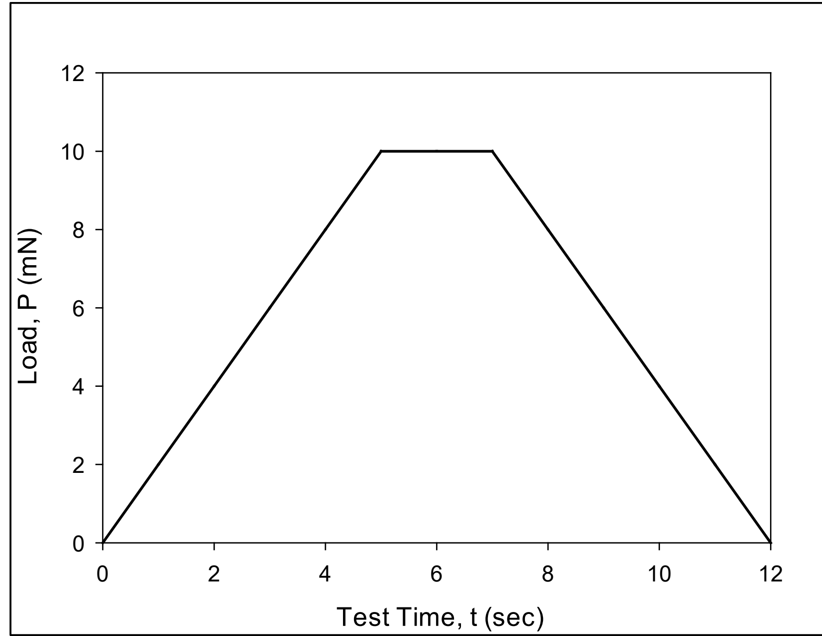

Figure 3.26 An Example of The Loading Profile Used During Nanoindentation Testing

A typical load (P) versus displacement (h) curve, obtained after a nanoindentation test, is presented in Figure 3.26. This curve has three different segments where the first, second, and third segments represent the displacements during the loading, holding and unloading period, respectively.

During a nanoindentation experiment, the effects of the non-rigidity of an indenter, during a nanoindentation experiment, can be addressed by introducing a term called reduced modulus (E_r) through the following equation:

$$\frac{1}{E_r} = \frac{(1-\nu^2)}{E} + \frac{(1-\nu_i^2)}{E_i} \tag{3.12}$$

where E is the elastic modulus of the test specimen, E_i is the known elastic modulus of the indenter tip material, ν and ν_i are the Poisson's ratio of the test specimen and the indenter tip, respectively.

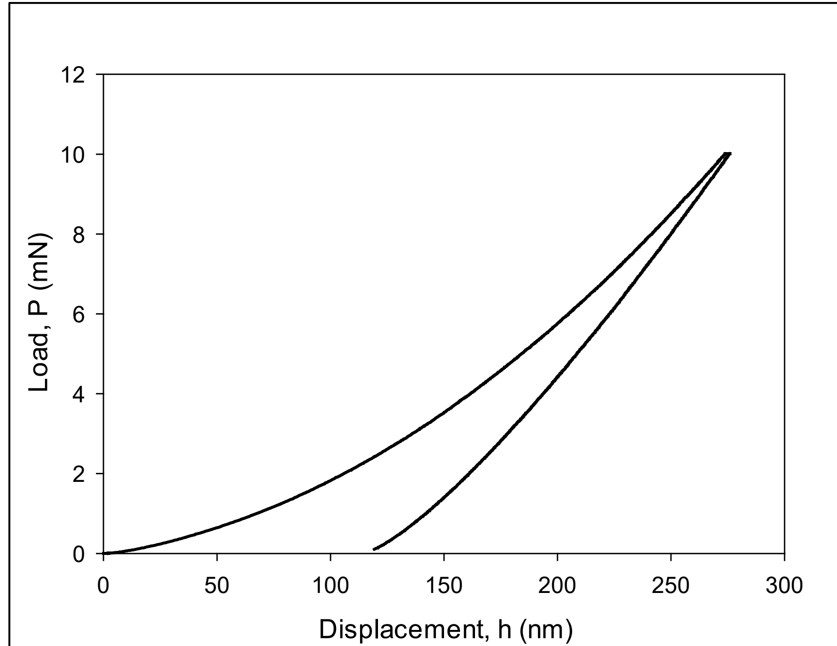

Figure 3.27 An Example of Load-Displacement Curve Obtained

After Nanoindentation Test

Typically reduced modulus was measured from an indentation experiment using the following equation.

$$E_r = \frac{\sqrt{\Pi}}{2} \cdot \frac{S}{\sqrt{A}} \tag{3.13}$$

Where S is the stiffness of the test specimen at the maximum load and A is the projected contact area at the maximum load. Stiffness was determined from the initial slope ($\frac{dP}{dh}$) of the unloading segment of a load displacement curve. The contact area A was measured following the technique proposed by Oliver and Pharr [162] where they assumed the contact area to be a function of contact depth. For an ideal Berkovich tip, it can be expressed as

$$A(h_c) = 24.5h_c^2 \tag{3.14}$$

In order to address any deviation from the ideal Berkovich geometry due to tip blunting, a modified version of Equation 3.7 was utilized.

$$A(h_c) = 24.5h_c^2 + C_1h_c^1 + C_2h_c^{1/2} + C_3h_c^{1/4} + C_4h_c^{1/8} + C_5h_c^{1/16} \qquad (3.15)$$

Where C_1, C_2, C_3, C_4, and C_5 are fitting constants. In order to determine the values of these constants, multiple indents were made at multiple depths on a quartz sample with known elastic modulus (69.6 GPa). The contact areas at the different known depths were determined from Equation 3.13 and these values were plotted to get a A versus h_c plot. The values of constants C_1 to C_5 were determined by fitting the plot by Equation 3.14. Once the values of the constants are known for a particular tip geometry, Equation 3.12 was used to determine the value of reduced modulus (E_r) for any unknown material and Equation 3.11 was used to convert E_r to elastic modulus E.

Hardness is a material property that defines the resistance of the surface against plastic deformation. During a nanoindentation experiment, hardness H was determined by dividing the maximum load by the projected contact area.

$$H = \frac{P_{max}}{A} \qquad (3.16)$$

Tabor [163] developed an approximate relationship between hardness and yield stress of which is true for many metals.

$$H \approx 3\sigma_Y \qquad \text{or} \qquad \sigma_Y \approx \frac{H}{3} \qquad (3.17)$$

The above equation was used to determine stress during nanoindentation experiments.

3.8 Summary and Discussion

All the experimental procedures and the data processing steps were presented in this chapter. Micro-scale uniaxial tensile specimens were prepared in a rectangular shaped hollow glass tube using a vacuum suction method. Typical dimension of the uniaxial tensile specimens were 80 (length) X 3 (width) X 0.5 (height) mm. Uniaxial tensile tests were performed using a micro tension torsion testing system. Nanoindentation experiments were conducted on solder joints which were 3x3 BGA solder with ball diameter 30 mils. Nanoindentation experiments were performed using Hysitron TI950 TriboIndenter. Nanoindenter can be used to indent vary small volume element to extract various mechanical properties like elastic modulus and hardness.

CHAPTER 4

MECHANICAL CHARACTERIZATION OF SAC305 SOLDER MATERIAL UNDER DIFFERENT THERMAL EXPOSURES

4.1 Introduction

During the service life of electronic packages, solder joints undergo thermal cycling which occurs between low to high temperature extreme. Also, solder joints can experience same exposure during accelerated thermal cycling testing which is being used for characterizing thermal-mechanical fatigue behavior. Mechanical behavior of solder joints evolves due to this variation in temperature and microstructure evolution of solder materials. In addition, during dwell at high temperature extreme, thermal aging phenomena occurs in the solder material which causes the microstructural evolution and leads to the material property degradation. Additional aging effects may occur during ramping between low to high temperature extremes in thermal cycling. In literature, many studies showed the evolution of mechanical properties of solder materials under isothermal aging [164] whereas studies on evolution under thermal cycling exposure is limited. Mechanical behaviors of lead free solder alloys under thermal cycling temperatures are necessary to support several harsh environment electronics applications. In this chapter, we have characterized the stress-strain and creep behavior evolution of SAC305 (96.5Sn3.0Ag0.5Cu) lead free solder material under different thermal exposures, which is

the most popular low cost lead free solder alloy in electronic packaging industries. Different thermal exposures used in this study were (1) Isothermal aging at high temperature extreme (no cycling), (2) 150 minutes cycles with 45 minutes ramps and 30 minutes dwells, (2) air-to-air thermal shock exposures with 30 minutes dwells and near instantaneous ramps, (3) 90 minute cycles with 45 minutes ramps and 0 minutes dwells (thermal ramp only). Tensile and creep specimens were formed in rectangular cross-section glass tubes using a vacuum suction process, and a water quenched (WQ) solidification profile was utilized to yield fine microstructures and the upper limits of the mechanical properties for each alloy. The samples were then placed into the chambers for preconditioning for 1, 2, 5, 20, 50, and 100days of exposures. After preconditioning, tensile testing was performed at room temperature and at strain rate 0.001 sec^{-1}. Stress-strain results were presented in terms of effective elastic modulus, ultimate tensile stress (UTS), and yield strength (YS). Stress-strain behavior were then compared under different thermal exposures. Creep testing was performed at room temperature and three different stress levels (10, 12, and 15 MPa). Creep behavior was presented in terms of secondary creep strain rate. For each stress level, creep performance was compared between different thermal exposures. For tensile testing, 8-10 samples and for creep testing 5 specimens were tested for each condition.

4.2 Alloy Composition and Experimental Test Matrix

In this study, uniaxial tensile tests and creep tests were carried out on SAC305 lead free solder alloy. Table 4.1 represents the vendor recommended chemical compositions.

Table 4.1 Vendor Specified Compositions of SAC305 Solder Material

Alloy	Sn	Ag	Cu	Bi	Ni	Sb
SAC 305	96.50	3.00	0.50	0.00	0.00	0.00

A large test matrix of experiments was studied here for determining stress-strain properties of SAC305 solder material under isothermal aging, slow thermal ramping, thermal shock, and slow thermal cycling. All samples tested in this study had reflowed (RF) microstructures. For this study, the samples were aged at T = 125 °C and thermally cycled between -40-125°C for various durations including 0 (no aging), 1, 2, 5, 20, 50, and 100 days. For each thermal exposures, tensile testing was performed at a single strain rate 0.001 sec^{-1}. The test matrix is shown in Table 4.2.

Table 4.2 Test Matrix of Tensile Testing Under Different Thermal Exposures

Thermal Exposures	Exposure Time (Days)						
	0	1	2	5	20	50	100
Isothermal Aging	√	√	√	√	√	√	√
Slow Thermal Ramping	√	√	√	√	√	√	√
Thermal Shock	√	√	√	√	√	√	√
Slow Thermal Cycling	√	√	√	√	√	√	√

4.3 Stress vs. Strain Data of SAC305 Solder Under Different Thermal Exposures

Figure 4. 1 (a-d) represents the stress vs. strain plot of SAC305 solder material under isothermal aging, slow thermal ramping, thermal shock, and slow thermal cycling respectively for 0, 1, 2, 5, 20, 50, and 100 days of exposures. The seven colored curves in each plot are for different exposure time. Each colored curve is the "average" experimental curve for each exposure time at a strain rate 0.001 sec^{-1}. They were fitted (8-10 recorded curves) by four parameter hyperbolic tangent model in equation 3.2 (chapter 3). In these plots, black curve represents as reflowed condition whereas red, green, blue, pink, cyan, and orange represents 1, 2, 5, 20, 50 and 100 days results respectively.

From these plots, it can be observed that, initially, E, UTS, and YS reduced drastically under isothermal aging compared to other thermal cyclic conditions. But, with the increasing elapsed time, the reduction of E, UTS, and YS becomes higher under other thermal exposures. For instance, the E reduced by 31% after 1 day of isothermal aging at T = 125 ^{o}C. But, after 1 day of slow thermal ramping, thermal shock, and slow thermal cycling, the reductions are 25%, 23%, and 26%, respectively at T = 125 ^{o}C. On the other hand, after 1 day, UTS reduction is 34% under isothermal aging whereas 22%, 26%, and 23% at T = 125 ^{o}C under slow thermal ramping, thermal shock, and slow thermal cycling, respectively. However, after 100 days of isothermal aging, E reduced by 54% while it was reduced by 62%, 62%, and 70% under slow thermal ramping, thermal shock, as well as slow thermal cycling, respectively. Table 4.2 represents additional numerical comparisons for bulk solder.

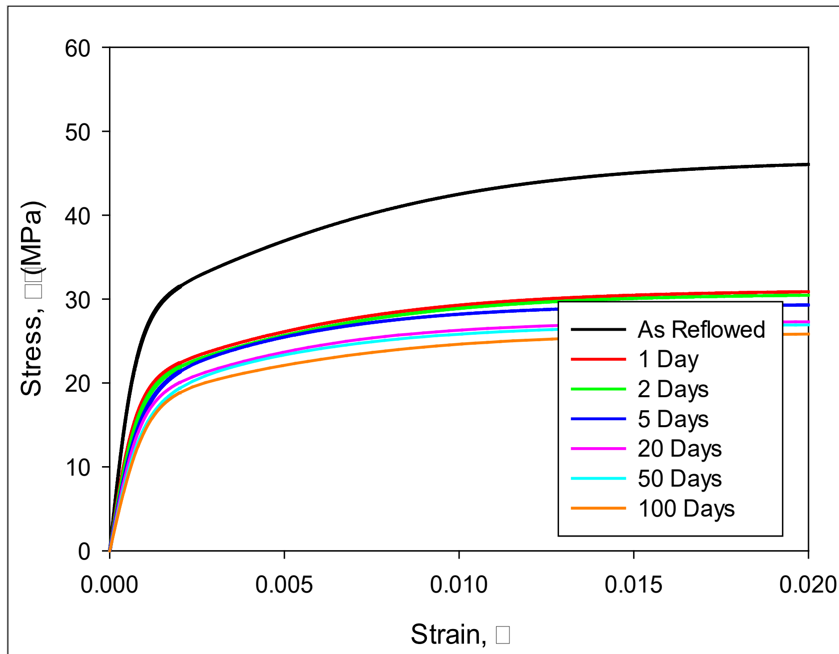

(a) Isothermal Aging

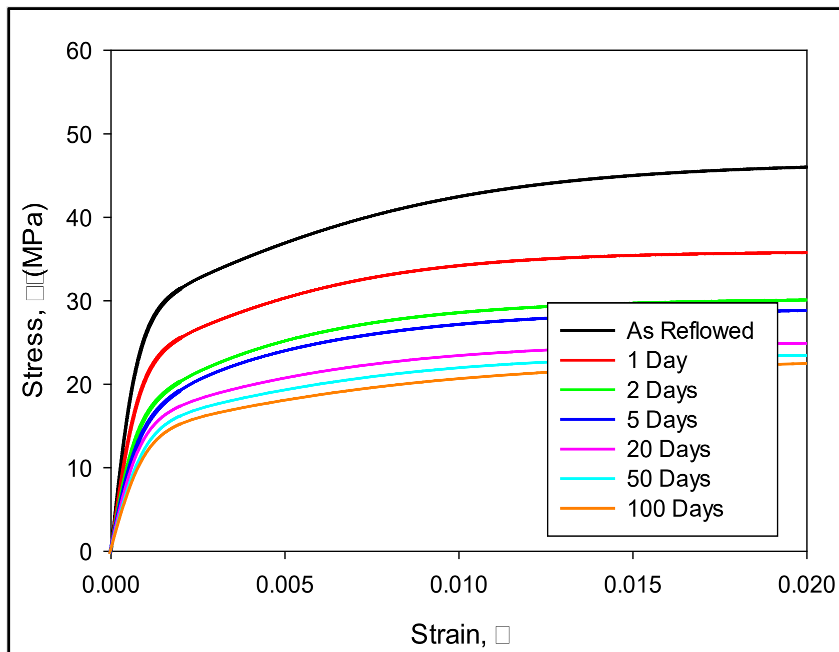

(b) Slow Thermal Ramping

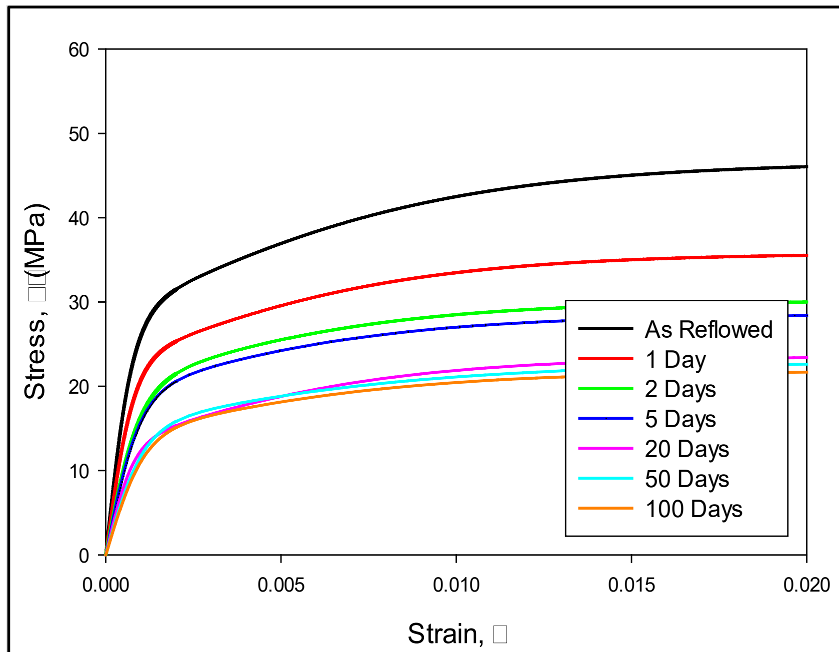

(c) Thermal Shock

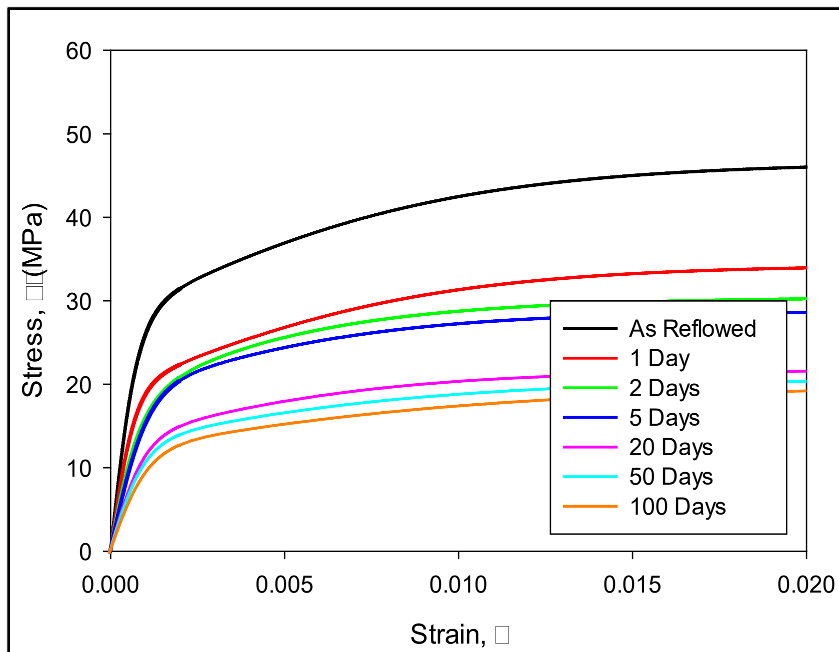

(d) Slow Thermal Cycling

Figure 4.1 Stress-Strain Behavior of SAC305 Alloy Under Different Thermal Exposures

Table 4.2 Mechanical Property of SAC305 Solder Under Different Thermal Exposures

Thermal Exposure		Effective Elastic Modulus, (GPa)	% Change	UTS (MPa)	% Change	YS (MPa)	% Change
None	0 Day	39.62	0.0	47.06	0.0	33.5	0.0
Aging	1 Day	27.32	31.0	30.88	34.3	24.0	28.3
	2 Days	25.18	36.5	30.47	35.3	22.5	32.8
	5 Days	23.23	41.1	29.30	37.7	22.0	34.3
	20 Days	21.87	44.8	27.77	41.0	21.5	35.8
	50 Days	19.81	50.0	27.47	42.0	21.2	36.7
	100 Days	18.40	53.6	26.48	43.8	20.5	38.8
Slow Thermal Ramping	1 Day	29.61	25.3	36.49	22.5	27.4	18.2
	2 Days	23.88	39.7	30.87	34.3	22.5	32.8
	5 Days	21.14	46.6	30.33	35.6	21.4	36.1
	20 Days	18.88	52.3	25.67	45.4	18.9	43.6
	50 Days	16.17	59.1	24.10	48.8	17.8	46.8
	100 Days	15.09	61.9	23.36	50.4	16.7	50.1
Thermal Shock	1 Day	1 Day	30.20	23.8	30.05	22.9	26.9
	2 Days	2 Days	22.07	44.3	28.39	35.2	23.5
	5 Days	5 Days	20.32	48.7	26.83	39.7	21.3
	20 Days	20 Days	17.86	54.9	23.95	49.3	17.4
	50 Days	50 Days	14.82	62.6	23.33	50.4	16.6
	100 Days	100 Days	13.73	65.3	22.13	53.0	16.4

Slow Thermal Cycling	1 Day	29.17	26.4	34.98	25.7	24.2	27.8
	2 Days	21.02	46.9	30.72	34.7	23.7	29.3
	5 Days	16.22	59.1	27.90	40.7	22.0	34.3
	20 Days	14.65	63.1	22.13	52.9	16.5	50.8
	50 Days	13.66	65.5	21.28	54.8	15.6	53.4
	100 Days	11.72	70.4	20.21	57.1	14.2	57.6

4.4 Comparison Between Aging and Different Thermal Exposures

Figure 4.2 (a-f) represent the comparisons of the stress-strain results for 1, 2, 5, 20, 50, and 100 days between aging and different thermal exposures. In these plots, the black curve shows the result for as reflowed (no aging or cycling), while the red, green, dark blue, cyan curves show the exposure to pure aging, slow thermal ramping, thermal shock, and slow thermal cycling, respectively. From figure 4.4 (a) it can be observed that after 1 day of thermal exposure mechanical properties reduced significantly which is presented by red curve. But after 2 days of thermal exposures, all other curves merged with red curve and crossed it after 5 days of thermal exposures irrespective to the thermal cycling loading. It indicates that after 5 days of thermal exposures, the degradation in mechanical properties under all other thermal exposures were higher compared to the isothermal aging. In addition, after 100 days of thermal exposure mechanical properties degradation were higher under slow thermal cycling presented by cyan curve (figure 4.4 (f)) compared to the isothermal aging and other thermal loadings.

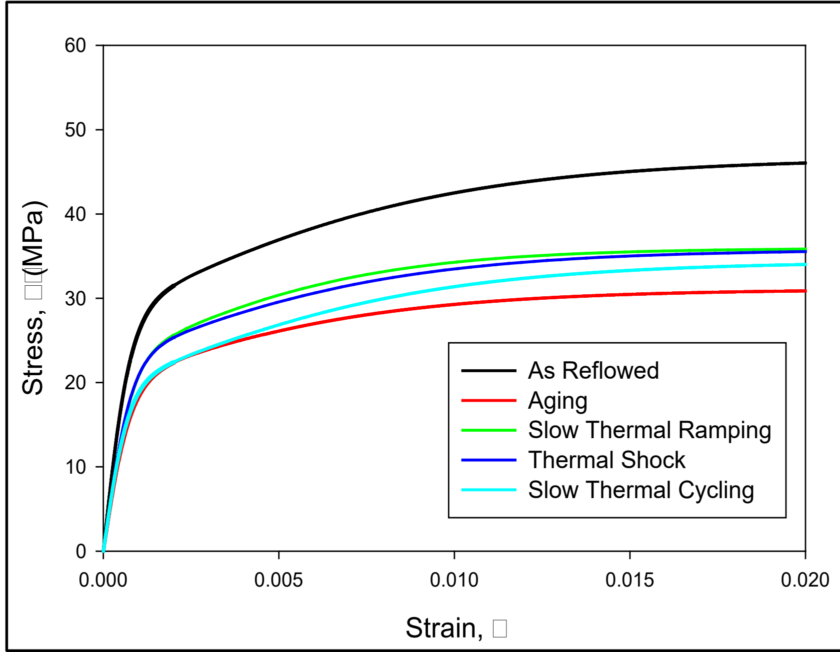

(a) 1 Day Result

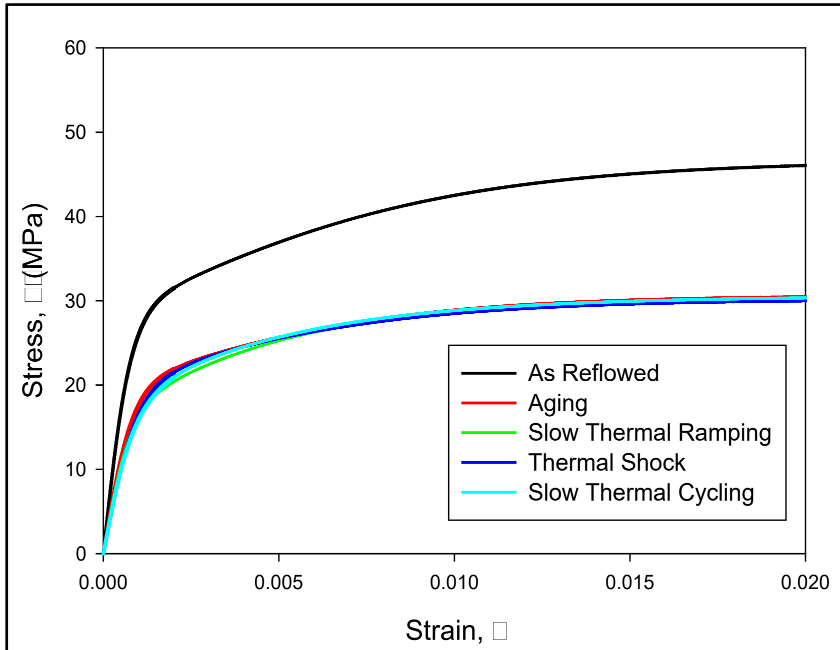

(b) 2 Days Result

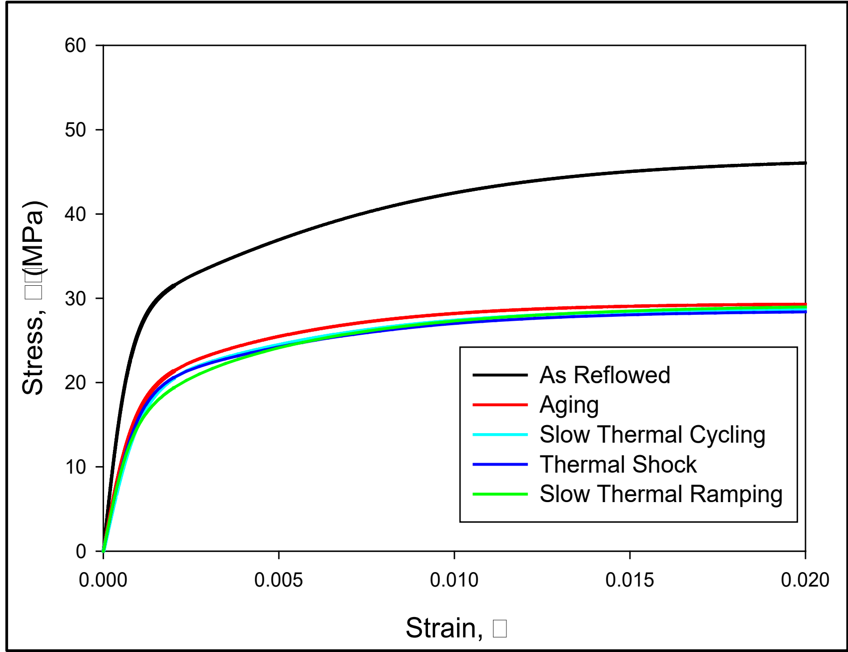

(c) 5 Days Result

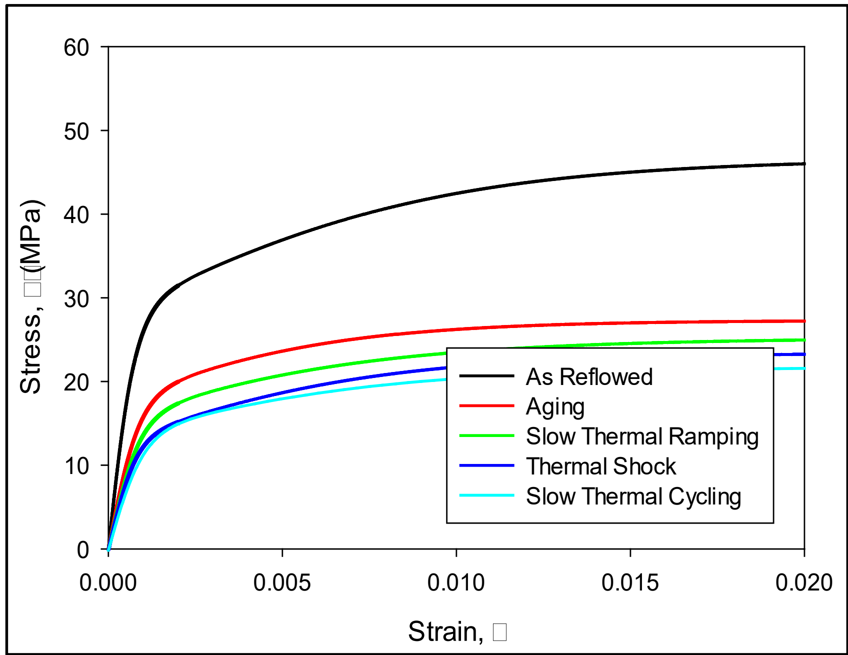

(d) 20 Days Result

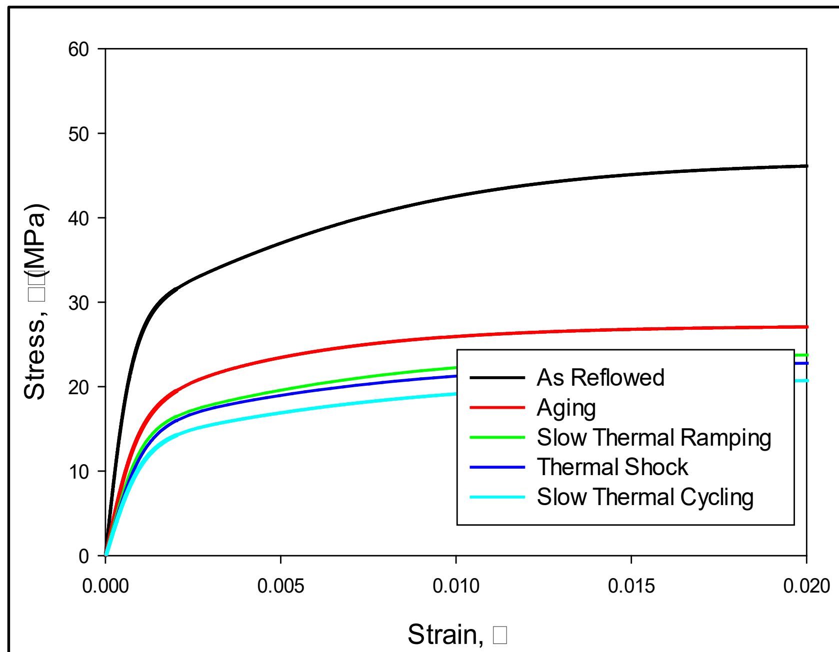

(e) 50 Days Result

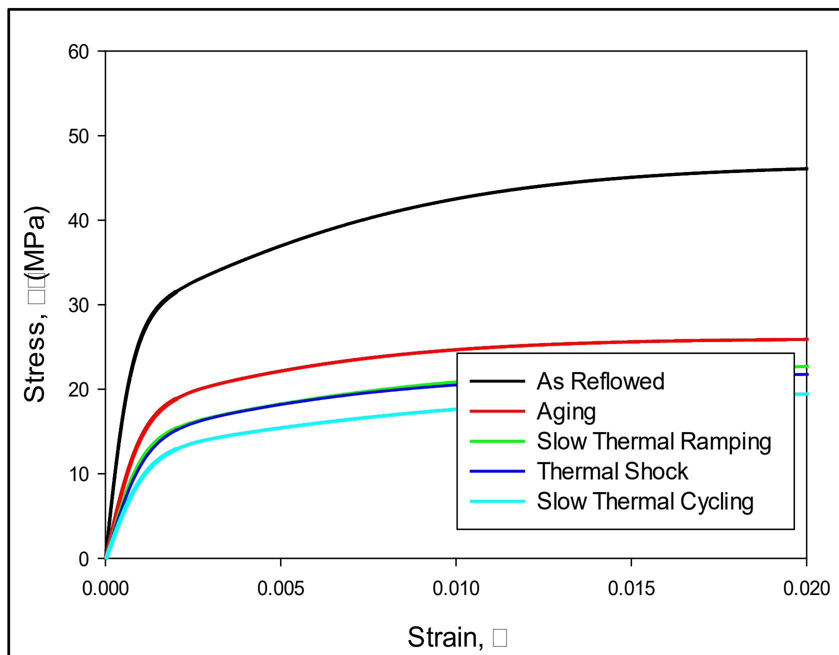

(f) 100 Days Result

Figure 4.2 Stress-Strain Behavior Comparison Under Different Thermal Exposure

4.5 Effective Elastic Modulus, UTS, and YS Evolution with Exposure Times

Figure 4.3 (a-c) show the evolution of E, UTS, and YS under aging and different thermal cycling conditions. These plots were drawn from the data of Table 4.2. In these plots, red, green, blue and cyan indicates aging, slow thermal ramping, thermal shock, and slow thermal cycling respectively. From these plots, it can be inferred that, E, UTS, and YS reduced exponentially with elapsed time irrespective to the thermal loading. Initially, the reduction rate is higher under isothermal aging compared to the other thermal cycling conditions after 1 day. On the contrary, the reduction of E, UTS, and YS are higher for slow thermal cycling, thermal shock, and slow thermal ramping after 100 days of exposures compared to isothermal aging. Moreover, slow thermal cycling showed more detrimental effect among all thermal exposures which depicts additional aging during slow ramping period.

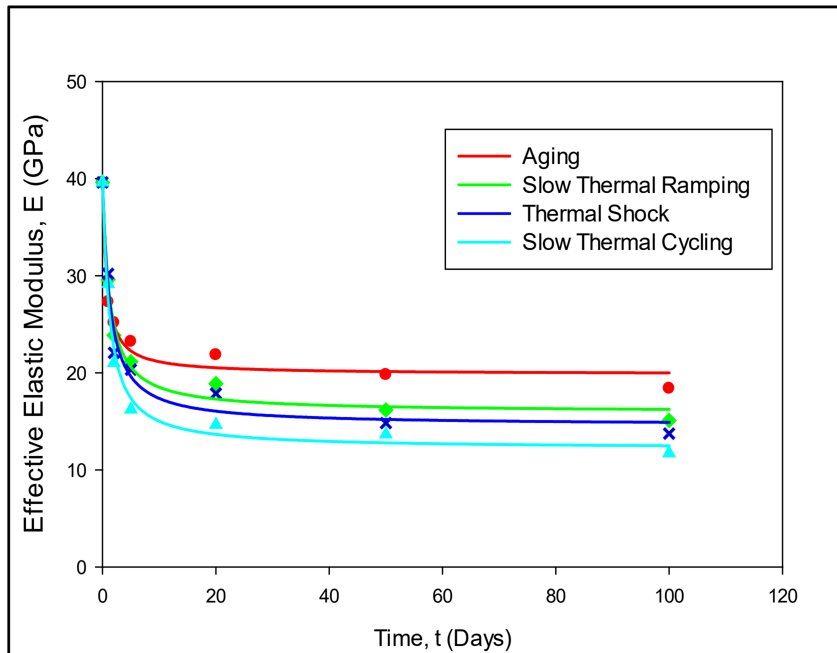

(a) Effective Elastic Modulus

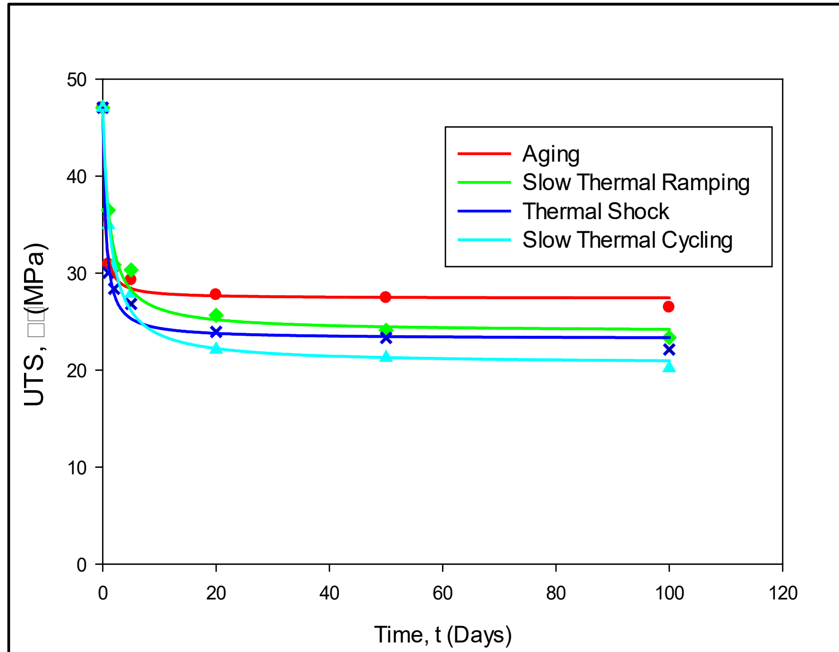

(b) Ultimate Tensile Strength

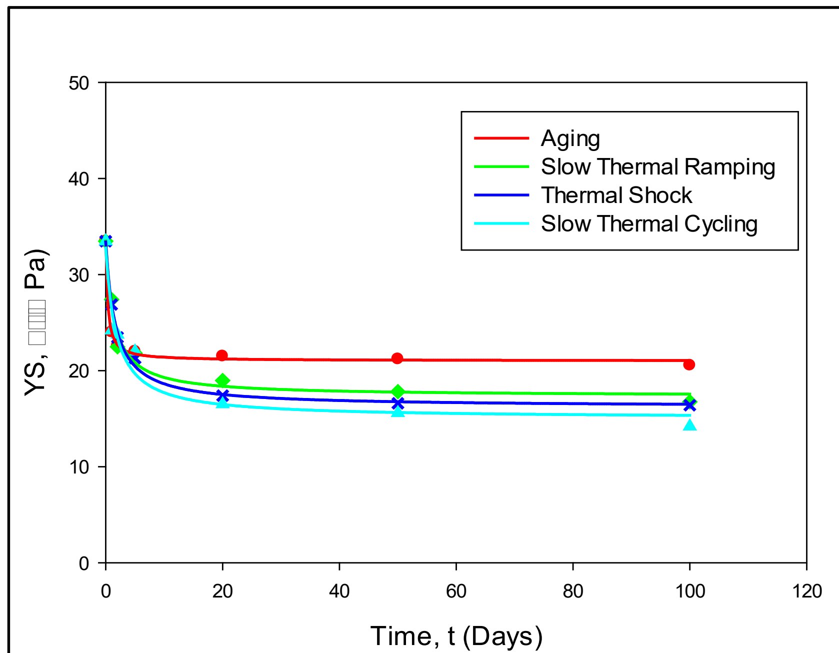

(c)Yield Strength

Figure 4.3 Stress-Strain Behavior Evolution Under Different Thermal Exposures

4.6 Creep Test Matrix of SAC305 Solder Under Different Thermal Exposures

A large test matrix of experiments was studied here for determining creep behavior of SAC305 solder material under different thermal exposures. Five samples were tested for each condition and each stress level. In this study, three different stress level were used such as 10, 12, and 15 MPa. All the tests were performed at room temperature and continued up to 6000 second. The test matrix is shown in Table 4.4.

Table 4.4 Creep Test Matrix of SAC305 Solder Material

Thermal Exposure	Time (Days)	Applied Stress		
		10 MPa	12 MPa	15 MPa
None	0	√	√	√
Aging	1	√	√	√
	2	√	√	√
	5	√	√	√
	20	√	√	√
Slow Thermal Ramping	1	√	√	√
	2	√	√	√
	5	√	√	√
	20	√	√	√
Slow Thermal Cycling	1	√	√	√
	2	√	√	√
	5	√	√	√
	20	√	√	√

4.7 Creep Response Under Different Thermal Exposures

Figure 4.4 (a-c) depict the evolution of creep response of SAC305 solder material under isothermal aging for 0, 1, 2, 5, and 20 days at fixed stress levels 10, 12, and 15 MPa, respectively. In these plots, each curve was fitted by equation 3.4 (chapter 3) to obtain the "average" of recorded experimental strain-time data. The black, red, green, blue, and cyan curves show the average strain-time data for 0, 1, 2, 5, and 20 days of isothermal aging, respectively. It can be inferred from these plots that secondary creep strain rate increases with the aging time. Besides, the variation in creep rate with aging time becomes significant at higher stress level. For example, creep curves of 1, 2, and 5 days aging are close to the As-reflowed condition at 10 MPa, whereas at 12 and 15 MPa, after 1 day of isothermal aging the creep curves were moving toward the higher strain compared to the as-reflowed condition.

An analogous plot of slow thermal ramping is shown in figure 4.5 (a-c). In these plots, the black, red, green, and blue, and cyan curves show the results for 0, 1, 2, 5, and 20 days of slow thermal ramping (no high-temperature dwell), respectively. From figure 4.5, it can be observed that the secondary creep strain rate increases with the elapsed time under slow thermal ramping as isothermal aging. In addition, secondary creep strain rate increases with the stress level. But the change in secondary creep strain rate was lower under slow thermal ramping compared to the isothermal aging up to 2 days thermal exposures. Unlike aging, after 5 days of slow thermal ramping, the variation in secondary creep strain rate was significantly higher compared to the as-reflowed conditions and drastic change can be observed after 20 days of thermal exposures. This variation in creep rate can be attributed to the increasing dislocation movement with stress level and elapsed

time. Figure 4.6 (a-c) represent another analogous plot of slow thermal cycling. Average secondary creep strain rate for aging, slow thermal ramping, as well as slow thermal cycling are tabulated in Table 4.5. Similar phenomena under slow thermal cycling can be observed as slow thermal ramping in secondary creep rate up to 2 days of thermal exposures. But after 5, and 20 days of thermal exposures, secondary creep strain rate change was severe compared to both slow thermal ramping, and aging. It will be clearer in figure 4.7. Moreover, this variation may be due to the additional aging during low to high and high to low temperature ramping which eventually leads to the higher dislocation movement.

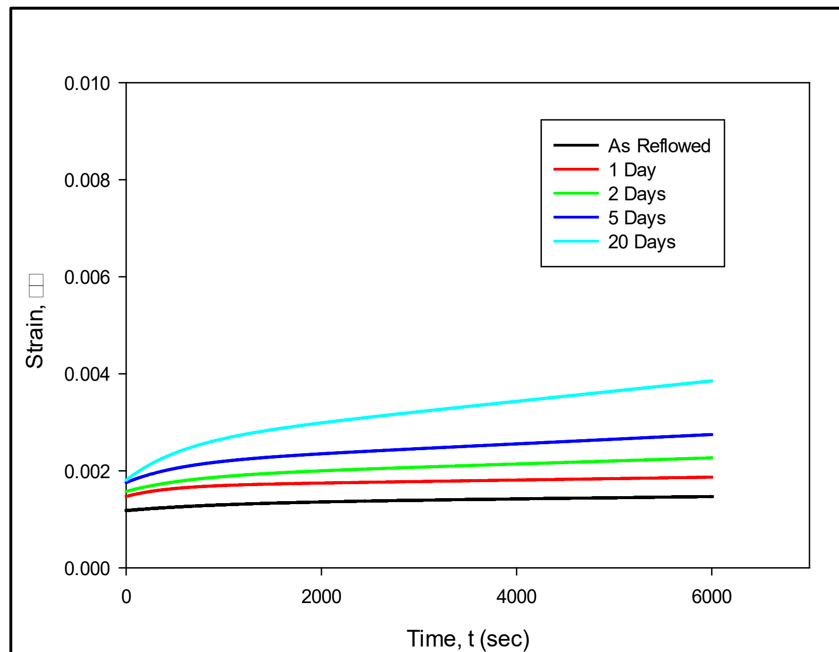

(a) 10 MPa

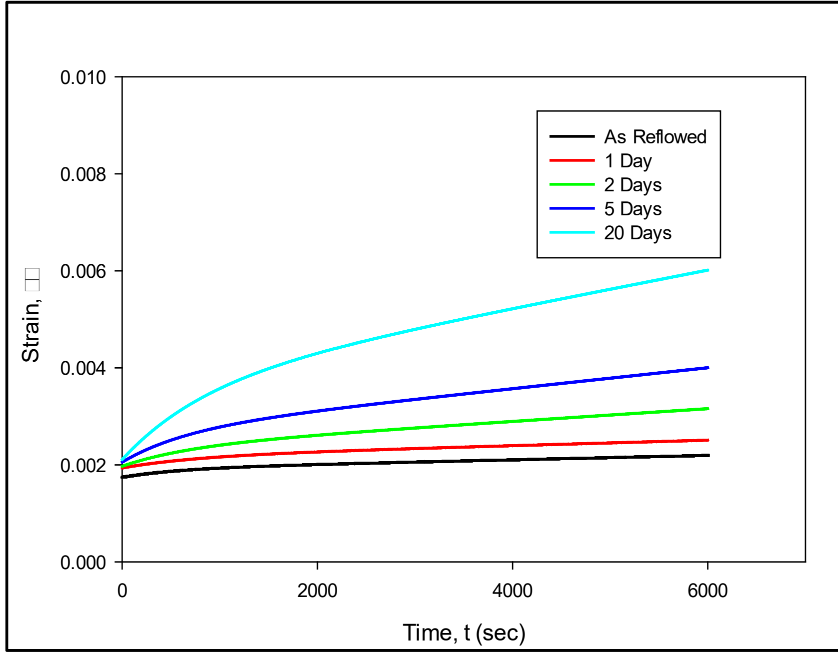

(b) 12 MPa

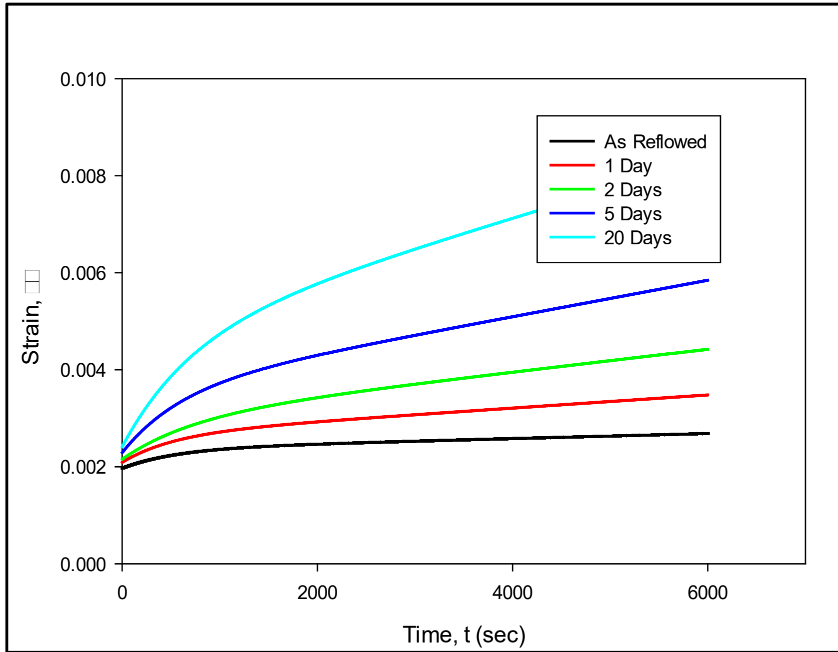

(c) 15 MPa

Figure 4.4 Creep Data of SAC305 Solder at Different Stress Levels Under Aging

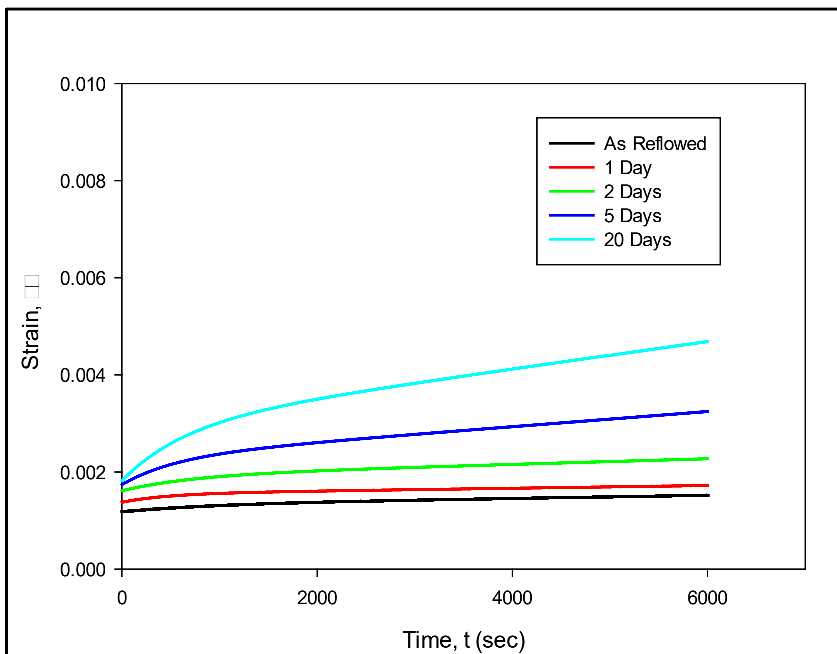

(a) 10 MPa

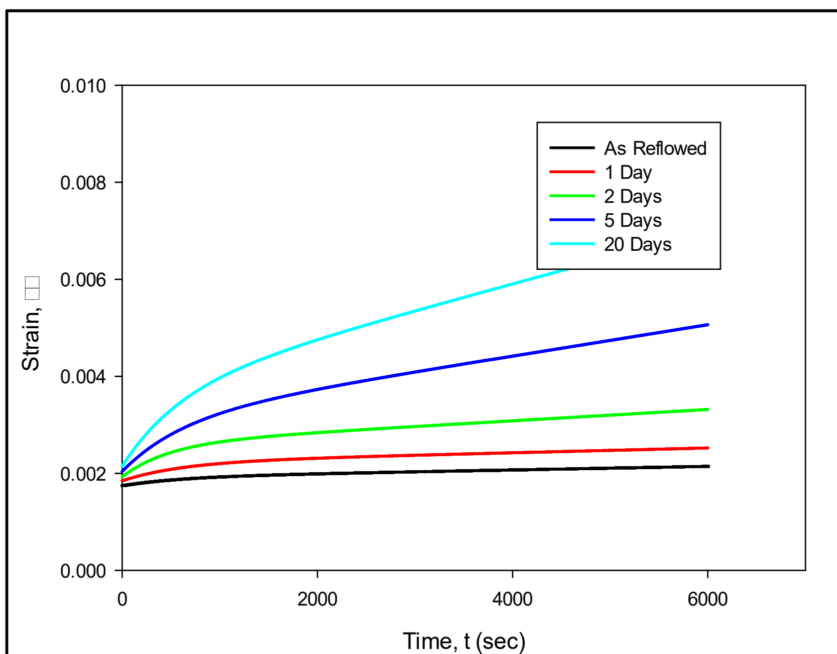

(b) 12 MPa

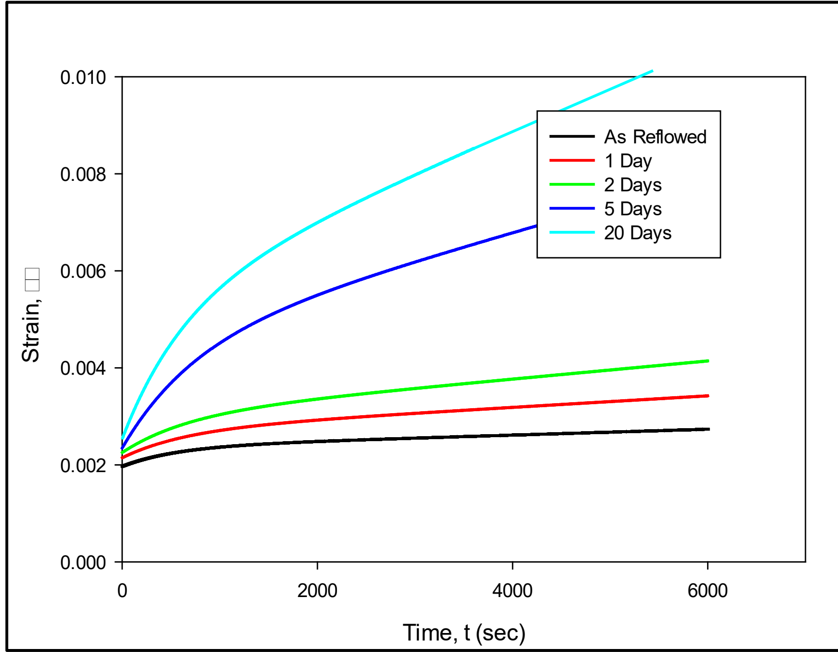

(c) 15 MPa

Figure 4.5 Creep Data of SAC305 Solder Under Slow Thermal Ramping

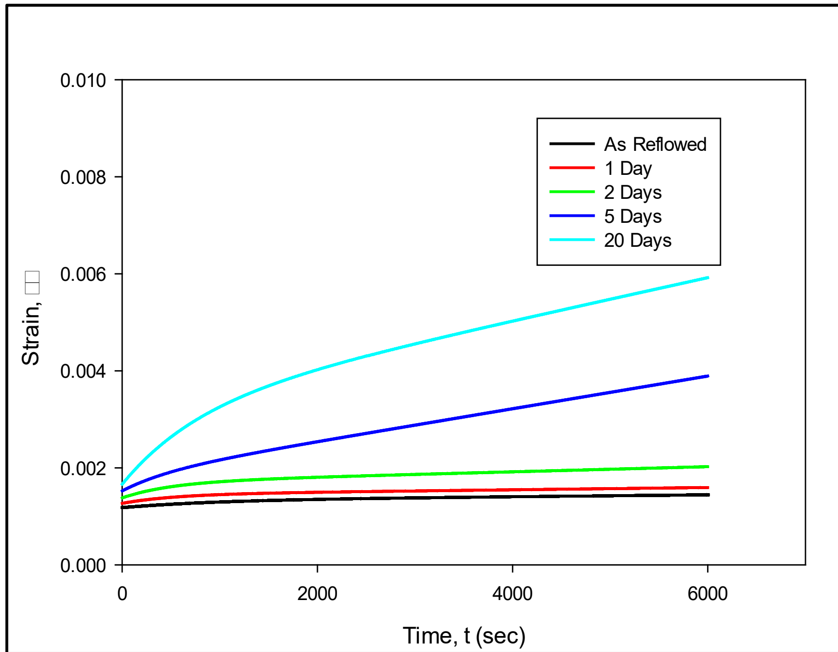

(a) 10 MPa

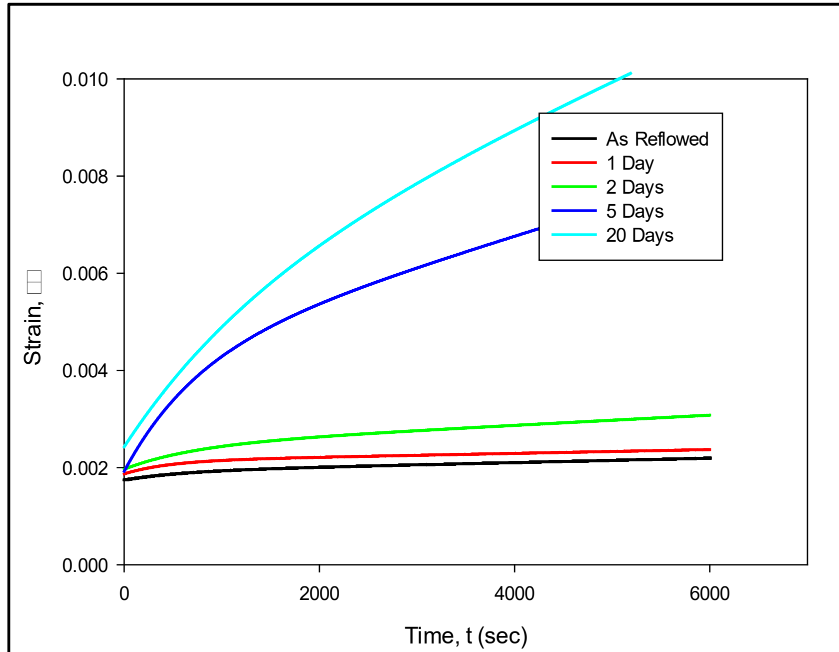

(b) 12 MPa

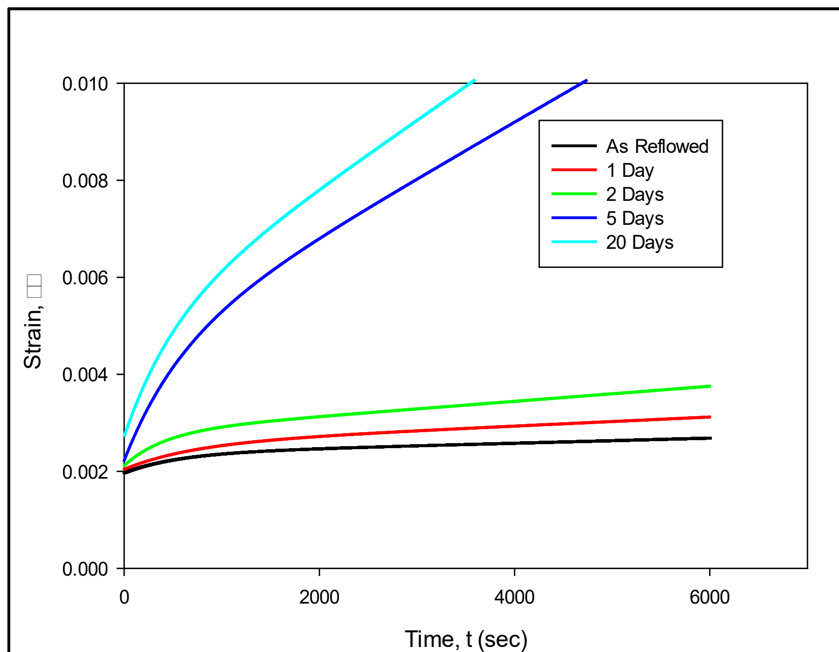

(c) 15 MPa

Figure 4.6 Creep Data of SAC305 Solder at Under Slow Thermal Cycling

Table 4.5 Increase Ratio of Creep Rate at Different Stress Levels and Time

Thermal Exposure	Time (Days)	Secondary Creep Strain Rate (sec^{-1})		
		Increase Ratio at σ= 10 MPa	Increase Ratio at σ= 12 MPa	Increase Ratio at σ= 15 MPa
None	0 Day	1X	1X	1X
Aging	1 Day	2.09 X	1.93 X	3.07 X
	2 Days	4.44 X	4.54 X	5.35 X
	5 Days	6.80 X	8.53 X	8.53 X
	20 Days	14.87 X	13.63 X	13.83 X
Slow Thermal Ramping	1 Day	1.96 X	1.70 X	2.67 X
	2 Days	4.04 X	4.10 X	4.22 X
	5 Days	11.02 X	11.30 X	13.10 X
	20 Days	20.11 X	19.11 X	20.00 X
Slow Thermal Cycling	1 Day	1.65 X	1.34 X	2.10 X
	2 Days	3.74 X	3.60 X	3.53 X
	5 Days	23.90 X	21.56 X	26.45 X
	20 Days	31.46 X	31.41 X	31.65 X

4.8 Comparison Between Aging and Different Thermal Exposures with Elapsed Time

Figure 4.7 was plotted by pulling up the data of 20 Days from figure 4.4a, 4.5a, and 4.6a for the stress level of 10 MPa. Similar phenomenon can be seen in other stress levels. From this plot, it is visible that for a particular stress level secondary creep strain rate increases with any thermal exposures compared to as-reflowed condition. But the rate of increase is much higher under slow thermal cycling (Solid cyan line) compared to the isothermal aging (red line). For example, after 20 days of exposures, secondary creep strain rate increased ~15x and ~32x for isothermal aging, and slow thermal cycling, respectively.

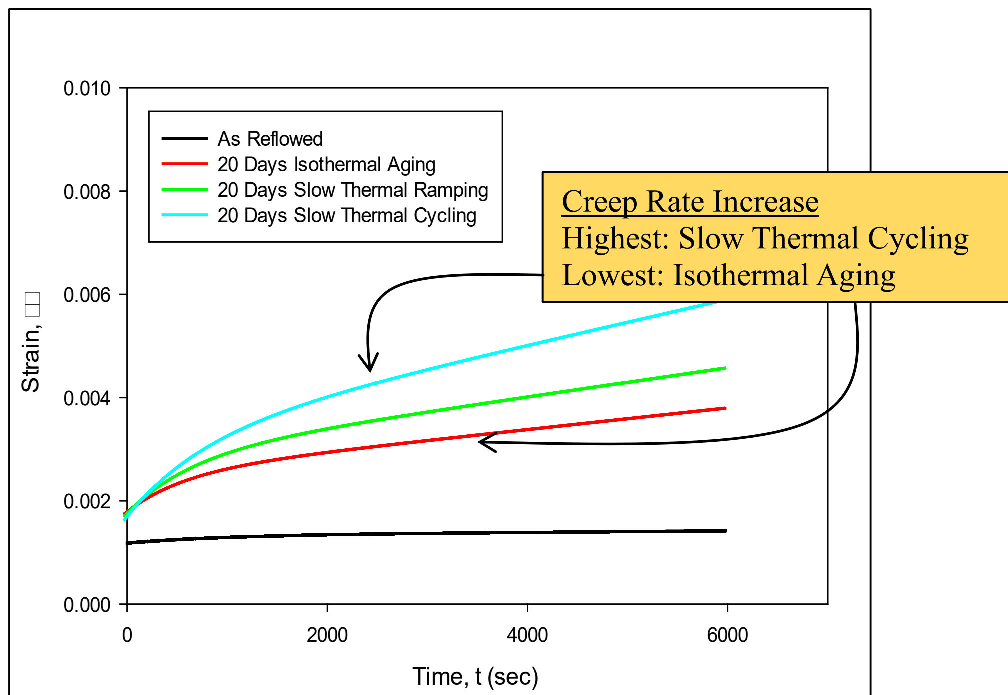

Figure 4.7 Representative Strain vs. Time Plot at Stress level 10 MPa

4.9 Evolution of Creep Response Under Different Exposures with Stress Level

Figure 4.8(a-d) show the evolution of secondary creep strain rate with stress level (10, 12, 15 MPa) for 1, 2, 5, and 20 days of isothermal aging, slow thermal ramping, and slow thermal cycling. Vertical axis (log scale) represents secondary creep strain rate. In these plots, the black curve shows the result for as reflowed SAC305 solder (no aging or cycling), while the red, green, and cyan curves show pure isothermal aging, slow thermal ramping (STR), and slow thermal cycling (STC), respectively. From all these plots, it is obvious that the secondary creep strain rate increases exponentially with stress level for any thermal cycling profile exposures. Also, secondary creep strain rate increases with elapsed time under all thermal cycling profile exposures irrespective of the stress level. But initially, the secondary creep strain rate change under isothermal aging was higher compared to STR, and STC with stress levels. After 5 days of thermal exposures, the secondary creep strain rate change becomes higher under STR, and STC compared to isothermal aging, but, drastically under STC. For instance, after 1 day of isothermal aging secondary creep strain rate increased maximum of 3.1x whereas, for STR and STC, it was 2.7x, and 2.1x, respectively. Contrarily, after 5 days of isothermal aging secondary creep strain rate increased maximum 8.5x while it was increased by 13.1x, and 26.5x for STR, and STC, respectively.

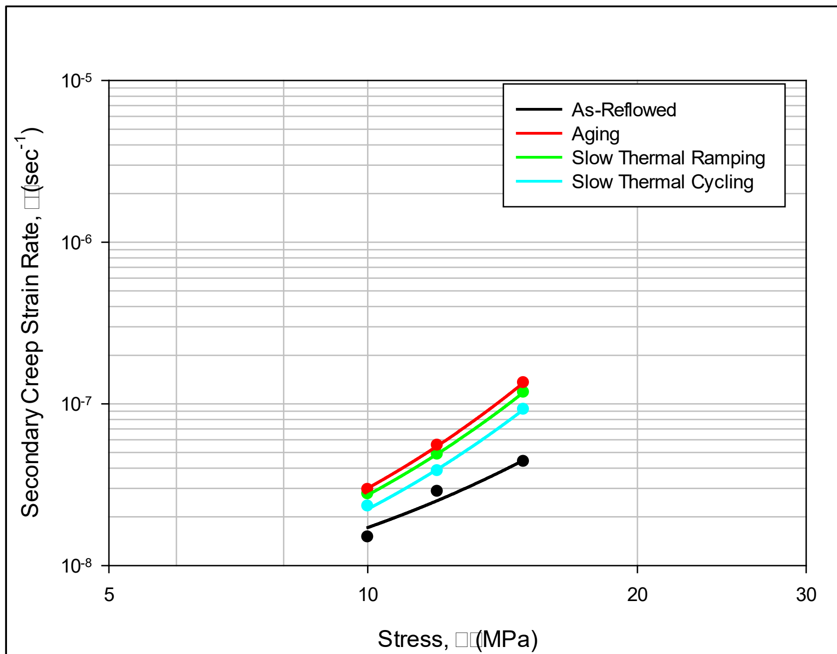

(a) 1 Day Result

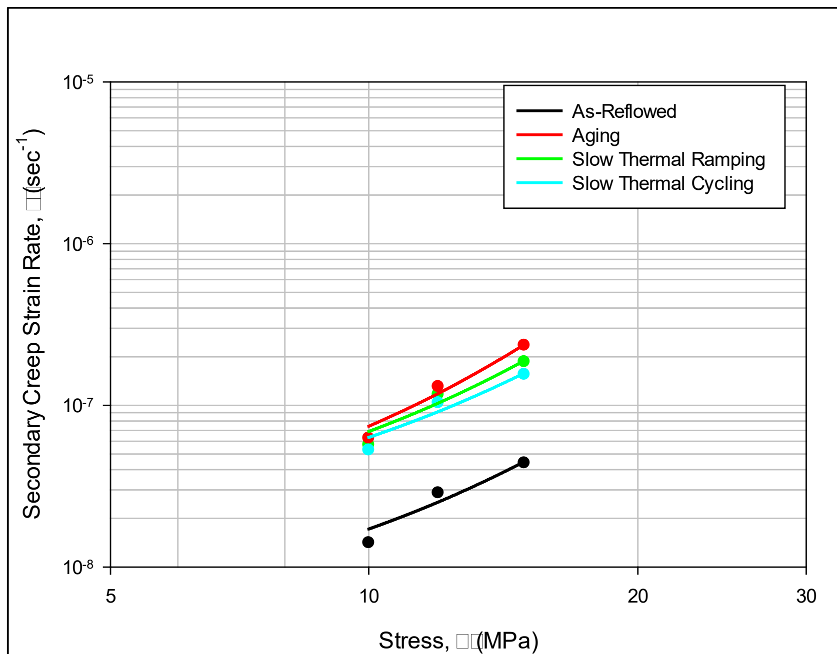

(b) 2 Days Result

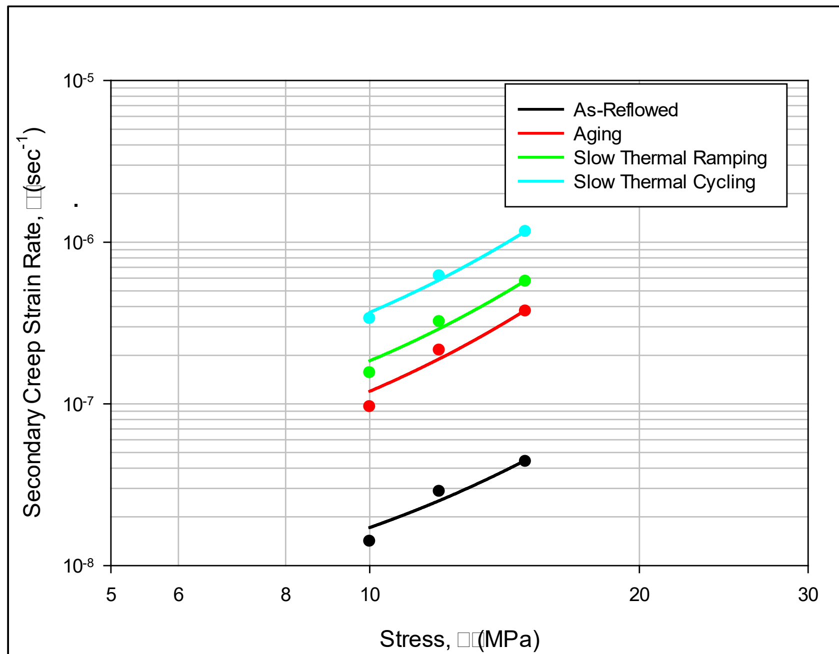

(c) 5 Days Result

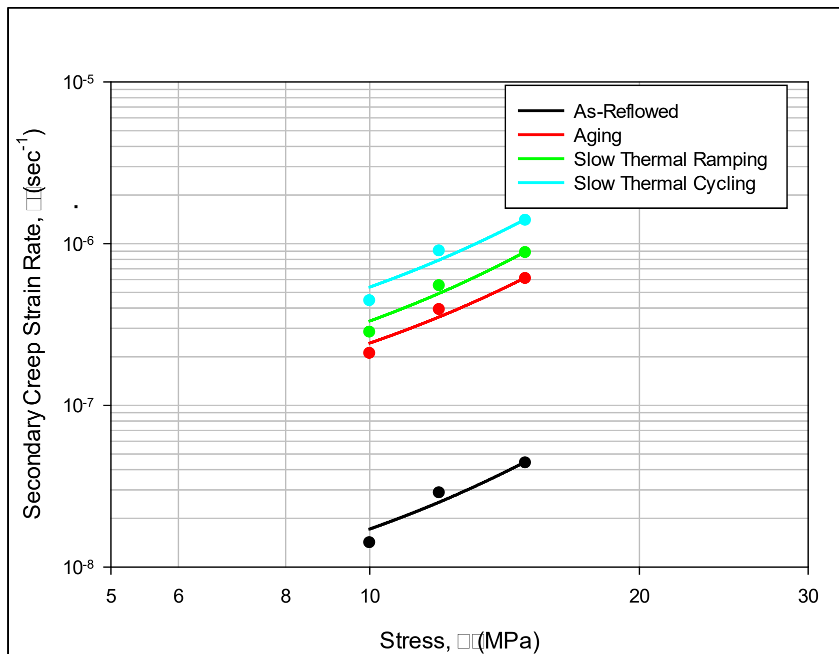

(d) 20 Days Result

Figure 4.8 Creep Rate Evolution Under Different Thermal Exposures with Stress Levels

4.10 Summary and Discussion

In this chapter, mechanical behavior evolution of SAC305 solder material under different thermal cycling exposures was investigated. The thermal cycles were (1) 150 minute cycles with 45 minutes ramps and 30 minutes dwells, (2) air-to-air thermal shock exposures with 30 minutes dwells and near instantaneous ramps, and (3) 90 minute cycles with 45 minutes ramps and 0 minutes dwells, (4) no cycling (simple aging at high temperature extreme). Sets of bulk solder were cycled and aged for the duration of 1, 2, 5, 20, 50, and 100 days at the high temperature extreme of T = 125 C followed by uniaxial tensile testing and creep testing respectively to measure the mechanical properties evolution in terms of E, UTS, YS, and secondary creep strain rate. Uniaxial test samples were prepared by vacuum suction method and submerging into room temperature water followed by reflow solidification.

Results showed that the mechanical properties degradation of SAC305 solder material under slow thermal cycling was severe compared to the aging and other thermal profiles. For example, after 100 days of isothermal aging, E, UTS, and YS of bulk solder was degraded by 54%, 44%, and 39%, respectively. On the other hand, the degradation under slow thermal cycling was 70% ,57%, and 58%, respectively. Even though, the reduction in mechanical properties under pure aging after 1 day was higher compared to other thermal profiles, but with increasing exposure the degradation becomes more prominent in other thermal profiles, particularly, thermal cycle with longest ramp rate (slow thermal cycling).

Also, in this present study, evolution of creep behavior of SAC305 solder material under isothermal aging and different thermal cycling profile exposures have been investigated. Evolution of creep behavior was measured in terms of secondary creep strain rate. Comparison of secondary creep strain rate change as a function of stress level at different elapsed time were also observed between isothermal aging and different thermal cycling profile exposures.

Sets of five samples were exposed to different thermal exposures for various durations such as 1, 2, 5, and 20 days. Then creep testing was performed on thermally cycled samples to observe the evolution of creep behavior with elapsed time under different thermal cycling profile exposures at different stress levels (10, 12, 15 MPa). Afterward, comparative results of isothermal aging, slow thermal ramping, and slow thermal cycling were presented in terms of secondary creep strain rate. For isothermal aging, slow thermal ramping, and slow thermal cycling, secondary creep strain rate increased with the stress level and elapsed time. Even though secondary creep strain rate increased for all thermal cycling exposures with all stress levels, but the initial (up to 2 days) increase ratio of secondary creep rate under isothermal aging was higher compared to other thermal cycling profile exposures. But with increased elapsed time such as 5 days of exposures, the increase ratio becomes higher under slow thermal ramping, and slow thermal cycling. The secondary creep strain rate change was much dramatic under slow thermal cycling compared to isothermal aging and slow thermal ramping. For example, the secondary creep strain rate increased maximum 8.5x after 5 days of isothermal aging whereas it was increased by maximum 13.5x and 26.5x under slow thermal ramping, and slow thermal cycling, respectively compared to the as reflowed condition. This investigation

demonstrates that irrespective of stress level the creep property of SAC305 is severely affected by slow thermal cycling exposures after 5 days of exposures compared to the isothermal aging and slow thermal ramping.

CHAPTER 5

INVESTIGATION ON MECHANICAL PROPERTIES OF SAC+X SOLDER MATERIAL AND COMPARISON WITH SAC305 SOLDER MATERIAL UNDER DIFFERENT THERMAL EXPOSURES

5.1 Introduction

Mechanical properties degradation of lead free solder materials occurs under isothermal aging and thermal cycling. In thermal cycling, dwelling at high temperature extreme causes microstructural evolution due to aging. Also, additional aging occurs during ramping between low and high temperature extreme. This aging of lead-free Sn-Ag-Cu (SAC) solder material leads to growth of intermetallic (IMC) particles in the bulk solder. The IMCs in bulk and solder joints are primarily Ag_3Sn particles which forms along the recrystallization area during thermal cycling in solder joint. Besides recrystallization occurs in β-Sn phases and coarsening of precipitates in the solder joints [165]. The coarsening of IMC particles causes the degradation of mechanical properties. In the prior chapter, it was reported that mechanical behavior degradation of SAC305 solder material under different thermal exposure was severe compared to the isothermal aging. Even though initially, the degradation is much higher under isothermal aging but with increasing exposure time both mechanical properties i.e. stress-strain and creep degraded more under other thermal exposures particularly, with long ramp period stated as slow thermal cycling. In the literature, it was reported that addition of dopant strongly

affects the mechanical property of Pb-free solder. For example, several advantages were recorded due to the addition of Bi as a dopant. Increase of strength due to precipitation hardening, reduction of the IMC layers thickness, and solidification temperatures were the contribution of Bi addition [123]. But most of the study focused on the effect of aging on Bi-doped SAC alloy. Limited amount of work has been found to work on the effect of thermal cycling on Bi-doped SAC solder.

In this chapter, the effect of different thermal exposures such as isothermal aging, slow thermal ramping, thermal shock, and slow thermal cycling on mechanical behavior evolution of SAC+Bi solder material has been presented. Prior to the tensile and creep testing for mechanical properties extraction, all the uniaxial samples were preconditioned for 1, 2, 5, 20,50, and 100 days. After preconditioning, tensile tests and creep tests were performed using the similar condition recorded in chapter 4. Tensile properties were presented in terms of E, UTS, and YS. The creep behavior was presented in terms of secondary creep strain rate. The evolution of E, UTS, and YS under isothermal aging and other thermal exposures with exposure time was presented for SAC+Bi. Stress-strain property comparison of SAC305 and SAC+Bi was also evaluated in this Creep testing was performed at three different stress levels such as 10, 12, and 15 MPa. All the creep data was fitted using four parameters Burger's model. Creep behavior evolution was presented in terms of secondary creep strain rate with exposure time at three stress levels for SAC+Bi Solder. Comparison of secondary creep strain rate under different thermal exposures with stress level (10, 12, and 15 MPa) was also presented between SAC305 and SAC+Bi solder material.

5.2 Alloy Composition and Experimental Test Matrix

In this study, uniaxial tensile tests and creep tests were carried out on SAC305 and SAC+X lead free solder alloy. Vendor recommended name in this study of SAC+X (X=Bi) solder material was SAC_Q. Table 5.1 represents the vendor recommended chemical compositions.

Table 5.1 Vendor Specified Compositions of SAC305 and SAC+X Solder Material

Alloy	Sn	Ag	Cu	Bi	Ni	Sb
SAC 305	96.50	3.00	0.50	0.00	0.00	0.00
SAC_Q	92.50	4.00	0.50	3.00	0.00	0.00

A large test matrix of experiments was studied here for determining stress-strain properties of SAC+X solder material under isothermal aging, slow thermal ramping, thermal shock, and slow thermal cycling. All samples tested in this study had reflowed (RF) microstructures. For this study, the samples were aged at T = 125 ºC and thermally cycled between -40-125ºC for various durations including 0 (no aging), 1, 2, 5, 20, 50, and 100 days. For each thermal exposures, tensile testing was performed at a single strain rate 0.001 sec^{-1}. The test matrix is shown in Table 5.2.

Table 5.2 Test Matrix of Tensile Testing Under Different Thermal Exposures

Thermal Exposures	Exposure Time (Days)						
	0	1	2	5	20	50	100
Isothermal Aging	√	√	√	√	√	√	√
Slow Thermal Ramping	√	√	√	√	√	√	√
Thermal Shock	√	√	√	√	√	√	√
Slow Thermal Cycling	√	√	√	√	√	√	√

5.3 Stress vs. Strain Data of SAC+X Solder Under Different Thermal Exposures

Stress vs. strain plot of SAC+Bi (SAC_Q) solder for 1, 2, 5, 20, 50, and 100 days of exposures under isothermal aging, slow thermal ramping, thermal shock, and slow thermal cycling was presented in figure 5.1 (a-d) respectively. In these plots, each curve is an "average" stress-strain curve representing the fit of the empirical model in equation 3.2 (chapter 3) to the recorded stress-strain curves. The black, red, green, blue, pink, cyan, and orange curves show the average stress-strain data for 0, 1, 2, 5, 20, 50, and 100 days result, respectively. From these plot, small change in the effective elastic modulus E (initial slope), ultimate tensile strength (UTS), and yield strength (YS) with exposure time was observed irrespective to thermal exposure type. For example, E, UTS, and YS decreased by around 14%, 11%, and 20% (Table 5.3), respectively, after 5 days of aging. Also, E, UTS, and YS decreased around 17%, 20%, and 25% after 5 days of exposure under slow thermal cycling. Even though the change under isothermal aging or other thermal exposures was not significant but the change under slow thermal cycling was higher compared to aging as well as other thermal exposures. This small change in SAC+Bi under harsh environment can be attributed to the solid solution strengthening effect of Bi.

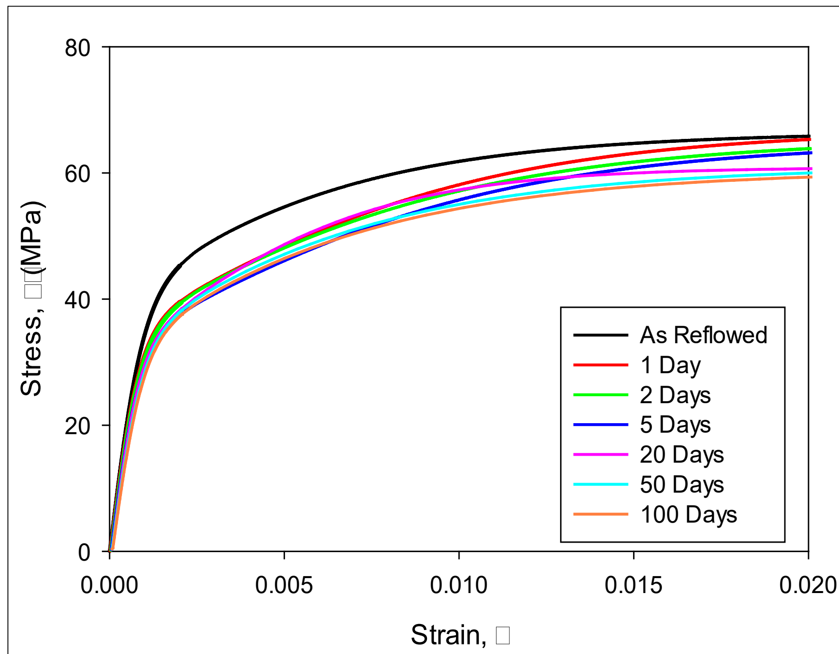

(a) Isothermal Aging

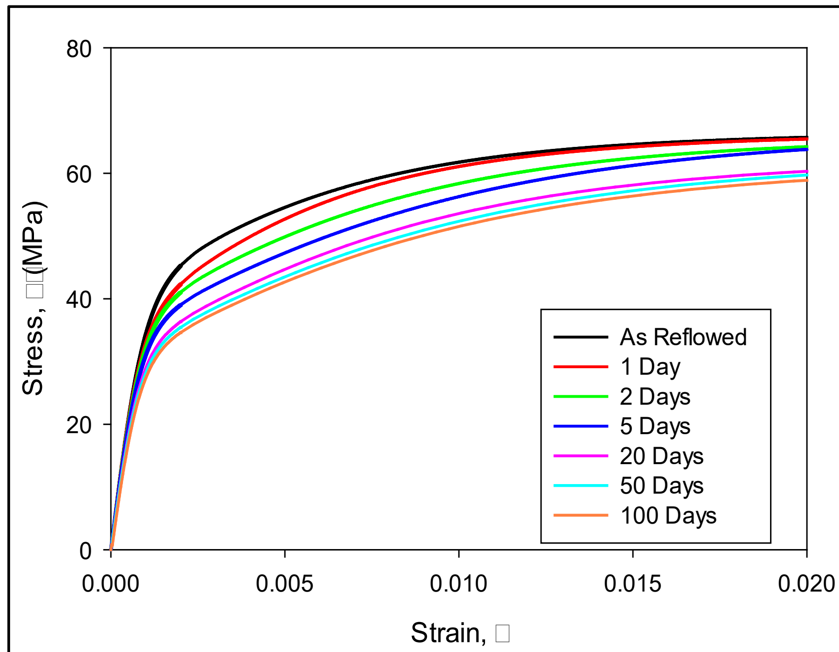

(b) Slow Thermal Ramping

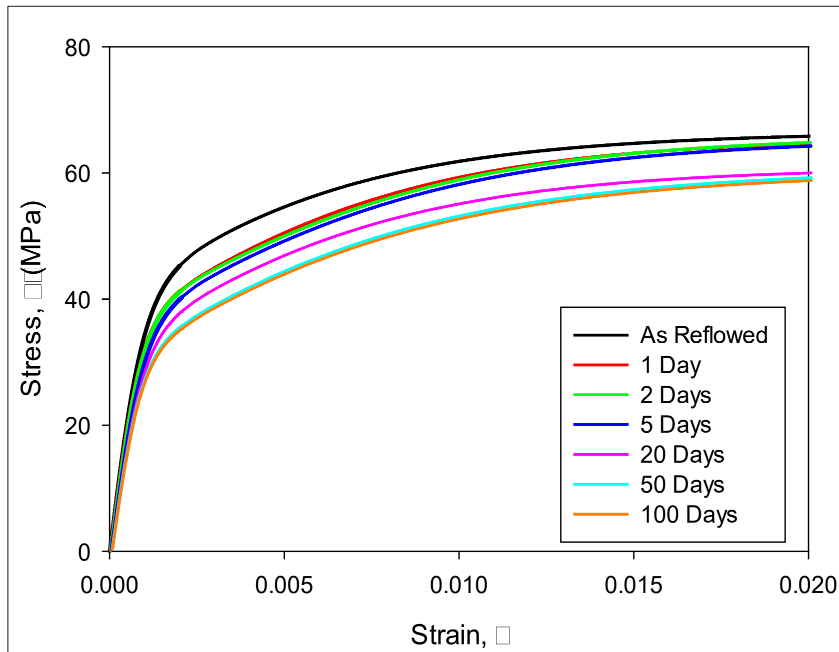

(c) Thermal Shock

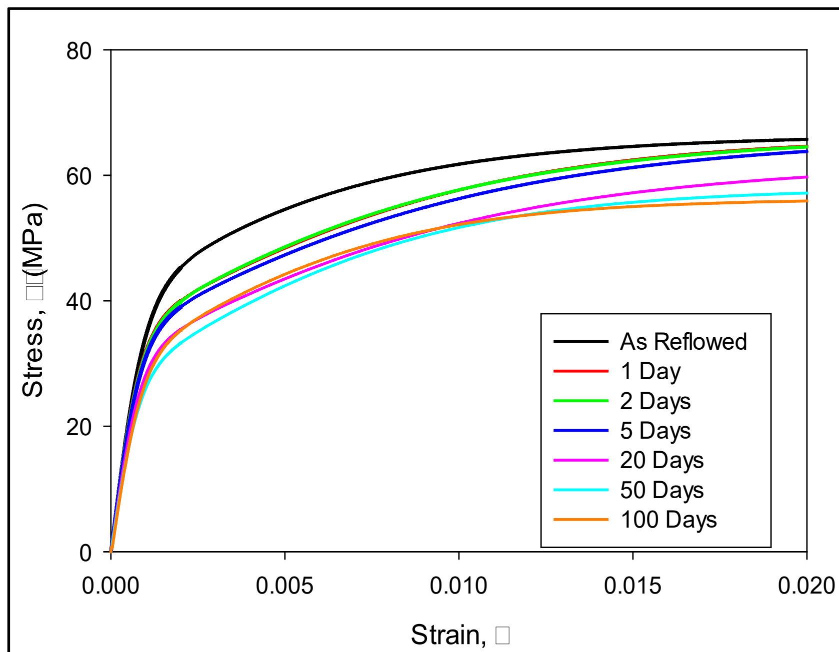

(d) Slow Thermal Cycling

Figure 5.1 Stress-Strain Behavior of SAC+Bi Under Different Thermal Exposures

Table 5.3 Mechanical Property of SAC+Bi Solder Under Different Thermal Exposures

Thermal Exposure		Effective Elastic Modulus, (GPa)	% Change	UTS (MPa)	% Change	YS (MPa)	% Change
None	0 Day	45.17	0.0	65.47	0.0	49.70	0.0
Aging	1 Day	44.31	1.90	65.10	0.57	43.00	13.4
	2 Days	44.02	3.72	64.25	1.86	42.50	14.5
	5 Days	42.14	6.71	63.00	3.77	41.60	16.3
	20 Days	41.49	8.14	60.17	8.09	40.75	18.0
	50 Days	39.39	12.8	59.17	9.62	40.37	18.8
	100 Days	38.90	13.9	58.50	10.6	40.00	19.5
Slow Thermal Ramping	1 Day	44.92	0.55	65.06	0.63	49.00	1.41
	2 Days	44.19	2.17	64.93	0.83	43.28	12.9
	5 Days	43.43	3.85	63.93	2.35	42.07	15.3
	20 Days	40.76	9.76	61.70	5.75	40.00	19.5
	50 Days	39.55	12.44	60.40	7.74	39.10	21.3
	100 Days	38.50	14.76	59.57	9.01	38.10	23.3
Thermal Shock	1 Day	44.87	0.66	65.03	0.67	45.81	7.82
	2 Days	44.16	2.24	64.54	1.42	44.50	10.5
	5 Days	42.36	6.22	63.80	2.55	41.70	16.1
	20 Days	39.22	13.1	59.57	9.10	40.80	17.9
	50 Days	38.48	14.8	58.36	10.9	39.00	21.5
	100 Days	37.70	16.5	57.90	11.6	38.70	22.1

Slow Thermal Cycling	1 Day	44.90	0.60	65.08	0.60	46.76	5.91
	2 Days	44.34	1.80	64.30	1.80	44.86	9.72
	5 Days	43.21	4.34	64.41	1.62	42.43	14.7
	20 Days	38.14	15.6	56.27	14.1	40.81	18.0
	50 Days	36.75	18.6	55.10	15.8	38.50	22.6
	100 Days	35.80	20.7	54.34	17.0	37.50	24.7

5.4 Comparison Between Aging and Different Thermal Exposures

Figure 5.2 (a-f) represent the comparisons of stress-strain results for 1, 2, 5, 20, 50, and 100 days between aging and different thermal exposures. In these plots, the black curve shows the result for as reflowed (no aging or cycling), while the red, green, dark blue, cyan curves show the exposure to pure aging, slow thermal ramping, thermal shock, and slow thermal cycling, respectively. From these plots it can be inferred that stress-strain properties did not change significantly up to 5 days exposures. After 20 days of exposure small change can be observed under isothermal aging and other thermal exposures. But the change was higher under slow thermal cycling which was indicated by cyan color curve. Even though the change was small but stress-strain properties change was smaller under isothermal aging which is noticeable (red curve on top) after 100 days of exposure.

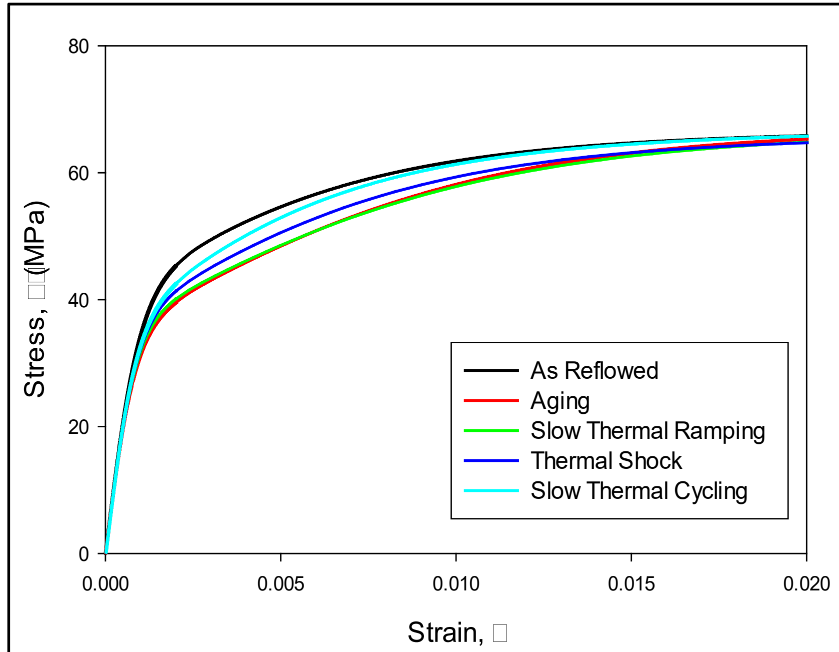

(a) 1 Day Result

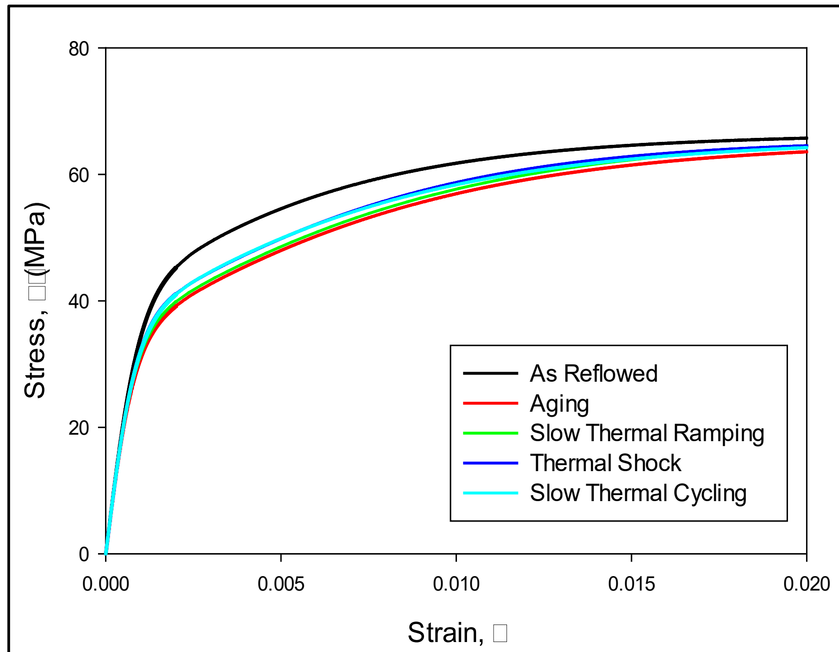

(b) 2 Days Result

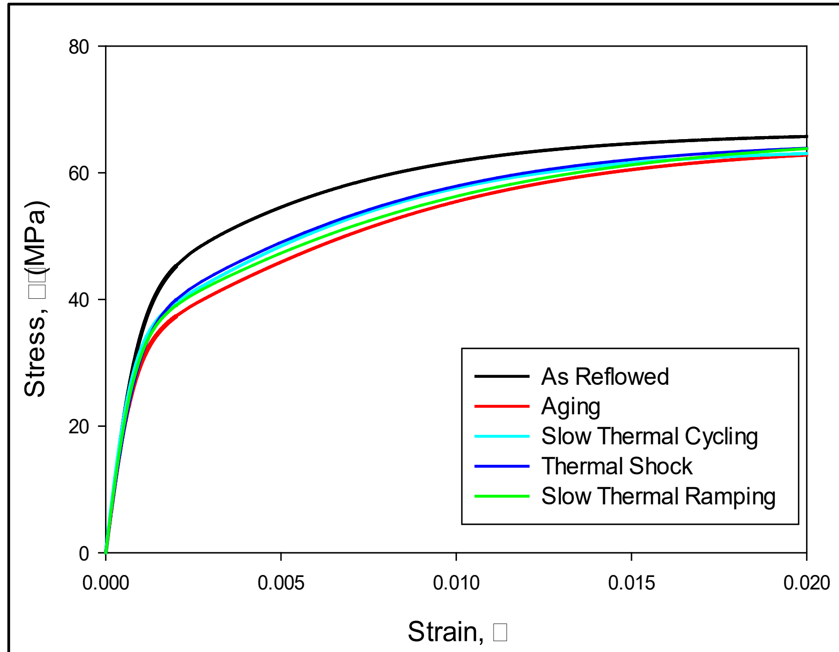

(c) 5 Days Result

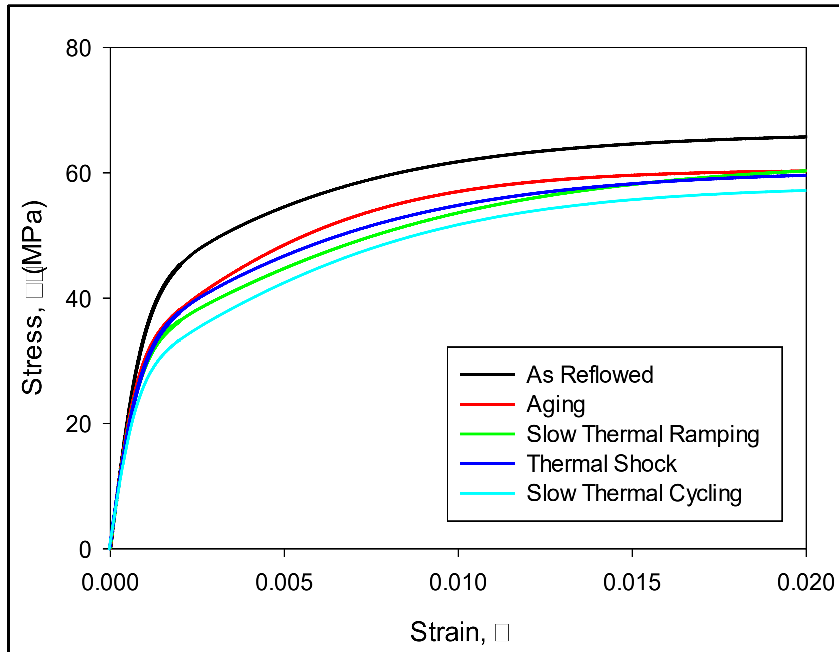

(d) 20 Days Result

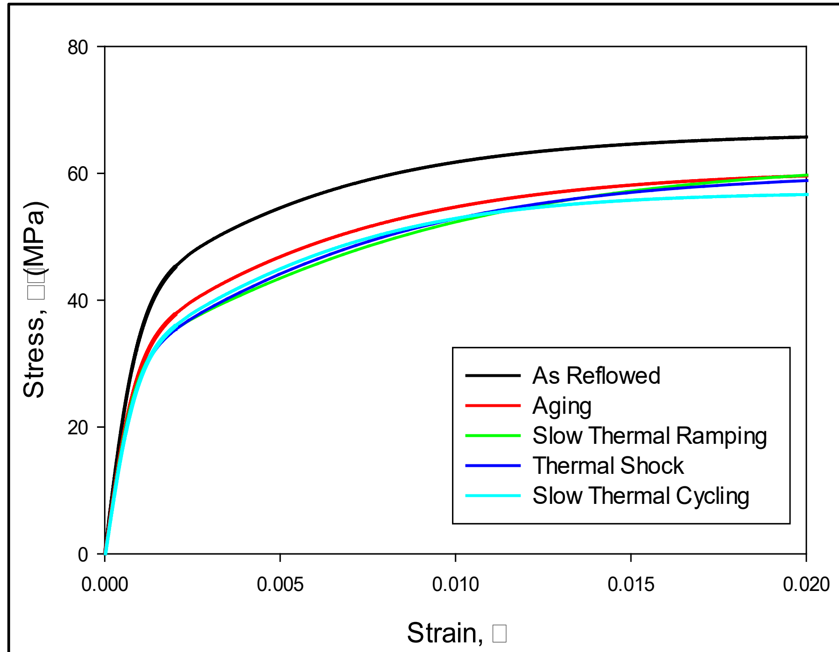

(e) 50 Days Result

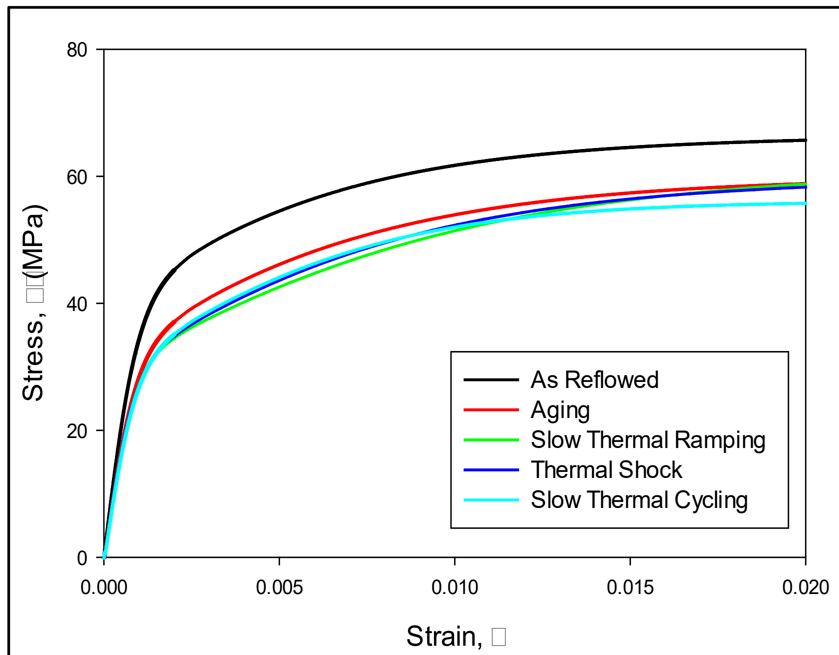

(f) 100 Days Result

Figure 5.2 Comparison of Stress-Strain Behavior of SAC+Bi

5.5 E, UTS, and YS Evolution of SAC+Bi Solder with Exposure Time

Figure 5.3 (a-c) show the evolution of E, UTS, and YS under aging and different thermal cycling conditions. From these plots, it can be inferred that, E, UTS, and YS degrade exponentially with elapsed time. Initially, the degradation rate was very insignificant until 5 days of exposure irrespective to the thermal loading conditions. After 5 days, small degradation in E, UTS, and YS was observed under all the thermal cycling conditions. Also, after 20 days, the degradation starts to slow down. The degradation rate in E, UTS, and YS was slightly higher in slow thermal ramping, thermal shock, as well as slow thermal cycling compared to aging after 20 days of exposure. After 100 days of exposure the degradation of stress-strain properties was small under isothermal aging compared to other thermal exposures presented by red colors in these plots. But the degradation was slightly higher under slow thermal cycling (cyan color curve) compared to the other thermal exposures.

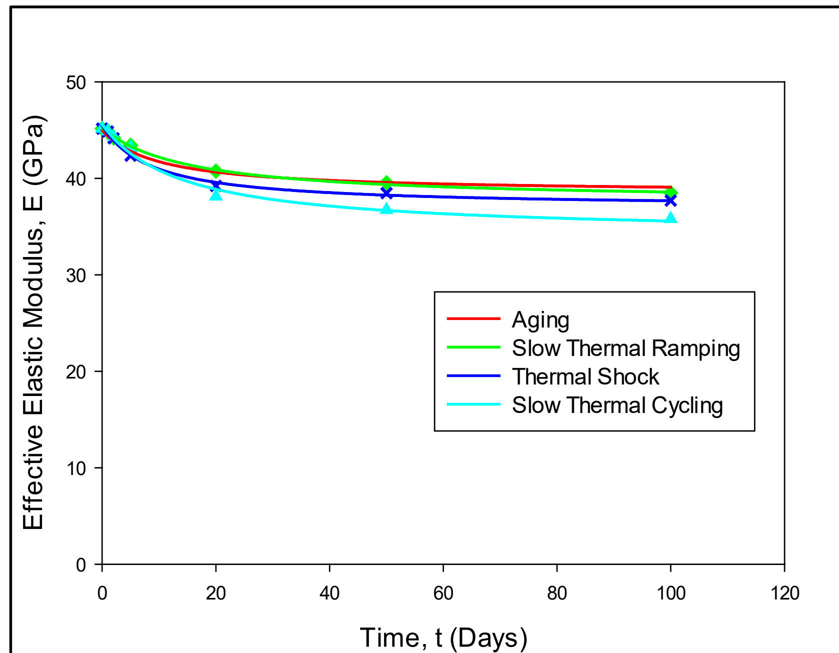

(a) Effective Elastic Modulus

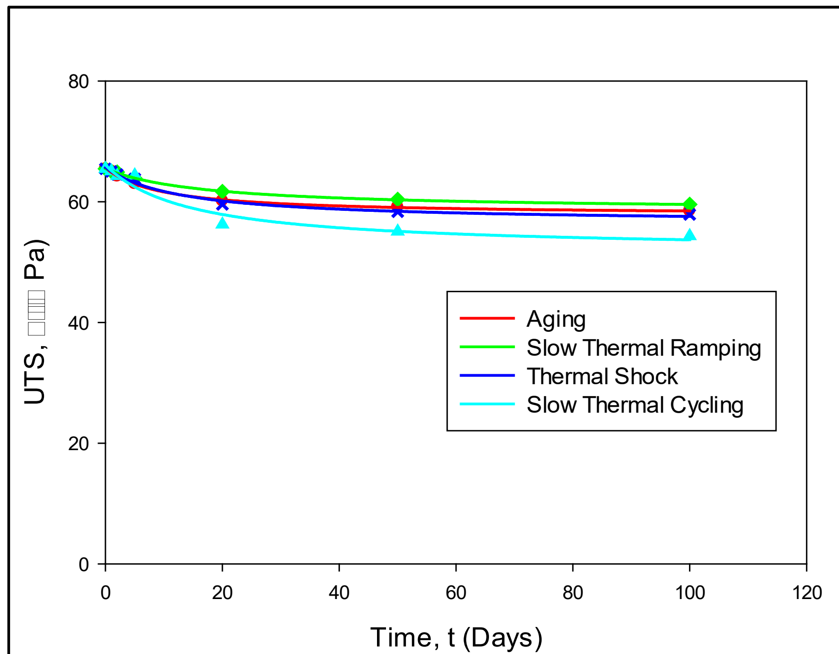

(b) UTS

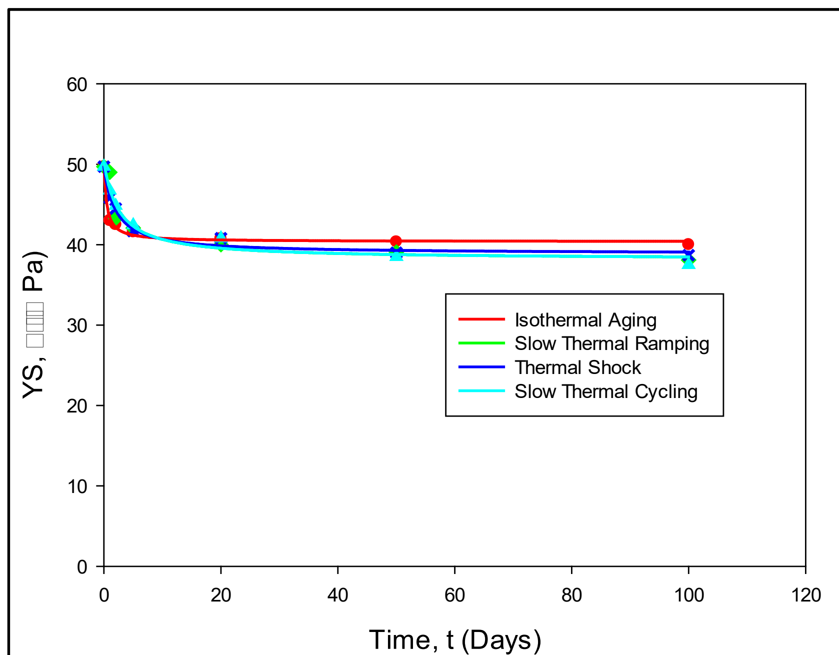

(c) YS

Figure 5.3 Tensile Properties Evolution Under Different Thermal Exposure

5.6 Creep Test Matrix of SAC305 Solder Under Different Thermal Exposures

A large test matrix of experiments was studied here for determining creep behavior of SAC+Bi solder material under different thermal exposures. Similar condition applied here as mentioned in chapter 4. The test matrix is shown in Table 5.4.

Table 5.4 Creep Test Matrix of SAC+Bi Solder Material

Thermal Exposure	Time (Days)	Applied Stress		
		10 MPa	12 MPa	15 MPa
None	0	√	√	√
Aging	1	√	√	√
	2	√	√	√
	5	√	√	√
	20	√	√	√
Slow Thermal Ramping	1	√	√	√
	2	√	√	√
	5	√	√	√
	20	√	√	√
Slow Thermal Cycling	1	√	√	√
	2	√	√	√
	5	√	√	√
	20	√	√	√

5.7 Creep Response of SAC+Bi Solder Under Different Thermal Exposures

Figure 5.4 (a-c) depict the evolution of creep response of SA+Bi solder material under isothermal aging for 0, 1, 2, 5, and 20 days at fixed stress levels 10, 12, and 15 MPa, respectively. In these plots, each curve was fitted by equation 3.4 (chapter 3) to obtain the "average" of recorded experimental strain-time data. The black, red, green, blue, and cyan curves show the average strain-time data for 0, 1, 2, 5, and 20 days of isothermal aging, respectively. It can be observed from these plots that secondary creep strain rate did not change significantly with exposure time for any stress level under isothermal aging. For example, secondary creep strain rate increased only 3X, 2X, and 2X (Table 5.5) under isothermal aging after 20 days of exposure at stress level 10, 12, and 15 MPa respectively.

An analogous plot of slow thermal ramping is shown in figure 5.5 (a-c). In these plots, the black, red, green, and blue, and cyan curves show the results for 0, 1, 2, 5, and 20 days of slow thermal ramping (no high-temperature dwell), respectively. From figure 4.5, it can be observed that the secondary creep strain rate showed similar trend as isothermal aging. But after 20 days of exposure, at higher stress level (15 MPa) secondary creep strain rate under slow thermal ramping increased small in amount compared to isothermal aging (cyan color curve). Figure 5.6 (a-c) represent another analogous plot of slow thermal cycling. Average secondary creep strain rate for aging, slow thermal ramping, as well as slow thermal cycling are tabulated in Table 4.5. Similar phenomena under slow thermal cycling can be observed as aging, and slow thermal ramping in secondary creep strain rate. Even though the change in secondary creep strain rate was not significant but after 20 days of thermal exposures, secondary creep strain rate change was comparatively higher under slow thermal cycling than isothermal aging and slow thermal ramping at 15

MPa. The small change in secondary creep strain rate under isothermal aging and different thermal exposures can be attributed to the lower dislocation movement caused by Bi doping. Moreover, this variation at 15 MPa under slow thermal cycling after 20 days may be due to the additional aging during low to high and high to low temperature ramping which eventually leads to the higher dislocation movement.

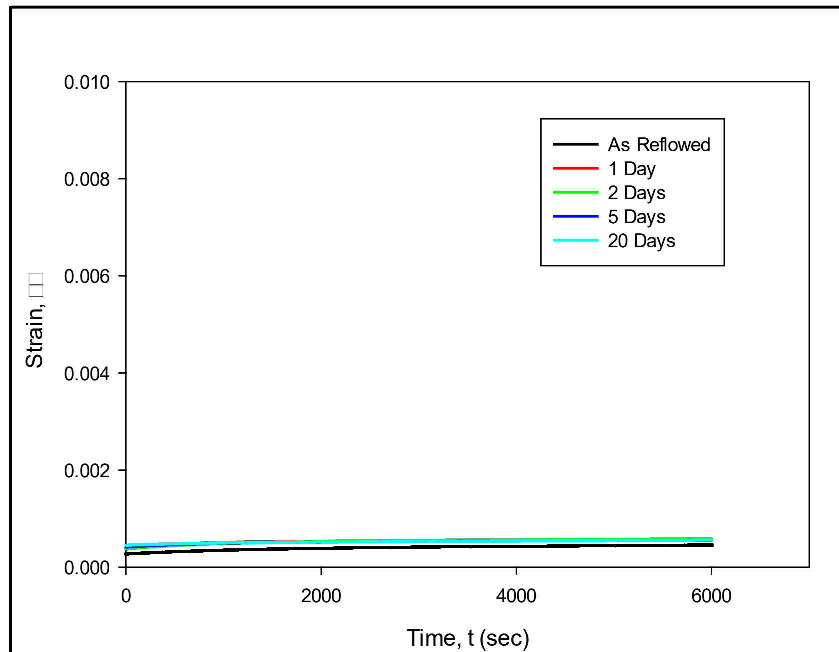

(a) 10 MPa

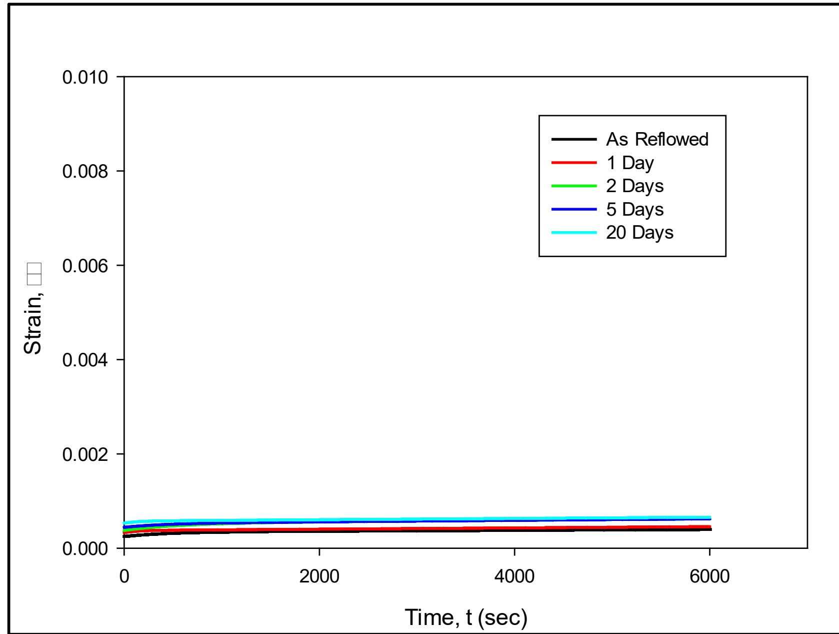

(b) 12 MPa

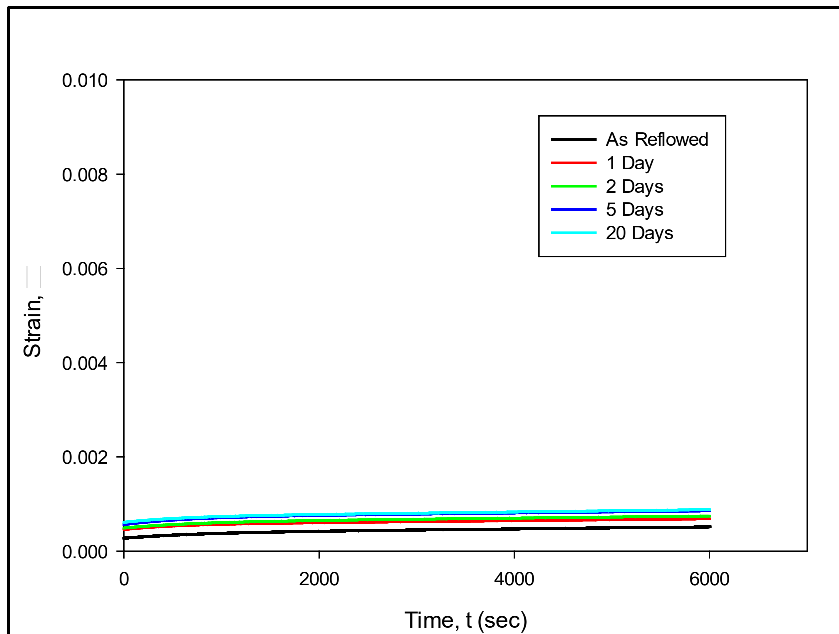

(c) 15 MPa

Figure 5.4 Creep Data of SAC+Bi Under Isothermal Aging

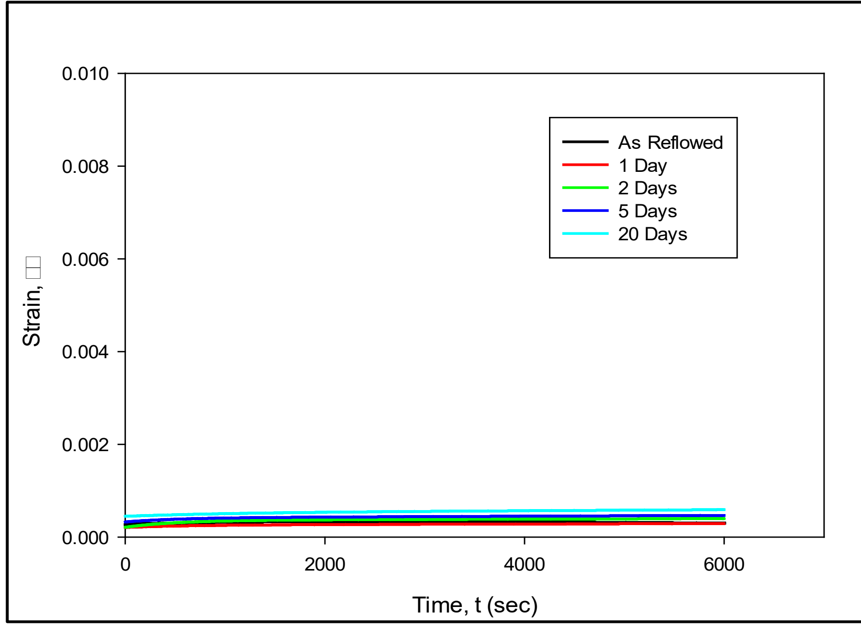

(a) 10 MPa

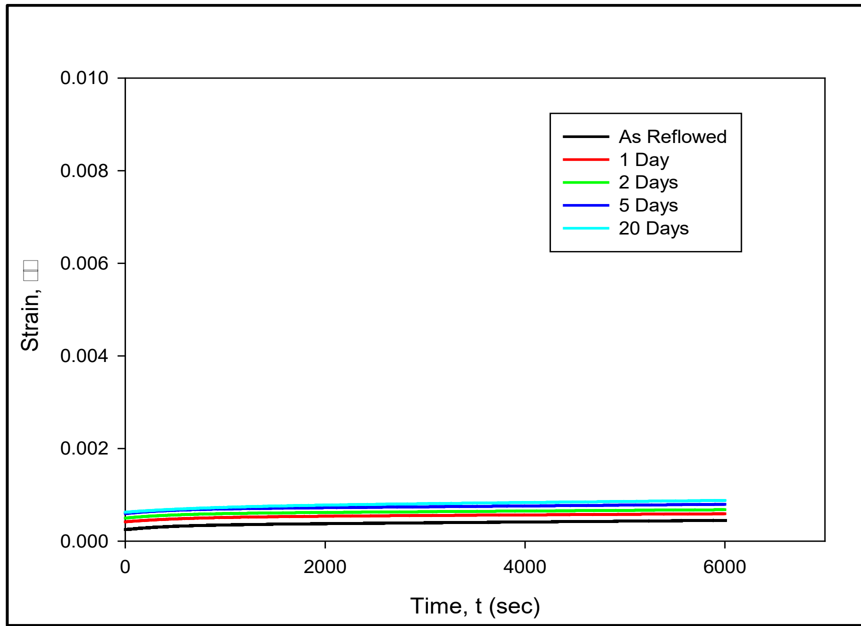

(b) 12 MPa

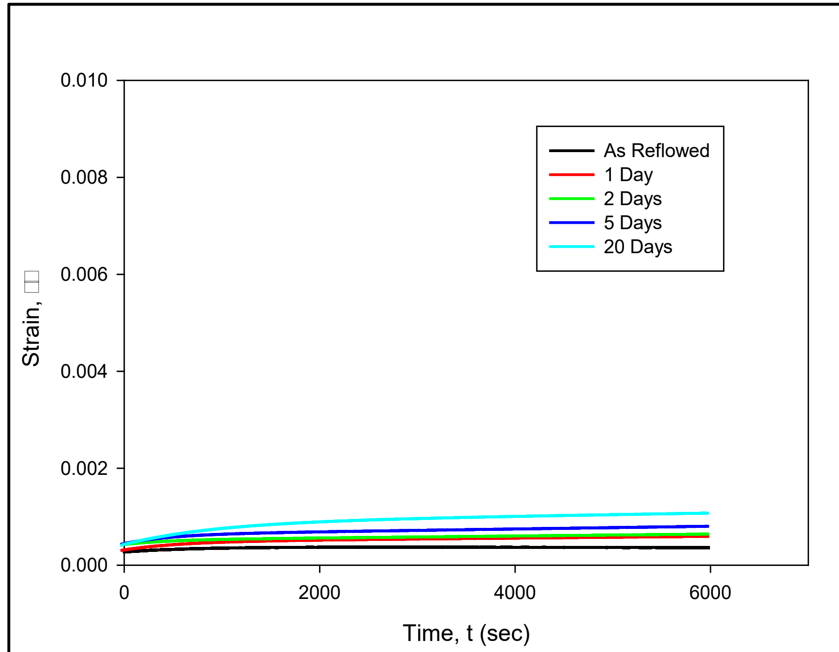

(c) 15 MPa

Figure 5.5 Creep Data of SAC+Bi Solder Under Slow Thermal Ramping

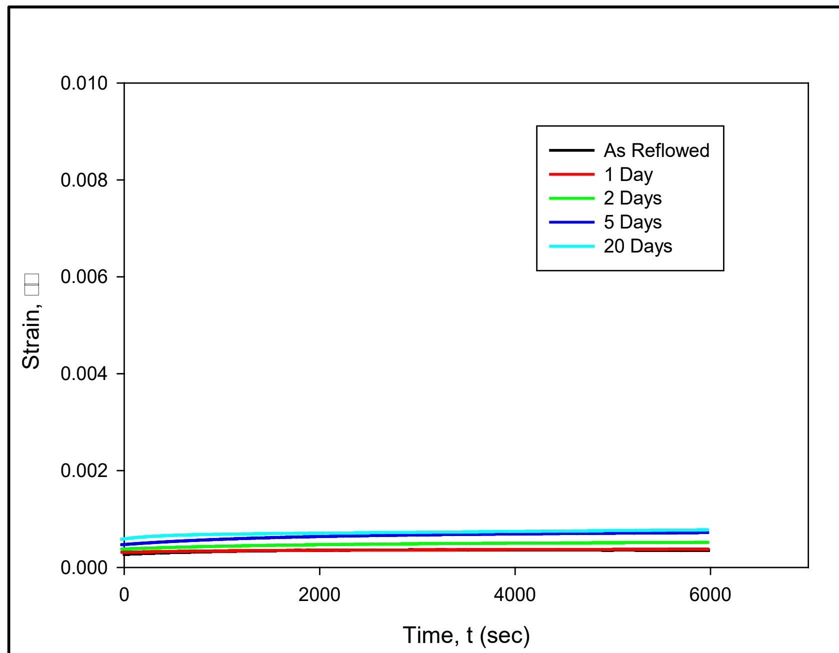

(a) 10 MPa

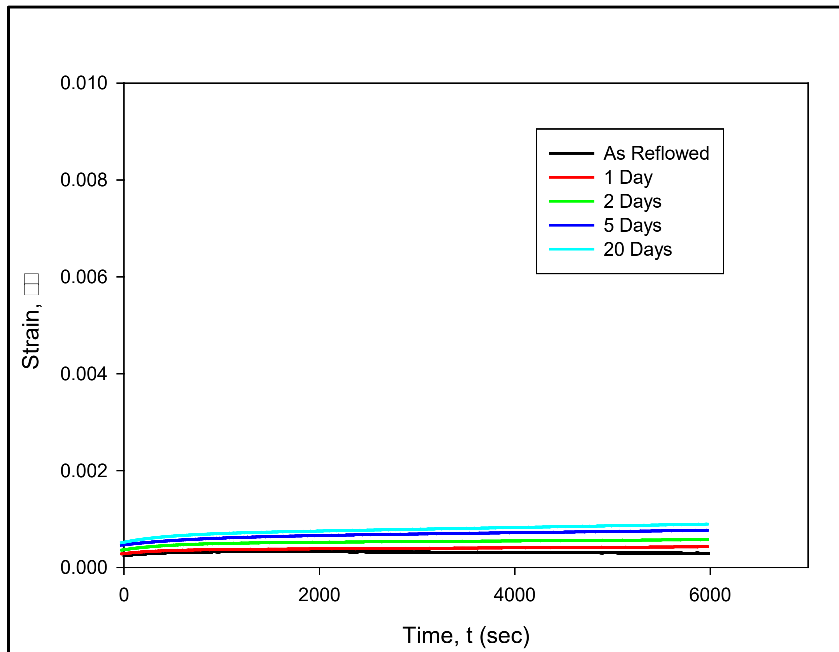

(b) 12 MPa

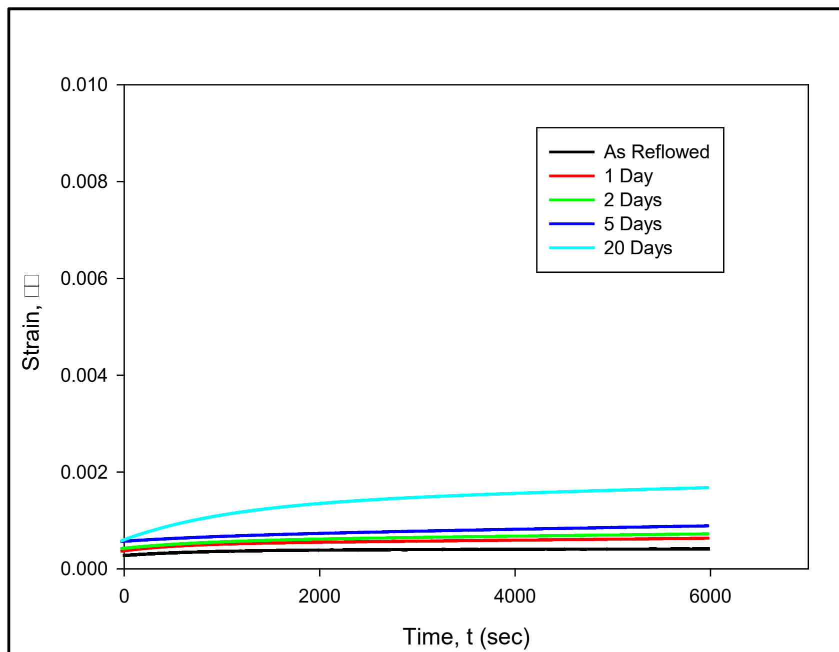

(c) 15 MPa

Figure 5.6 Creep Data of SAC+Bi Under Slow Thermal cycling

Table 5.5 Increase Ratio of Creep Rate at Different Stress Levels and Time

Thermal Exposure	Time (Days)	Secondary Creep Strain Rate (sec^{-1})		
		Increase Ratio at σ= 10 MPa	Increase Ratio at σ= 12 MPa	Increase Ratio at σ= 15 MPa
None	0 Day	1X	1X	1X
Aging	1 Day	2.00 X	1.53 X	1.55 X
	2 Days	2.36 X	1.72 X	1.70 X
	5 Days	2.70 X	1.81 X	1.77 X
	20 Days	3.16 X	1.94 X	1.92 X
Slow Thermal Ramping	1 Day	1.77 X	1.35 X	1.47 X
	2 Days	2.06 X	1.62 X	1.64 X
	5 Days	3.16 X	2.02 X	2.29 X
	20 Days	3.70 X	2.44 X	2.55 X
Slow Thermal Cycling	1 Day	1.57 X	1.28 X	1.59 X
	2 Days	2.17 X	1.56 X	1.86 X
	5 Days	3.73 X	2.87 X	2.74 X
	20 Days	5.96 X	4.04 X	4.10 X

5.8 Comparison Between Aging and Different Thermal Exposures with Elapsed Time

Figure 5.7 was plotted by pulling up the data of 20 Days from figure 5.4a, 5.5a, and 5.6a for the stress level of 15 MPa. Similar phenomenon can be seen in other stress levels. From this plot, it is visible that for a particular stress level secondary creep strain rate increases with any thermal exposures compared to as-reflowed condition. Also, compared to isothermal aging the increase in secondary creep strain rate under slow thermal cycling was higher (solid cyan line). But unlike SAC305 the rate of increase is not significant. For example, after 20 days of exposures, secondary creep strain rate increased ~2x and ~4x for isothermal aging, and slow thermal cycling, respectively.

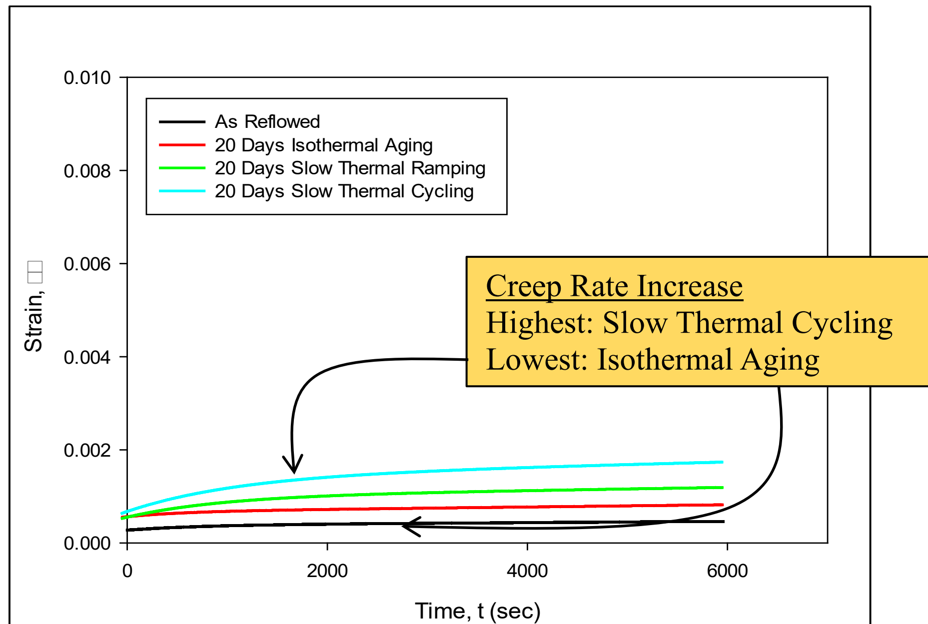

Figure 5.7 Representative Strain vs. Time Plot Under Different Thermal Exposures at Stress level 15 MPa

5.9 Evolution of Creep Response of SAC+Bi Solder Under Different Exposures with Stress Level

Figure 5.8(a-d) show the evolution of secondary creep strain rate with stress level (10, 12, 15 MPa) for 1, 2, 5, and 20 days of isothermal aging, slow thermal ramping, and slow thermal cycling. Vertical axis (log scale) represents secondary creep strain rate. In these plots, the black curve shows the result for as reflowed SAC+Bi solder (no aging or cycling), while the red, green, and cyan curves show pure isothermal aging, slow thermal ramping (STR), and slow thermal cycling (STC), respectively. From all these plots, it is obvious that the secondary creep strain rate change was not significant irrespective to the thermal exposures. For example, after 2 days of exposures, for any stress level three curves (red, green, cyan solid line) merged on top of each other (Figure 5.8 (1-b)). Also, with increased exposure time, secondary creep strain rate change was not significant but after 20 days of exposures secondary creep strain rate change was higher under slow thermal cycling presented by cyan color which is top of red and green color curve (Figure 5.8 (d)). The small change in secondary creep strain rate for SAC+Bi solder material under isothermal aging and other thermal exposures can be attributed to the lower dislocation movement caused by Bi doping. But after 20 days of exposures, higher creep rate change under slow thermal cycling compared to aging and STR was due to the additional aging phenomena occurred during ramping period.

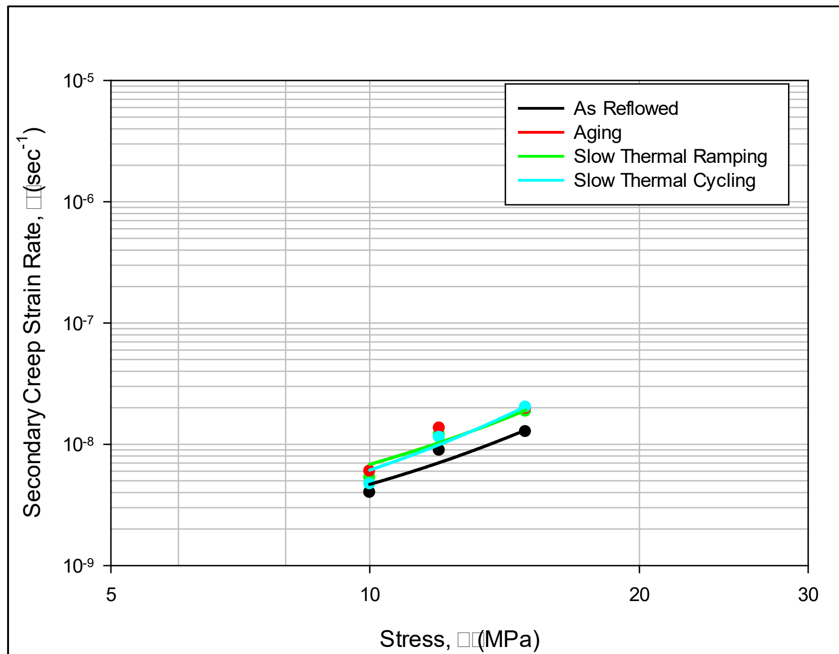

(a) 1 Day Result

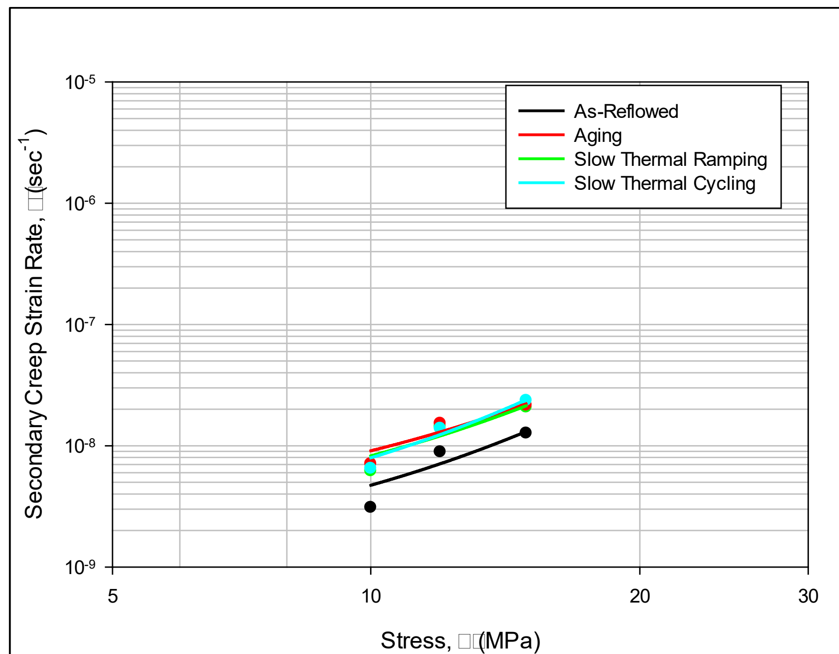

(b) 2 Days Result

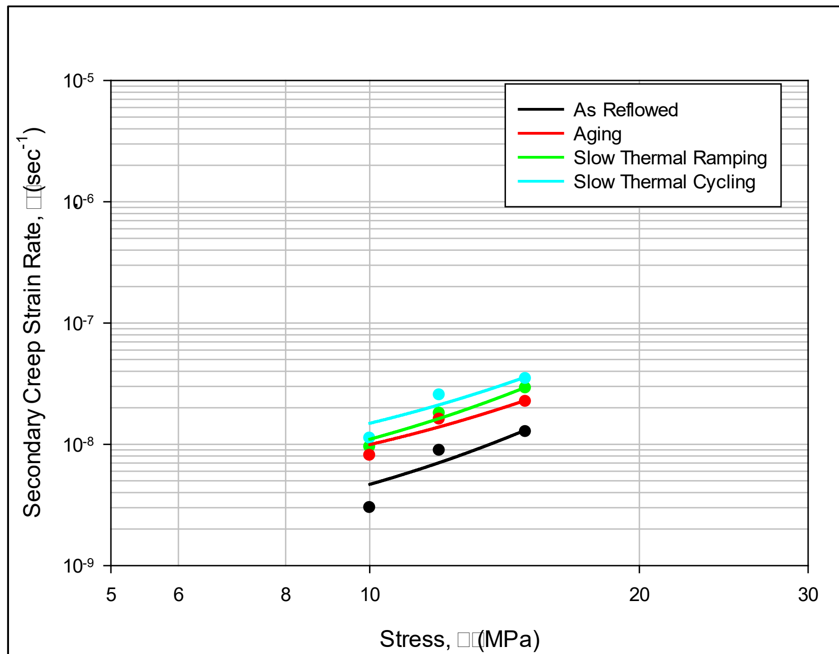

(c) 5 Days Result

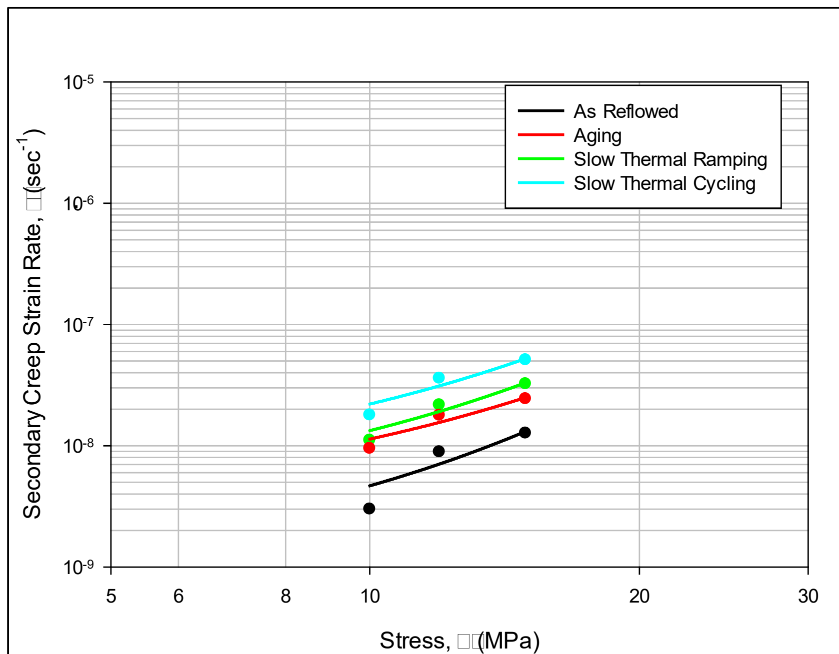

(d) 20 Days Result

Figure 5.8 Creep Rate vs. stress plot of SAC+Bi Under Different Thermal Exposures

5.10 Comparison of Modulus, UTS, and YS Between SAC305 and SAC+Bi Solder Material Under Different Thermal Exposures

Figure 5.9 (a-d) represents the evolution of normalized modulus with exposure time under isothermal aging, slow thermal ramping, thermal shock, and slow thermal cycling, respectively. In these plots, red curve indicates SAC305 solder material whereas blue curve indicates SAC+Bi solder material. For both lead free solder material, it is obvious that normalized modulus evolution showed exponential decay irrespective to the thermal exposures. Also, initially, the degradation rate is higher and slowing down with time. But the normalized modulus degradation was insignificant for SAC+Bi solder material (blue curve) compared to the SAC305 (red curve) solder material under isothermal aging and other thermal exposures. Even though the degradation of SAC+Bi solder is not significant, but the degradation is higher under slow thermal cycling as SAC305 compared to aging and other thermal exposures.

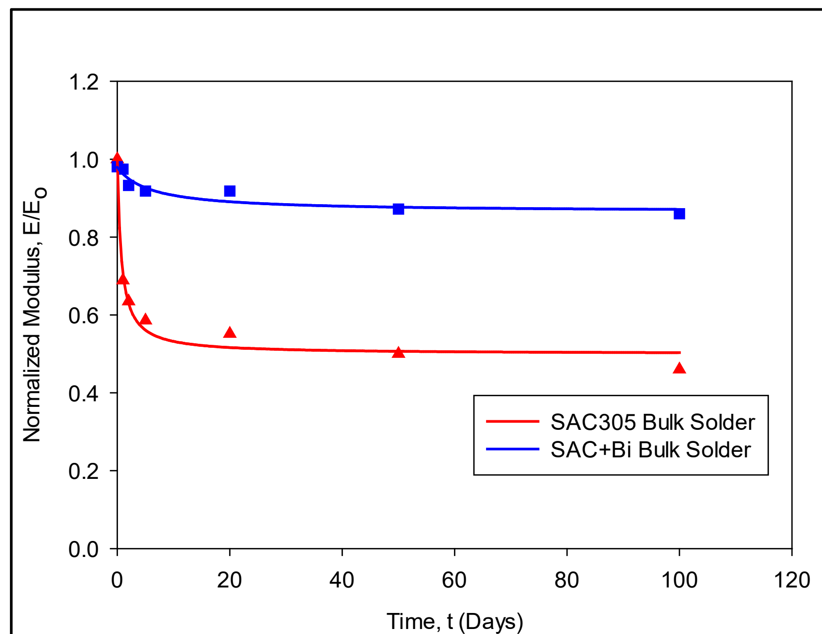

(a) Isothermal Aging

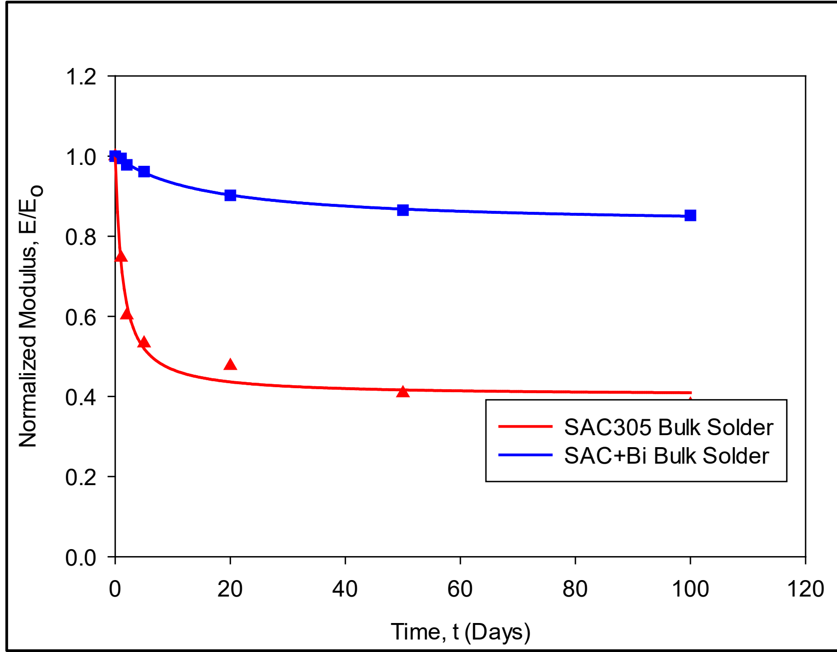

(b) Slow Thermal Ramping

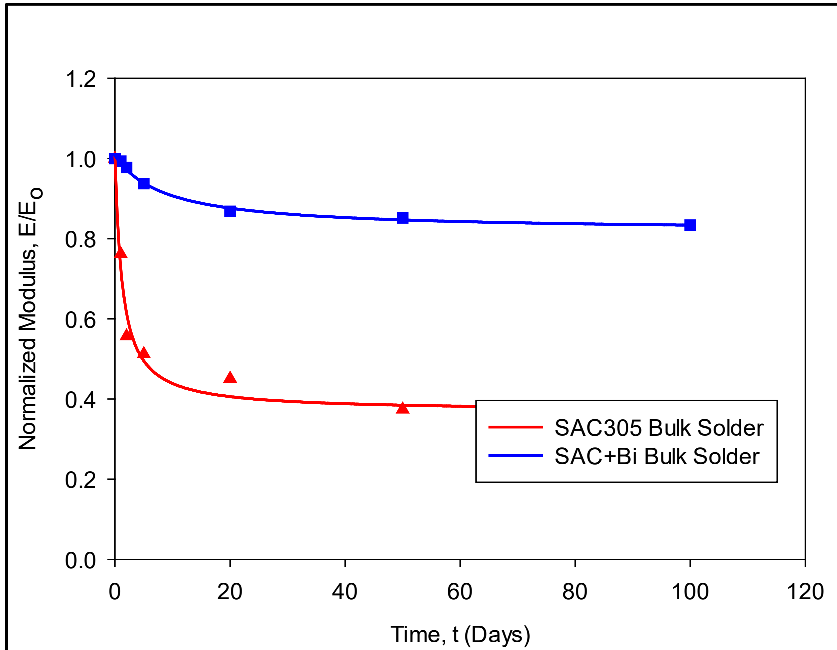

(c) Thermal Shock

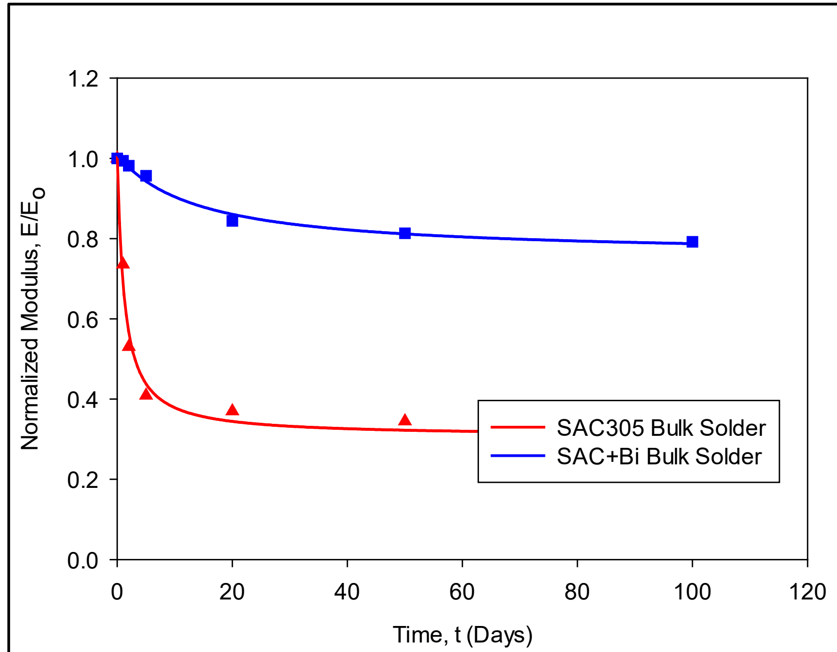

(d) Slow Thermal Cycling

Figure 5.9 Comparison of Effective Elastic Modulus Evolution Between SAC305 and SAC+Bi Solder Material Under Different Thermal Exposures

Figure 5.10 (a-d) and Figure 5.11 (a-d) show the analogous plot of normalized UTS and normalized YS evolution with exposure time under isothermal aging, STR, TS, and STC, respectively. Similar to normalized modulus, both UTS and YS reduced exponentially for both SAC305 and SAC+Bi solder material irrespective to the thermal exposures. Unlike SAC305, the degradation of normalized UTS and YS was not significant for SAC+Bi due to the solid solution hardening effect. But the degradation for both material was higher under slow thermal cycling due to additional aging during ramp period.

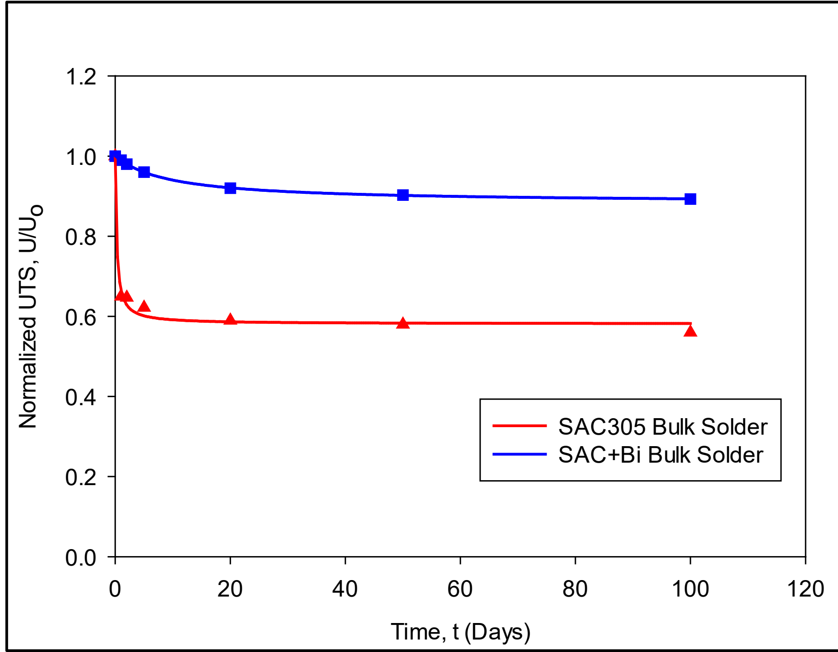

(a) Isothermal Aging

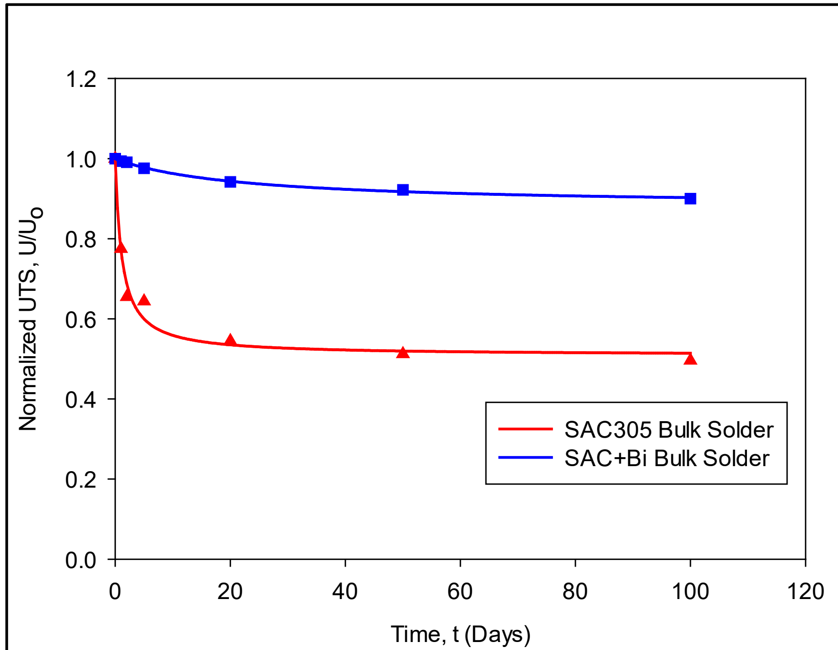

(b) Slow Thermal Ramping

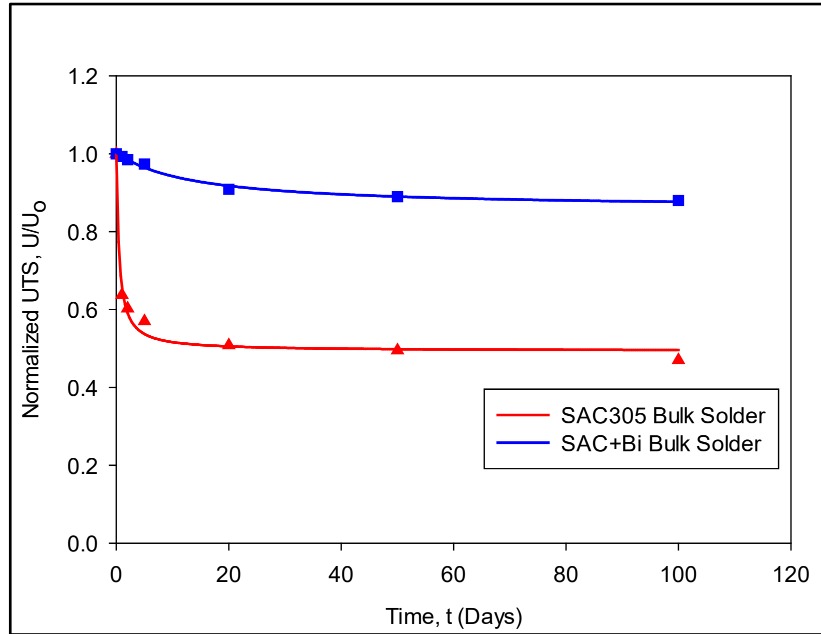

(c) Thermal Shock

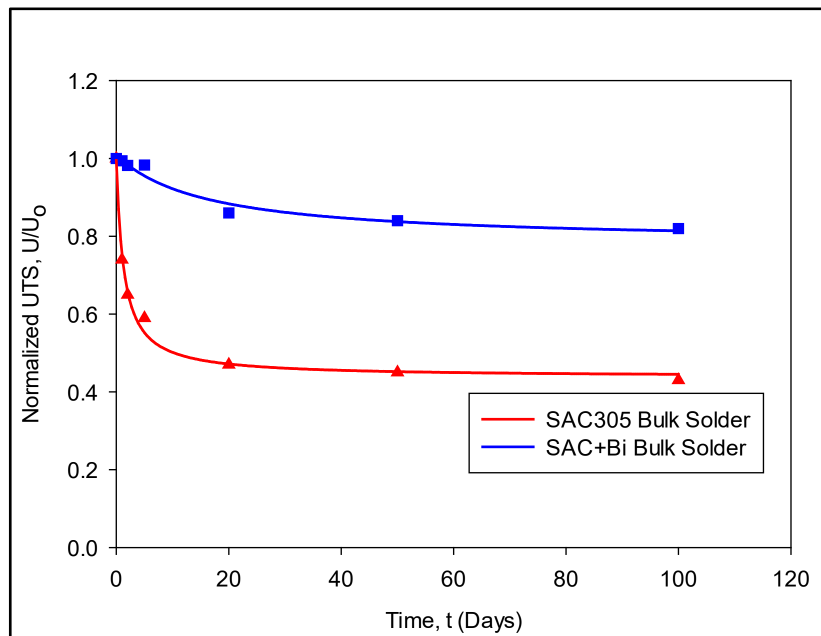

(d) Slow Thermal Cycling

Figure 5.9 Comparison of Ultimate Tensile Strength Evolution Between SAC305 and SAC+Bi Solder Material Under Different Thermal Exposures

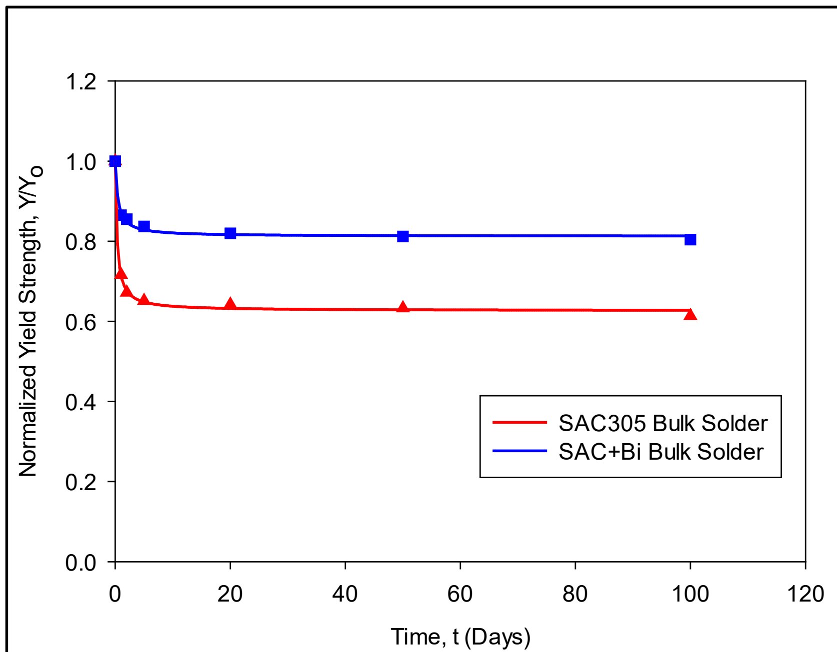

(a) Isothermal Aging

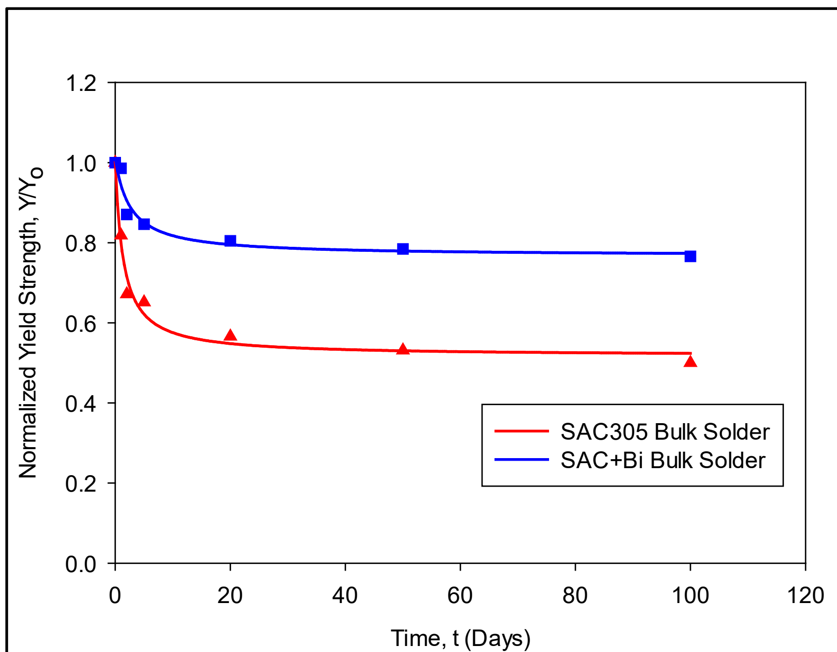

(b) Slow Thermal Ramping

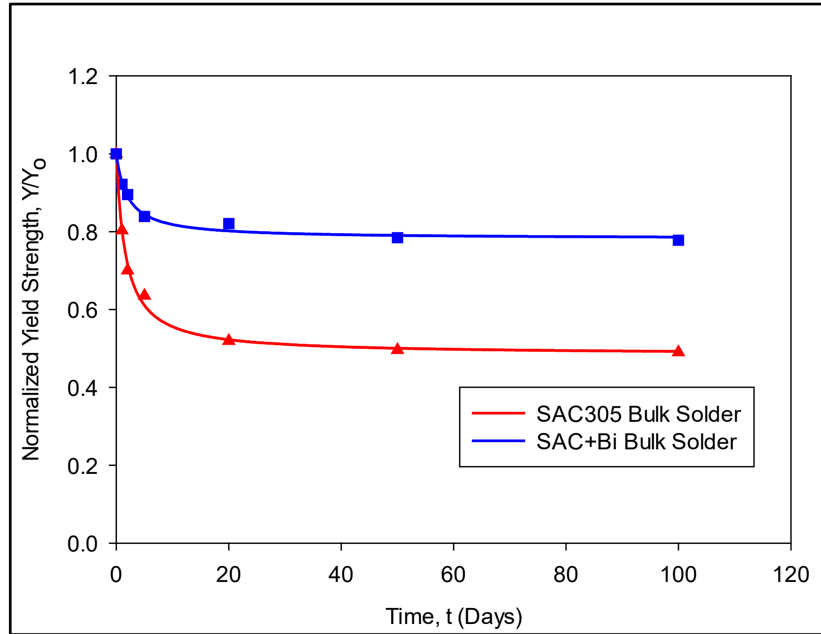

(c) Thermal Shock

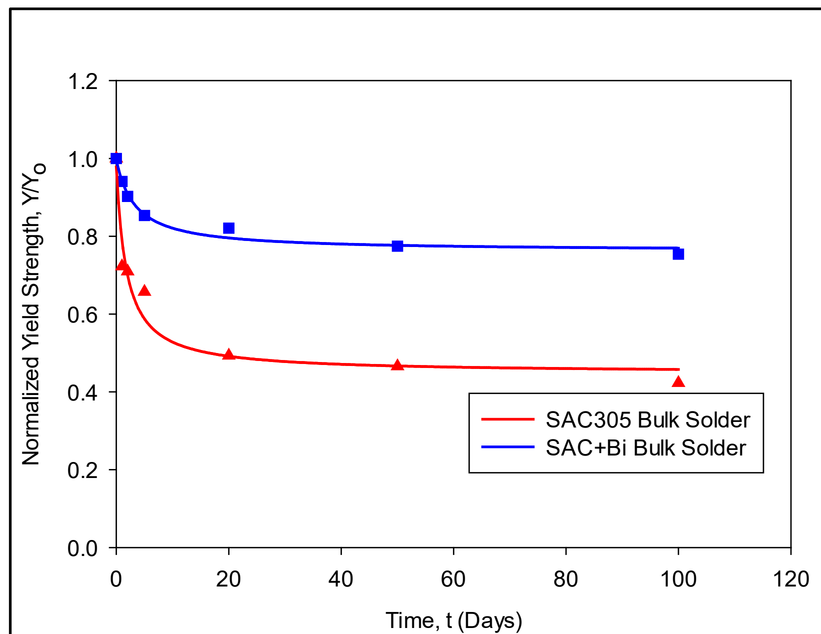

(d) Slow Thermal Cycling

Figure 5.10 Comparison of Yield Tensile Strength Evolution Between SAC305 and SAC+Bi Solder Material Under Different Thermal Exposures

5.11 Comparison of Creep Response Between SAC305 and SAC+Bi Solder Material Under Different Thermal Exposures

Figure 5.11(a-d) show the evolution of secondary creep strain rate with stress level (10, 12, 15 MPa) for 1, 2, 5, and 20 days of isothermal aging for both SAC305 and SAC+Bi solder material. Vertical axis (log scale) represents secondary creep strain rate. In these plots, the dotted line indicates SAC+Bi solder and solid line indicates SAC305 solder material. Also, black line indicates (both solid and dotted) as reflowed condition and red line indicates preconditioned. From these plots, it is clear that the secondary creep strain rate change of SAC305 with stress level was exponential whereas for SAC+Bi, it was almost linear. Secondary creep strain rate changes with exposure time for SAC+Bi solder material, but the change was insignificant compared to SAC305 solder material. For example, after 20 days of exposures, the gap between black solid line and red solid line increased significantly (figure 5.11(d)). It indicates the increase of creep rate of SAC305 solder with stress level. But after 20 days of thermal exposures, the gap between black dotted line (as reflowed) and red dotted line (preconditioned) did not change which indicates insignificant change in secondary creep strain rate of SAC+Bi solder material with stress level.

Analogous plots have shown in figure 5.12 (a-d) and figure 5.13 (a-d) for slow thermal ramping and slow thermal cycling respectively. Similar phenomena have been observed in these plots. Comparing figure 5.11 (d), 5.12 (d), and 5.13 (d), it can be concluded that for both SAC305 and SAC+Bi, the change in secondary creep strain rate with stress level was higher under slow thermal cycling. But the creep rate change of SAC+Bi is much lower with exposure time and stress level than SAC305 solder.

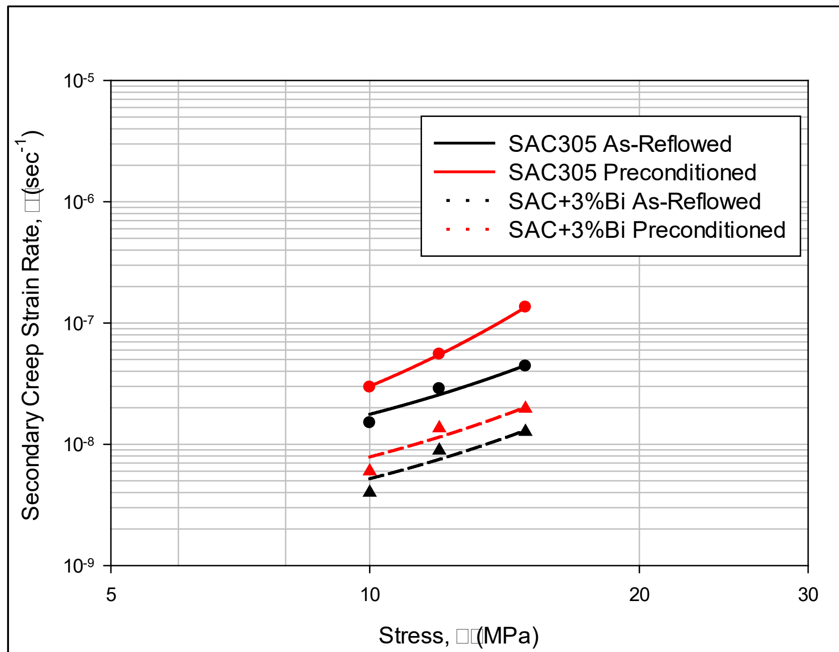

(a) 1 Day Result

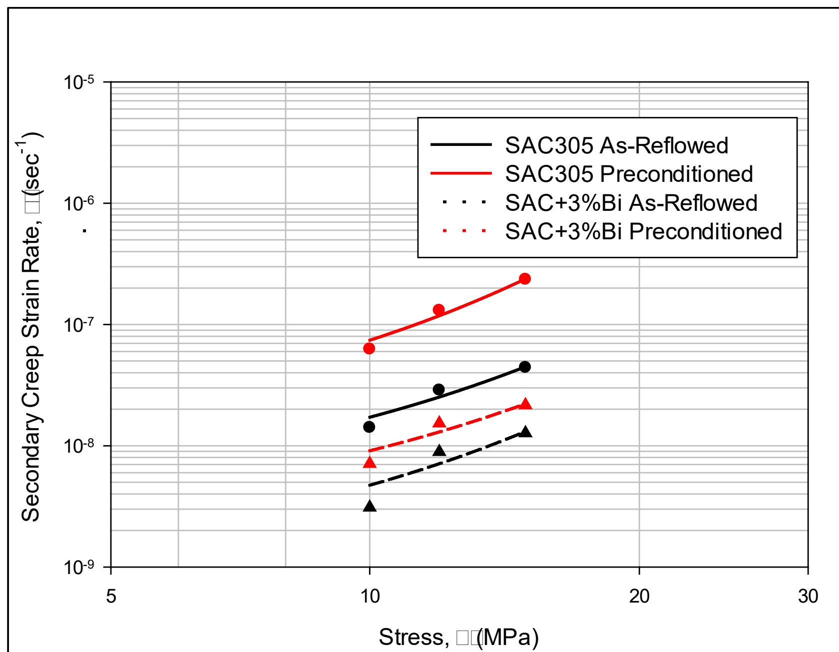

(b) 2 Days Result

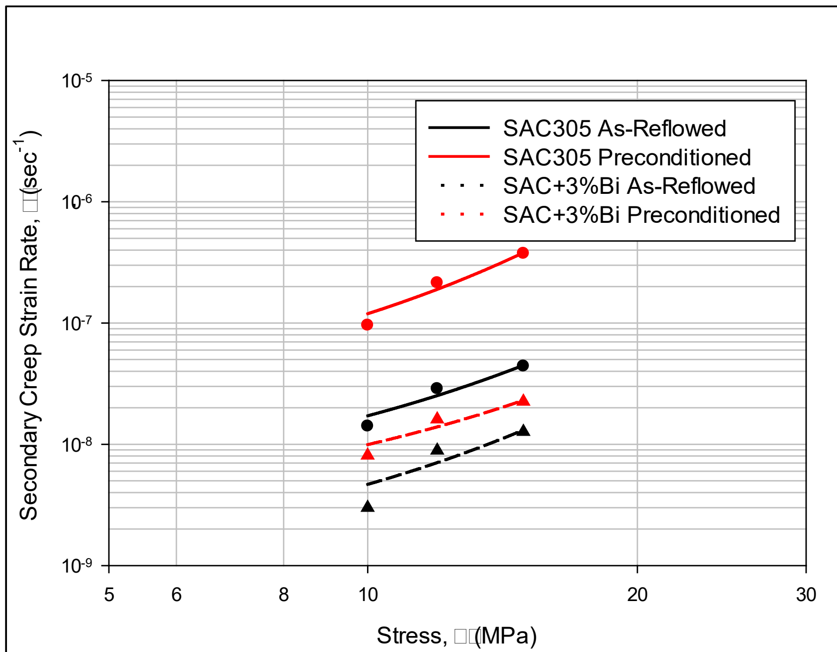

(c) 5 Days Result

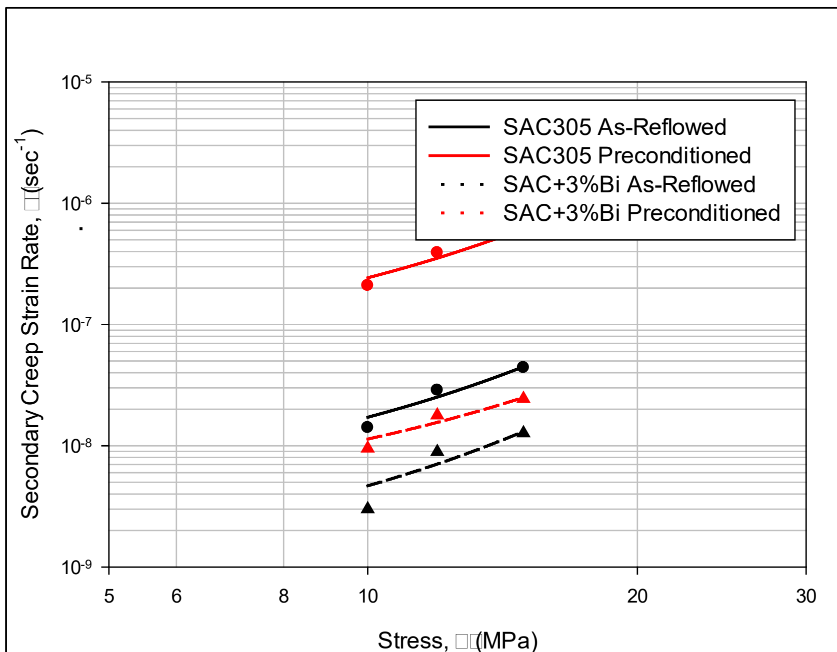

(d) 20 Days Result

Figure 5.11 Creep Rate Evolution of SAC305 and SAC+Bi Under Isothermal Aging

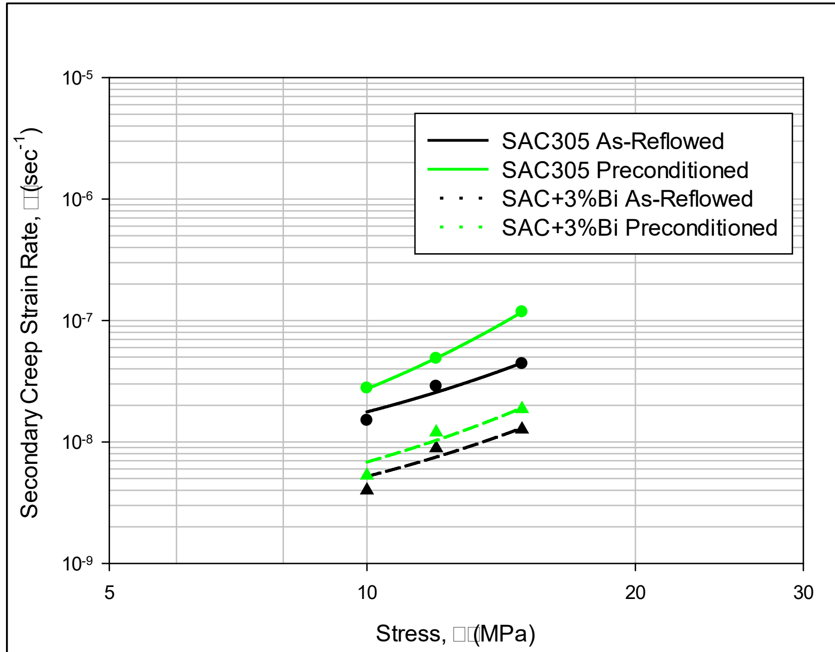

(a) 1 Day Result

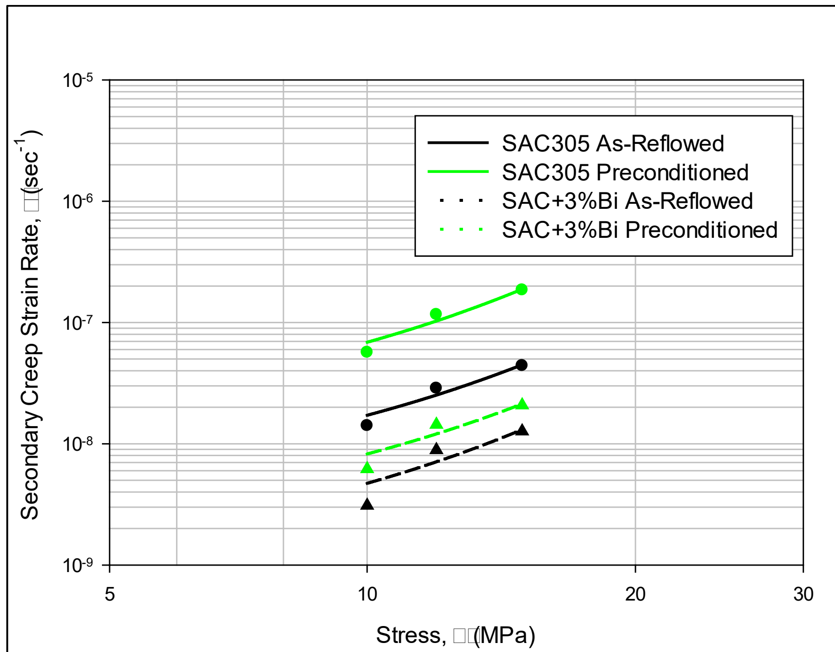

(b) 2 Days Result

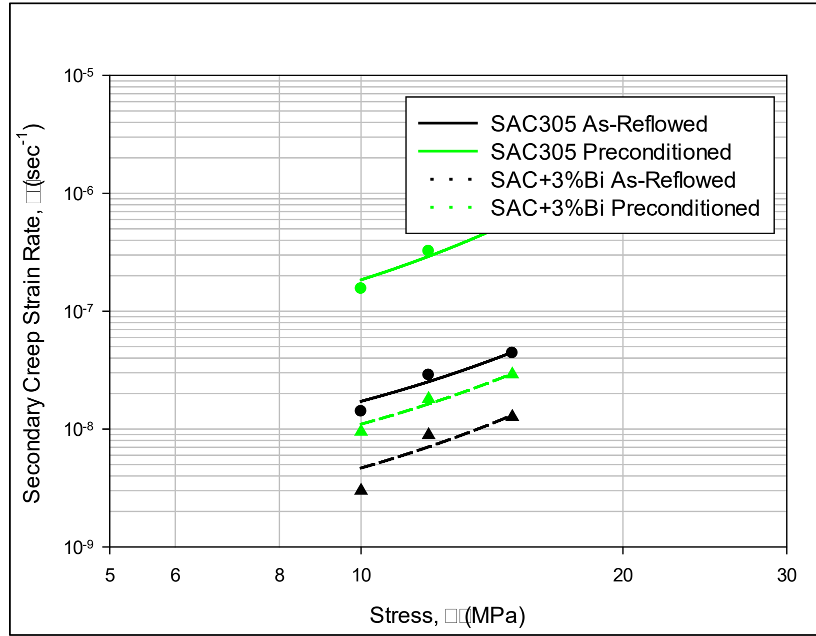

(c) 5 Days Result

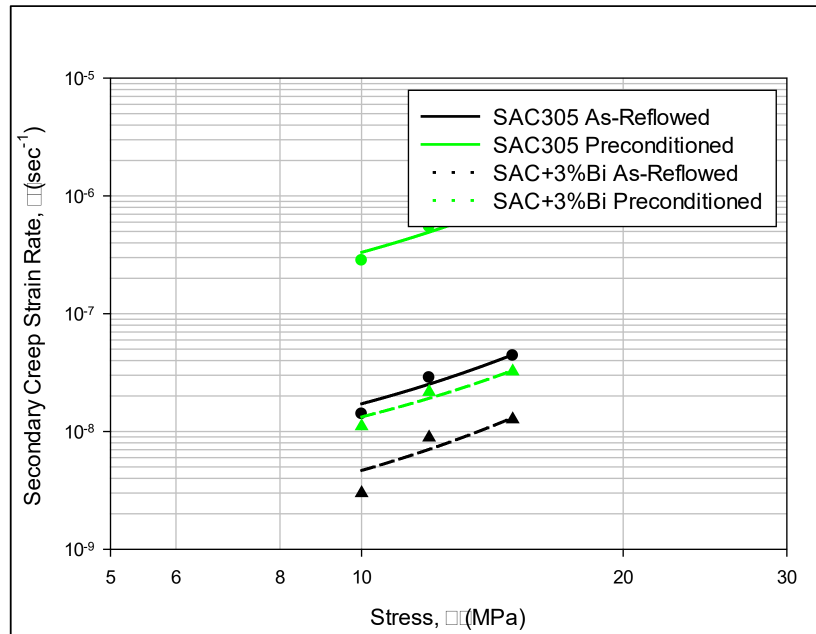

(d) 20 Days Result

Figure 5.12 Creep Rate Evolution of SAC305 and SAC+Bi Under STR

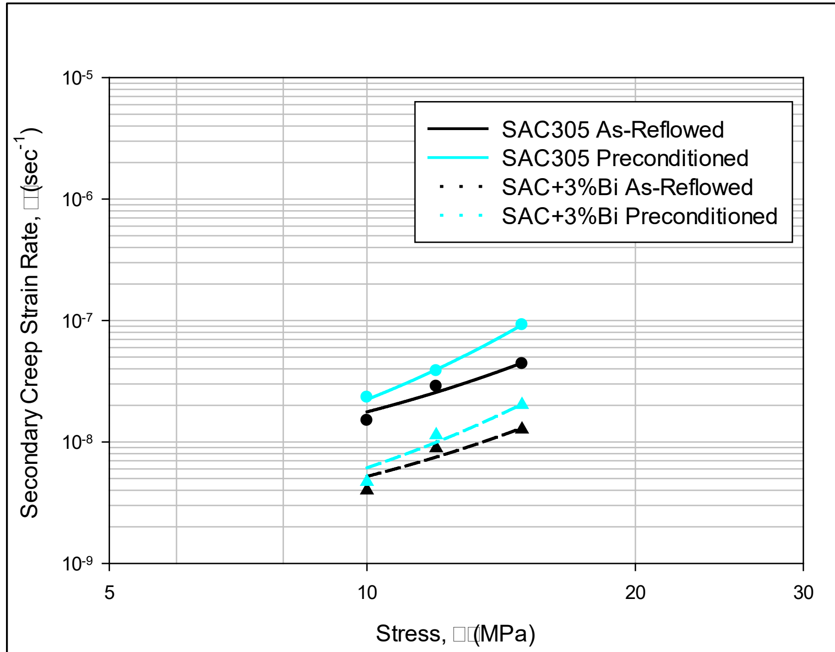

(a) 1 Day Result

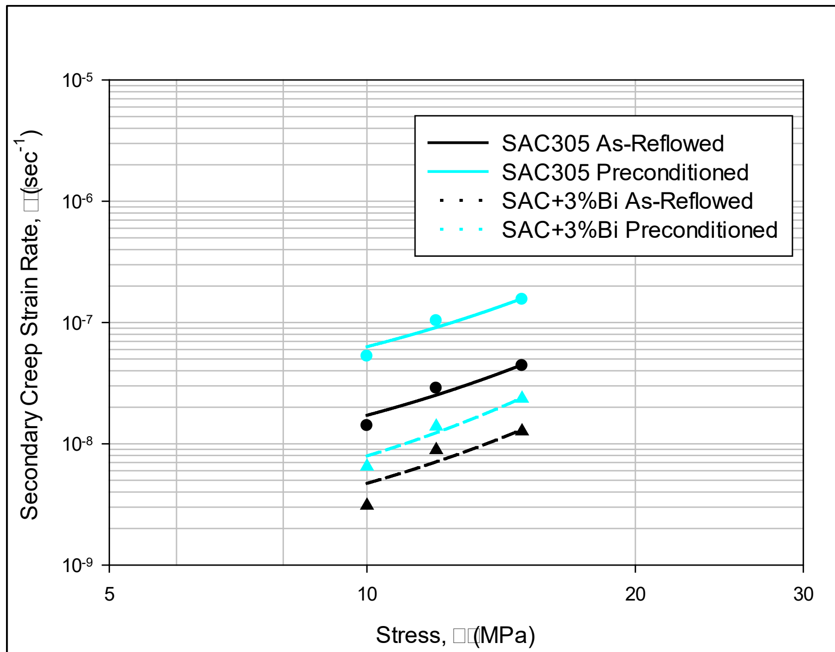

(b) 2 Days Result

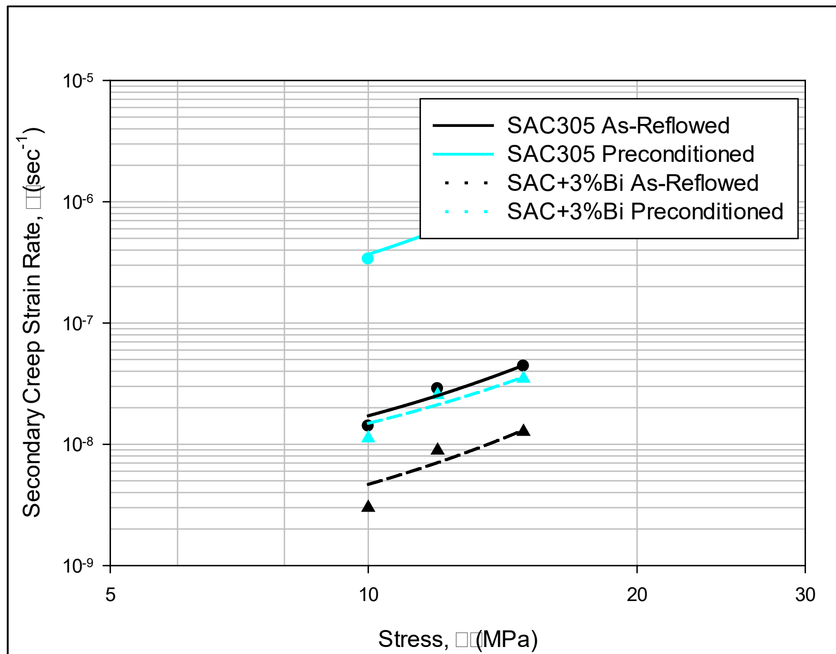

(c) 5 Days Result

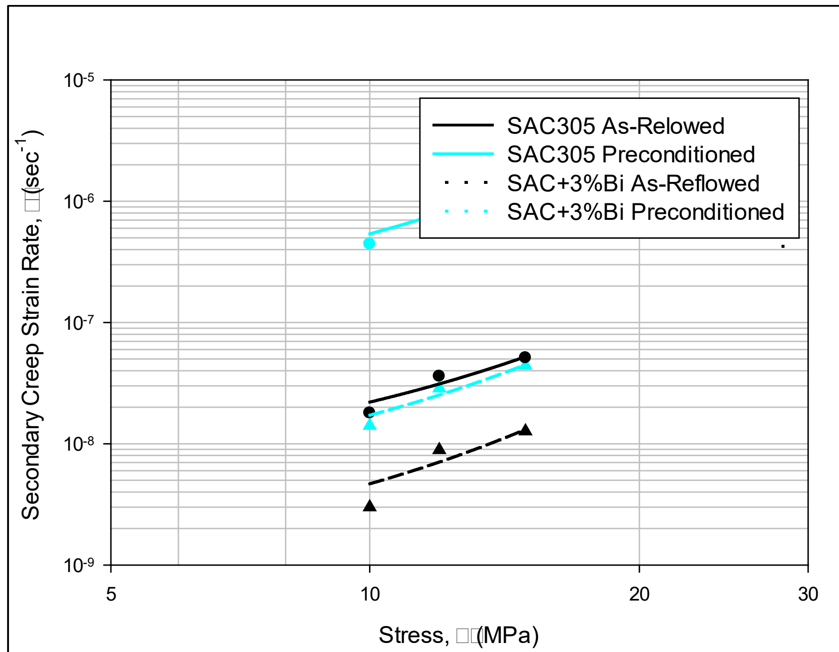

(d) 20 Days Result

Figure 5.13 Creep Rate Evolution of SAC305 and SAC+Bi Under STC

5.12 Summary and Discussion

In this chapter, the Effects of Various Thermal Exposures on the Evolution of the Mechanical Behavior of SAC+Bi Lead Free Solder were Investigated. For mechanical properties extraction, uniaxial test samples have been used. Tensile tests were performed at room temperature and strain rate 0.001 sec^{-1}. Creep tests were performed at three different stress levels such as 10, 12, and 15 MPa. From stress-strain properties, it was found that unlike SAC305, the elasic modulus, ultimate tensile strength, and yield strength of SAC+Bi did not change significantly with any of the thermal exposures. Secondary Creep rate did not increase significantly like SAC305 with exposure time. Little increase has been observed under slow thermal cycling exposures at 15 MPa compared to isothermal Aging. Even though the Degradation of Mechanical Properties (Stress-Strain, Creep Response) of SAC+Bi has not changed significantly, the degradation of thermal cycling with the longest ramp periods has a greater rate compared to the other thermal profiles.

The evolutions of the Mechanical Properties of SAC+Bi and SAC305 Solder Materials were Compared for Various Thermal Exposures in this study. The Mechanical Property Degradations of the SAC+Bi Solder Alloy with Exposure Time were Relatively Small When Compared to Those for the SAC305 Solder Alloy. This was True Irrespective of the Thermal Exposure Chosen. Secondary Creep Rate of SAC+Bi Solder Alloy did not Increase Significantly like SAC305 with Exposure Time. Creep Deformation of SAC+Bi Solder Alloy was Much Lower Than As-Reflowed SAC305 Solder Alloy. After 20 Days of Thermal Exposures under Slow Thermal Cycling, Secondary Creep Strain Rate of SAC+Bi Reaches the As-Reflowed Creep Rate of SAC305 Solder Alloy.

CHAPTER 6

INVESTIGATION ON MECHANICAL PROPERTIES EVOLUTION OF SAC305 AND SAC+Bi SOLDER JOINT BY NANOINDENTATION TECHNIQUE

6.1 Introduction

Electronic devices are subjected to severe conditions during service that exposes solder joints to elevated temperatures. This causes significant change in the performance of SAC solder alloys due to evolution of the microstructure, which consists primarily of β-Sn, eutectic Sn, and Ag–Sn and Cu–Sn intermetallic compounds (IMCs). The entire mechanical properties of the solder joints are dictated by the IMCs, which are generally hard and brittle in nature. Exposure to high temperatures causes thermal coarsening due to which the size of these IMCs grows. Since the mechanical properties of a lead free solder are strongly influenced by its microstructure, hence mechanical response, failure and fatigue behaviors of lead free solder joints in electronic assemblies are affected when subjected to isothermal aging and/or thermal cycling operating conditions. Moreover, additional aging phenomena during ramping from low to high and high to low temperature during thermal cycling can further deteriorate the solder joints since the microstructure is constantly evolving (degrading) with time. This alters the structural reliability of the whole assembly and thus become a concern for the researchers for past decades. Many researchers have studied constitutive and failure behaviors of SAC solder alloys due to

aging affect extensively. But very few studies have been conducted on the effect of thermal cycling on the solder joint.

In this chapter, mechanical behavior evolution of SAC305 (96.5Sn-3.0Ag-0.5Cu) and SAC+Bi (92.5Sn-4.0Ag-0.5Cu-3Bi) solder joints in terms of modulus and hardness under isothermal aging, slow thermal ramping, thermal shock, and slow thermal cycling was investigated using nanoindentation technique. Berkovich pyramidal indenter tip (chapter 1) was used to measure the mechanical properties in this study. Solder joints were extracted from 3x3 BGA having ball diameter of 30 mils. The solder joint used in this study was special type which did not have copper pad on both sides to make sure there is no CTE mismatch during thermal cycling. The purpose was to replicate bulk solder into small scale and make it more realistic. Also, observe the mechanical properties evolution of solder joints at stress free condition. Since the properties of SAC solder joints are highly dependent on crystal orientation, polarized light microscopy was utilized to determine the orientation of the tested joints. For all of the experiments, only single grain solder joints were used to avoid introducing any unintentional variation from changes in the crystal orientation across the joint cross-section. To study the aging and different thermal exposure effect, solder joints were preconditioned for 0, 1, 2, 5, 20, 50, and 100 days at T = 125 °C in a box oven for aging and thermally cycled into a chamber from -40-125ºC. Nanoindentation testing was then performed on the preconditioned specimens to extract the elastic modulus, hardness, and YS. For each thermal exposure 10 indents were made in a row to measure the average property. Throughout this study, a constant force of 30 mN was applied and holding time was maintained as 50 seconds to avoid the creep effect

during unloading. Thermal drift in this study was ≤ 0.05 nm/sec and all the tests were performed at room temperature.

6.2 Sample Preparation for Nanoindentation Technique

Sample grinding, and polishing procedure outlined in chapter 3, section 3.7 and figure 3.23 was followed to prepare samples for nanoindentation experiments. Since the mechanical behavior of solder alloys depends on crystal orientation, the orientation of the SAC305 and SAC+Bi solder joints were initially determined using polarized light microscopy. Only single-grain solder joints were identified and used in this study to avoid any variation in properties associated with different crystal orientation (figure 3.24). Three different solder joints of both SAC305 and SAC+Bi with single grain orientation and uniform IMC distributions were chosen used for the nanoindentation study.

6.3 Room Temperature Nanoindentation System and Test Procedure

The Hysitron TI 950 TriboIndenter system (figure 6.1) was utilized to analyze the global mechanical properties of solder joints and at room temperature. Nanoindentation testing was carried out by selecting arrays of regularly spaced indentations or by selecting random individual locations for indentation. While performing each indentation experiment, the load versus indentation displacement normal to the cross-sectional surface was measured. Peak load was reached at a loading rate of 5 mN/sec, and then the indenter tip was held at the peak load of 30 mN for 50 sec for each individual indent. Finally, the indenter was unloaded at the same rate of 5 mN/sec. The indents were made in 70 μm apart to avoid locations that were deformed plastically by the previous indents. The elastic

modulus of the solder joints was obtained using the approach proposed by Oliver and Pharr by calculating the slope of the load-displacement curve in the unloading region of the test. In all test conditions, as shown in Figure 6.2, the indentation marks were ensured to cover the available phases of the material. Thus, the nanoindentation tests represents the global properties of the solder joints, instead of the localized mechanical properties of the phases (β-Sn dendrites or Ag_3Sn and Cu_6Sn_5 IMC particles). To maintain accuracy of the results, indenter axis calibration followed by hardness and elastic modulus measurement calibrations were performed on standard fused silica and quartz samples. Moreover, every test included a drift measurement and correction prior to the main indent that minimized the effects due to temperature fluctuations.

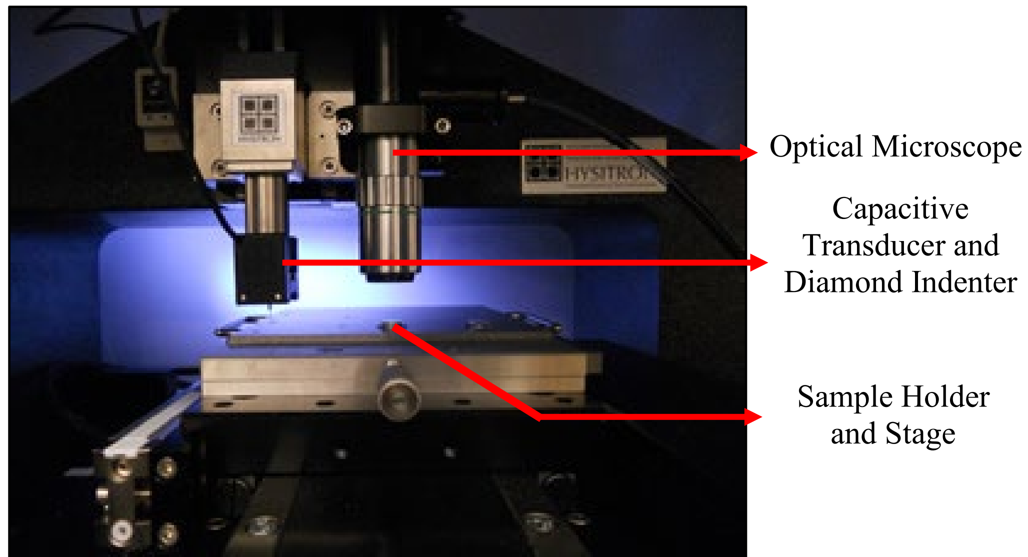

Figure 6.1 Nanoindentation System for Room Temperature Testing

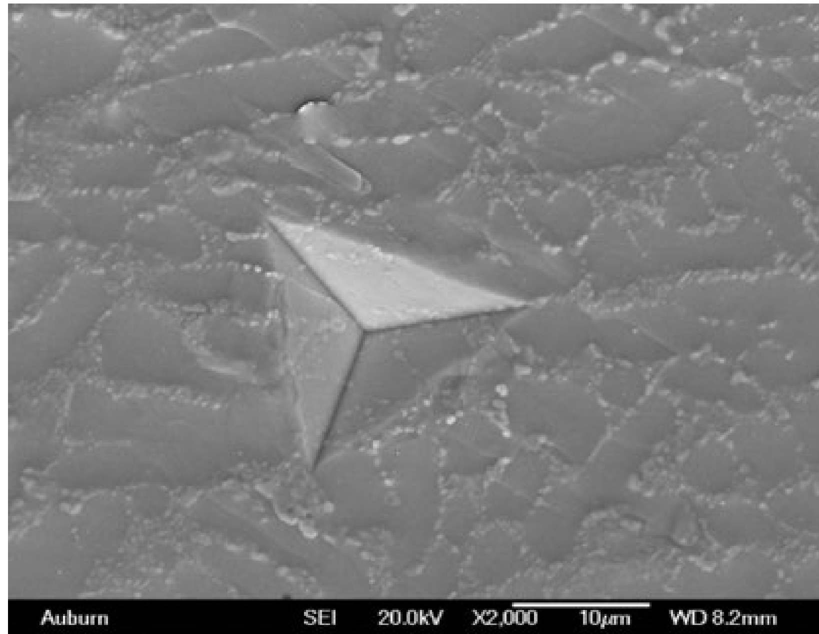

Figure 6.2 Permanent Indentation After Nanoindentation Testing

6.4 Factors Influence in Nanoindentation Test Results

During indentation, two factors affect the nanoindentation test results which need to be considered carefully. First factor is holding time and second factor is surface effect. These two factors need to be established before indenting on solder joints.

6.4.1 Influence of Holding Time on Modulus and Hardness

The SAC solder alloys are soft and shows deformation due to creep. Creep affect influences the initial portion of the nanoindentation-unloading curve by producing bulging affect and thus provide erroneous modulus and hardness value. Figure 6.3 (a) and 6.3 (b) reveals the typical load-displacement curves on standard polycarbonate and β-Sn between without holding between loading and unloading respectively. The bulging out at the initial part of the unloading curve shows the primary creep effect clearly, which indicates that the

creep of β-Sn is unavoidable during nanoindentation tests on SAC with no holding time. Apparently if those creep effects were not accounted for, the mechanical properties determined from fitting the unloading curves would be highly unreal and contain errors. However, for the standard quartz and IMCs this creep effect was not that prominent at no holding time (figure 6.4 (a) and 6.4 (b)). The IMCs are hard and expected to be resistant to creep.

In order to investigate the creep effect on the mechanical properties (modulus and hardness) of SAC solder alloy measured by nanoindentation, different holding times were tried out in the test to find the optimal holding time to minimize the creep affect. In Fig. 6.5 (a) and (b), one can see that the creep effect became ignorable and gives stable value when the holding time (HT) was longer than 15 sec. Thus, in order to minimize the effect of creep, a 50-second holding time was chosen for the present study.

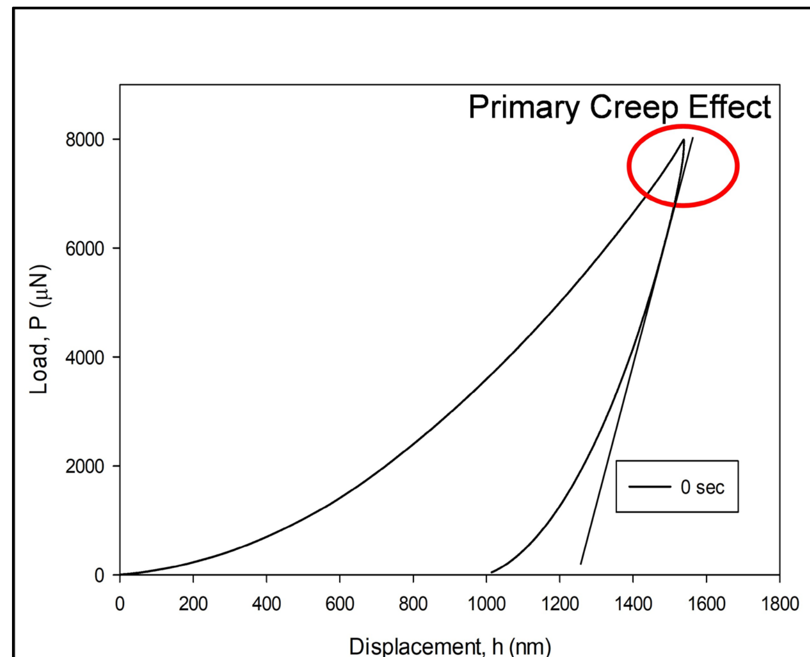

(a) Standard Polycarbonate

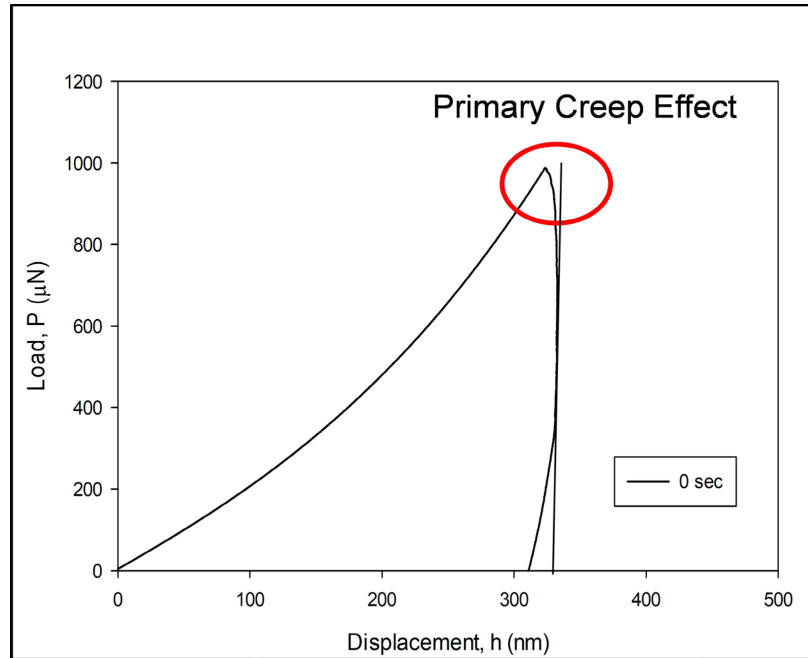

(b) Solder Joint

Figure 6.1 Load –Displacement Curve (a) Standard Polycarbonate and (b) Solder

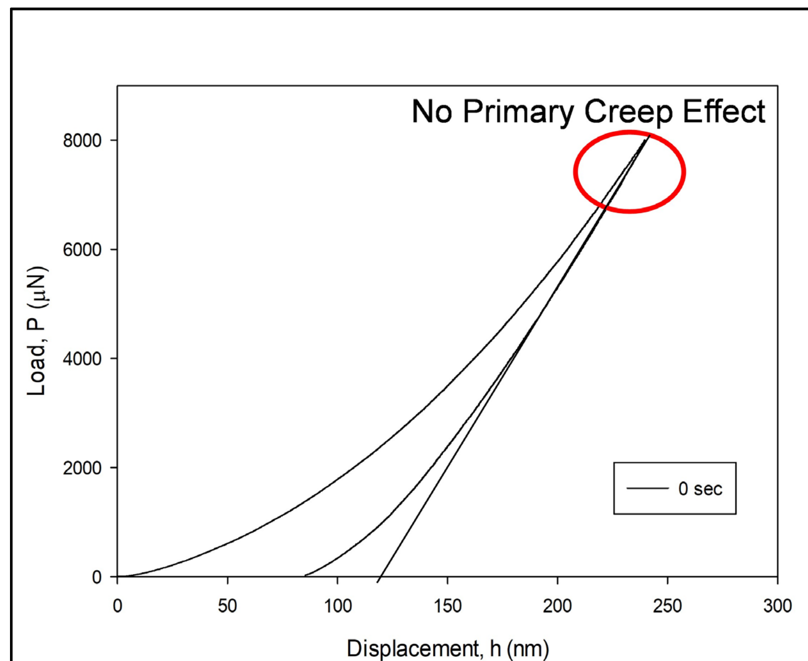

(a) Standard Quartz

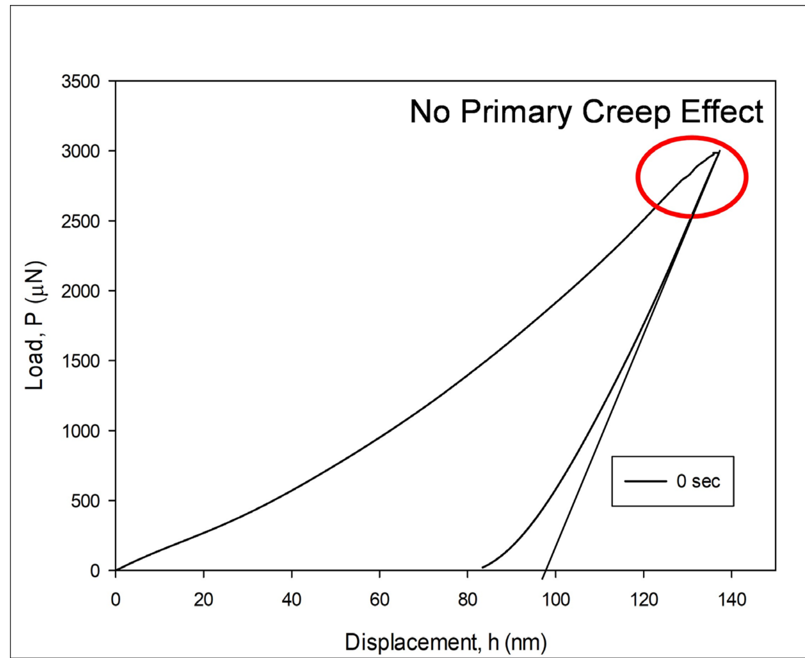

(b) IMC

Figure 6.2 Load –Displacement Curve (a) Standard Quartz and (b) IMCs

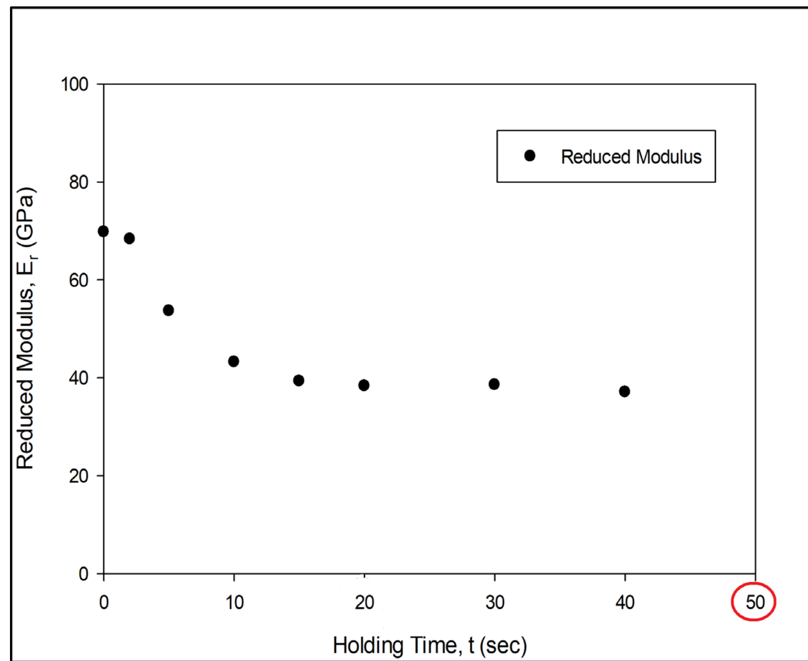

(a) Modulus

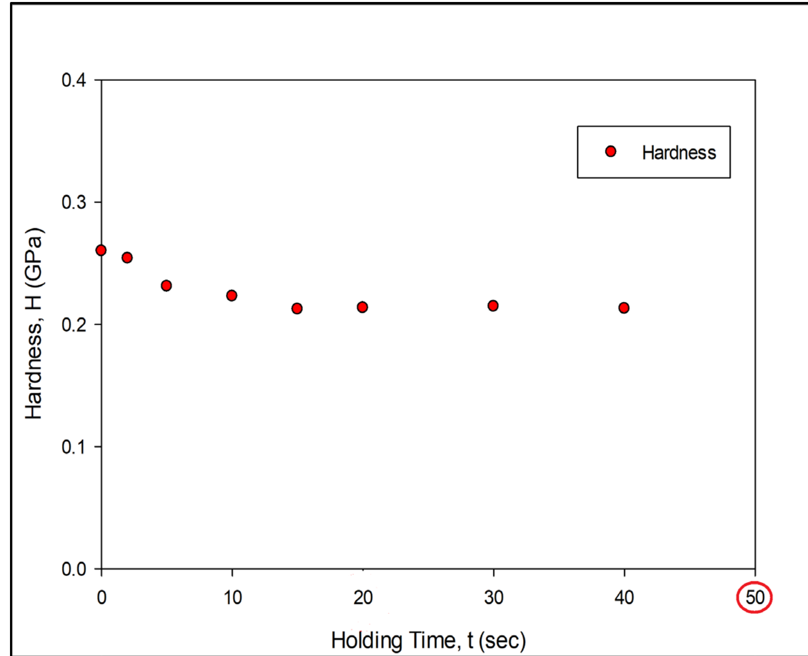

(b) Hardness

Figure 6.3 Variation of (a) Modulus and (b) Hardness with Different Holding Time

6.4.2 Influence of Surface Effect on Modulus and Hardness

Another parameter that affects the nanoindentation results is the surface affect. The modulus and hardness value does not show constant value at all indentation depths. The strain hardening effect during sample polishing and/or presence of surface inclusions could provide unstable properties for small indentations. To obtain a stabilized value, the modulus and hardness as a function of indentation depth were characterized. To accomplish this, a multiple load-partial unload testing protocol was performed on the β-Sn and IMC phases where a gradual loading, hold, and then a 50% unloading routine was utilized (Fig. 6.6). Each unload segment was then fitted to calculate the unloading slope and extract the modulus and hardness at a certain depth. Using this procedure multiple times, the modulus and hardness as a function of indentation depth were obtained. Result of this approach is

shown in Fig. 6.7 for solder. The results were found to stabilize and be independent of depth after approximately 200 nm of indentation depth for β-tin and 60 nm for the IMC phase. Thus, we have determined the E and H values in this work by choosing a load, which gives results at indentation depths higher than the above-mentioned values.

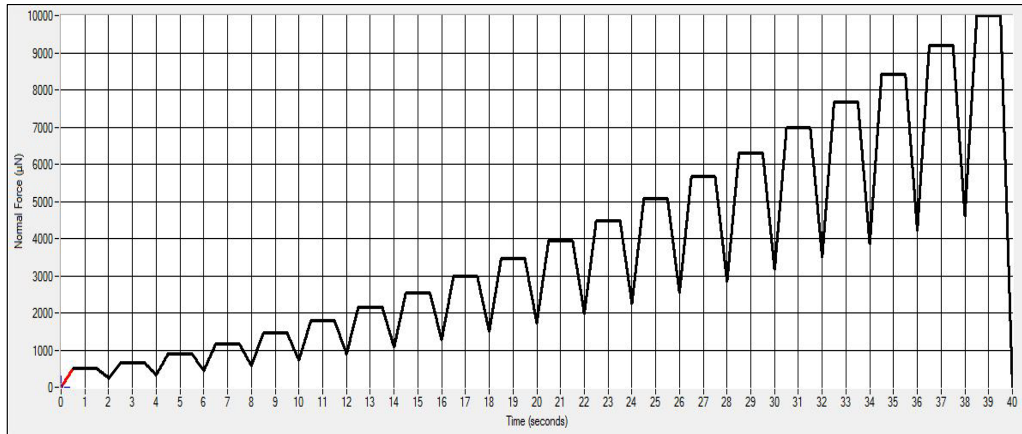

Figure 6.4 Multiple Load-unload Load Function

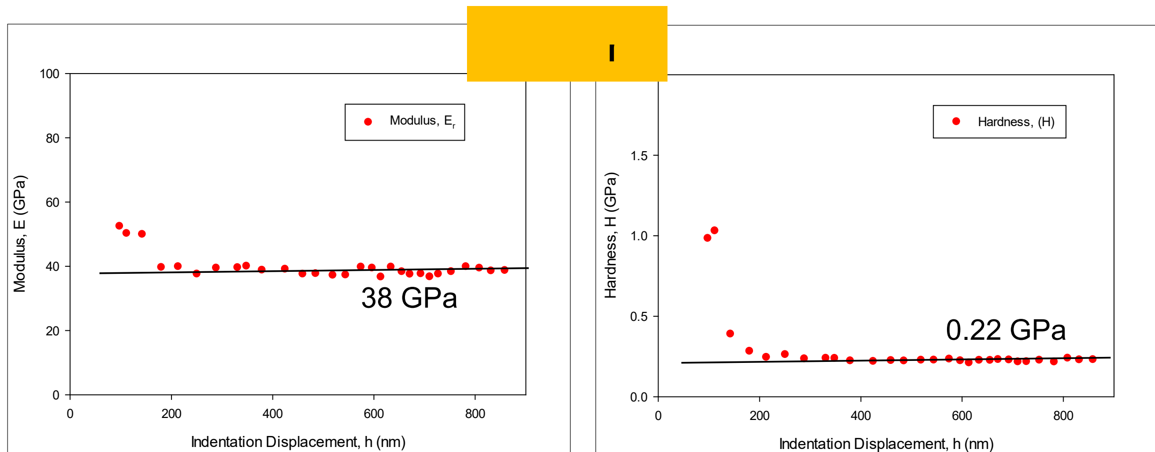

(b)

Figure 6.5 Variation of Modulus and Hardness of Solder Joint

6.5 Modulus, Hardness, and Yield Strength Measurement of SAC305 Solder Joints Under Different Thermal Exposures

After preconditioning, sets of solder joints for each thermal exposures were indented for each exposure time. Ten indentations were made in a row presented in figure 6.8 to extract the mechanical properties. As mentioned earlier, from the unloading part of load-displacement curve, the modulus and hardness values were obtained using the Oliver and Pharr method and applying maximum load that provides maximum indentation depth at a stable region. Nanoindentation was performed using 30 mN peak load so that the indentation covers both β-Sn and Ag_3Sn IMC's. Average of ten indentations were calculated which represents the modulus and hardness of each solder joint. But for each thermal profiles and exposure time, three joints have been used. As the grain orientation of each joint is different so the normalized values of all mechanical properties were considered for plotting figure 6.9. Figure 6.9 (a-c) show representative normalized modulus, hardness and yield strength with exposure time, respectively. In these plot, modulus and hardness were plotted for three different solder joint and then average property was calculated by fitting them. Modulus and hardness values of SAC305 solder under different thermal exposures have been tabulated in Table 6.1 and 6.2 respectively.

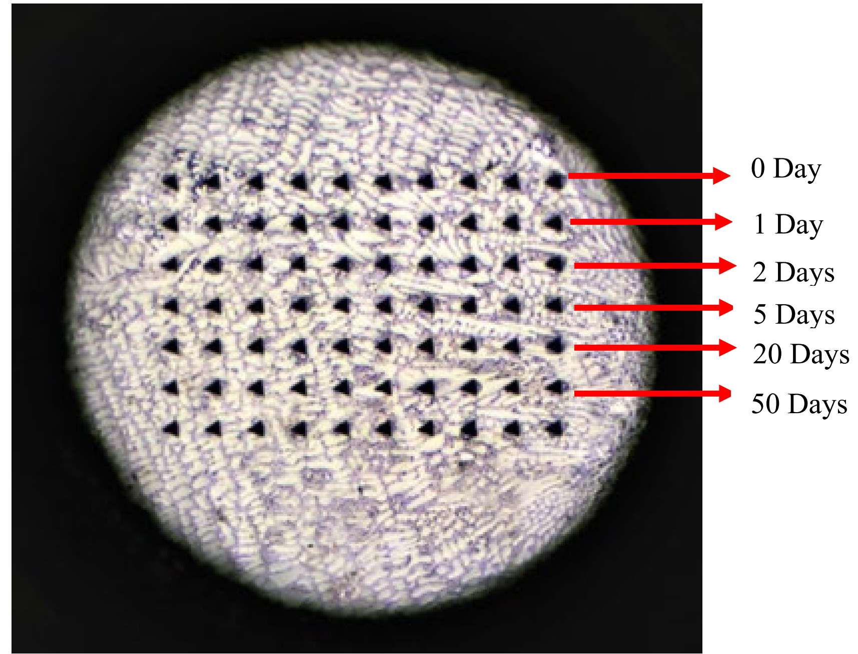

Figure 6.8 Indentation Marks on SAC+Bi Solder Joint For Property Extraction

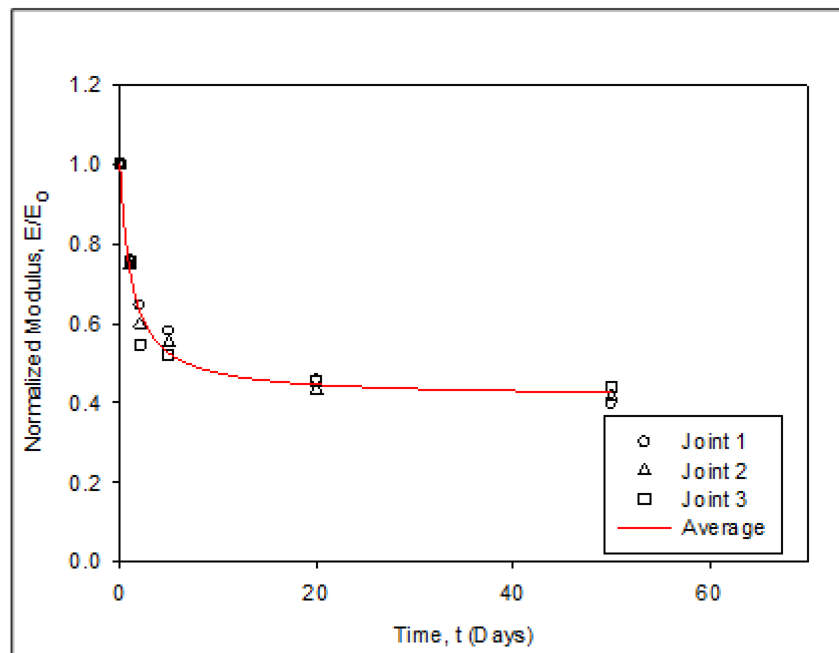

(a) Modulus

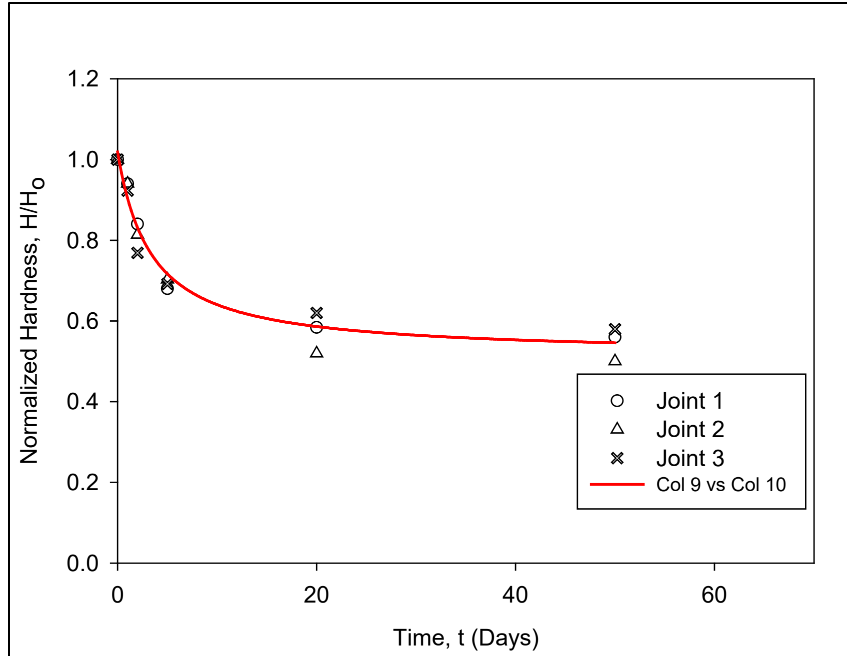

(b) Hardness

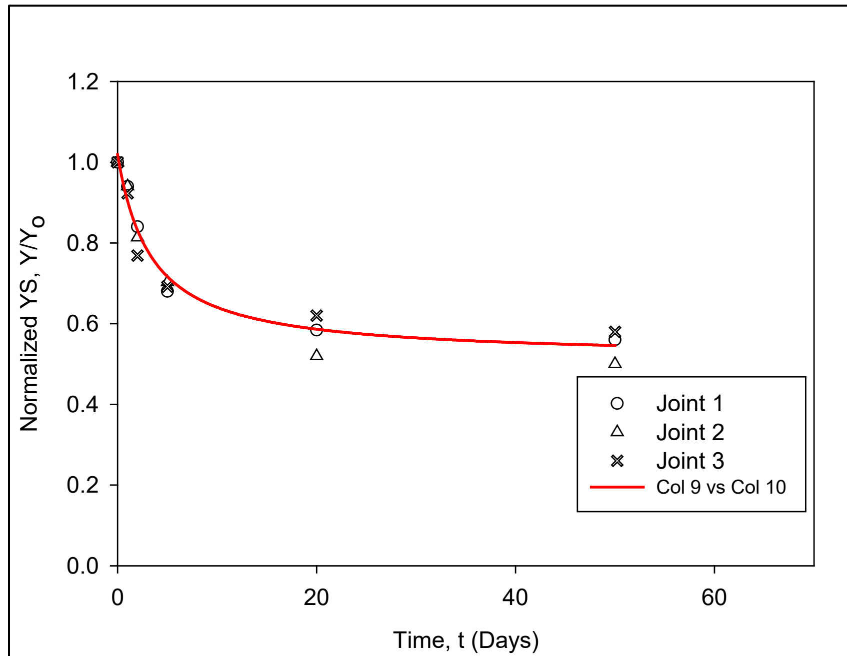

(c) Yield Strength

Figure 6.9 Representative Normalized Modulus vs. Time Pot for SAC305 Alloy

Table 6.1 Modulus of SAC305 Solder Joints Under Different Thermal Exposures

Thermal Expsoures	Time (Days)	Joint-1 (GPa)	Joint-2 (GPa)	Joint-3 (GPa)
Aging	0	40.2 ± 3.1	49.7 ± 4.4	35.5 ± 1.2
	1	30.1 ± 2.3	35.5 ± 2.6	25.3 ± 2.2
	2	28.9 ± 0.9	34.7 ± 1.8	24.4 ± 3.1
	5	27.1 ± 2.5	33.0 ± 2.5	22.9 ± 1.7
	20	24.9 (1.2)	31.3 ± 0.8	22.0 ± 0.9
	50	24.1 (2.3)	30.9 ± 2.9	20.5 ± 1.2
Slow Thermal Ramping	0	43.3 ± 3.5	51.0 ± 1.7	39.9 ± 2.1
	1	35.7 ± 1.5	45.5 ± 1.4	33.9 ± 1.4
	2	33.1 ± 2.1	40.3 ± 3.2	30.9 ± 1.6
	5	29.5 ± 1.5	31.0 ± 1.8	26.4 ± 0.9
	20	24.9 ± 0.5	29.4 ± 3.1	21.7 ± 2.1
	50	23.6 ± 2.6	26.2 ± 4.2	20.8 ± 0.2
`Thermal Shock	0	56.5 ± 4.3	54.1± 1.2	32.6 ± 1.8
	1	44.8 ± 2.1	43.2 ± 2.3	26.7 ± 1.5
	2	41.8 ± 1.8	36.3 ± 1.8	21.3 ± 0.9
	5	36.3 ± 1.6	34.1 ± 1.6	20.5 ± 3.2
	20	28.9 ± 5.2	25.8 ± 0.9	16.1 ± 2.7
	50	26.7 ± 3.3	25.3 ± 2.2	14.76 ± 1.4
Slow Thermal Cycling	0	47.0 ± 3.5	54.0 ± 4.1	59.5 ± 4.5
	1	35.7 ± 2.5	40.3 ± 1.4	45.0 ± 0.2
	2	30.3 ± 1.3	32.3 ± 2.1	32.55 ± 0.8
	5	27.3 ± 0.6	29.8 ± 1.6	30.97 ± 1.2
	20	21.5 ± 0.9	23.3 ± 3.8	26.9 ± 1.1
	50	18.7 ± 3.1	22.5 ± 0.8	26.1 ± 2.4

Table 6.2 Hardness of SAC305 Solder Joints Under Different Thermal Exposures

Thermal Exposures	Days	Joint-1 (GPa)	Joint-2 (GPa)	Joint-3(GPa)
Aging	0	0.22 ± 0.02	0.23 ± 0.09	0.21 ± 0.18
	1	0.20 ± 0.02	0.21 ± 0.02	0.19 ± 0.03
	2	0.19 ± 0.02	0.20 ± 0.01	0.18 ± 0.04
	5	0.18 ± 0.01	0.195 ± 0.01	0.17 ± 0.01
	20	0.17 ± 0.03	0.183 ± 0.05	0.16 ± 0.02
	50	0.16 ± 0.05	0.18 ± 0.08	0.156 ± 0.03
Slow Thermal Ramping	0	0.24 ± 0.03	0.245 ± 0.03	0.236 ± 0.03
	1	0.23 ± 0.01	0.235 ± 0.02	0.215 ± 0.02
	2	0.21 ± 0.02	0.212 ± 0.01	0.204 ± 0.01
	5	0.18 ± 0.03	0.196 ± 0.02	0.19 ± 0.04
	20	0.16 ± 0.07	0.175 ± 0.07	0.17 ± 0.03
	50	0.15 ± 0.09	0.16 ± 0.05	0.16 ± 0.08
Thermal Shock	0	0.28 ± 0.02	0.25 ± 0.04	0.23 ± 0.02
	1	0.26 ± 0.02	0.237 ± 0.02	0.216 ± 0.03
	2	0.23 ± 0.01	0.20 ± 0.03	0.18 ± 0.02
	5	0.20 ± 0.03	0.185 ± 0.01	0.17 ± 0.04
	20	0.17 ± 0.03	0.153 ± 0.02	0.147 ± 0.06
	50	0.165 ± 0.07	0.151 ± 0.12	0.138 ± 0.04
Slow Thermal Cycling	0	0.25 ± 0.03	0.27 ± 0.03	0.26 ± 0.02
	1	0.235 ± 0.02	0.254 ± 0.02	0.24 ± 0.01
	2	0.21 ± 0.04	0.22 ± 0.01	0.20 ± 0.03
	5	0.17 ± 0.01	0.19 ± 0.03	0.18 ± 0.04
	20	0.146 ± 0.08	0.14 ± 0.05	0.16 ± 0.08
	50	0.14 ± 0.01	0.135 ± 0.02	0.15 ± 0.05

6.6 Evolution of Modulus, Hardness, and Yield Strength of AC305 Solder Joints with Elapsed Time

Figure 6.10 shows the evolution of representative normalized modulus of SAC305 solder balls under slow thermal cycling. Other thermal cycling conditions showed the similar trend. In each thermal condition, three single grain joints have been chosen to perform nanoindentation (Table 6.1, 6.2). From the load-displacement curve, modulus, hardness, and yield strength were calculated. The average results of three joints were used under all thermal cycling conditions to compare the evolution of normalized modulus. In this plot black, red, green, blue, pink, and cyan curves presented 0, 1, 2, 5, 20, and 50 days results. From this plot it is obvious that with increased exposure time load-displacement curve shifts to the right. This shifting indicates higher displacement or mechanical properties degradation with exposure time.

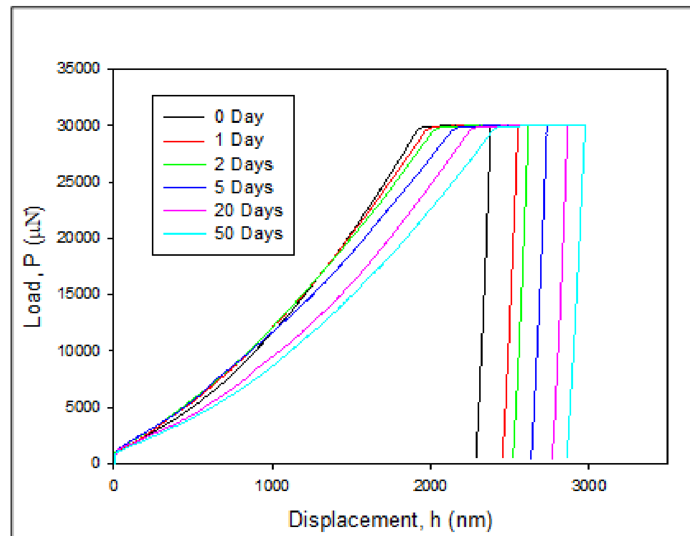

Figure 6.10 Representative Load vs. Displacement curve of SAC305 Solder Joint for Different Thermal Profiles with Exposure Time

Figure 6.11a and 6.11b represent the evolution of modulus, and yield strength with elapsed time for different thermal cycling conditions. From these plots, it can be inferred that, initially, the degradation of both E and yield strength was higher for isothermal aging compared to the other thermal cycling conditions. For example, after 1 days of aging, the degradation of modulus was 27%, whereas it was 14%, 20%, and 25% for slow thermal ramping, thermal shock, and slow thermal cycling, respectively. Similar phenomena can be observed for yield strength. But, with the increasing exposure time, the degradation of modulus and yield strength become higher under slow thermal ramping, thermal shock, as well as slow thermal cycling compared to the isothermal aging. Moreover, the degradation rate was higher under thermal cycling with longer ramping time. For example, after 50 days of thermal exposure, modulus reduced by 40% for isothermal aging while under slow thermal cycling, it was 58%. Similarly, after 50 days exposure, yield strength reduced by 25% and 45%, respectively under isothermal aging and slow thermal cycling. The higher degradation under slow thermal cycling can be attributed by the higher rate of IMC coarsening in SAC solder [166-169].

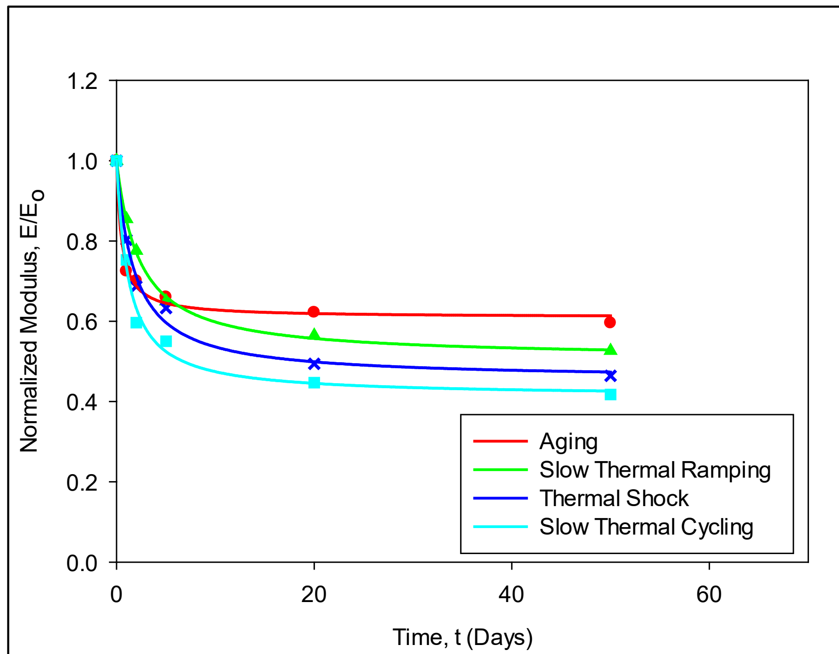

(a) Modulus

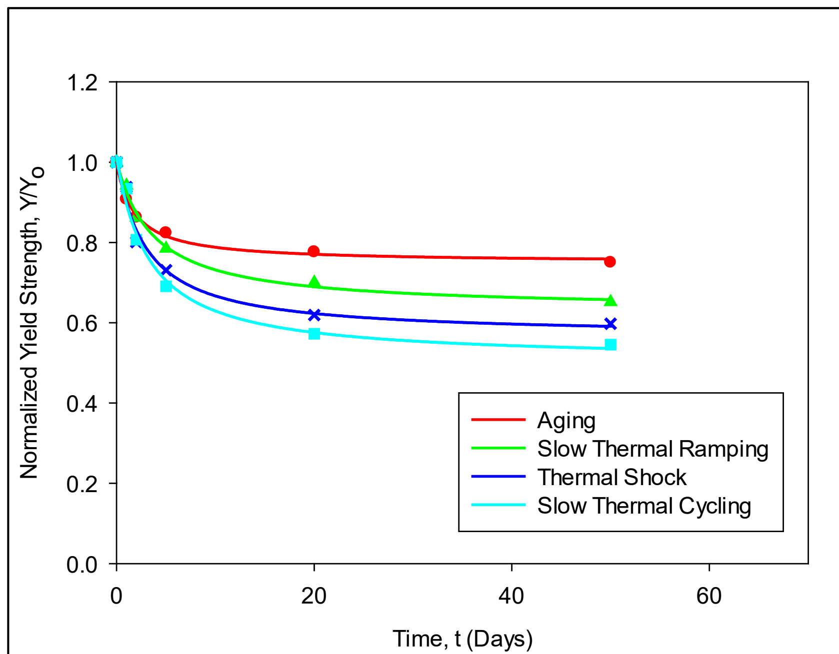

(b) Yield Strength

Figure 6.11 Evolution of Mechanical Properties of SAC305 Solder Joints under Aging and Different Thermal Exposures

6.7 Modulus, Hardness, and Yield Strength Measurement of SAC+Bi Solder Joints Under Different Thermal Exposures

Single grain solder joints of SAC+Bi (chapter 3) were used for nanoindentation technique to observe the evolution of mechanical properties. Similar testing conditions and fitting model was used as described in chapter 3. In addition, three solder joints were used for each thermal cycling conditions to investigate the mechanical properties evolution. Similar to SAC305 solder joint 10 indents were made in a row presented in figure 6.12. From the load-displacement curve, mechanical properties were extracted. Modulus and hardness values under aging and different thermal exposures have been recorded in Table 6.3 and 6.4. As the grain orientation for each solder joint is not same so similar to SAC305, normalized properties have been used to understand the evolution in the next section.

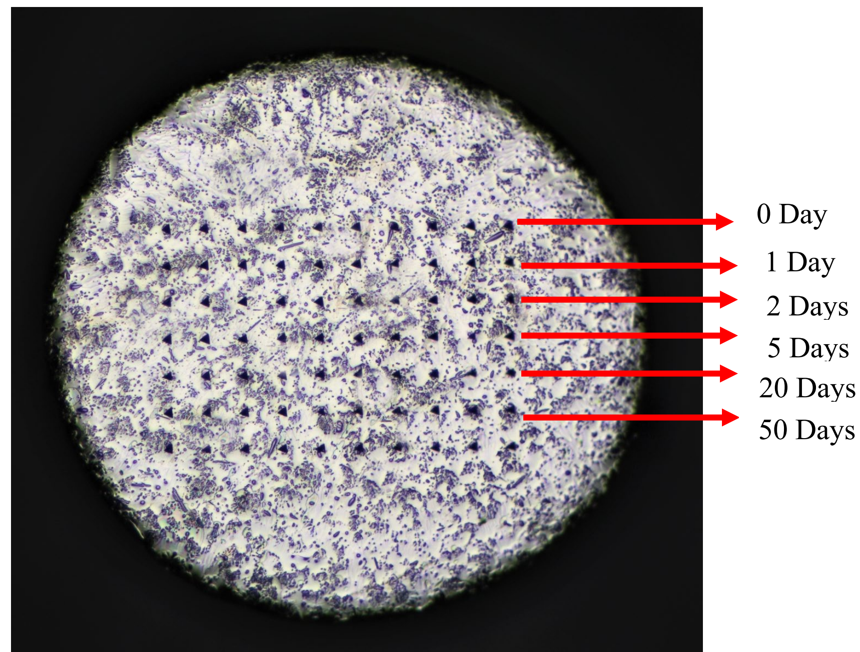

Figure 6.12 Indentation Marks on SAC+Bi Solder Joint For Property Extraction

Table 6.3 Modulus of SAC+Bi Solder Joints Under Different Thermal Exposures

Profiles	Days	Joint-1 (GPa)	Joint-2 (GPa)	Joint-3 (GPa)
Aging	0	57.40 ± 3.5	51.00 ± 2.4	41.7 ± 3.7
	1	56.78 ± 4.8	49.87 ± 2.7	41.4 ± 2.8
	2	56.23 ± 3.3	49.53 ± 5.4	40.8 ± 3.2
	5	55.09 ± 2.6	48.74 ± 4.7	39.8 ± 4.4
	20	54.32 ± 4.5	48.39 ± 2.3	39.7 ± 3.7
	50	53.09 ± 6.3	46.69 ± 3.6	38.2 ± 2.3
Slow Thermal Ramping	0	42.00 ± 3.5	63.00 ± 3.4	51.20 ± 2.1
	1	41.79 ± 2.2	62.90 ± 1.9	50.90 ± 1.6
	2	41.24 ± 3.1	62.22 ± 2.2	50.00 ± 4.1
	5	40.87 ± 5.1	61.25 ± 3.9	49.73 ± 2.7
	20	38.93 ± 4.1	58.15 ± 4.2	47.15 ± 3.1
	50	37.79 ± 1.9	56.57 ± 3.5	46.03 ± 4.4
`Thermal Shock	0	57.30 ± 5.1	51.00 ± 2.5	41.70 ± 2.2
	1	56.84 ± 2.1	50.57 ± 4.5	41.32 ± 3.2
	2	56.15 ± 4.4	50.03 ± 2.3	40.90 ± 2.2
	5	55.29 ± 1.2	49.23 ± 2.7	40.36 ± 5.1
	20	51.90 ± 3.4	45.39 ± 4.4	38.41 ± 6.3
	50	50.48 ± 2.8	44.78 ± 2.3	36.57 ± 1.6
Slow Thermal Cycling	0	63.46 ±5.5	45.00 ± 2.8	68.30 ± 4.7
	1	63.02 ± 4.8	44.68 ± 3.7	67.80 ± 2.5
	2	62.55 ± 3.3	44.33 ± 1.4	66.90 ± 5.1
	5	61.23 ± 5.4	43.30 ± 2.3	65.70 ± 3.3
	20	56.17 ± 2.1	39.47 ± 3.7	59.83 ± 1.1
	50	54.96± 5.2	39.38 ± 1.6	58.97 ± 2.4

Table 6.4 Hardness of SAC+Bi Solder Joints Under Different Thermal Exposures

Profiles	Days	Joint-1 (GPa)	Joint-2 (GPa)	Joint-3 (GPa)
Aging	0	0.59 ± 0.05	0.49 ± 0.05	0.57 ± 0.01
	1	0.55 ± 0.04	0.46 ± 0.02	0.54 ± 0.08
	2	0.53 ± 0.14	0.44 ± 0.03	0.51 ± 0.02
	5	0.51 ± 0.03	0.43 ± 0.04	0.50 ± 0.06
	20	0.505 ±0.07	0.42 ± 0.07	0.49 ± 0.05
	50	0.496±0.05	0.416 ±0.03	0.48 ± 0.04
Slow Thermal Ramping	0	0.52 ± 0.04	0.55 ± 0.03	0.57 ± 0.01
	1	0.515 ±0.05	0.546 ±0.06	0.565 ±0.02
	2	0.478 ±0.03	0.504 ±0.04	0.515 ±0.03
	5	0.467 ±0.04	0.495 ±0.02	0.503 ±0.06
	20	0.435 ±0.07	0.465 ±0.04	0.479 ±0.05
	50	0.426 ± 0.03	0.450 ± 0.06	0.465 ± 0.03
`Thermal Shock	0	0.47 ±0.05	0.46 ± 0.06	0.48 ± 0.08
	1	0.45 ± 0.03	0.44 ± 0.07	0.46 ± 0.08
	2	0.43 ± 0.06	0.42 ± 0.02	0.43 ± 0.04
	5	0.41 ± 0.01	0.40 ± 0.04	0.415 ± 0.02
	20	0.39 ± 0.04	0.38 ± 0.02	0.40 ± 0.05
	50	0.38 ± 0.06	0.375 ± 0.08	0.394 ± 0.03
Slow Thermal Cycling	0	0.47 ± 0.07	0.49 ± 0.12	0.47 ± 0.10
	1	0.46 ± 0.08	0.48 ± 0.10	0.45 ± 0.06
	2	0.445 ± 0.09	0.46 ± 0.08	0.44 ± 0.10
	5	0.42 ± 0.05	0.43 ± 0.09	0.415 ± 0.08
	20	0.385 ± 0.05	0.40 ± 0.06	0.382 ± 0.10
	50	0.38 ± 0.06	0.39 ± 0.04	0.381 ± 0.09

6.8 Evolution of Modulus, Hardness, and Yield Strength of SAC+Bi Solder Joints with Elapsed Time

Figure 6.13 (a), and 6.13 (b) show the evolution of mechanical properties of SAC+Bi solder joints under different thermal exposures. Exponential decay can be observed in the mechanical properties with exposure time under different thermal cycling condition. From these plots, it can be depicted that the degradation in E and YS was insignificant up to 5 days exposure. After 20 days of exposure, small degradation in E and YS was observed irrespective to the thermal cycling condition. But the degradation under slow thermal ramping, thermal shock, and slow thermal cycling was higher compared to the aging. Moreover, slow thermal cycling showed higher effect among all thermal cycling conditions. For example, after 50 days of exposure, E, hardness, and YS degraded by 8%, 16%, and 16% respectively under isothermal aging where these were 13%, 19%, and 19%, respectively under slow thermal cycling. Although, the degradation of SAC+Bi under different thermal cycling conditions was not significant compared to the degradation of SAC305 with the same time duration. But among isothermal aging and different thermal exposures, thermal cycling with long ramping time had adverse effect on mechanical properties. It is true for both SAC305 and SAC+Bi solder materials.

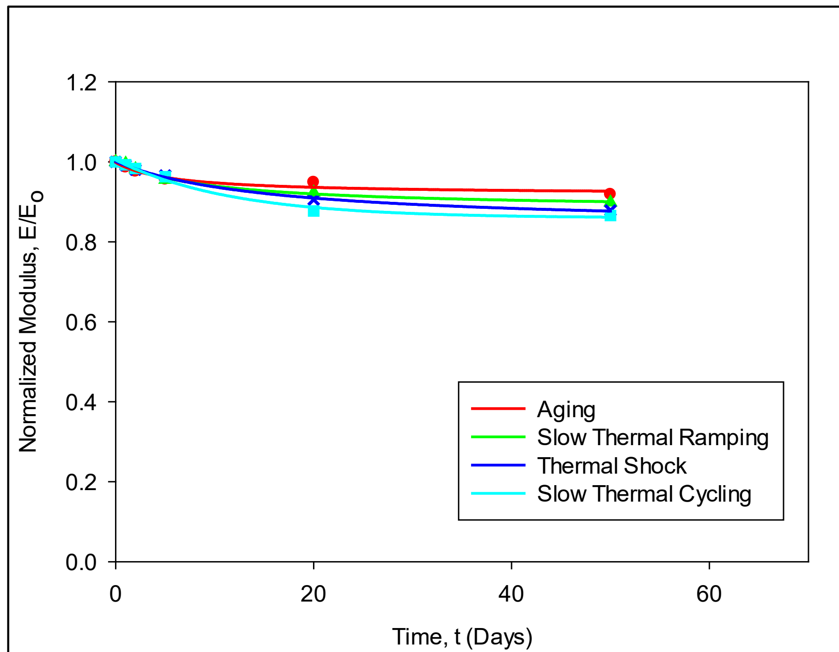

(a) Modulus

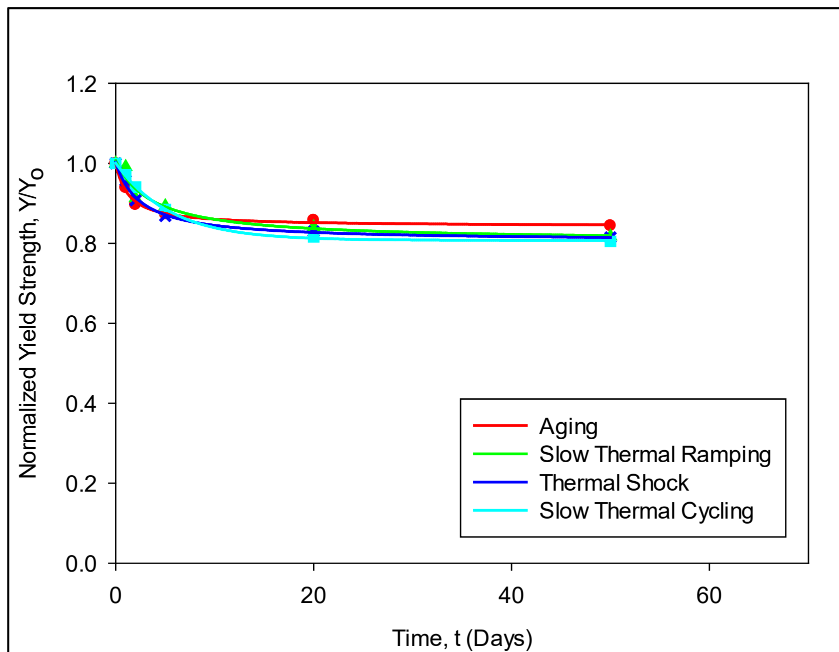

(b) Yield Strength

Figure 6.13 Evolution of Mechanical Properties of SAC+Bi Solder Joints under Different Thermal Exposures

6.9 Comparison of Modulus Between Bulk Solder and Solder Joint

Evolution of normalized modulus for both bulk solder and solder balls with elapsed time under different thermal cycling conditions are presented in figure 6.14 (a-d). In these plots, red and pink curves present the evolution of SAC305 and SAC+Bi bulk solder, respectively. On the other hand, green and blue curves present the evolution of SAC305 and SAC+Bi solder balls, respectively. From these plots, it can be demonstrated that for both SAC305 and SAC+Bi solder balls and bulk solder, normalized modulus showed exponential decay with time irrespective to the thermal exposures. But the degradation of normalized modulus is higher under slow thermal cycling conditions for both solder balls and bulk solder. Also, irrespective to the thermal exposure conditions, the degradation of normalized modulus of solder balls are less compared to the bulk solder for both SAC305 as well as SAC+Bi. For instance, after 50 days of exposure, under slow thermal cycling, normalized modulus of SAC305 solder balls degrade 58% while for bulk solder it degrades 66%. Also, the modulus of SAC+Bi solder ball and bulk solder degrade by 13%, and 18%, respectively. Besides, it can be seen from these plot that the degradation in modulus of SAC305 under any thermal exposure is much higher than the degradation of SAC+Bi solder material. In addition, compared to SAC305, the degradation in modulus after 50 days of exposure is not significant. It can also be observed that the drop in normalized modulus under slow thermal ramping, thermal shock, and slow thermal cycling is higher compared to isothermal aging for both SAC305 and SAC+Bi.

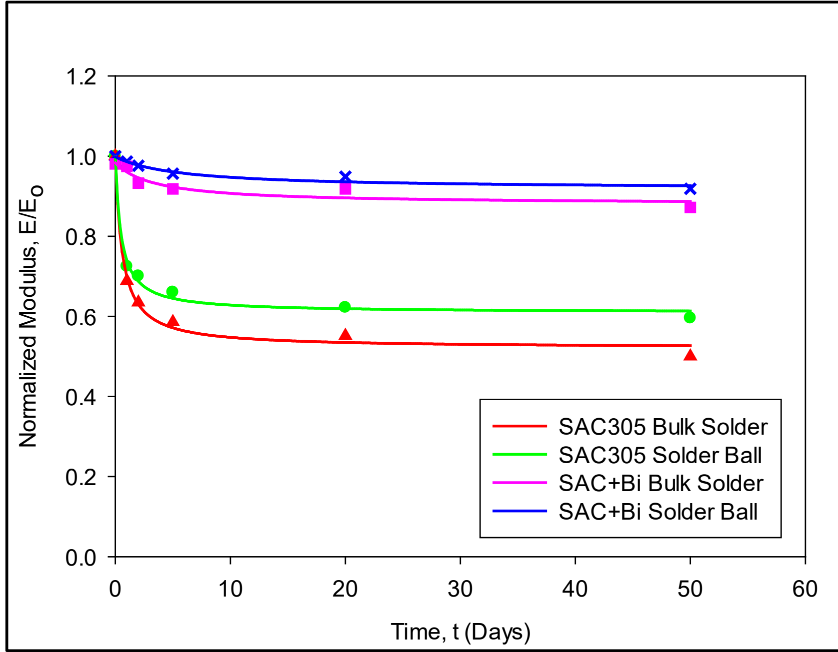

(a) Isothermal Aging

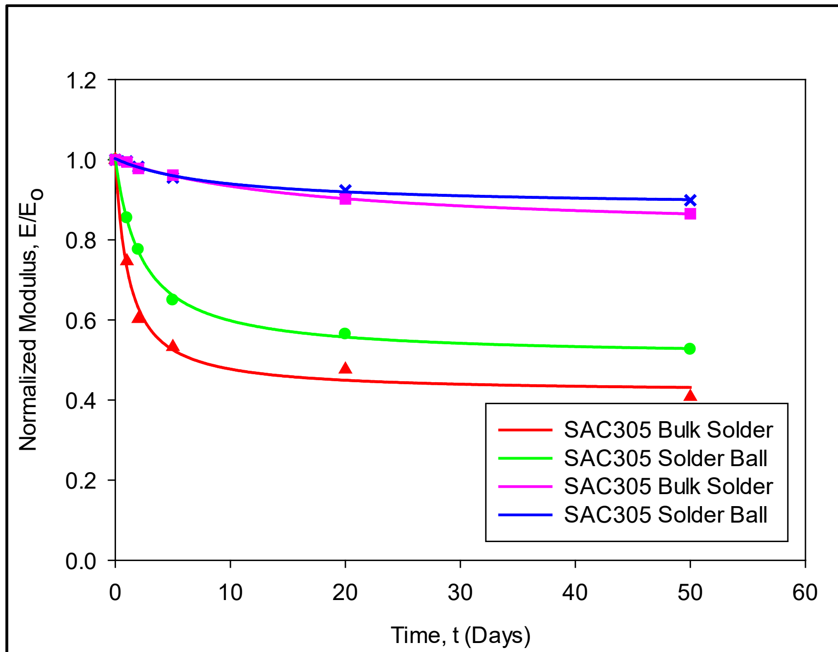

(b) Slow Thermal Ramping

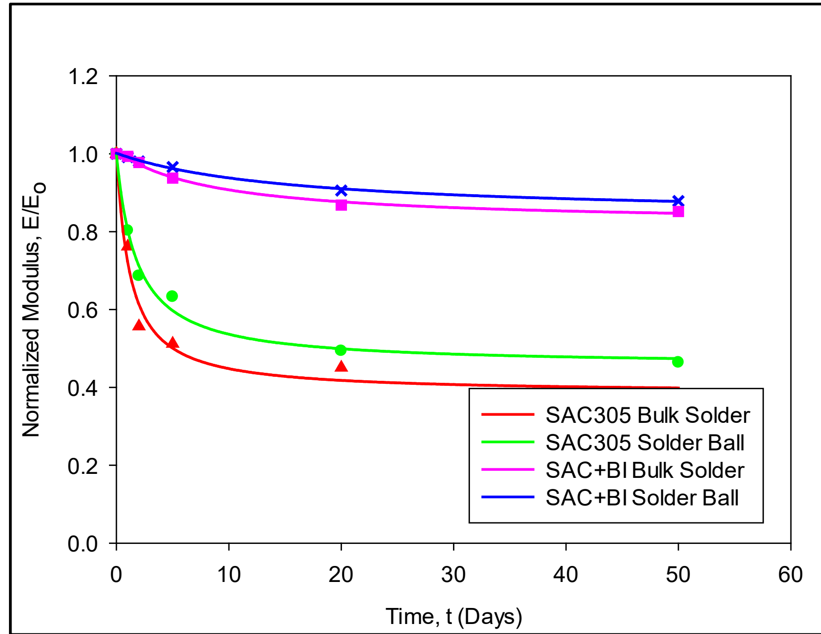

(c) Thermal Shock

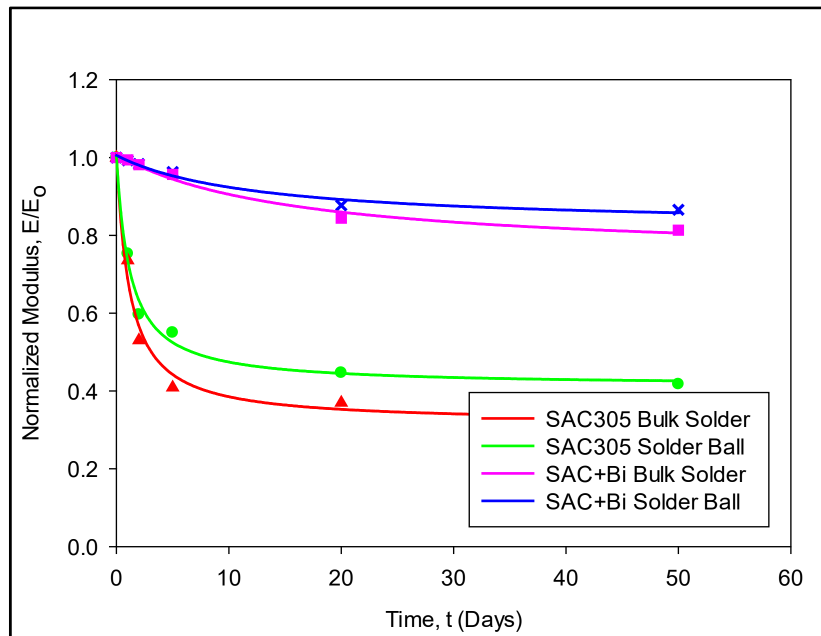

(d) Slow Thermal Cycling

Figure 6.14 Normalized Modulus Evolution Under Different Thermal Exposures

6.10 Comparison of Yield Strength Between Bulk Solder and Solder Joint

Figure 6.15 (a-d) represent the evolution of normalized YS for both bulk solder and solder balls with elapsed time under different thermal cycling conditions. The degradation in YS for both SAC305 and SAC+Bi shows exponential decay.

The evolution of YS under different thermal cycling conditions for both SAC305 and SAC+Bi solder material show the similar trend as modulus evolution (section 6.9). For both SAC305 and SAC+Bi solder material, the degradation in solder joint is smaller compared to the bulk solder. For SAC+Bi solder material, the degradation of YS for both bulk and solder joint was insignificant compared to SAC305 solder material. But a similarity can be observed between bulk solder and solder joint. Even though the degradation is insignificant but the degradation under slow thermal cycling is higher than other thermal exposures (6.15 (d)).

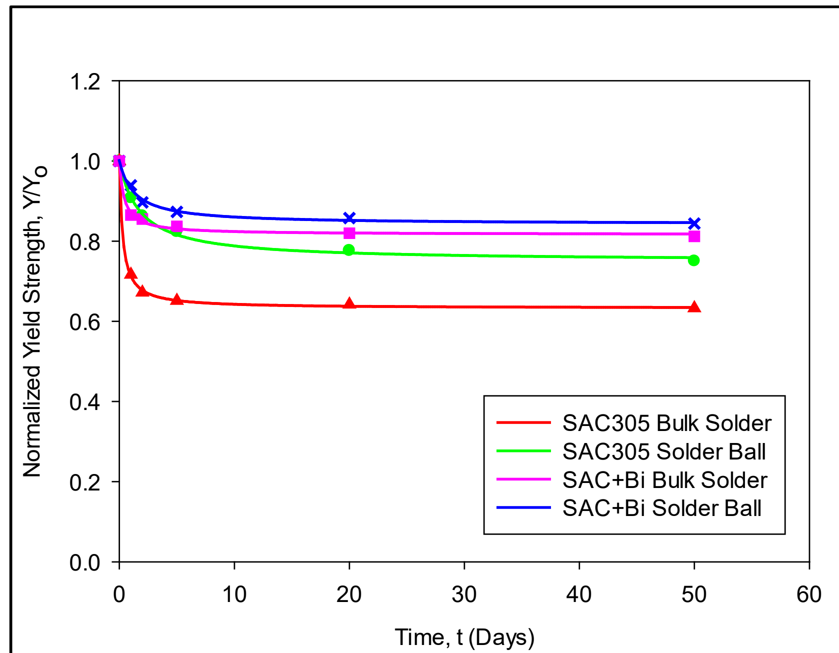

(a) Isothermal Aging

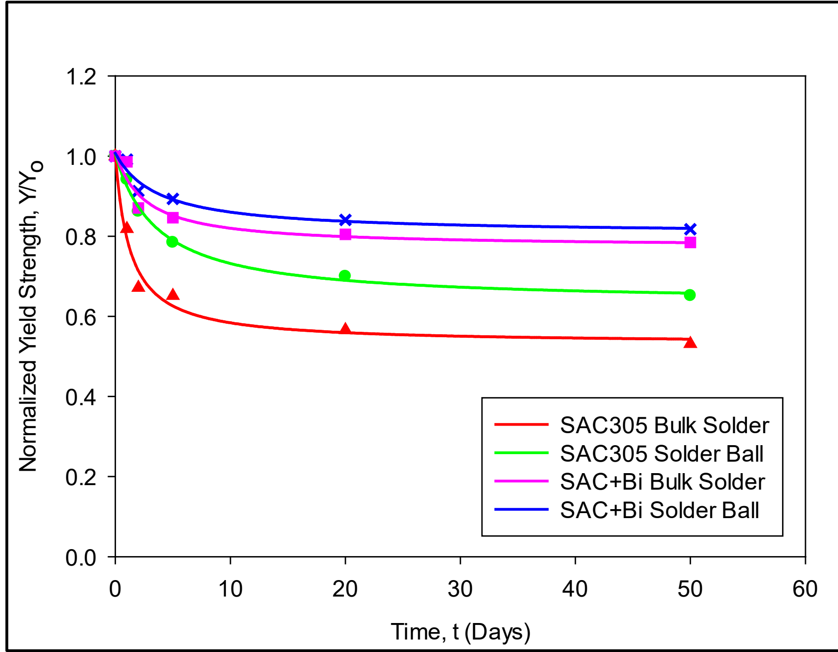

(b) Slow Thermal Ramping

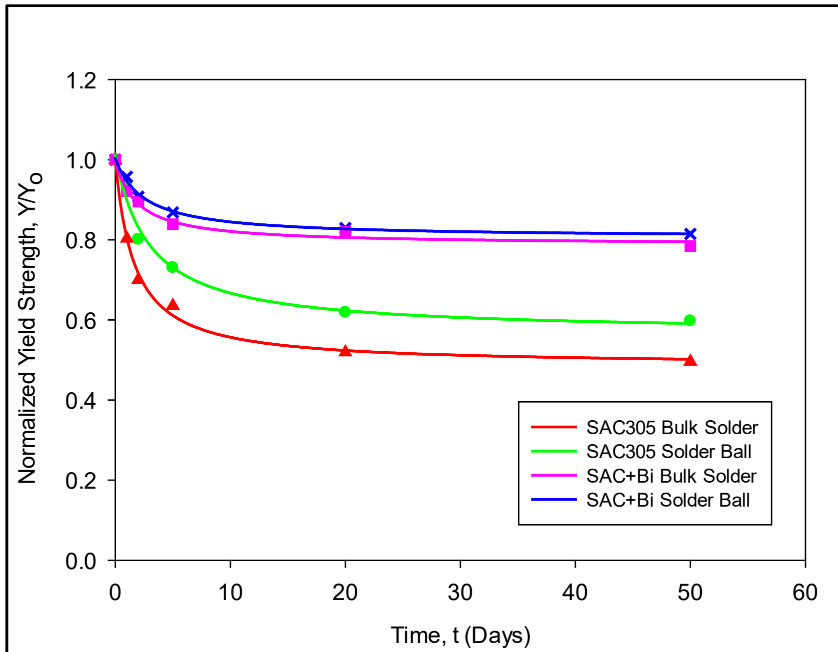

(c) Thermal Shock

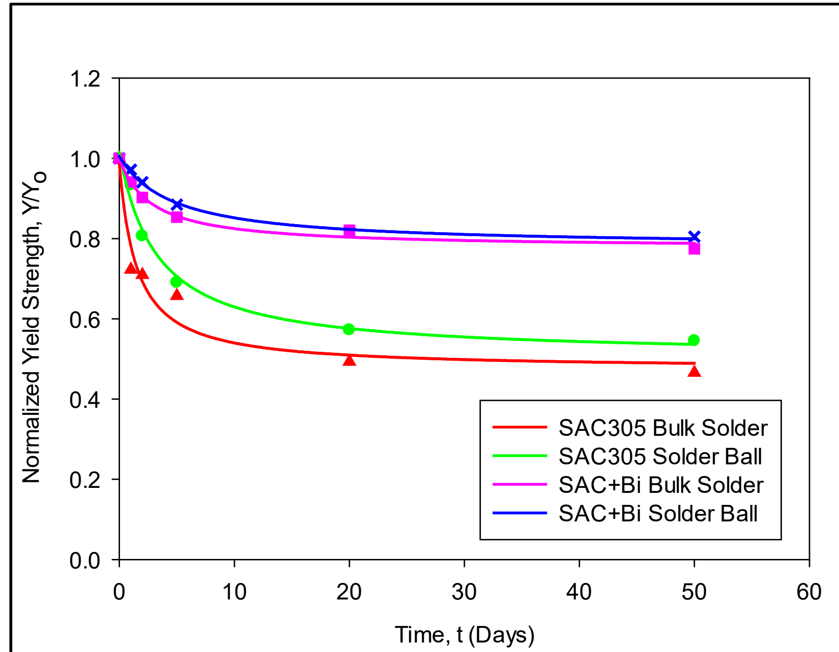

(d) Slow Thermal Cycling

Figure 6.15 Normalized Yield Strength Evolution Under Different Thermal Exposures

6.11 Summary and Discussion

In this chapter, the effects of various thermal exposures on the evolutions of the mechanical properties of SAC305 and SAC+Bi solder joints (balls) were investigated using nanoindentation. Sets of solder balls were cycled and aged for the duration of 1, 2, 5, 20, and 50 days at the high temperature extreme of T = 125 C followed by nanoindentation testing to measure the mechanical properties evolution in terms of E, and YS. As Expected, elastic Modulus, hardness, and yield strength of the solder joints decreased with exposure time for isothermal aging, slow thermal ramping, thermal shock, as well as slow thermal cycling. But for both bulk solder and solder balls, the mechanical properties degradation of SAC305 solder material under slow thermal cycling was severe compared to the aging and other thermal profiles. For example, after 50 days of isothermal aging, E, UTS, and

YS of bulk solder was degraded by 50%, 42%, and 36%, respectively. On the other hand, the degradation under slow thermal cycling was 66%, 55%, and 53%, respectively. Similarly, the average percentage change in modulus and YS of solder balls after 50 days of isothermal aging was found as 40%, and 25%, respectively, whereas, under slow thermal cycling it was observed as 58%, as well as 45%, respectively. Even though, the reduction in mechanical properties under pure aging after 1 day was higher compared to other thermal profiles, but with increasing exposure the degradation becomes more prominent in other thermal profiles, particularly, thermal cycle with longest ramp rate (slow thermal cycling). Results also showed that compared to the SAC305 solder material, SAC+Bi showed insignificant change in E, UTS as well as YS for both bulk solder and solder joint up to 5 days of exposure. Small change was observed in mechanical properties after 20 days exposure. As SAC305, the degradation in solder balls was found less compared to the bulk solder irrespective to the thermal cycling condition. Also, for both bulk solder and solder balls, slow thermal cycling showed more effect on mechanical properties evolution of SAC+Bi solder material compared to the isothermal aging and other thermal cycling condition. For all of the thermal exposures, the mechanical property degradations of both SAC305 and SAC+Bi solder materials were larger in the bulk solder relative to those in the solder joints. The degradations using the slow thermal cycling profile were largest for both solder joints and bulk Solder.

CHAPTER 7

MICROSTRUCTURAL EVOLUTION OF SAC305 AND SAC+Bi SOLDER UNDER DIFFERENT THERMAL EXPOSURES

7.1 Introduction

The degradation of mechanical properties of solder alloys are result of the microstructural evolution during isothermal aging and thermal cycling. The most well-known and widely observed changes are coarsening of the Ag_3Sn and Cu_6Sn_5 intermetallic compounds (IMCs) present in the eutectic regions between β-Sn dendrites. Some researchers have proposed empirical models to describe the growth of these secondary phase particles as a function of aging temperature and aging time, and related this growth to mechanical property changes. In most of the prior investigations, microstructural changes during aging have been observed by comparing two different solder joints subjected to different aging conditions. Thus, the comparisons made were qualitative in nature (e.g. average IMC particle size) since the two microstructures were from different samples and could not be directly compared. Besides, very limited studies have been conducted to understand the microstructural evolution during thermal cycling to correlate with mechanical properties evolution. This chapter aims to provide a better understanding of the SAC305 and SAC+Bi microstructure evolution and changes in mechanical properties occurring during the thermal cycling that is characteristic of thermomechanical fatigue tests. Also, compare the microstructure evolution of both solder material under

different thermal exposures in terms of average particle diameter as well as number of particles with exposure time.

7.2 Microstructural Evolution of SAC305 Solder

In this current work, the microstructural evolution of SAC305 solder material under different thermal exposures has been investigated for different exposure time such as 0, 1, 2, 5, and 20 days. The topography of the microstructure of a fixed region was captured using the SEM system. The fixed region was marked by nanoindentation tool. SEM system generated several images of the microstructure as the preconditioning progressed. These images were used to predict the microstructural evolution in SAC305 bulk solder exposed to isothermal aging and slow thermal ramping, and slow thermal cycling exposure. Image analysis software was utilized to quantify microstructural changes (total area, number, and average diameter of IMC particles, interparticle spacing etc.) with respect to exposure time.

The microstructure of SAC305 solder consists of β-Sn dendrites surrounded by eutectic region which is a mixture of Ag_3Sn, Cu_6Sn_5, and β-Sn phase. The IMCs (Ag_3Sn, Cu_6Sn_5) in the eutectic region helps to improve strength of the solder alloy restricting dislocation motion. Due to their low melting temperatures, lead free solders are exposed to high homologous temperatures in most product applications. Thus, there is a continuous state of active diffusion processes in the solder alloys, and their microstructures are inherently unstable and will continually evolve during normal operating temperature conditions of electronic packaging assemblies. Typical microstructure evolution in lead free solders includes coarsening of intermetallic phases and subgrains, breakdown of

dendrite structures, as well as potential recrystallization at Sn grain boundaries. Such changes in solder microstructure are accompanied by dramatic changes in mechanical response and failure behavior, and these multifaceted evolutions occurring in the material are typically referred to as solder aging phenomena. An example of SAC305 solder microstructure evolution after 1 year of aging at 100 °C is presented in Figure 7.1.

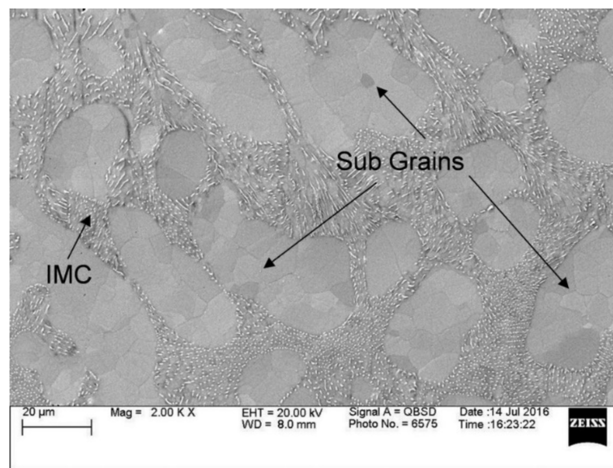

(a)

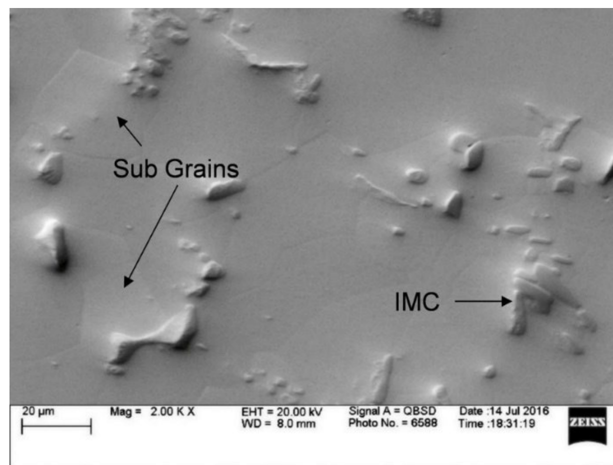

(b)

Figure 7.1 Microstructure of SAC305 Solder (a) Before Aging and (b) After Aging

During thermal cycling, dwelling at high temperature causes aging induced microstructural evolution. In addition, during ramping period, additional aging induced evolution occurs which causes additional microstructural and mechanical properties evolution. Many researchers have studied effects of aging on the evolution of solder microstructure. The most well-known and widely observed changes are coarsening of the Ag_3Sn and Cu_6Sn_5 IMCs present in the eutectic regions between β-Sn dendrites. Several researchers [57, 61, 70, 154, 170, 171-174] have also proposed empirical models to describe the growth of IMC particles or layers as a function of aging temperature and aging time. In many studies on the effects of aging on solder microstructure, observations were made on two different solder joints (one non-aged and one aged). Thus, the comparisons made were often qualitative in nature since the two microstructures were from different samples and could not be directly compared. Figure 7.2 represents the variations of SAC305 microstructure based on the locations of the same sample. All the images were taken at the same magnification from the same sample but in different locations or regions. It is evident from all the images in Figure 7.2 (a-d) that the microstructure of SAC305 is also dependent on the locations. As a result, in order to avoid region based variation in the microstructure, aging study should conduct at a fixed location of the same sample (not different sample). This kind of careful studies are expected to produce a more realistic quantitative analysis results for both aging and thermal cycling induced IMC coarsening experiments.

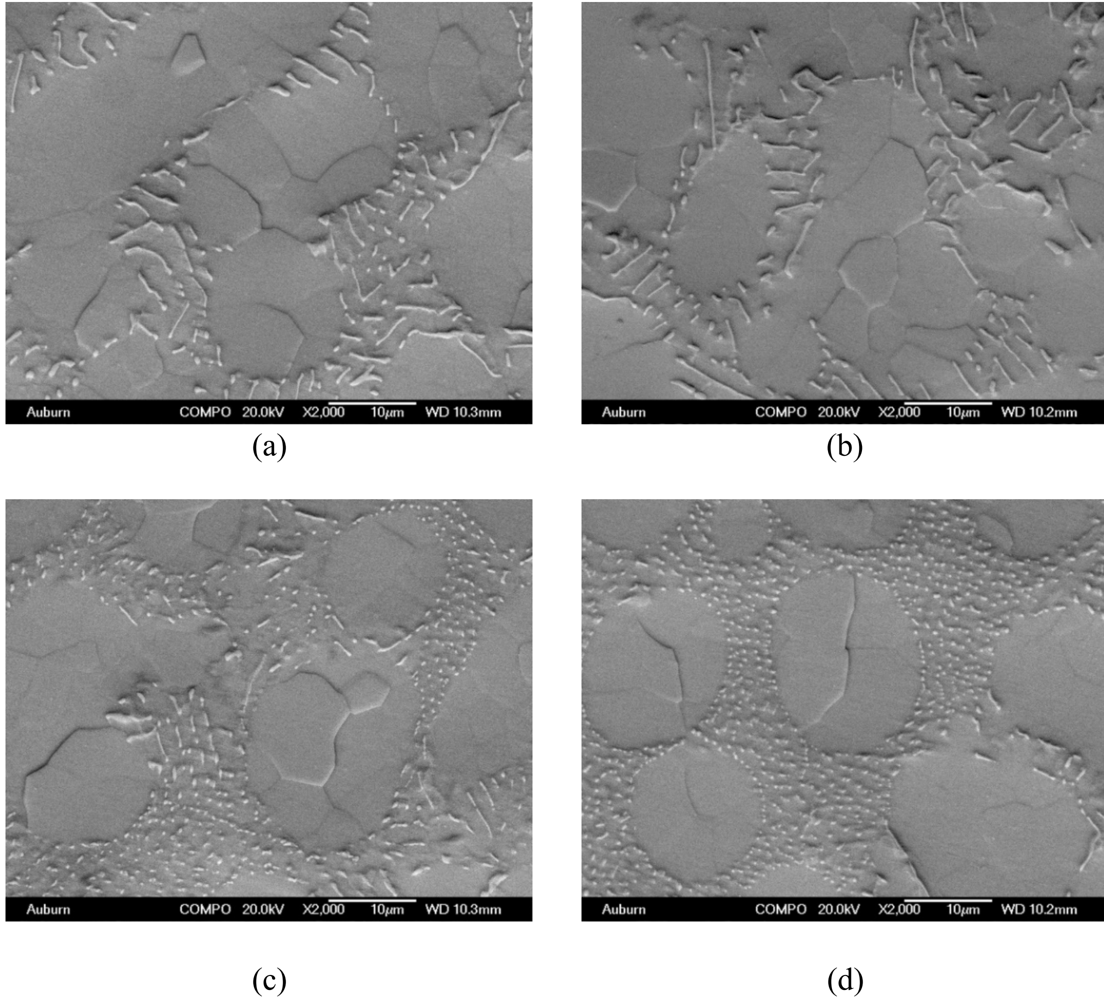

Figure 7.2 Location Based Variation in the Microstructure of SAC305 Solder

7.3 Sample Preparation and Experimental Procedure

The specimens for microstructure study were prepared by vacuum suction method. Rectangular specimen preparation procedure has been described in chapter 3. At first, an epoxy mold was taken, and a slot was made by IsoMet 1000 precision cutter. The size of slot was equivalent to the thickness of the rectangular sample. Afterwards, the rectangular sample was inserted into this slot and grinded flowed by autopolishing to obtain fine microstructure for SEM imaging. Figure 7.4 represents the flow chart of this sample preparation and experimental procedure. The detail of the grinding and polishing process

involves mechanical grinding with several SiC abrasive papers having different grits (300-1200) followed by polishing with 1 μm diamond paste and colloidal silica suspensions (0.02 μm). Finally, autoploisher has been used to remove any extra scratch left from grinding and polishing and to obtain mirror finish samples suitable for nanoindentation test and SEM microscopy, as shown in Figure 7.1.

Figure 7.3 IsoMet 1000 Precision Cutter

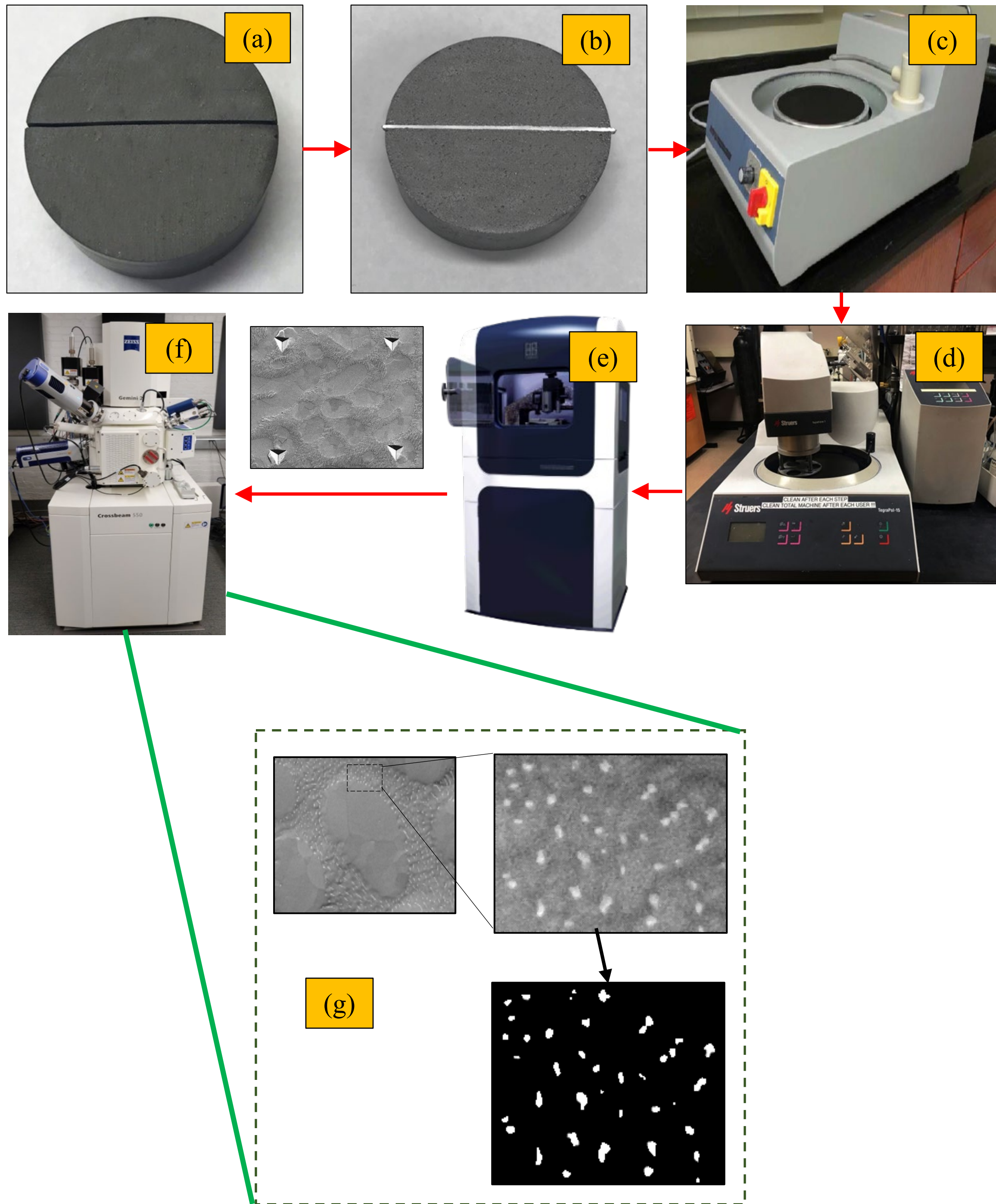

Figure 7.4 Flow Chart of Experimental Procedure (a) Slot Cutting, (b) Sample Insertion, (c) Grinding, (d) Autopolishing, (e) Nanoindentation, (f) Zeiss Cross Beam 500 SEM, (g) Image Processing

7.4 Thermal Cycling Chamber for Preconditioning

Thermotron SM series thermal cycling chamber from Thermal Product Solutions (figure 7.5) was used to perform slow thermal ramping (no dwell) and slow thermal cycling (both dwell and ramp) of the sample in this study. A programmable controller attached to the main chamber was utilized to program the thermal profile. The rectangular sample obtained after polishing was subjected to a temperature cycle profile with: Temperature excursion: -40 °C to 125 °C Ramp rate: 45 min and Dwell time: 30 min. Before running tests, the chamber was calibrated using a thermal profiler. Also, a dummy sample similar to original sample was placed inside the chamber and was monitored at three different positions attaching a K-type thermocouple to ensure that the original sample follows the same profile during test. Figure 7.5 (a) shows the thermal cycling chamber used for sloe thermal ramping (no dwell) and slow thermal cycling. Figure 7.5 (b) shows the thermal profiles used foe calibration. Using thermal profiler, it was found that the 45 min ramp and 30 min dwell periods were well maintained in the profile. All the thermal cycling profile have been mentioned in chapter 3.

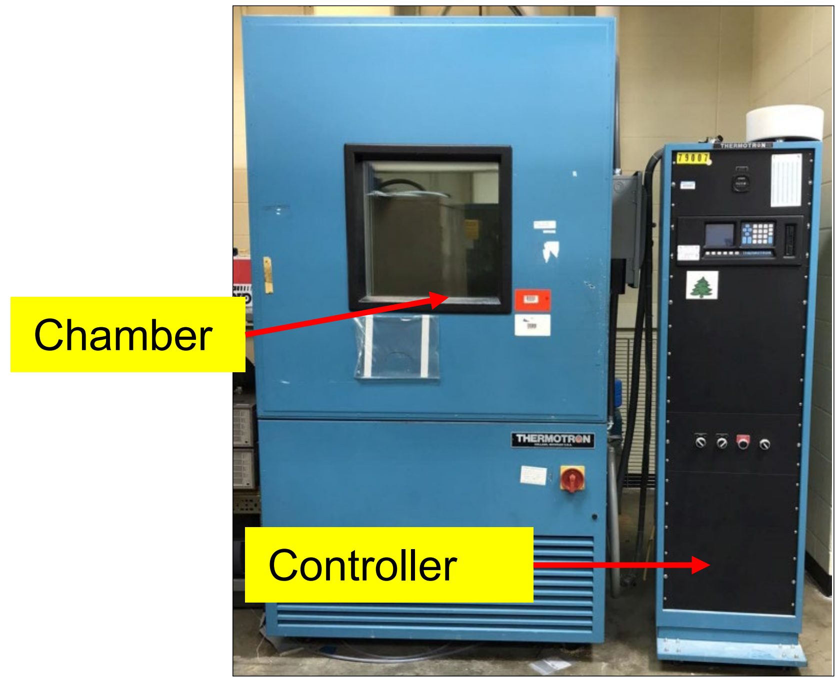

(a)

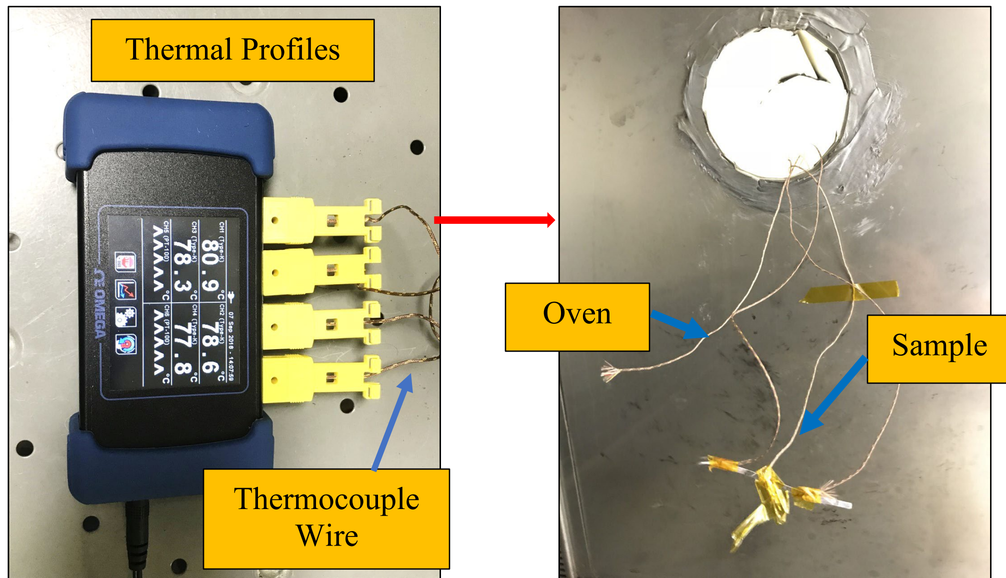

(b)

Figure 7.5 (a) Thermal cycling chamber (b) Thermal Profiler

7.5 Scanning Electron Microscopy (SEM) Imaging of SAC305 Solder

After preconditioning and nanoindentation, SEM analysis of the selected regions was performed on the non-aged as-polished samples. The same samples were then aged at high temperature (T= 125) for four different durations of aging (1, 2, 5, and 20 Days). Other two profiles were (1) slow thermal ramping: ramping between -40 – 125C for 45 minutes and ramping down for 45 minutes, and (2) slow thermal cycling: ramping between -40 – 125C for 45 minutes, dwelling at 125C for 30 minutes, and ramping down for 45 minutes. All the samples were cycled under these two profiles for same time durations as aging. The microstructures of the selected regions were captured after each exposure time. Three different regions of SAC305 bulk solder were chosen for each thermal exposure.

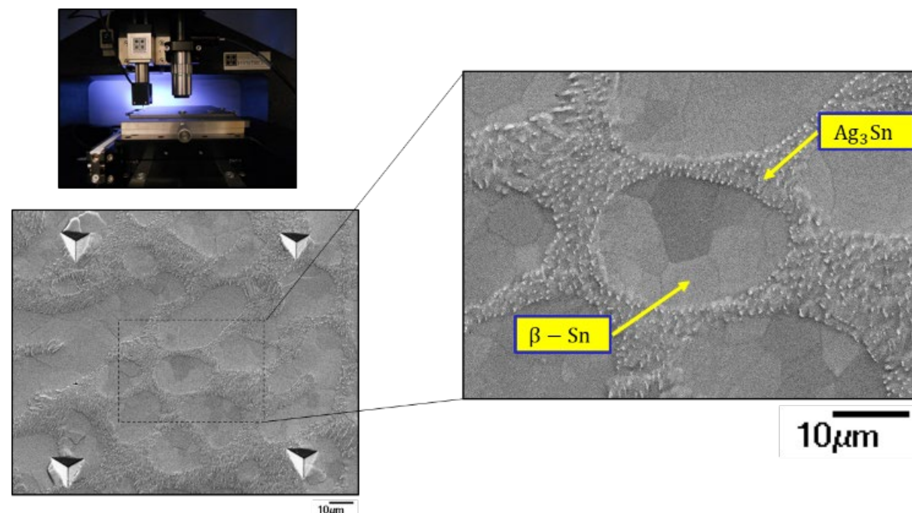

Figure 7.6 Example Region of Interest and Nanoindentation Markers

7.6 Effect of Thermal Exposure on Microstructure of SAC305 Solder

7.6.1 Effect of Aging

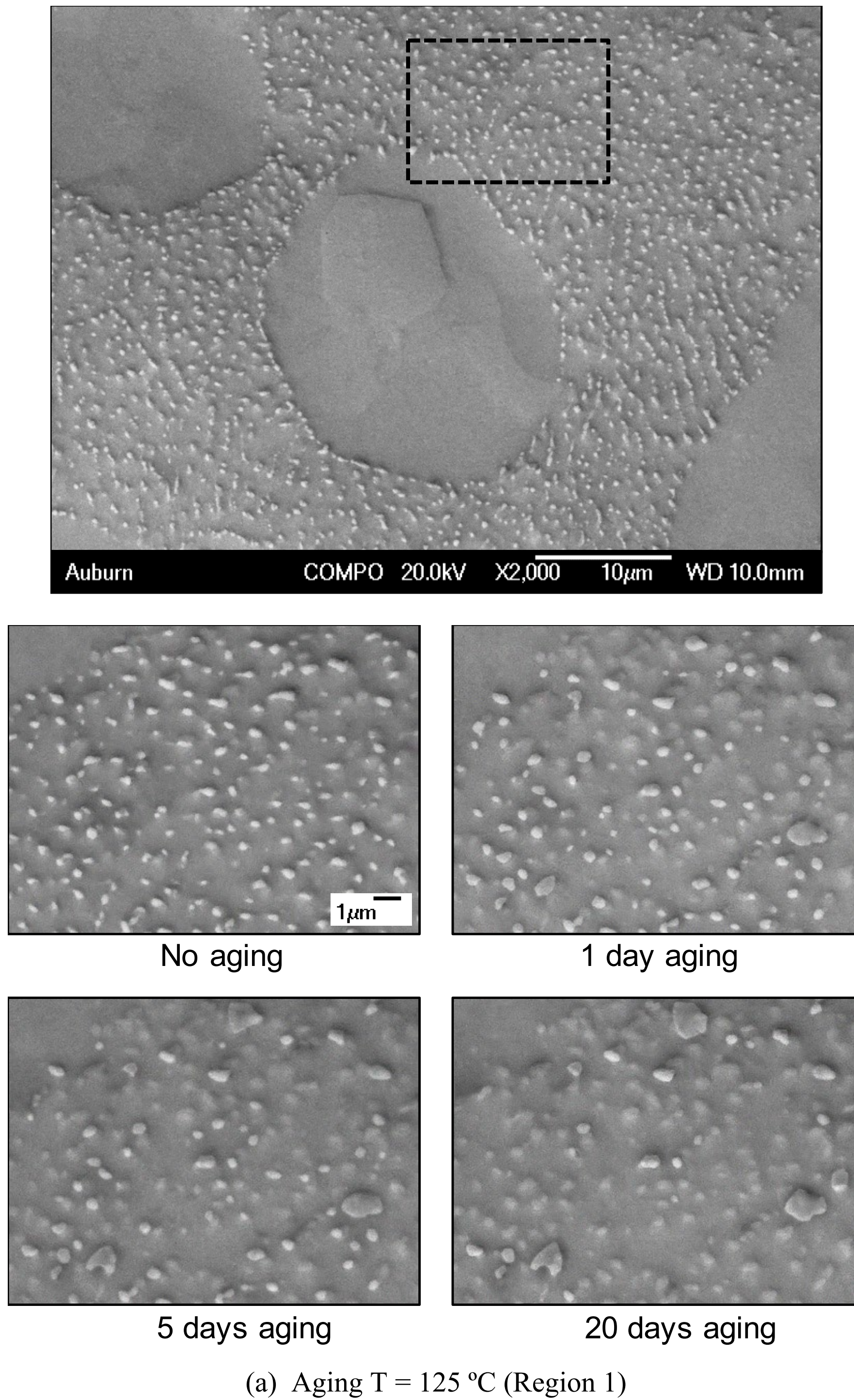

(a) Aging T = 125 ºC (Region 1)

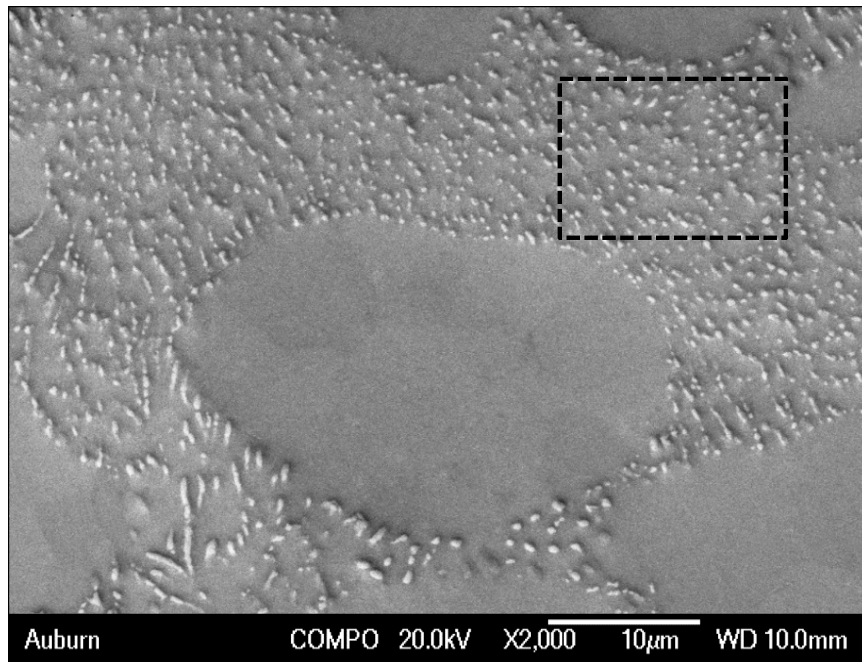

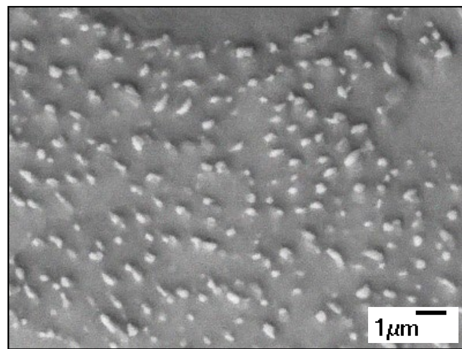

No aging

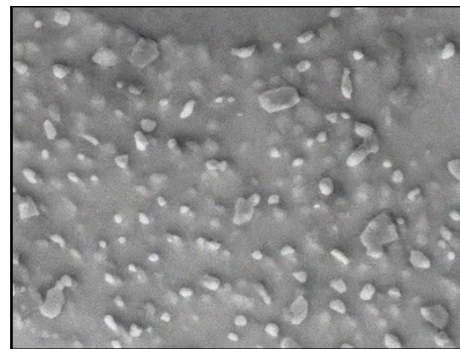

1 day aging

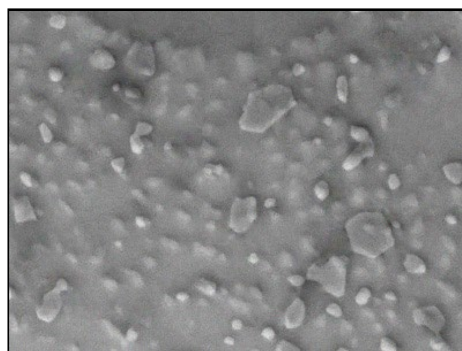

5 days aging

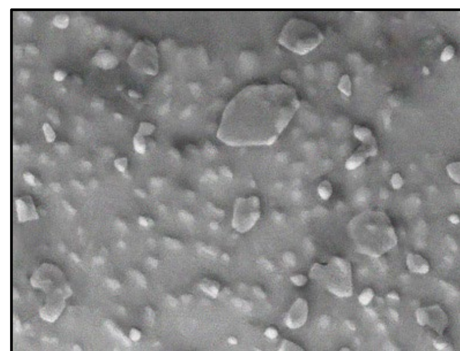

20 days aging

(b) Aging T = 125 ºC (Region 2)

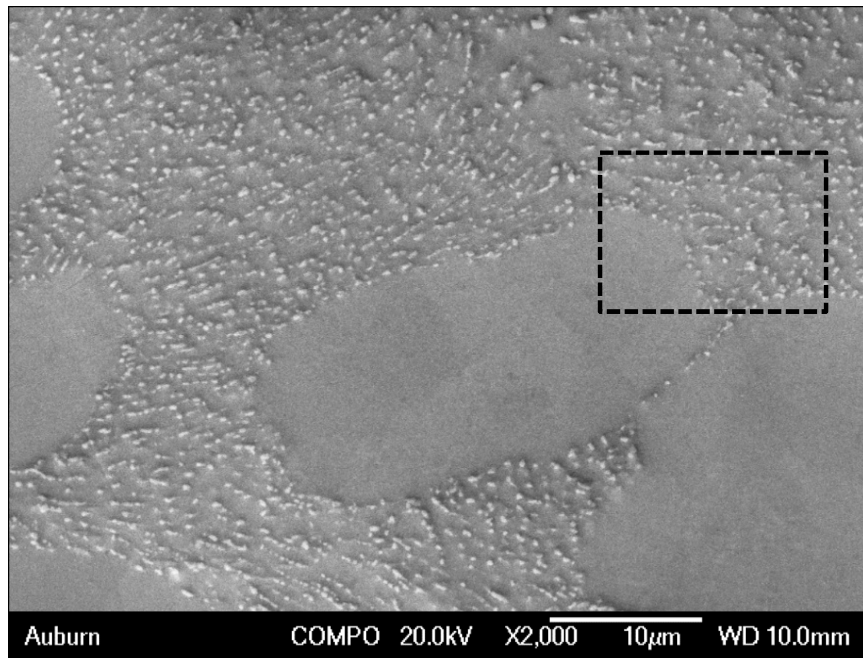

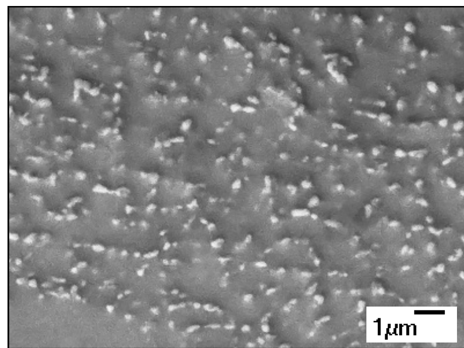

No aging

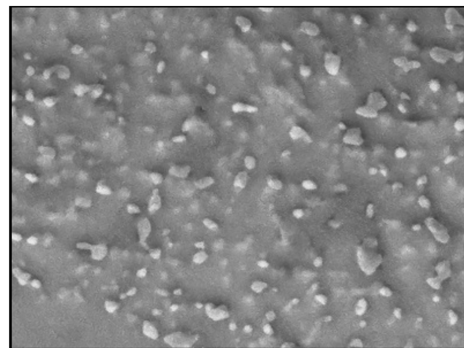

1 day aging

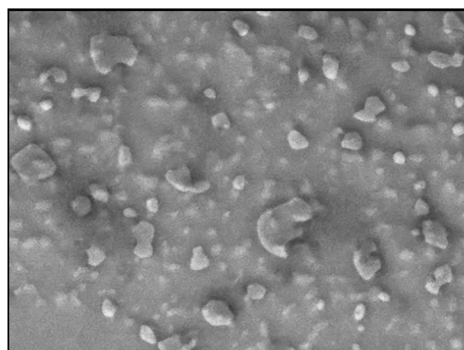

5 days aging

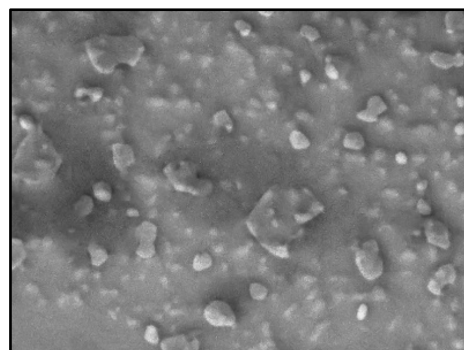

20 days aging

(c) Aging T = 125 ºC (Region 3)

Figure 7.7 Microstructure Evolution of SAC305 Solder Under Isothermal Aging

7.6.2 Effect of Slow Thermal Ramping (No Dwell)

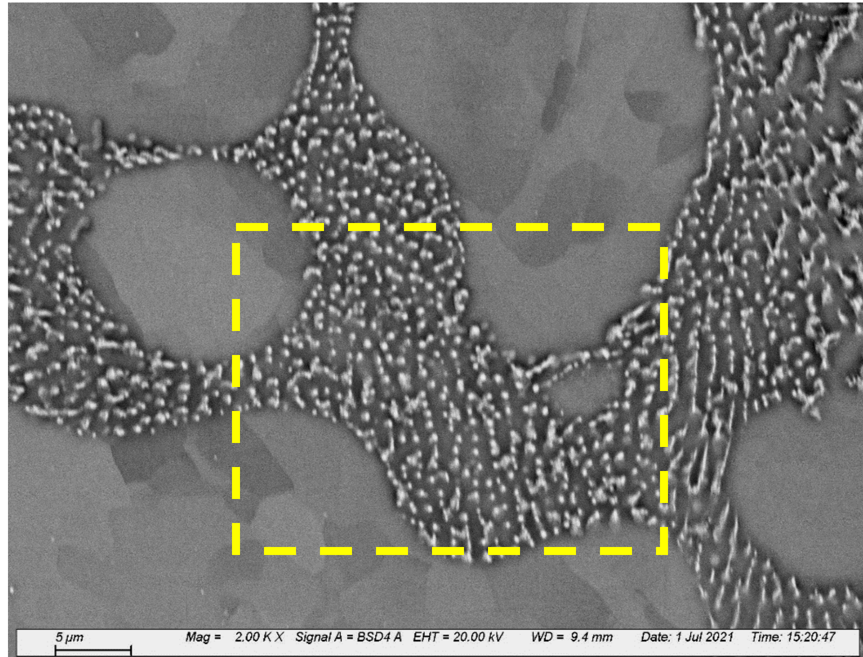

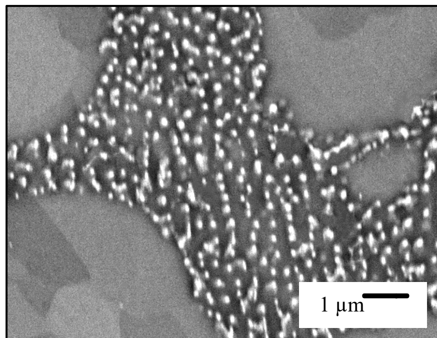

As Reflowed

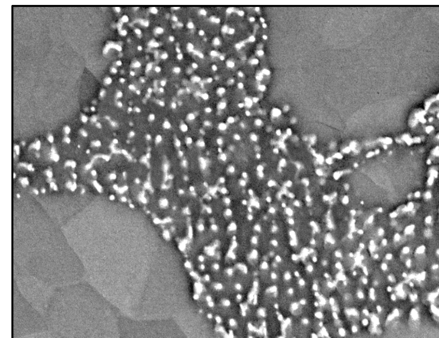

1 Day STR

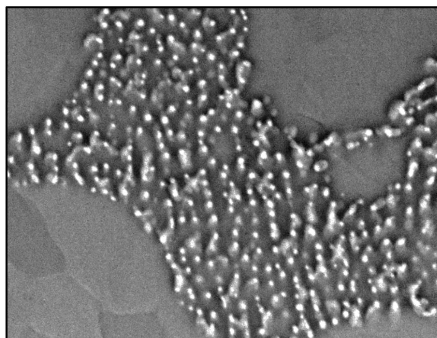

5 Days STR

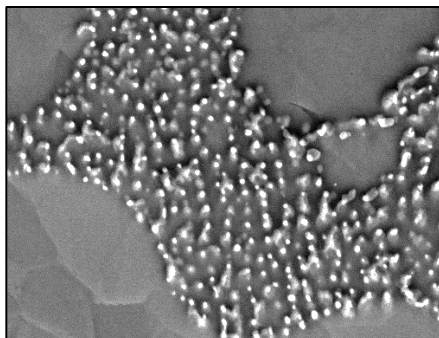

20 Days STR

(a) Slow Thermal Ramping (Region 1)

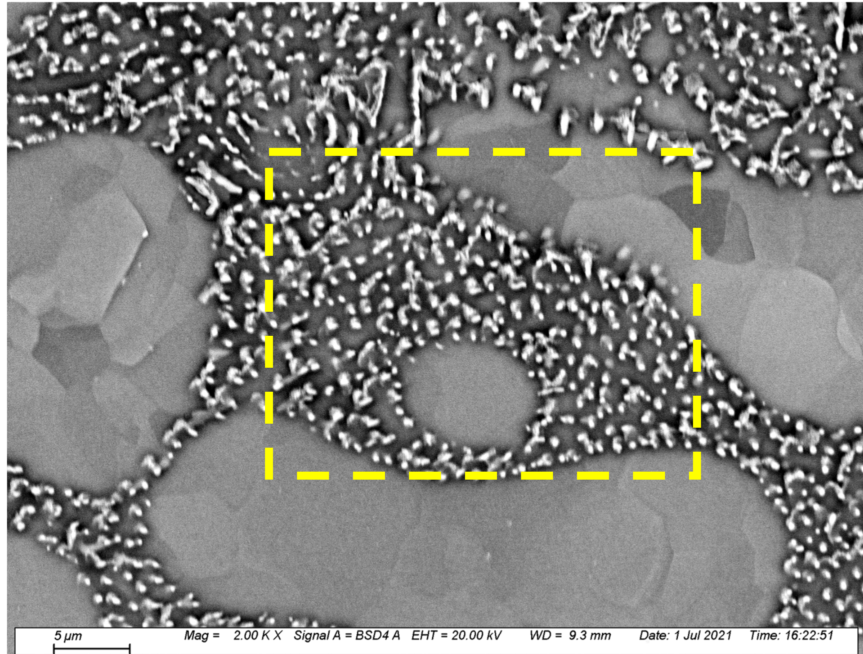

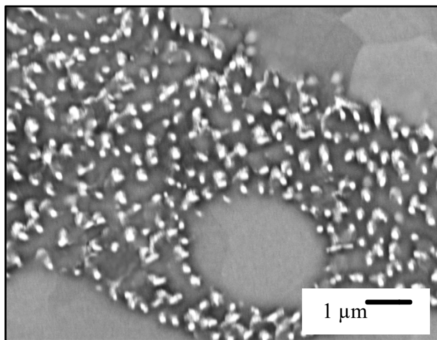

As Reflowed

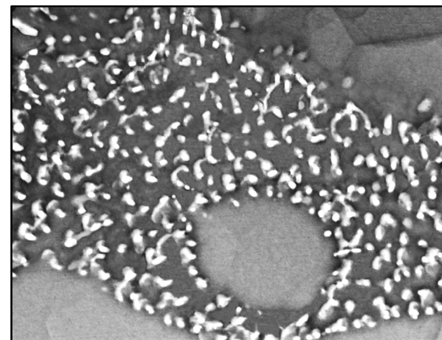

1 Day STR

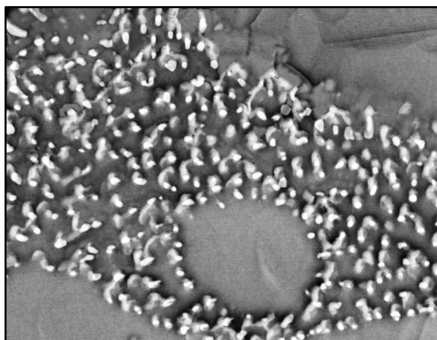

5 Days STR

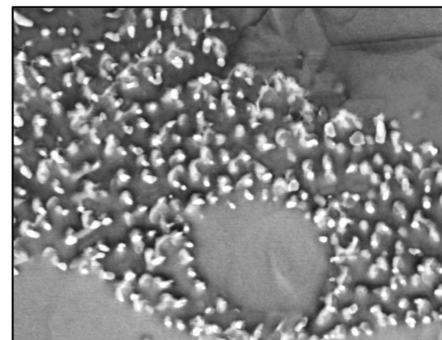

20 Days STR

(b) Slow Thermal Ramping (Region 2)

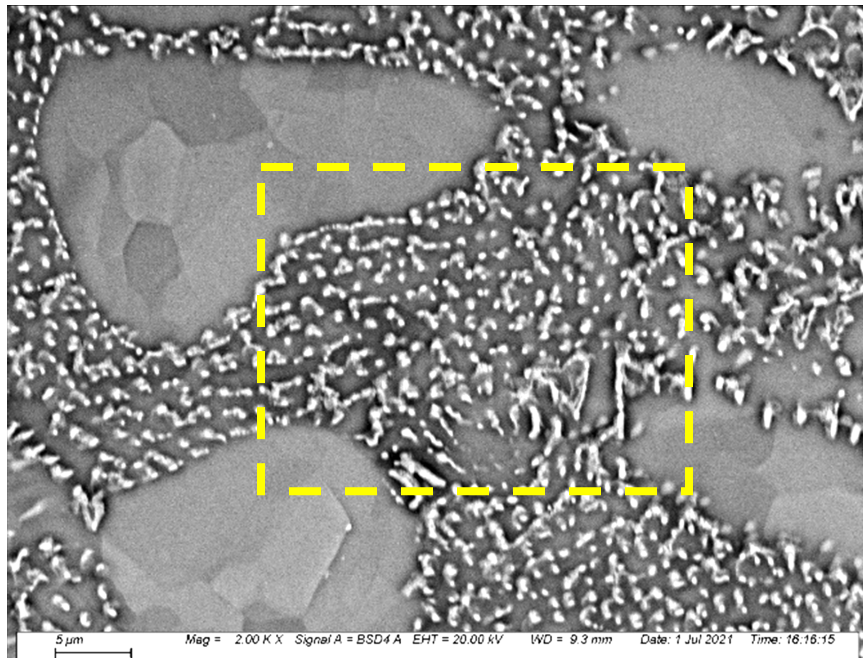

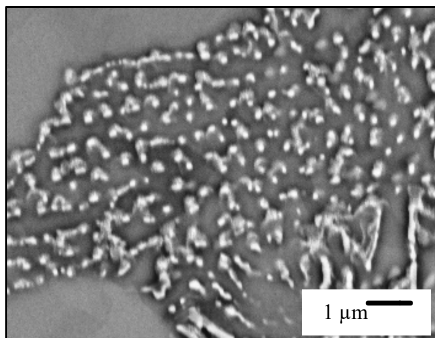

As Reflowed

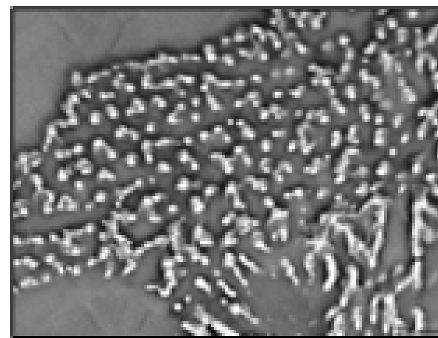

1 Day STR

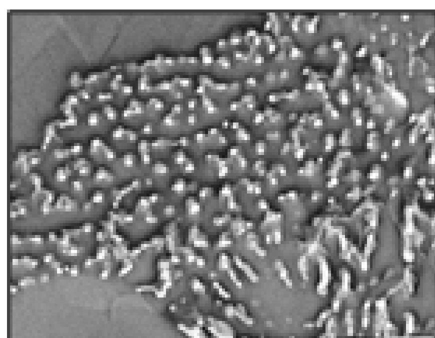

5 Days STR

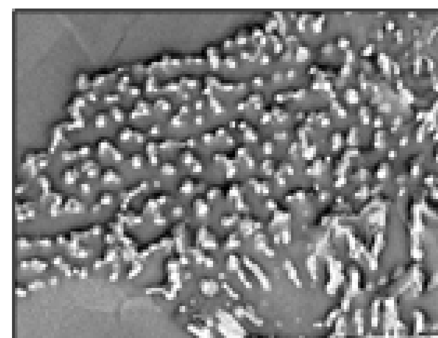

20 Days STR

(c) Slow Thermal Ramping (Region 3)

Figure 7.8 Microstructure Evolution of SAC305 Solder Under STR

7.6.3 Effect of Slow Thermal Cycling (Ramp+Dwell)

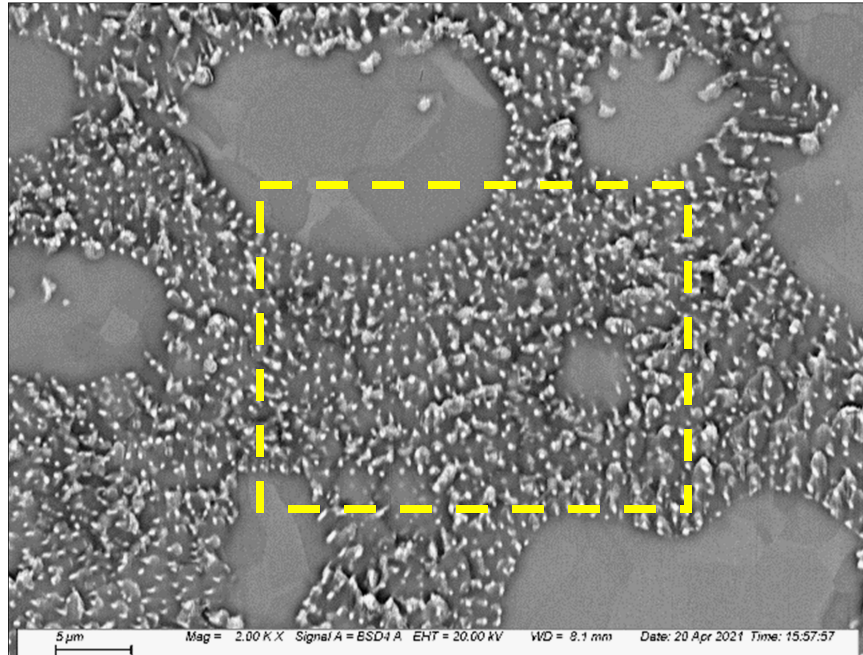

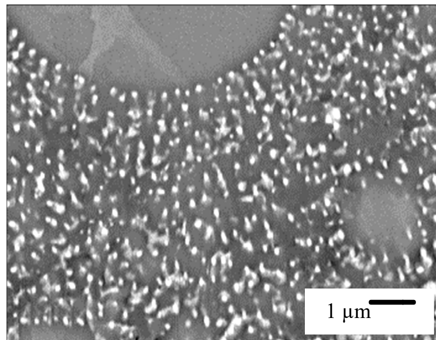

As Reflowed

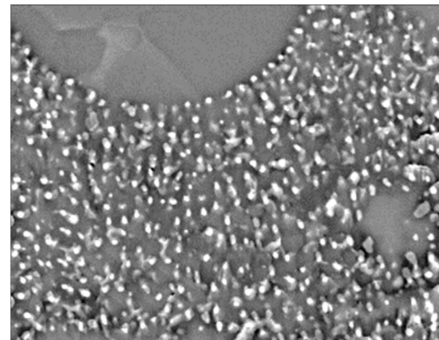

1 Day STC

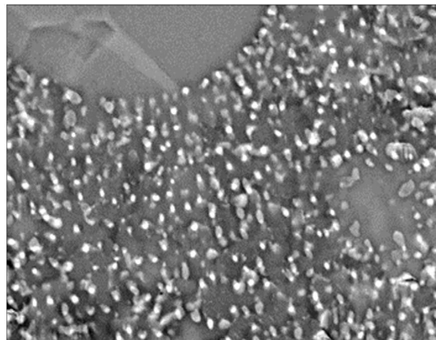

5 Days STC

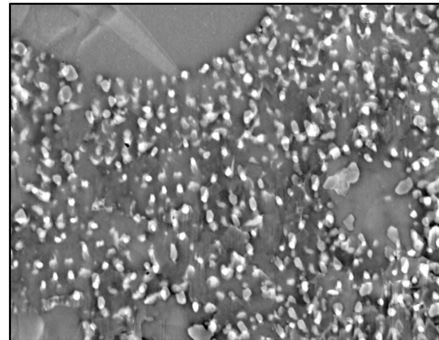

20 Days STC

(a) Slow Thermal Cycling (STC) (Region 1)

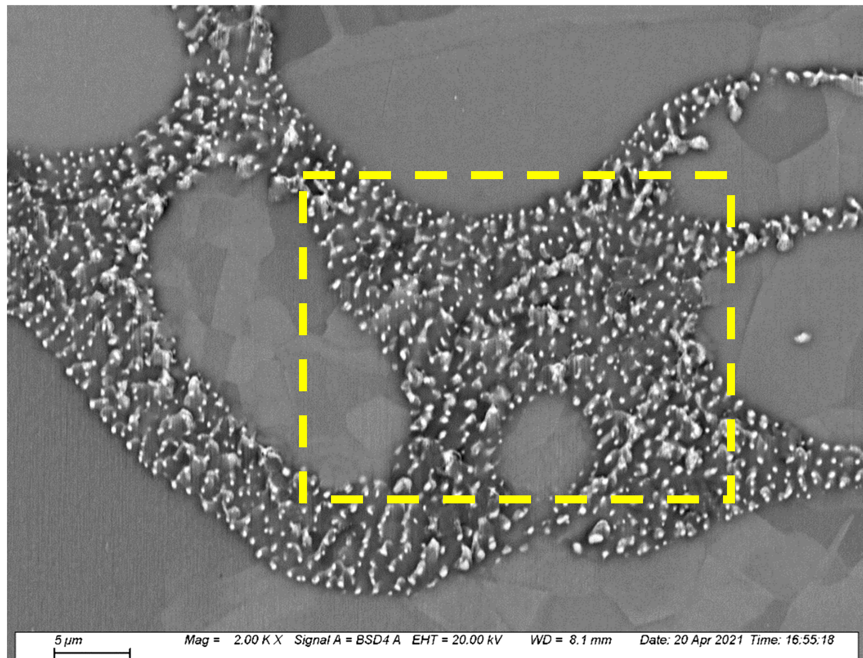

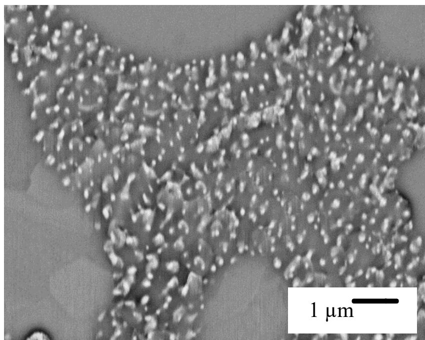

As Reflowed

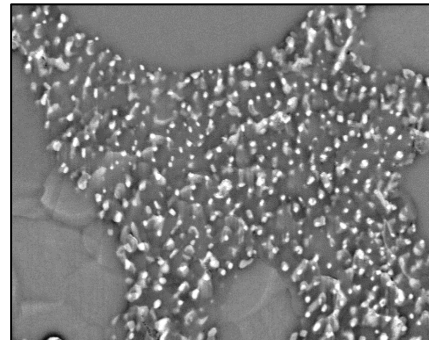

1 Day STC

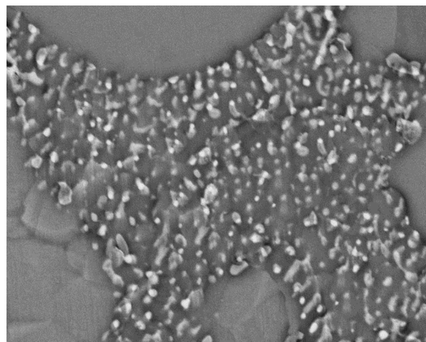

5 Days STC

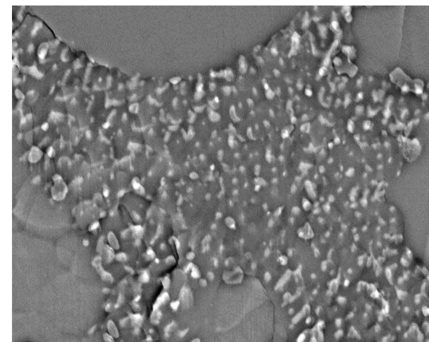

20 Days STC

(b) Slow Thermal Cycling (STC) (Region 2)

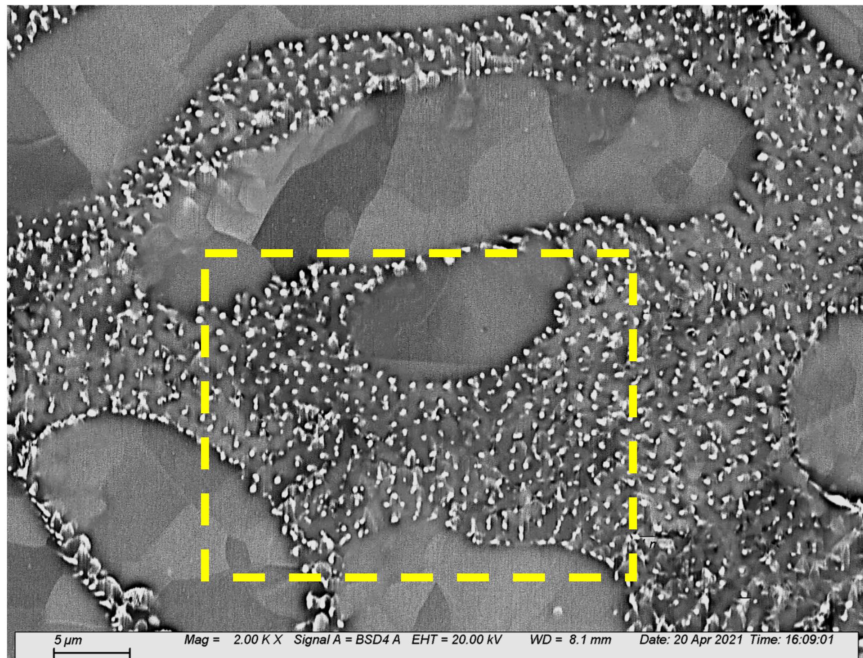

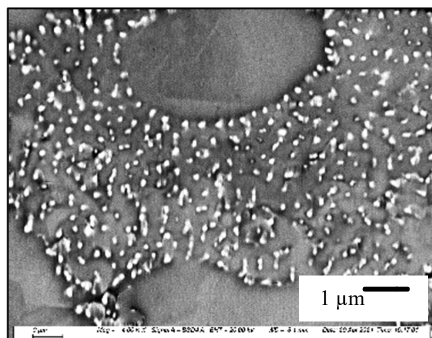

As Reflowed

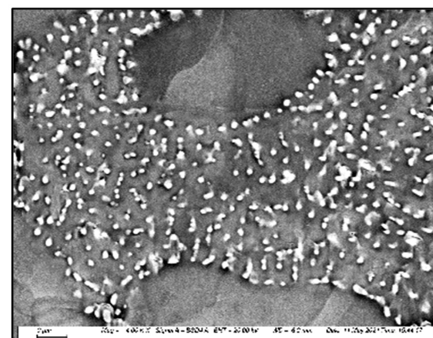

1 Day STC

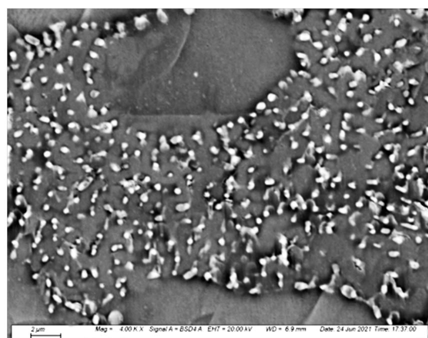

5 Days STC

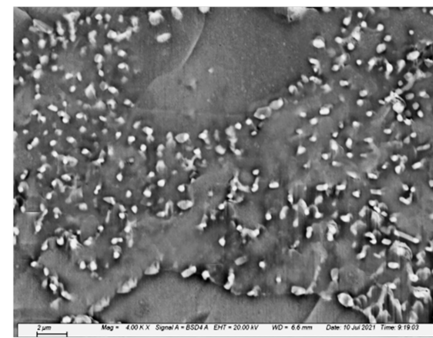

20 Days STC

(c) Slow Thermal Cycling (STC) (Region 3)

Figure 7.9 Microstructure Evolution of SAC305 Solder Under STC

7.7 Measurement of Area and Number of IMC

Quantitative analyses of the size metrics of the IMC particles were performed with all of the SEM images at different exposure times for the IMC particle evolutions. The analyzed regions were typically chosen to be interdendritic regions with a heavy concentration of IMC particles. For example, the images shown in Figure 7.10, were taken from a subregion of the images in Figure 7.7. The area of each particle, the total area of all of the particles, and the total number of particles in each selected region and aging time were determined using image analysis software (ImageJ and Adobe Photoshop) and Matlab. The particle size measurement process involves 3 major steps. First, all the particles were outlined in Adobe Photoshop. Then the gray scale image was converted into a binary image. Lastly, the average area of the particles (White spots), in the binary image, were calculated using MATLAB and the number of particles were determined using image analysis software (ImageJ). An example of image analysis process is shown in Figure 7.10. An SEM image with all the IMC particles is presented in Figure 7.10 (a). Figure 7.10 (b) represents the corresponding binary image with the outlined particles that was obtained after conversion. This image was used to calculate the area of particles in MATLAB. Figure 7.10 (c) shows the image obtained from the ImageJ software representing particles numbers. It is evident from this image that the software was capable to accurately identify all the individual particle in the field of view.

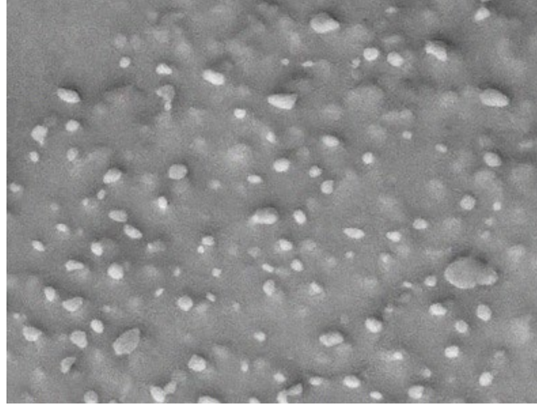

(a)

(b)

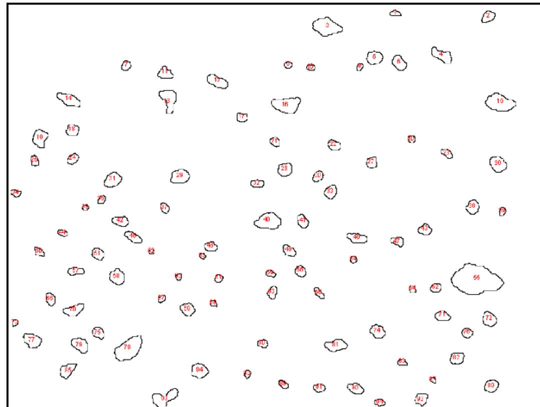

(c)

Figure 7.10 Image Processing Steps for IMC Particle Area Calculations (a) After Outlining All the Particles (b) Binary Image and (c) Final Image from ImageJ

7.8 Measurement of Particle Diameter and Evolution with Exposure Time

Average particle diameter of all the particles was calculated using the empirical model described in section 3.6.3. To observe the evolution of the average particle diameter under different thermal exposures was plotted with exposure time. In section 3.6.4, description of the model used to track the particle diameter evolution with exposure time has been reported. Table 7.1 represents the variations in particle numbers and average particle diameters with aging. The variations of the average IMC particle diameter exposure is shown in Figures 7.11.

Table 7.1 IMC Particle Diameter of Different Locations Under Different Thermal Exposure with Different Exposure Time

Thermal Exposure	Time (Days)	No. of Particles				Avg. Diameter (nm)			
		R- 1	R- 2	R- 3	Avg	R- 1	R- 2	R- 3	Avg
Aging	0	178	205	273	218	390	374	328	364
	1	94	88	101	94	550	645	587	537
	5	69	44	47	53	651	930	968	850
	20	60	35	33	42	753	1132	1225	1036
Slow Thermal Ramping	0	75	209	230	171	320	356	350	342
	1	45	130	69	81	384	455	382	407
	5	30	41	25	32	806	975	890	890
	20	21	20	18	19	1056	1111	1240	1136
Slow Thermal Cycling	0	252	193	151	198	326	292	428	349
	1	139	106	83	110	368	368	449	395
	5	32	18	35	28	906	808	1233	982
	20	17	11	12	13	1180	1153	1584	1300

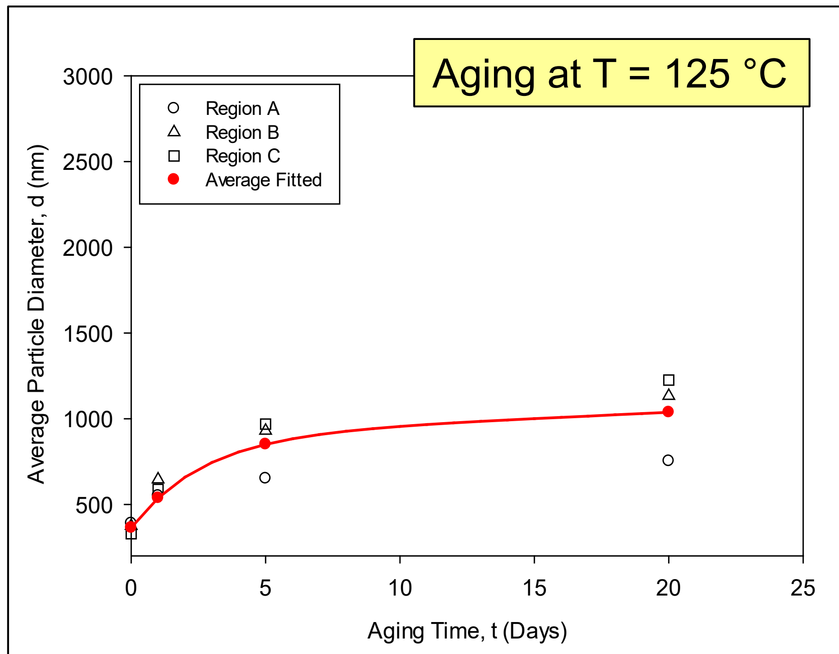

(a) Isothermal Aging

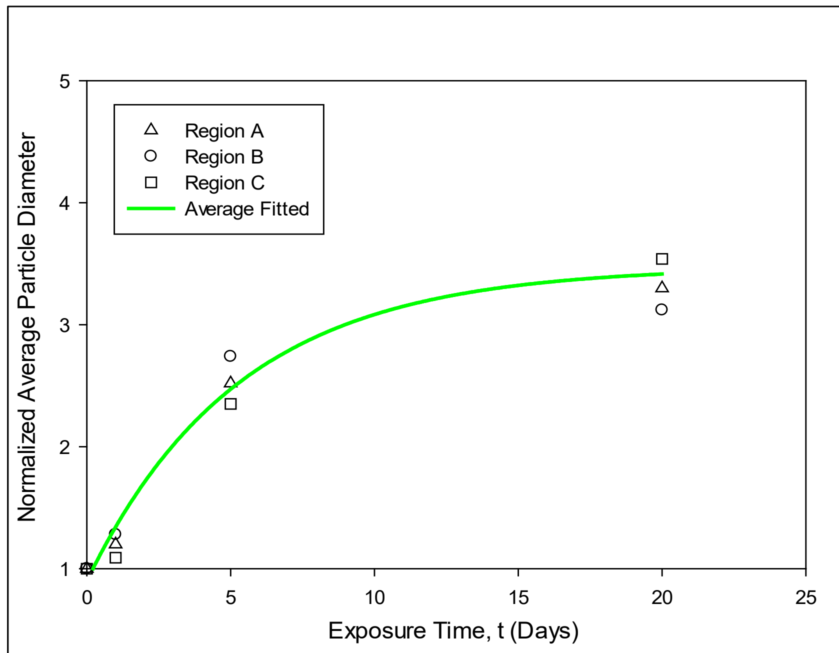

(b) Slow Thermal Ramping

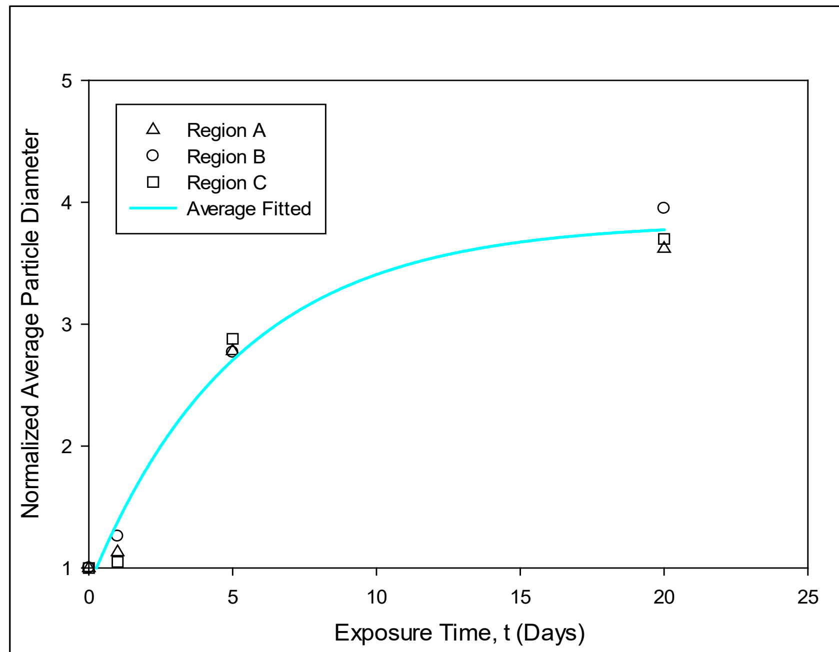

(c) Slow Thermal Cycling

Figure 7.11 Changes in IMC Particle Diameter with Exposure Time Under Different Thermal Exposure

7.9 Comparison of Normalized Average Particle Diameter Evolution

Figure 7.12 shows the comparison of average normalized particle diameter change under different thermal cycling exposures. In this plot, red, green, and pink curves are presenting the average normalized particle diameter change with elapsed time. It can be seen that initially, up to 1 day of thermal exposure, the change in normalized average particle diameter was higher under isothermal aging compared to the slow thermal ramping and slow thermal cycling. But, after 20 days of thermal exposures, it becomes significantly higher under slow thermal ramping, and slow thermal cycling compared to isothermal aging.

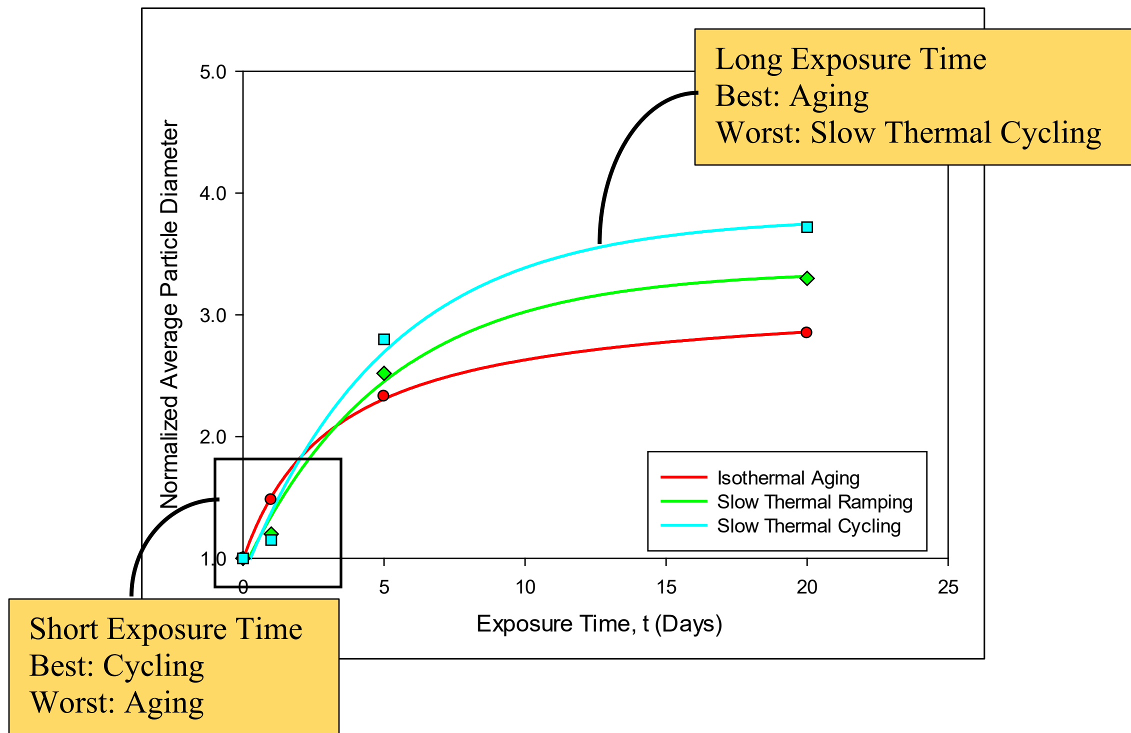

Figure 7.12 Comparison of Normalized Average Particle Diameter Evolution Under Different Thermal Exposure with Exposure Time

7.10 Correlation Between Mechanical and Microstructural Properties Evolution

In this study, it was found that mechanical properties degraded with exposure time under isothermal aging and any thermal cycling exposures. But initially, the degradation is higher under isothermal aging compared to other thermal exposures. After 5 days of exposures, the degradation under slow thermal ramping, thermal shock, and slow thermal cycling became higher compared to isothermal aging at 125C. But the degradation was higher under thermal cycling with longer ramp period. From section 7.9, similar phenomena can be observed for microstructural evolution. For example: After 1 day of isothermal aging, the average normalized particle diameter increased 48%, while under slow thermal ramping and slow thermal cycling it was 20%, as well as 15%. Contrarily, after 20 days of isothermal aging, it becomes 185% whereas under slow thermal ramping

and slow thermal cycling it was about 230%, and 275%, respectively. Figure 7.13 (a) and 7.13 (b) show the correlation between microstructure and tensile properties and creep properties respectively.

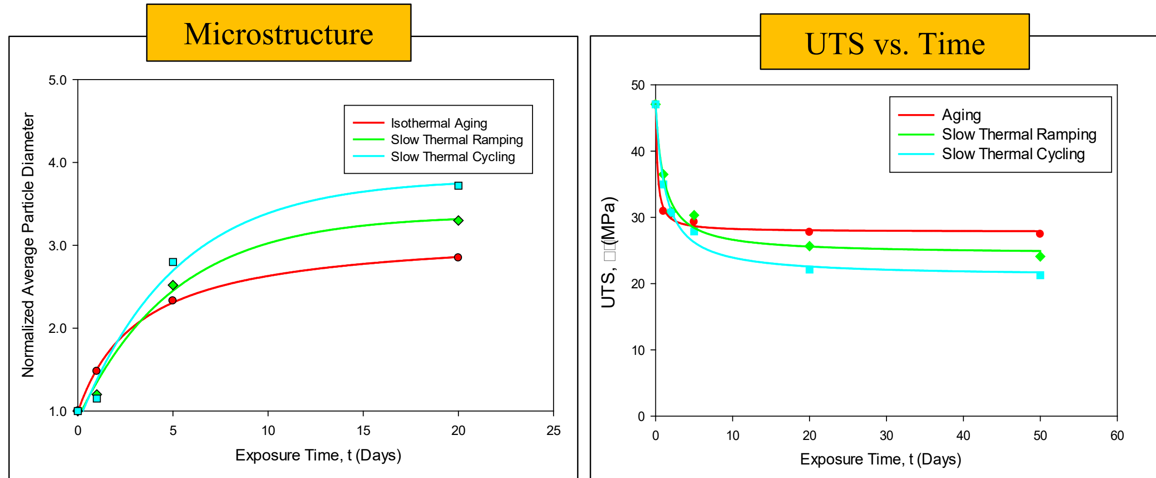

(a)

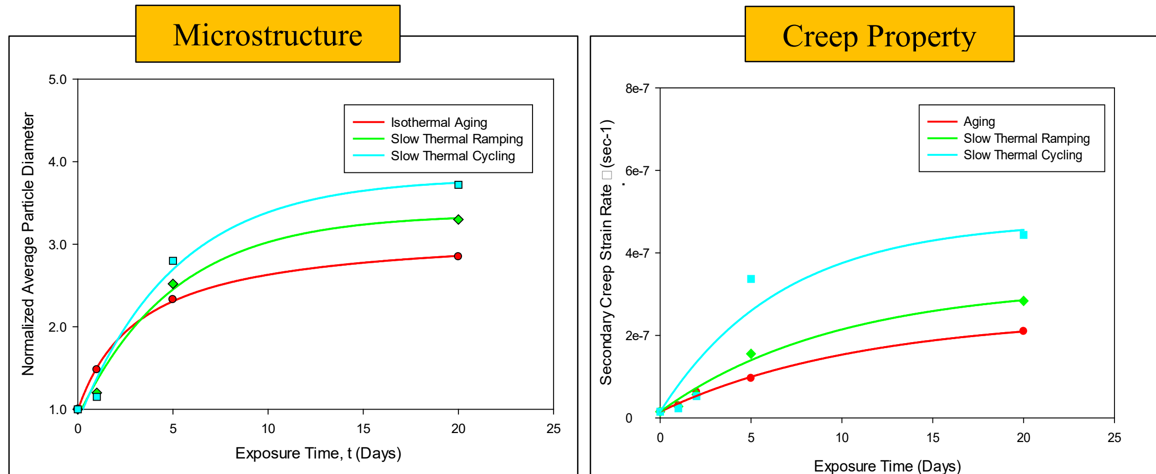

(b)

Figure 7.13 Correlation Between Microstructure and Mechanical Properties of SAC305 Solder Alloy

Figure 7.14 represents the evolution of normalized ultimate tensile strength with normalized average particle diameter. Red, green, and cyan colored curves present aging, ramping, and cycling results respectively. From this plot, it can be observed that irrespective to the thermal exposures, normalized ultimate tensile strength degraded exponentially with normalized average particle diameter. Also, all three curves are almost same which indicates the dependence of IMC particle diameter on ultimate tensile strength irrespective to the thermal exposure profiles. Figure 7.15 shows fitted curve that satisfies all data points and indicates that microstructure evolution depends on UTS not on thermal profiles.

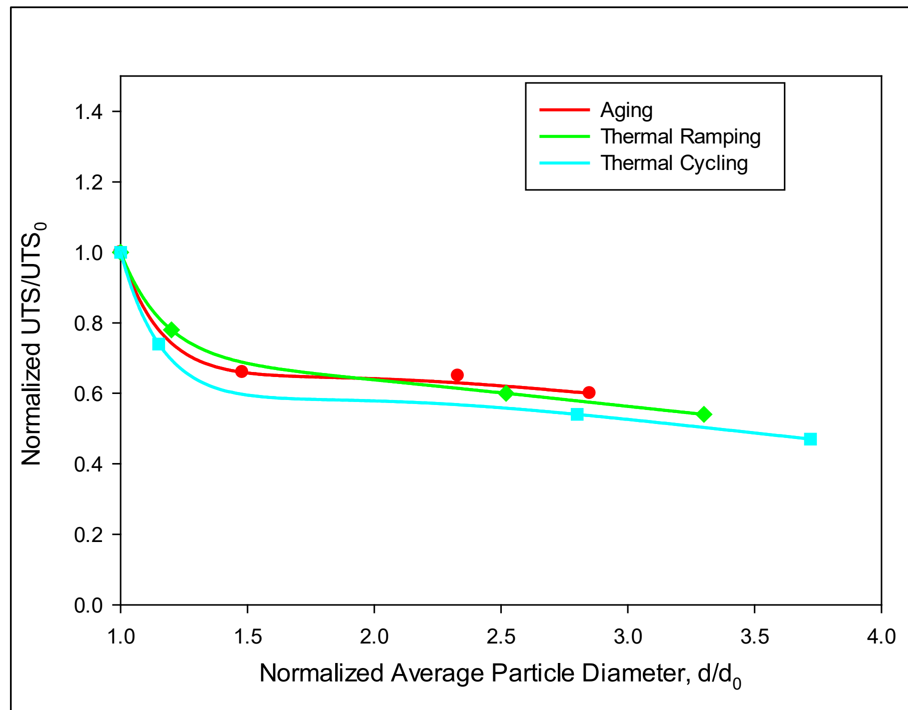

Figure 7.14 Change of Normalized Ultimate Tensile Strength with Normalized Average Particle Diameter

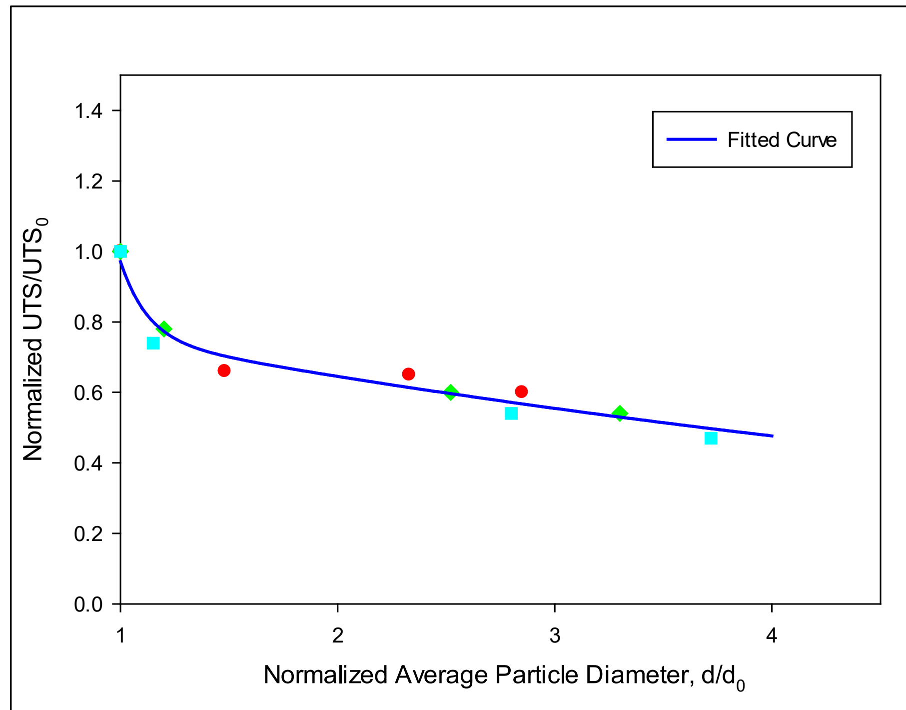

Figure 7.15 Relationship Between UTS and IMC Particle Diameter

Figure 7.16 depicts the effect of normalized average particle diameter on normalized creep rate. In this plot, red, green, and cyan curves present aging, ramping, and cycling results, respectively. It is obvious from this plot that normalized creep rate changes linearly with normalized average particle diameter. In addition, the curves are close to each one which demonstrates that irrespective to the microstructure evolution process, the IMC particle diameter changes depend on creep rate. Figure 7.17 shows best fit curve which goes through all data points and indicates that microstructure is tied up with creep rate not with thermal profiles.

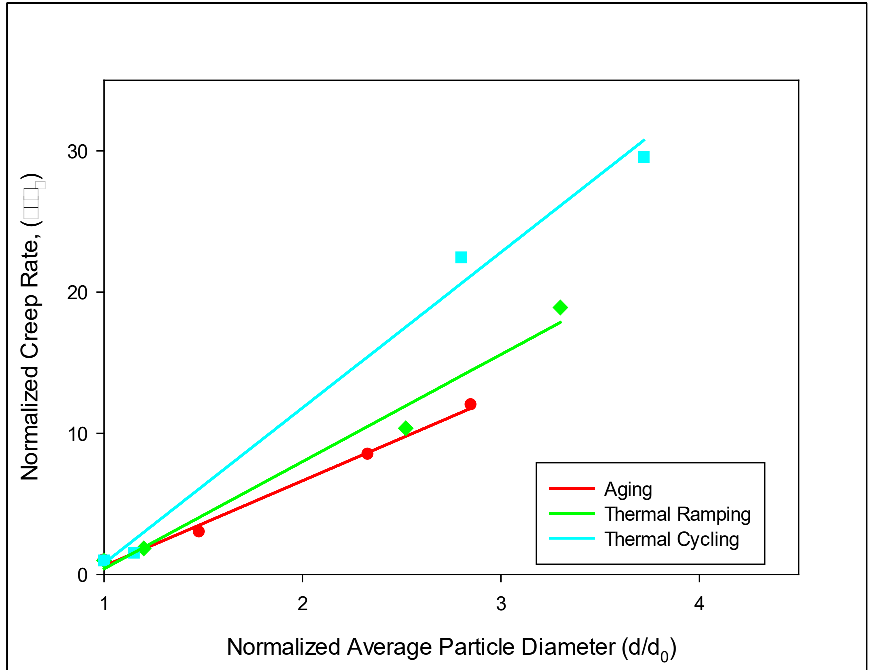

Figure 7.16 Change of Normalized Creep Rate with Normalized Average Particle Diameter

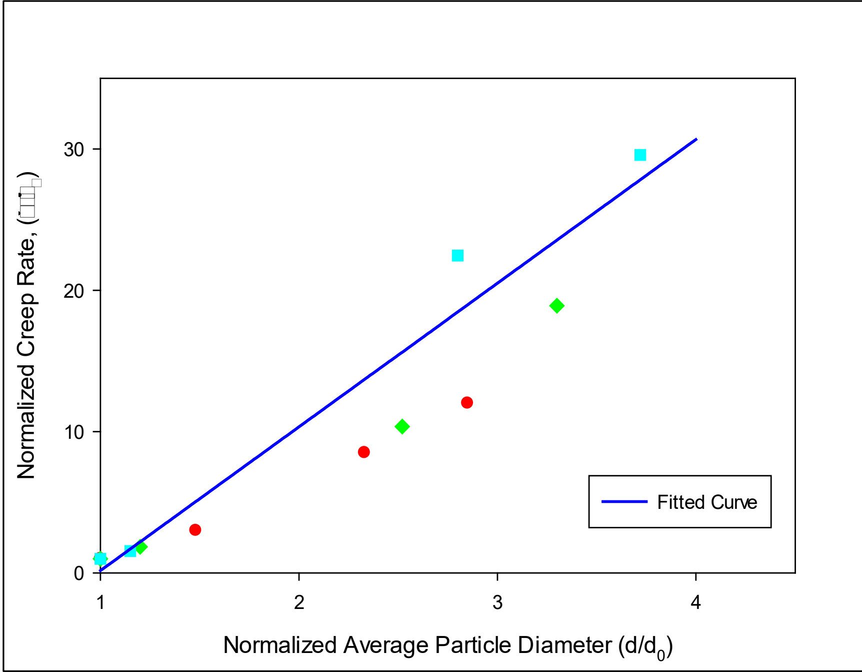

Figure 7.17 Relationship Between Creep Rate and IMC Particle Diameter

7.11 Microstructure Analysis of SAC+Bi Solder Alloy

As Mentioned in section 7.1, the microstructure of SAC305 is mainly composed of a β-Sn matrix and two different intermetallic compounds (IMC) namely, Ag_3Sn and Cu_6Sn_5. The reduction of strength of SAC305 after thermal exposure can be attributed to 2 major facts. First, coarsening of the Ag_3Sn and Cu_6Sn_5 intermetallic compounds and hence reduces their ability to block dislocation movements. Second, the β-Sn phase also coarsens/grows with thermal exposure, and hence reduces the strength of the alloy.

For the SAC-Bi alloy, the additional Bi content doesn't form any IMC with Sn. Therefore, the only IMCs that should present in microstructure of SAC_Q are Ag_3Sn and Cu_6Sn_5. However, Bi remains as a separate phase in the microstructure enhance the strength of the SAC-Bi alloys. Also, from the Sn-Bi phase diagram (see figure 7.18), it is observed that Bi has a good (~1.8%) solid solubility in Sn at room temperature. Hence Bi contributes more enhancement in strength of the SAC-Bi alloy before aging by the solid solution strengthening mechanism.

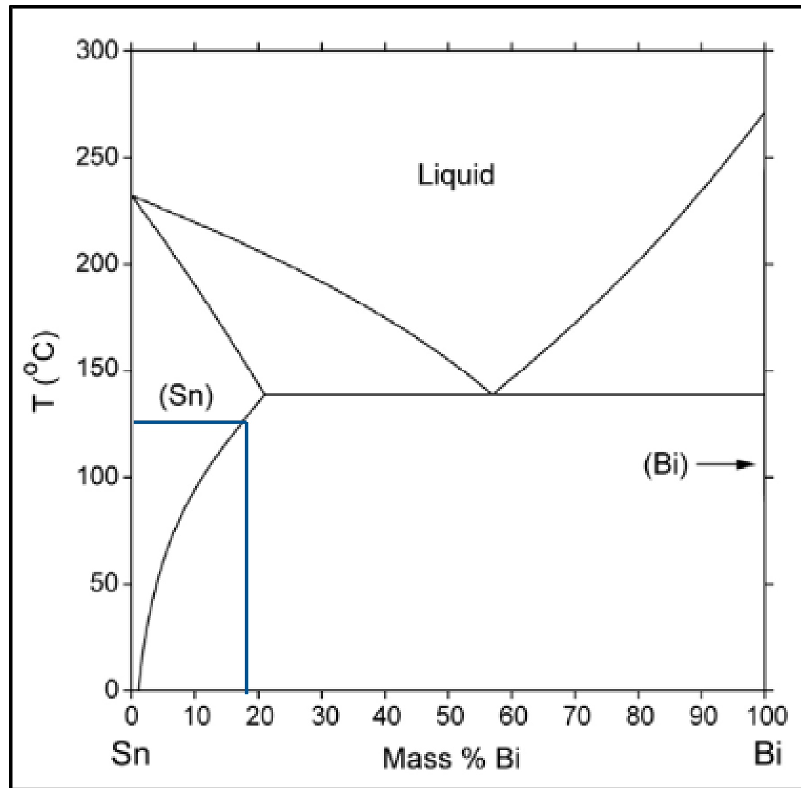

Figure 7.18 Sn-Bi Phase Diagram (http://www.metallurgy.nist.gov/)

Cai and coworkers [51] have demonstrated that additional Bi will go into solution in the β-Sn matrix during the aging of SAC-Bi alloys. As seen in Figure 7.18, the solid solution solubility of Bi increases from 1.8% at T = 25 °C, to about 17% at 125 °C. Thus, the Bi present in the as solidified microstructure of SAC-Bi alloys as a separate Bi phase will have the tendency to go into the solution with the β-Sn matrix during all thermal exposures. This will lead to additional solid solution strengthening of the SAC-Bi alloy. A hypothesis was developed to explain the experimental observation. According to the hypothesis, the observed negligible variations in strength of SAC_Q before and after thermal exposure is due to the increases in strength from solid solution strengthening exceeding any reductions in strength caused by the evolution of microstructure during high temperature aging.

To support the proposed mechanism for mitigation of different thermal exposure effect in SAC-Bi alloys, a study on the microstructure of SAC_Q was performed. At first, three different locations in a SAC_Q microstructure with β-Sn dendrites surrounded by interdendritic regions with IMC particles were selected and captured in SEM. The sample was then preconditioned with aging at 125 °C for 1, 5, and 20 days, and the images of the same locations were recaptured. These images were compared to see the effect of aging on the microstructure (figure 7.15). Similar images were captured for slow thermal ramping and slow thermal cycling exposure (figure 7.16, 7.17). The comparison shows that both the β-Sn dendrites and IMC particles presents in the microstructure of SAC_Q remains unaffected after thermal exposures in each of these three locations. These findings validate the experimental results of SAC-Bi alloys reported in this dissertation where the mechanical properties of SAC_Q showed negligible variations after aging and other thermal exposures.

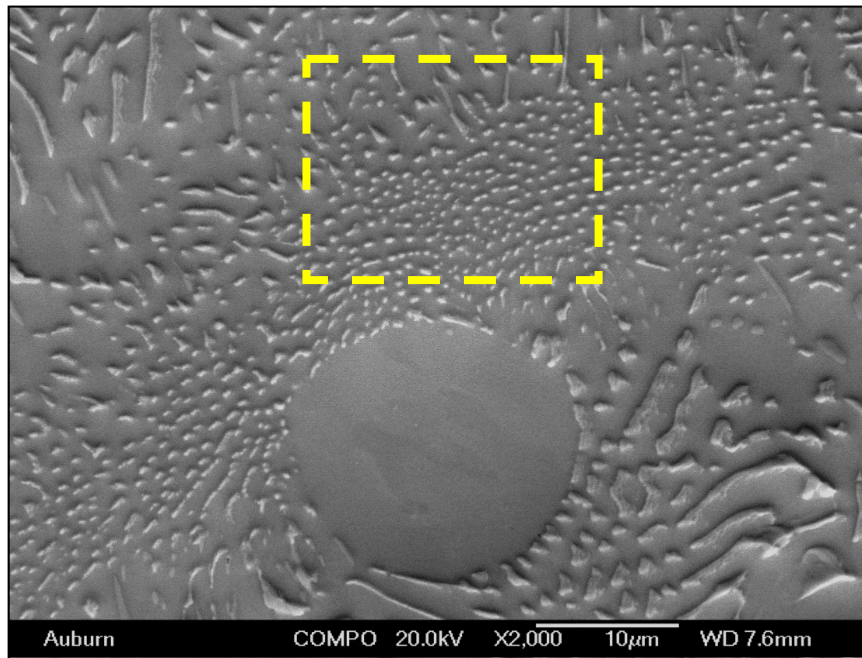

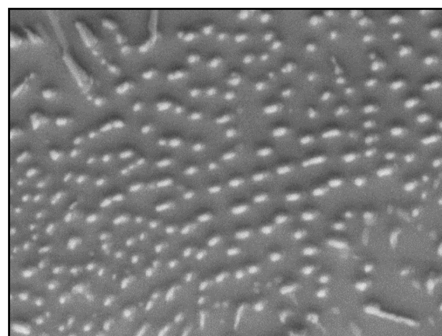

As Reflowed

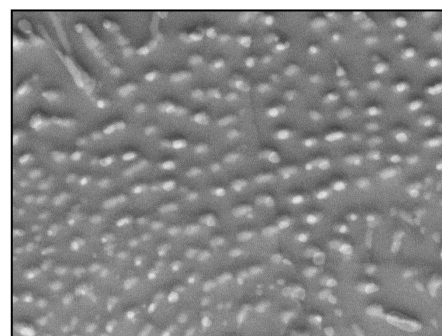

1 Day Aging

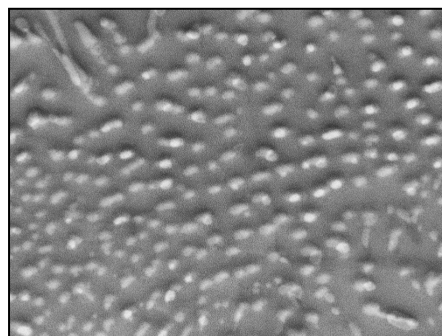

5 Days Aging

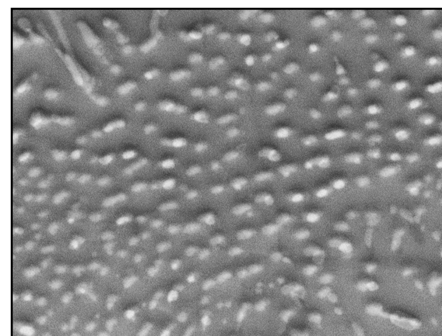

20 Days Aging

(a) Aging T=125ºC (Region 1)

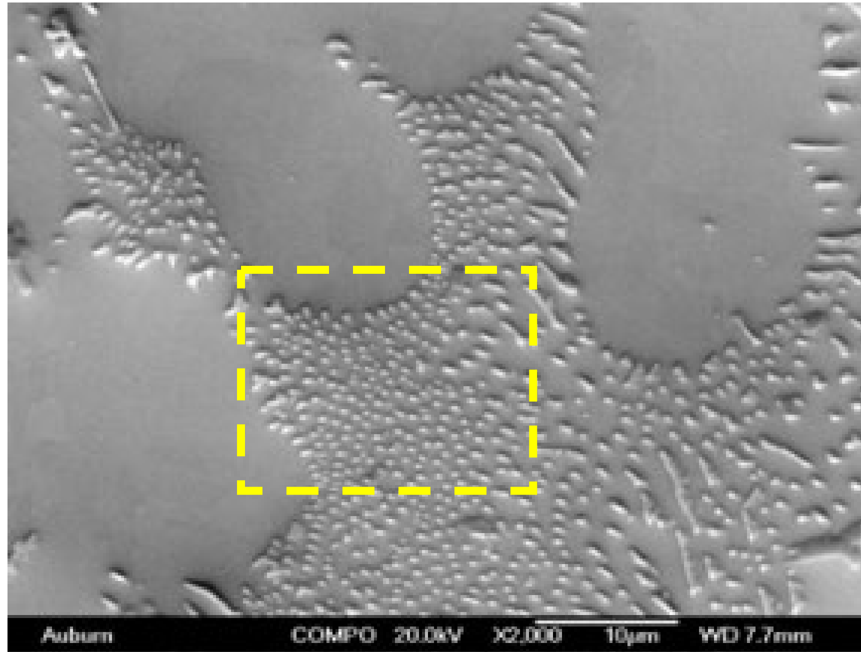

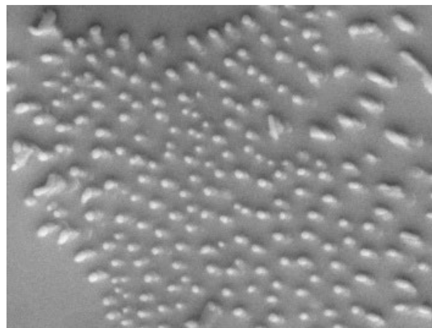
As Reflowed

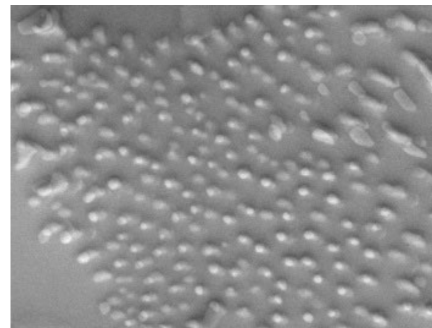
1 Day Aging

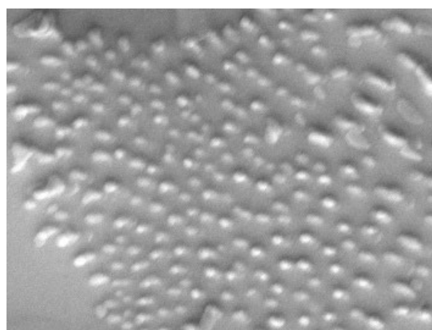
5 Days Aging

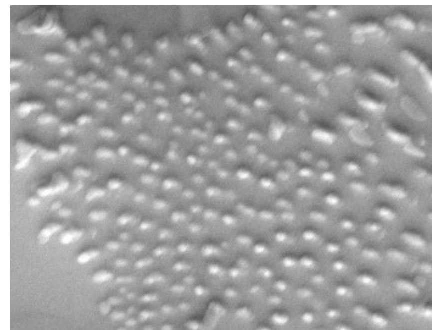
20 Days Aging

(b) Aging T=125ºC (Region 2)

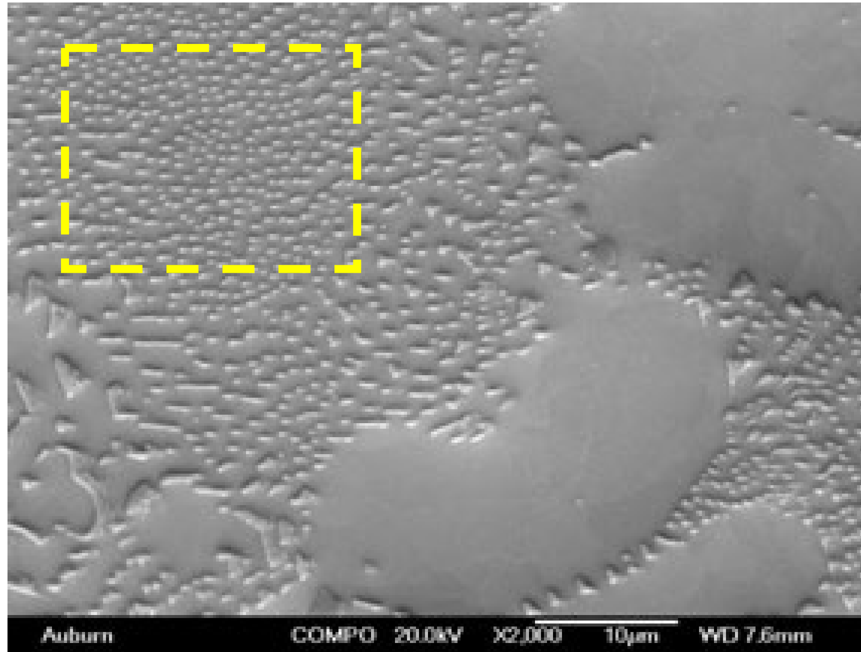

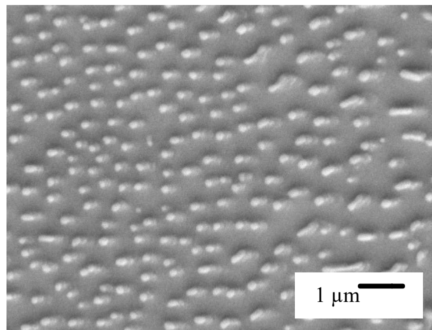

As Reflowed

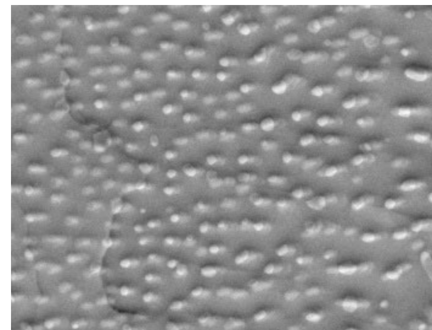

1 Day Aging

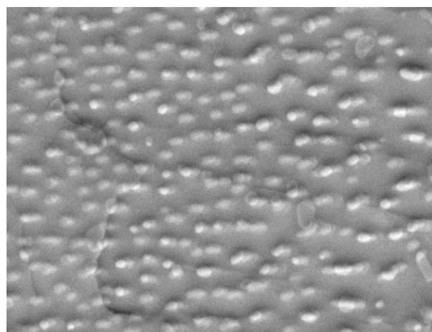

5 Days Aging

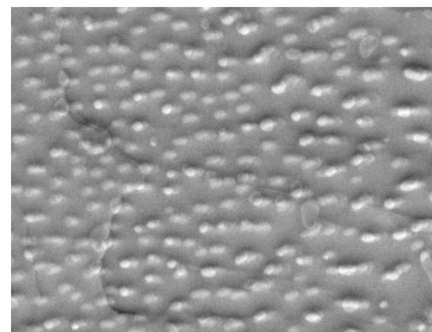

20 Days Aging

(a) Aging T=125ºC (Region 3)

Figure 7.19 Microstructure Evolution of SAC+Bi Solder Under Aging

Figure 7.19(a-c) and Figure 7.20 (a-c) contain images of Bi-rich regions illustrating example microstructural evolutions of the bismuth rich phases in SAC_Q joints subjected to slow thermal ramping, and slow thermal cycling for 1, 5, and 20 days of exposure. The images in the left sides were taken immediately after reflow. It exhibits a distribution of white Bi-rich phases throughout the lead free microstructure. EDS analysis of these white particles has confirmed that they are Bi rich phases with more than 80% of Bi. During cycling (images in the right side), bismuth was observed to go into solution within the β-Sn dendrites and also in the intermetallic rich regions between dendrites. As discussed previously, this leads to strengthening of the solder during aging by the mechanism of solid solution strengthening.

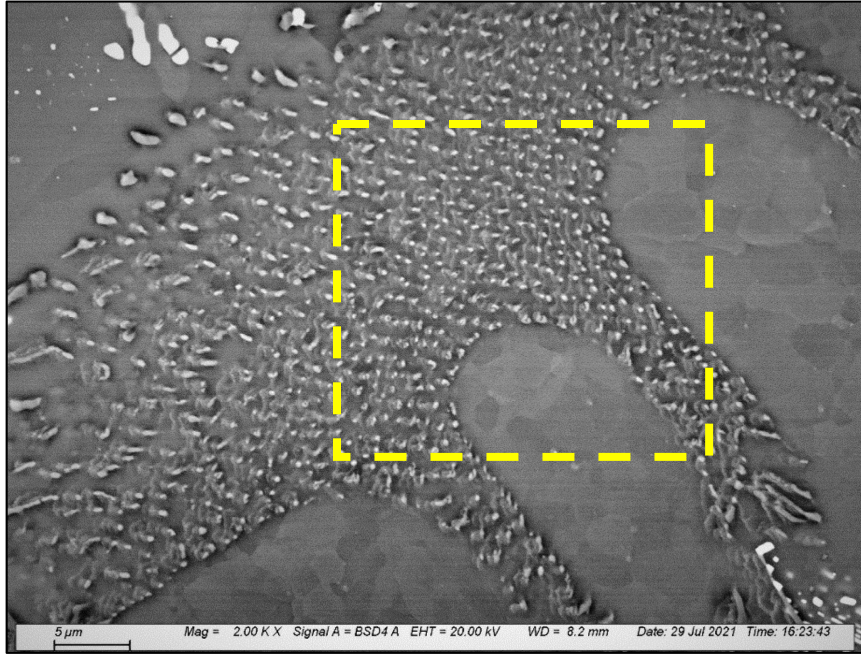

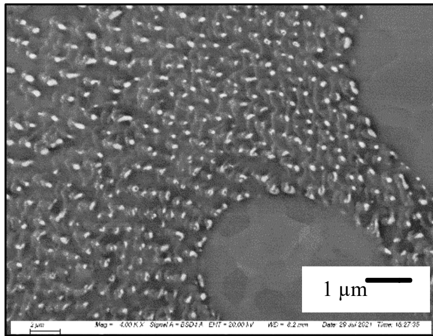

As Reflowed

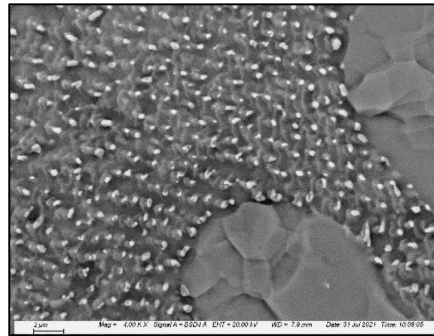

1 Day STR

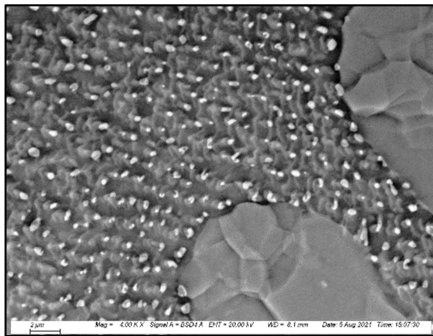

5 Days STR

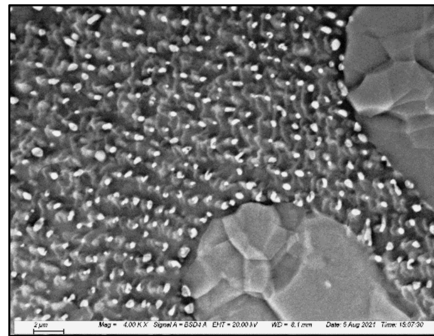

20 Days STR

(a) Slow Thermal Ramping (Region 1)

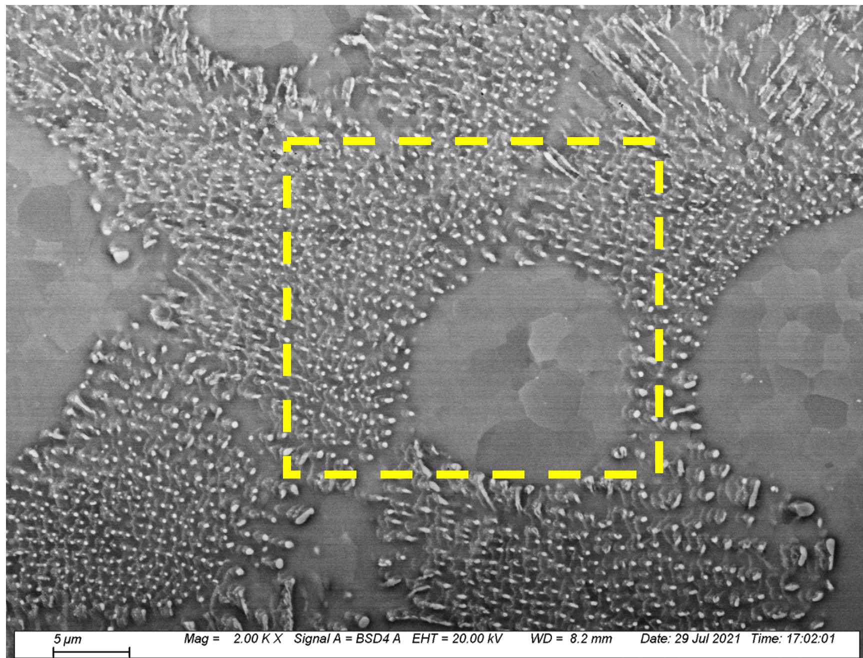

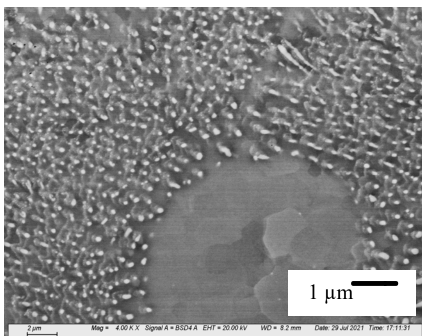

As Reflowed

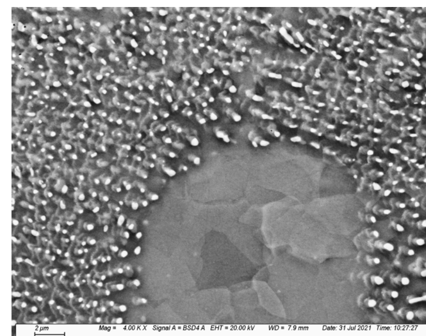

1 Day STR

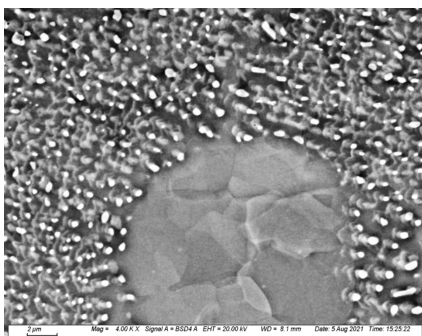

5 Days STR

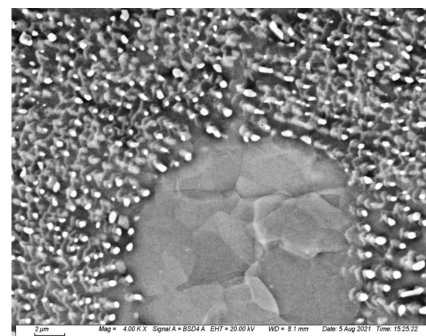

20 Days STR

(b) Slow Thermal Ramping (Region 2)

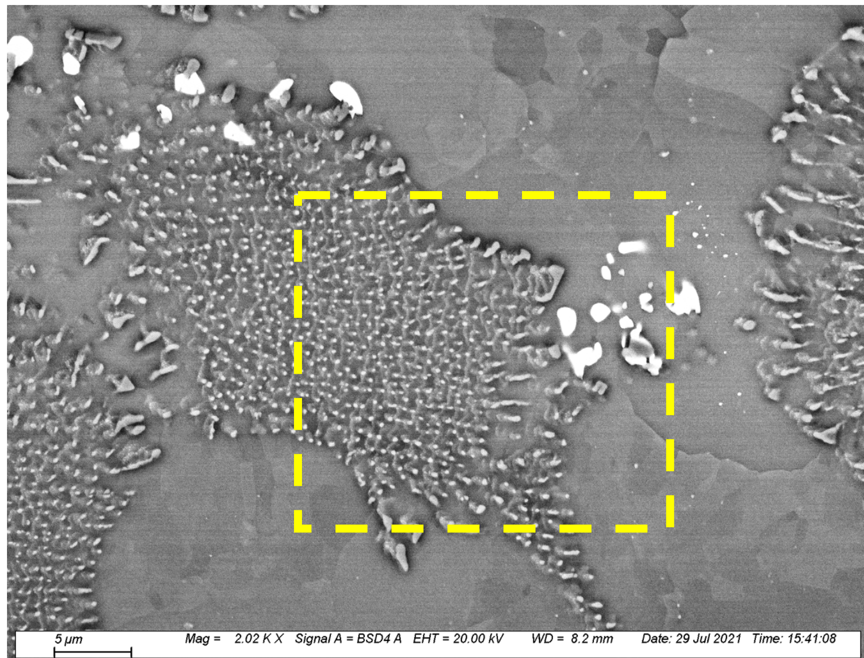

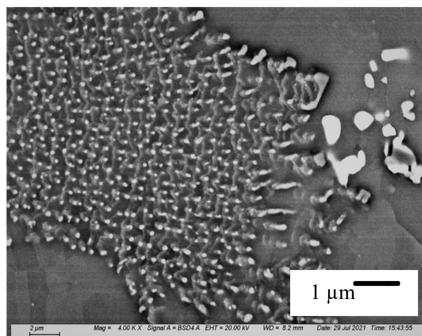

As Reflowed

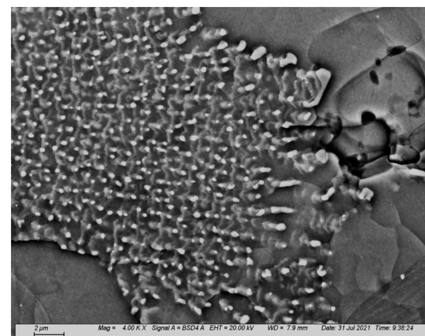

1 Day STR

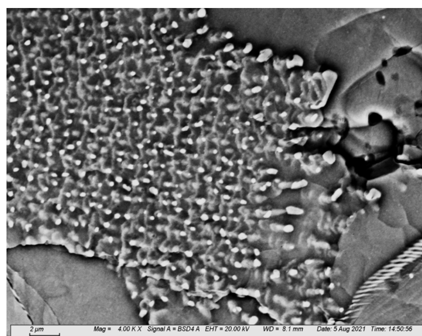

5 Days STR

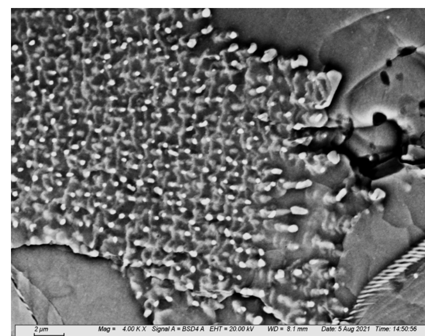

20 Days STR

(c) Slow Thermal Ramping (Region 3)

Figure 7.20 Microstructure Evolution of SAC+Bi Under Slow Thermal Ramping

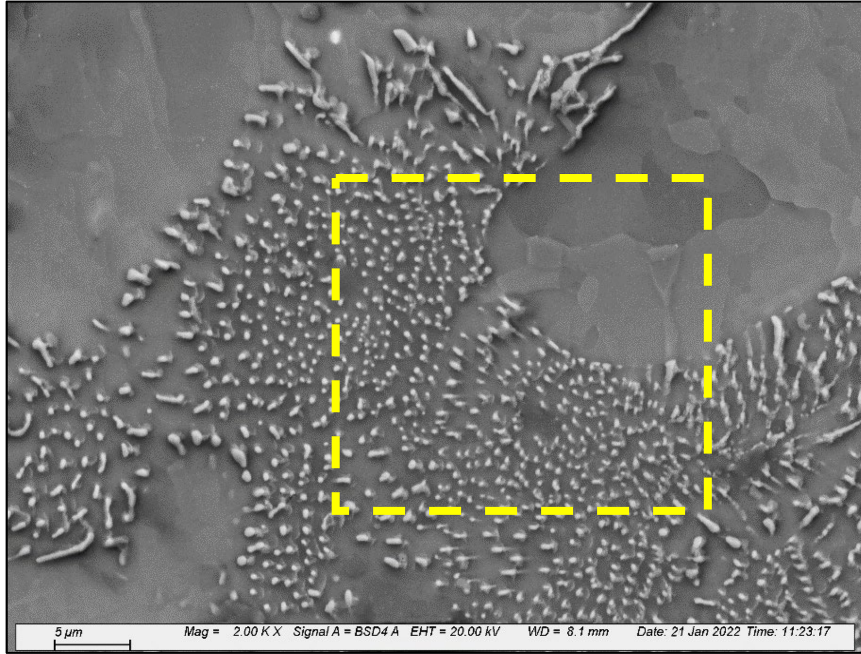

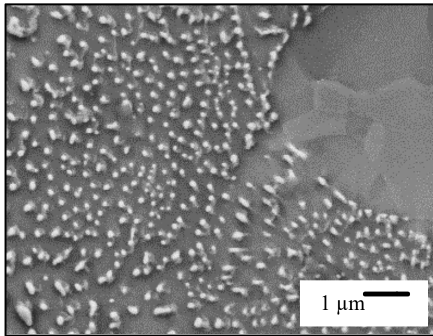

As Reflowed

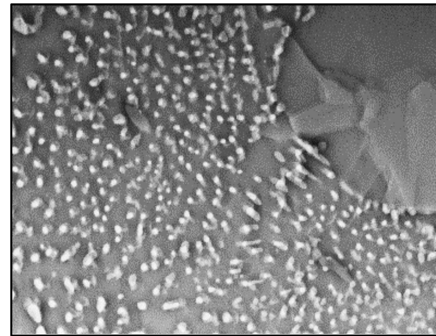

1 Day STC

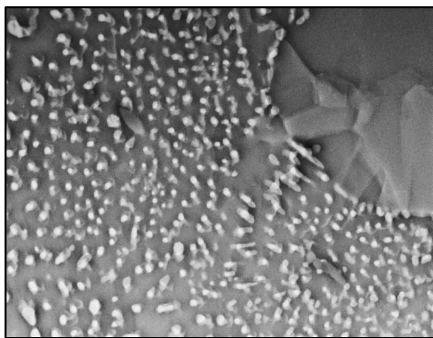

5 Days STC

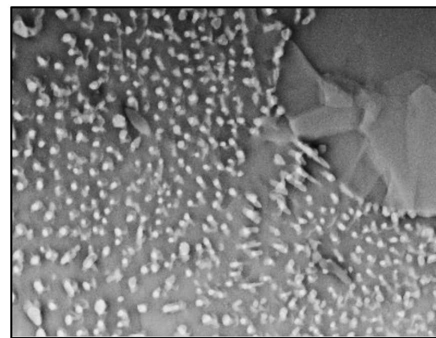

20 Days STC

(a) Slow Thermal Cycling (Region 1)

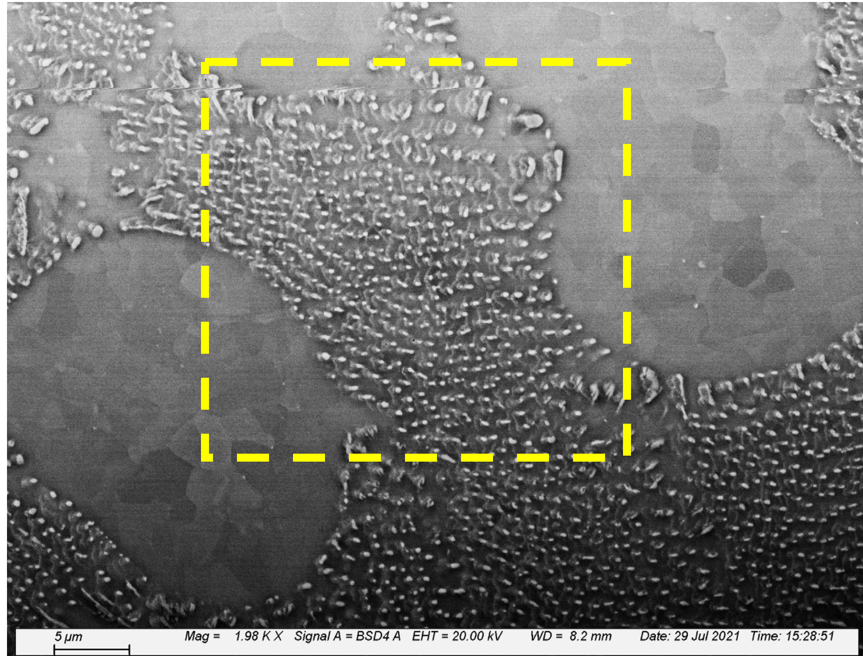

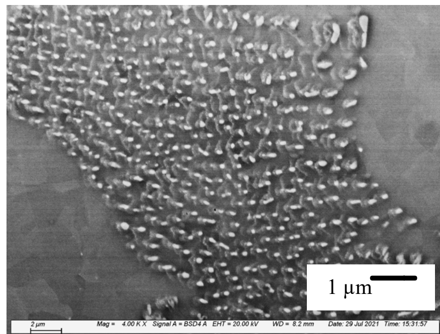

As Reflowed

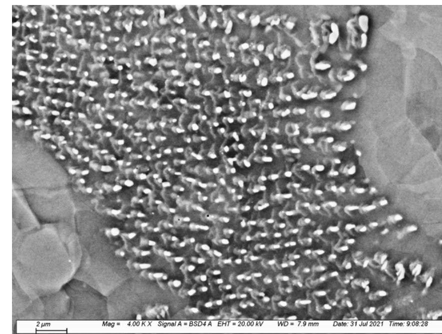

1 Day STC

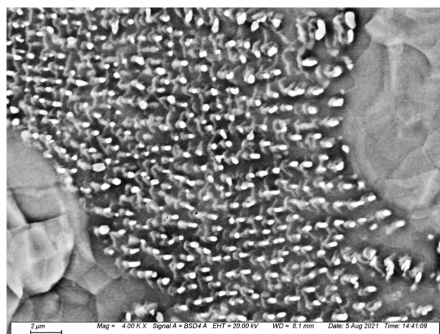

5 Days STC

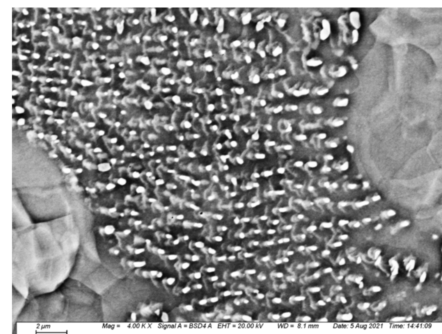

20 Days STC

(b) Slow Thermal Cycling (Region 2)

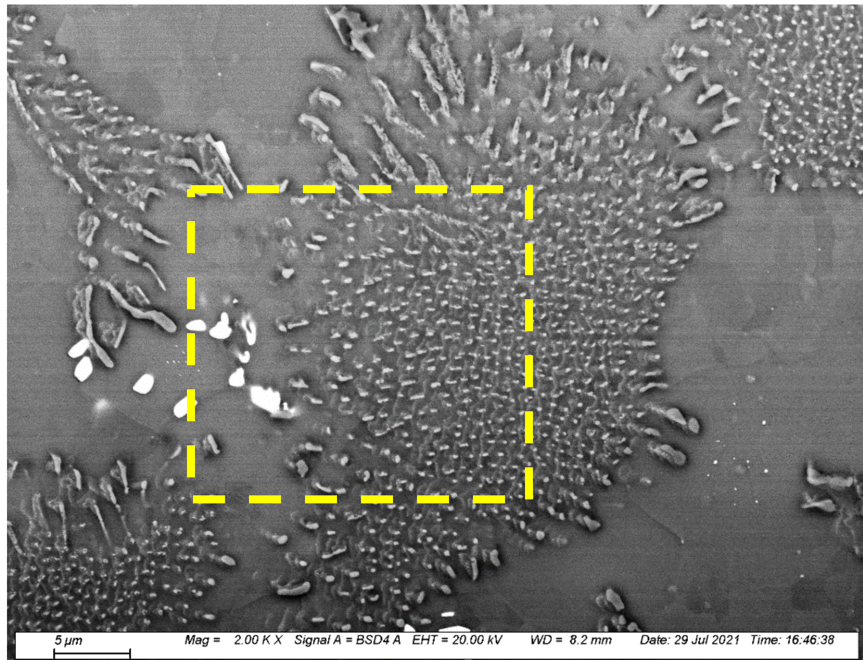

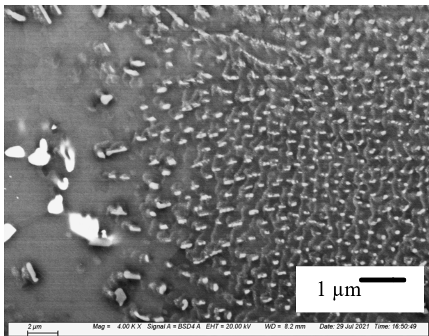

As Reflowed

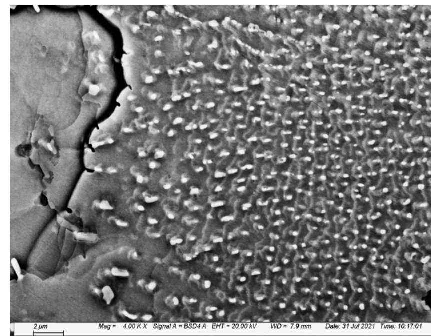

1 Day STC

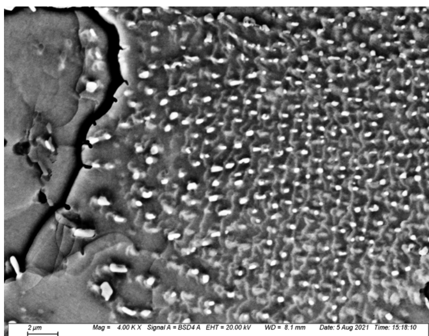

5 Days STC

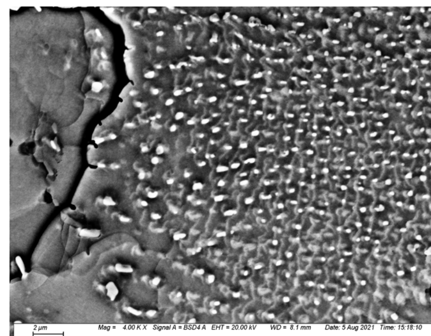

20 Days STC

(c) Slow Thermal Cycling (Region 3)

Figure 7.21 Microstructure Evolution of SAC+Bi Solder Under Slow Thermal Cycling

7.12 Comparison of Normalized Average Particle Diameter Evolution

Figure 7.21 shows the comparison of average normalized particle diameter change under different thermal cycling exposures. In this plot, red, green, and pink curves are presenting the average normalized particle diameter change with elapsed time. From this plot, it is can be inferred that the change in normalized average particle diameter under isothermal aging, slow thermal ramping, and slow thermal cycling was not significant with exposure time. Even though the degradation of SAC+Bi solder under all thermal exposures was not significant but after 20 days of exposure the degradation was relatively higher under thermal cycling with longer ramp period (solid cyan line). This insignificant change can be attribute to the solid solution strengthening of Bi.

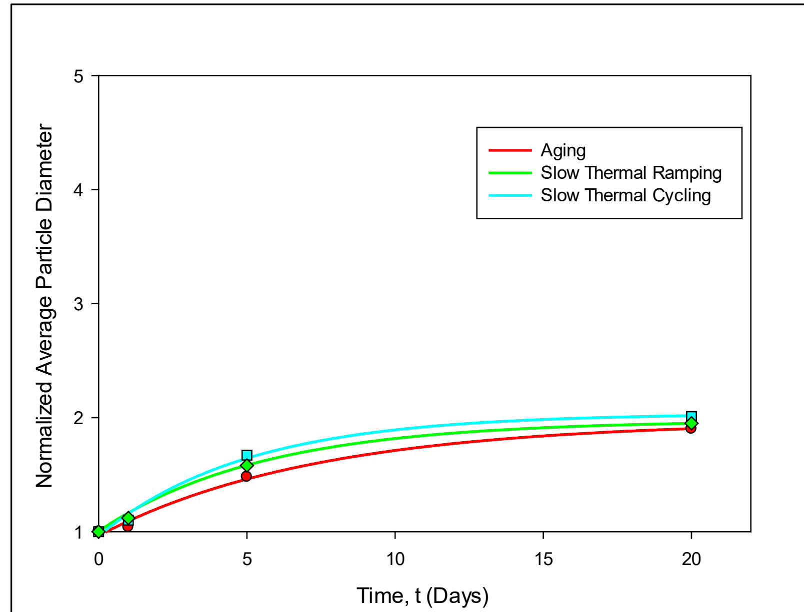

Figure 7.22 Comparison of Normalized Average Particle Diameter Evolution of SAC+Bi Alloy Under Different Thermal Exposure with Exposure Time

7.13 Correlation Between Mechanical and Microstructural Evolution

In this study, it was found that mechanical properties degraded with exposure time under isothermal aging and any thermal cycling exposures for SAC305 solder alloy. But from figure 7.19 (a) and 7.19 (b), both microstructure and mechanical properties are not changing significantly with exposure time irrespective to the thermal exposure condition.

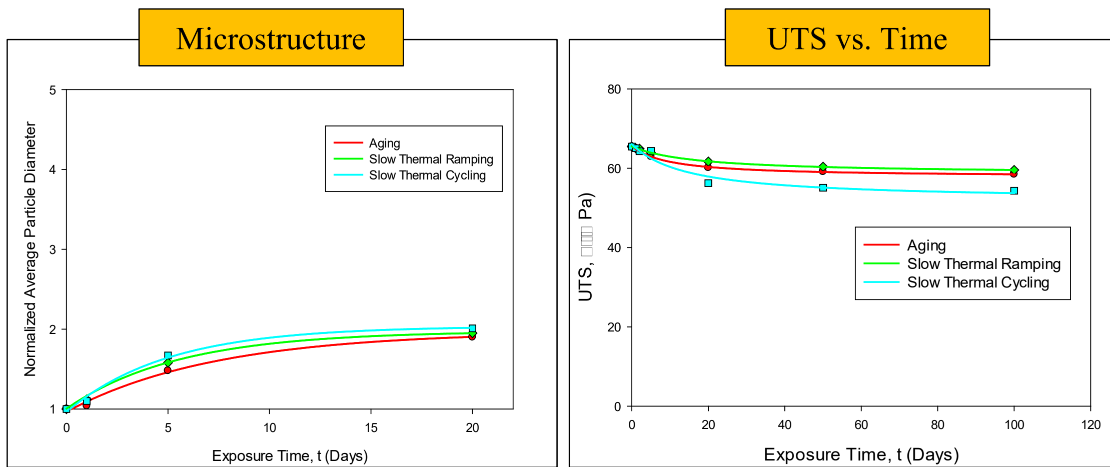

(a)

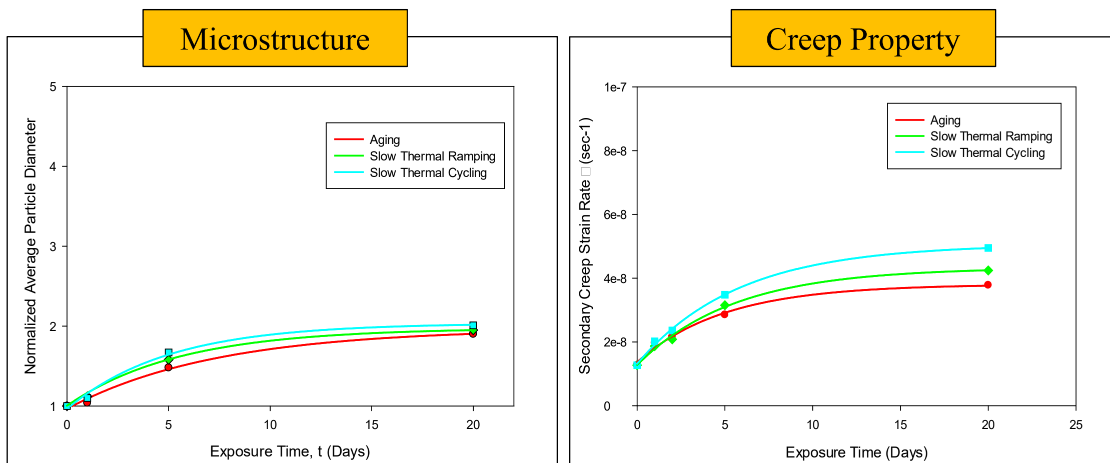

(b)

Figure 7.23 Correlation Between Microstructure and Mechanical Properties of SAC+Bi

Both tensile and creep property degradation after 20 days of exposure is little higher under thermal cycling with longer ramp period which is true for microstructure evolution. Even though the normalized average particle diameter did not change significantly but after 20 days of exposure particle diameter is little higher under thermal cycling with long ramp period supports the mechanical properties degradation.

7.14 Microstructural Evolution of SAC305 and SAC+Bi Solder Under Different Thermal Exposures with Exposure Time

Figure 7.20 presents the normalized average particle diameter vs. exposure time. In this plot, dotted red, green, and pink curves indicates SAC+Bi solder alloy under isothermal aging, slow thermal ramping, and slow thermal cycling respectively. Same color solid lines are indicating the SAC305 solder alloy under isothermal aging, slow thermal ramping, and slow thermal cycling respectively. From this plot, it is obvious that all three solid lines are on top of all three dotted lines. It indicates that the change of normalized average particle diameter is significantly higher for SAC305 solder alloy compared to the SAC+Bi solder alloy irrespective to the thermal exposure condition. For example, after 20 days of exposure for SAC305 solder material normalized average particle diameter increased 185%, 230%, and 275% respectively. On the other hand, for SAC+Bi the increase was 19%, 19.5%, and 20% respectively under isothermal aging, slow thermal ramping, and slow thermal cycling. Even though the particle diameter did not change significantly but the increase rate was higher under slow thermal cycling compared to other thermal exposures.

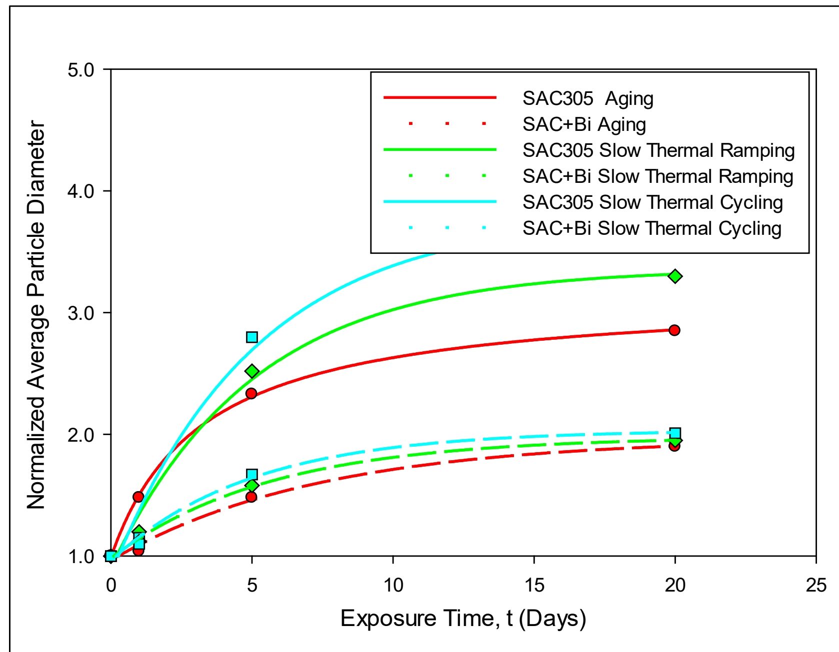

Figure 7.24 Normalized Particle Diameter Evolution with Time for SAC305 and SAC+Bi Under Different Thermal Exposure

7.15 Summary and Discussion

Microstructural evolutions in SAC305 lead free solder were observed via SEM for the various thermal exposure profiles. For all three thermal exposures, coarsening of IMC particles was observed. The average particle diameter increased, and the total number of particles decreased with exposure time. Initially (First 2 Days of Exposure), the rate of average particle diameter increase with aging was higher compared to slow thermal ramping and slow thermal cycling. However, with the increased exposure time it became higher under slow thermal ramping and slow thermal cycling compared to isothermal aging. Even though average particle diameter increased irrespective to the thermal cycling exposure profiles, the effect on IMC was largest under slow thermal cycling, which supports the mechanical behavior evolution observations. Microstructural evolutions in SAC+Bi lead free solder were observed via SEM for the various thermal exposure profiles.

The rate of normalized average particle diameter increase was not significant in SAC+Bi solder material compared to SA305 irrespective of the thermal exposures. Even though average particle diameter increase rate was not significant irrespective to the thermal cycling exposures, the effect on IMC was higher under slow thermal cycling, which supports the mechanical behavior evolution observations.

CHAPTER 8

SUMMARY AND CONCLUSIONS

8.1 Literature Review

The mechanical properties of a solder are strongly influenced by its microstructure, which is controlled by its thermal history including its solidification rate and thermal exposures after solidification. Aging of lead free solders leads to degradations in their constitutive and failure behaviors. For example, research in the literature has shown that aging leads to large reductions in solder material properties including shear strength, elastic modulus, nanoindentation joint modulus and hardness, high strain rate mechanical behavior and creep response. Other studies have shown that aging causes severe degradations in uniaxial cyclic stress-strain curves and fatigue life, shear cyclic stress-strain curves and fatigue life, fracture behavior, drop reliability, and thermal cycling reliability.

Dopants have been found to strongly influence the properties and behaviors of lead free solders. For Example, Bi helps to reduce solidification temperature, increases strength by means of precipitation hardening, helps to reduce IMC (Intermetallic Compound) layer thickness, and also reduce aging induced degradation of mechanical properties in lead free solder materials. Ni helps to improve thermal fatigue life and drop test performance by refining Sn grain size and reducing the IMC layer formation near the Cu pad. The effects

of rear earth (RE) elements and nanoparticle addition on the properties of lead free solder was also discussed in this chapter.

Nanoindentation methods have shown great potential for characterizing solder materials and aging effects at the joint scale. Nanoindentation is mainly used to extract elastic modulus and hardness of solder joints. Many of the prior works have also used nanoindentation technique to characterize the creep properties although most of the nanoindentation experiments, on solder joints, were conducted at room temperature.

The changes in solder mechanical behavior are a result of the evolution of the SAC solder microstructure that occurs during aging. The most well-known and widely observed changes are coarsening of the Ag_3Sn and Cu_6Sn_5 intermetallic compounds (IMCs) present in the eutectic regions between beta-Sn dendrites. Several researchers have proposed empirical models to describe the growth of these secondary phase particles as a function of aging temperature and aging time, and related this growth to mechanical property changes.

8.2 Experimental Procedures

All the experimental procedures and the data processing steps were presented in chapter 3. Micro-scale uniaxial tensile specimens were prepared in a rectangular shaped hollow glass tube using a vacuum suction method. Typical dimension of the uniaxial tensile specimens were 80 (length) $\times$ 3 (width) $\times$ 0.5 (height) mm. Uniaxial tensile tests were performed using a micro tension torsion testing system. Nanoindentation experiments were conducted on solder joints which were typically extracted from 3x3 BGA. The diameter of the solder joints was 30 mils. Nanoindentation experiments were performed using Hysitron TI950 TriboIndenter.

8.3 Mechanical Behavior Evolution of SAC305 Solder Under Different Thermal Exposure

In this chapter, mechanical behavior evolution of SAC305 solder material under different thermal cycling exposures was investigated. The thermal cycles were (1) 150 minute cycles with 45 minutes ramps and 30 minutes dwells, (2) air-to-air thermal shock exposures with 30 minutes dwells and near instantaneous ramps, and (3) 90 minute cycles with 45 minutes ramps and 0 minutes dwells, (4) no cycling (simple aging at high temperature extreme). Sets of bulk solder were cycled and aged for the duration of 1, 2, 5, 20, 50, and 100 days at the high temperature extreme of T = 125 C followed by uniaxial tensile testing and creep testing respectively to measure the mechanical properties evolution in terms of E, UTS, YS, and secondary creep strain rate. Uniaxial test samples were prepared by vacuum suction method and submerging into room temperature water followed by reflow solidification.

Results showed that the mechanical properties degradation of SAC305 solder material under slow thermal cycling was severe compared to the aging and other thermal profiles. For example, after 100 days of isothermal aging, E, UTS, and YS of bulk solder was degraded by 54%, 44%, and 39%, respectively. On the other hand, the degradation under slow thermal cycling was 70% ,57%, and 58%, respectively. Even though, the reduction in mechanical properties under pure aging after 1 day was higher compared to other thermal profiles, but with increasing exposure the degradation becomes more prominent in other thermal profiles, particularly, thermal cycle with longest ramp rate (slow thermal cycling).

Also, in this present study, evolution of creep behavior of SAC305 solder material under isothermal aging and different thermal cycling profile exposures have been investigated. Evolution of creep behavior was measured in terms of secondary creep strain rate. Comparison of secondary creep strain rate change as a function of stress level at different elapsed time were also observed between isothermal aging and different thermal cycling profile exposures.

Sets of five samples were exposed to different thermal exposures for various durations such as 1, 2, 5, and 20 days. Then creep testing was performed on thermally cycled samples to observe the evolution of creep behavior with elapsed time under different thermal cycling profile exposures at different stress levels (10, 12, 15 MPa). Afterward, comparative results of isothermal aging, slow thermal ramping, and slow thermal cycling were presented in terms of secondary creep strain rate. For isothermal aging, slow thermal ramping, and slow thermal cycling, secondary creep strain rate increased with the stress level and elapsed time. Even though secondary creep strain rate increased for all thermal cycling exposures with all stress levels, but the initial (up to 2 days) increase ratio of secondary creep rate under isothermal aging was higher compared to other thermal cycling profile exposures. But with increased elapsed time such as 5 days of exposures, the increase ratio becomes higher under slow thermal ramping, and slow thermal cycling. The secondary creep strain rate change was much dramatic under slow thermal cycling compared to isothermal aging and slow thermal ramping. For example, the secondary creep strain rate increased maximum 8.5x after 5 days of isothermal aging whereas it was increased by maximum 13.5x and 26.5x under slow thermal ramping, and slow thermal cycling, respectively compared to the as reflowed condition. This investigation

demonstrates that irrespective of stress level the creep property of SAC305 is severely affected by slow thermal cycling exposures after 5 days of exposures compared to the isothermal aging and slow thermal ramping.

8.4 Response of SAC+Bi Solder Alloy Under Different Thermal Exposure

In this chapter, the Effects of Various Thermal Exposures on the Evolution of the Mechanical Behavior of SAC+Bi Lead Free Solder were Investigated. For mechanical properties extraction, uniaxial test samples have been used. Tensile tests were performed at room temperature and strain rate 0.001 sec^{-1}. Creep tests were performed at three different stress levels such as 10, 12, and 15 MPa. From stress-strain properties, it was found that unlike SAC305, the elasic modulus, ultimate tensile strength, and yield strength of SAC+Bi did not change significantly with any of the thermal exposures. Secondary Creep rate did not increase significantly like SAC305 with exposure time. Little increase has been observed under slow thermal cycling exposures at 15 MPa compared to isothermal Aging. Even though the Degradation of Mechanical Properties (Stress-Strain, Creep Response) of SAC+Bi has not changed significantly, the degradation of thermal cycling with the longest ramp periods has a greater rate compared to the other thermal profiles.
The evolutions of the Mechanical Properties of SAC+Bi and SAC305 Solder Materials were Compared for Various Thermal Exposures in this study. The Mechanical Property Degradations of the SAC+Bi Solder Alloy with Exposure Time were Relatively Small When Compared to Those for the SAC305 Solder Alloy. This was True Irrespective of the Thermal Exposure Chosen. Secondary Creep Rate of SAC+Bi Solder Alloy did not Increase Significantly like SAC305 with Exposure Time. Creep Deformation of SAC+Bi

Solder Alloy was Much Lower Than As-Reflowed SAC305 Solder Alloy. After 20 Days of Thermal Exposures under Slow Thermal Cycling, Secondary Creep Strain Rate of SAC+Bi Reaches the As-Reflowed Creep Rate of SAC305 Solder Alloy.

8.5 Nanoindentation Characterization of SAC305 and SAC+Bi Solder Joint

In this chapter, the effects of various thermal exposures on the evolutions of the mechanical properties of SAC305 and SAC+Bi solder joints (balls) were investigated using nanoindentation. Sets of solder balls were cycled and aged for the duration of 1, 2, 5, 20, and 50 days at the high temperature extreme of T = 125 C followed by nanoindentation testing to measure the mechanical properties evolution in terms of E, and YS. As Expected, elastic Modulus, hardness, and yield strength of the solder joints decreased with exposure time for isothermal aging, slow thermal ramping, thermal shock, as well as slow thermal cycling. But for both bulk solder and solder balls, the mechanical properties degradation of SAC305 solder material under slow thermal cycling was severe compared to the aging and other thermal profiles. For example, after 50 days of isothermal aging, E, UTS, and YS of bulk solder was degraded by 50%, 42%, and 36%, respectively. On the other hand, the degradation under slow thermal cycling was 66%, 55%, and 53%, respectively. Similarly, the average percentage change in modulus and YS of solder balls after 50 days of isothermal aging was found as 40%, and 25%, respectively, whereas, under slow thermal cycling it was observed as 58%, as well as 45%, respectively. Even though, the reduction in mechanical properties under pure aging after 1 day was higher compared to other thermal profiles, but with increasing exposure the degradation becomes more prominent in other thermal profiles, particularly, thermal cycle with longest ramp rate (slow thermal cycling).

Results also showed that compared to the SAC305 solder material, SAC+Bi showed insignificant change in E, UTS as well as YS for both bulk solder and solder joint up to 5 days of exposure. Small change was observed in mechanical properties after 20 days exposure. As SAC305, the degradation in solder balls was found less compared to the bulk solder irrespective to the thermal cycling condition. Also, for both bulk solder and solder balls, slow thermal cycling showed more effect on mechanical properties evolution of SAC+Bi solder material compared to the isothermal aging and other thermal cycling condition. For all of the thermal exposures, the mechanical property degradations of both SAC305 and SAC+Bi solder materials were larger in the bulk solder relative to those in the solder joints. The degradations using the slow thermal cycling profile were largest for both solder joints and bulk Solder.

8.6 Microstructure Study of SAC305 and SAC+Bi Solder Under Different Thermal Exposure

Microstructural evolutions in SAC305 lead free solder were observed via SEM for the various thermal exposure profiles. For all three thermal exposures, coarsening of IMC particles was observed. The average particle diameter increased, and the total number of particles decreased with exposure time. Initially (First 2 Days of Exposure), the rate of average particle diameter increase with aging was higher compared to slow thermal ramping and slow thermal cycling. However, with the increased exposure time it became higher under slow thermal ramping and slow thermal cycling compared to isothermal aging. Even though average particle diameter increased irrespective to the thermal cycling exposure profiles, the effect on IMC was largest under slow thermal cycling, which

supports the mechanical behavior evolution observations. Microstructural evolutions in SAC+Bi lead free solder were observed via SEM for the various thermal exposure profiles. The rate of normalized average particle diameter increase was not significant in SAC+Bi solder material compared to SA305 irrespective of the thermal exposures. Even though average particle diameter increase rate was not significant irrespective to the thermal cycling exposures, the effect on IMC was higher under slow thermal cycling, which supports the mechanical behavior evolution observations.

8.7 Summary

In this Dissertation, popular lead free solder SAC305 and SAC+Bi solder alloys have been characterized and the reliability of these alloys in harsh environment applications have been investigated. These alloys were subjected to different thermal exposures. Those were (1) isothermal aging at 125 C, (2) slow thermal cycling from -40 C to +125 C with 45 minutes ramps and 30 minutes dwells (3) thermal ramping with 45 minutes ramps and no dwells, (4) thermal shock with 30 minutes dwell and instantaneous ramping between hot and cold temperatures. After preconditioning, tensile test was performed at room temperature and at a strain rate 0.001 $sec^{-}1$ to extract mechanical properties, such as elastic modulus, ultimate tensile strength, and yield stress. It was found that stress-strain properties of SAC305 solder alloy degraded significantly with exposure time irrespective to the thermal exposure. But initially the degradation was higher under isothermal aging compared to other thermal exposure. With increasing exposure time, other thermal exposure passes the effect of isothermal aging. After long exposure time, slow thermal cycling effect was severe compared to isothermal aging and other thermal

exposure. Creep test was also performed on SAC305 alloy at three stress level e.g. 10, 12, and 15 MPa. Creep behavior showed similar response as stress-strain behavior. Secondary creep strain rate increase ratio was much higher under slow thermal cycling for long exposure time compared to isothermal aging and other thermal exposure. Then the effect of different thermal exposures on SAC+Bi solder alloy has been characterized. It was found that mechanical properties both stress-strain and creep properties did not change significantly with exposure time irrespective to the thermal exposure which is unlike SAC305. Even though the degradation of mechanical properties was not significant but with exposure time but the degradation under thermal cycling with longer ramp period was little higher compared to isothermal aging as well as other thermal exposures. Comparison of SAC305 and SAC+Bi solder was made in this study and it can be depicted that there is a similarity between mechanical properties degradation. For both material the degradation occurred exponentially. In this study, all the preconditioning was performed at stress free condition on bulk solder. But in real application, solder joints are very small and the total number of grain is very limited. So, to observe the effect of different thermal exposures on solder joints at stress free condition another study has been conducted. In this study both SAC305 and SAC+Bi solder joints have been chosen. These joints did not have copper pad on both side so the expansion due to thermal exposure was stress free. Also, to avoid the grain orientation effect, all single grain solder joint has been used in this study. It was found that mechanical properties degradation of both solder alloy showed exponential decay as bulk solder. Also, for both alloy, the degradation of bulk solder was higher compared to the solder joint. But for SAC+Bi solder material, for both bulk and solder joint the degradation of mechanical properties were insignificant compared to

SAC305 bulk solder and solder joint. In addition, irrespective to material and thermal exposure, the degradation under thermal cycling with long ramp period was higher than isothermal aging and other thermal exposures. Lower mechanical properties degradation of SAC+Bi can be attributed to the solid solution hardening effect of Bi. Finally, to better understand the change in mechanical properties with exposure time under different thermal exposure, microstructure study of SAC305 and SAC+Bi bulk solder has been conducted. From this study, it can be inferred that average particle (IMC) diameter of SAC305 increased with exposure time. Initially, the increase rate was higher under isothermal aging compared to other thermal exposure but after long exposure the rate was much higher under thermal cycling with long ramp period. This phenomenon correlates mechanical properties degradation very well. On the other hand, for SAC+Bi solder material, the particle diameter did not change significantly with exposure and with any thermal exposure compared to SAC305 solder alloy. Even though the particle diameter did not increase significantly but the rate was little higher under slow thermal cycling. This phenomena also supports the mechanical behavior evolution of SAC+Bi solder alloy.

8.8 Future Work

Following future work can be performed to extend the findings of this dissertation:

- Investigate Stress-Strain and Creep Behavior Evolution of SAC+1%Bi, and SAC+2%Bi Bulk Solder for Various Thermal Exposures.
- Compare Stress-Strain and Creep Behavior of SAC+1%Bi, SAC+2%Bi, and SAC+3%Bi Bulk Solder for Various Thermal Exposures
- Investigate the Creep Behavior Evolution for SAC305, SAC+(1%, 2%, 3%)Bi Solder Joints for Various Thermal Exposures Using Nanoindentation
- Compare the Creep Results for Bulk Solder and Solder Joints for Both Alloys
- Measure Microstructure Evolution of SAC1%Bi, and SAC+2%Bi Alloy and Compare to Both SAC305, and SAC+3%Bi

REFERENCES

[1] M. Abtew and G. Selvaduray, "Lead-Free Solders in Microelectronics," *Materials Science and Engineering: R: Reports,* vol. 27, no. 5, pp. 95-141, 2000.

[2] P. T. Vianco, "Development of Alternatives to Lead-Bearing Solders," *Proceedings of Surface Mount Technical Association International Conference,* 1993.

[3] J. S. Hwang, *Implementing Lead-Free Electronics*. McGraw-Hill, New York, 2005.

[4] Q. Zhang, A. Dasgupta, and P. Haswell, "Creep and High-Temperature Isothermal Fatigue of Pb-Free Solders," *Proceedings of* InterPACK*,* no. 36908a, pp. 955-960, 2003.

[5] NCMS, "Lead-Free Solder Project Final Report," *NCMS Report 0401RE96,* 1997.

[6] N. C. Lee, "Getting Ready for Lead-Free Solders," *Soldering & Surface Mount Technology,* vol. 9, no. 2, pp. 65-69, 1997.

[7] K. S. Kim, S. H. Huh, and K. Suganuma, "Effects of Intermetallic Compounds on Properties of Sn–Ag–Cu Lead-Free Soldered Joints," *Journal of Alloys and Compounds,* vol. 352, no. 1, pp. 226-236, 2003.

[8] J.-W. Yoon, S.-W. Kim, and S.-B. Jung, "IMC Morphology, Interfacial Reaction and Joint Reliability of Pb-Free Sn–Ag–Cu Solder on Electrolytic Ni BGA Substrate," *Journal of Alloys and Compounds,* vol. 392, no. 1, pp. 247-252, 2005.

[9] D. Q. Yu and L. Wang, "The Growth and Roughness Evolution of Intermetallic Compounds of Sn–Ag–Cu/Cu Interface During Soldering Reaction," *Journal of Alloys and Compounds,* vol. 458, no. 1, pp. 542-547, 2008.

[10] C. M. L. Wu, D. Q. Yu, C. M. T. Law, and L. Wang, "Properties of Lead-Free Solder Alloys with Rare Earth Element Additions," *Materials Science and Engineering: R: Reports,* vol. 44, no. 1, pp. 1-44, 2004.

[11] Y. C. Chan and D. Yang, "Failure Mechanisms of Solder Interconnects under Current Stressing in Advanced Electronic Packages," *Progress in Materials Science,* vol. 55, no. 5, pp. 428-475, 2010.

[12] C.-h. Wang and S.-w. Chen, "Sn–0.7wt.%Cu/Ni Interfacial Reactions at 250°C," *Acta Materialia,* vol. 54, no. 1, pp. 247-253, 2006.

[13] G. Zeng, S. D. McDonald, Q. F. Gu, K. Sweatman, and K. Nogita, "Effects of Element Addition on the β→α Transformation in Tin," *Philosophical Magazine Letters,* vol. 94, no. 2, pp. 53-62, 2014.

[14] W. J. Plumbridge, "Tin Pest Issues in Lead-Free Electronic Solders," in *Lead-Free Electronic Solders: A Special Issue of the Journal of Materials Science: Materials in Electronics*, pp. 307-318, 2007.

[15] S. Cheng, C.-M. Huang, and M. Pecht, "A Review of Lead-Free Solders for Electronics Applications," *Microelectronics Reliability,* vol. 75, pp. 77-95, 2017.

[16] M. Hasnine, B. Tolla, and M. Karasawa, "Effect of Ge Addition on Wettability, Copper Dissolution, Microstructural and Mechanical Behavior of SnCu–Ge Solder Alloy," *Journal of Materials Science: Materials in Electronics,* vol. 28, no. 21, pp. 16106-16119, 2017.

[17] Q. B. Tao, L. Benabou, L. Vivet, V. N. Le, and F. B. Ouezdou, "Effect of Ni and Sb Additions and Testing Conditions on the Mechanical Properties and Microstructures of Lead-Free Solder Joints," *Materials Science and Engineering: A,* vol. 669, pp. 403-416, 2016.

[18] J. Glazer, "Metallurgy of Low Temperature Pb-Free Solders for Electronic Assembly," *International Materials Reviews,* vol. 40, no. 2, pp. 65-93, 1995.

[19] M. McCormack, S. Jin, G. W. Kammlott, and H. S. Chen, "New Pb-Free Solder Alloy with Superior Mechanical Properties," *Applied Physics Letters,* vol. 63, no. 1, pp. 15-17 1993.

[20] K. Nogita, “Stabilisation of Cu6Sn5 by Ni in Sn-0.7 Cu-0.05 Ni Lead-Free Solder Alloys,” *Intermetallics,* vol. 18, no. 1, pp. 145-149, 2010.

[21] F. X. Che, J. E. Luan, and X. Baraton, “Effect of Silver Content and Nickel Dopant on Mechanical Properties of Sn-Ag-Based Solders,” *Proceedings of ECTC,* pp. 485-490, 2008.

[22] F. Guo, J. Lee, S. Choi, J. P. Lucas, T. R. Bieler, and K. N. Subramanian, “Processing and Aging Characteristics of Eutectic Sn-3.5 Ag Solder Reinforced with Mechanically Incorporated Ni Particles,” *Journal of Electronic Materials,* vol. 30, no. 9, pp. 1073-1082, 2001.

[23] Z. G. Chen, Y. W. Shi, Z. D. Xia, and Y. F. Yan, “Study on the Microstructure of a Novel Lead-Free Solder Alloy SnAgCu-Re and Its Soldered Joints,” *Journal of Electronic Materials,* vol. 31, no. 10, pp. 1122-1128, 2002.

[24] F. Gao, S. Mukherjee, Q. Cui, and Z. Gu, “Synthesis, Characterization, and Thermal Properties of Nanoscale Lead-Free Solders on Multisegmented Metal Nanowires,” *Journal of Physical Chemistry C,* vol. 113, no. 22, pp. 9546-9552, 2009.

[25] C. M. T. Law and C. M. L. Wu, “Microstructure Evolution and Shear Strength of Sn-3.5 Ag-Re Lead-Free BGA Solder Balls,” *Proceedings of High Density Microsystem Design and Packaging and Component Failure Analysis,* pp. 60-65, 2004.

[26] N.-C. Lee, “Lead-Free Soldering-Where the World Is Going,” *Advancing Microelectronics,* vol. 26, no. 5, pp. 29-35, 1999.

[27] A. Pirondi, “Mechanical Failure in Microelectronic Packaging,” 2008.

[28] S. Wiese, A. Schubert, H. Walter, R. Dukek, F. Feustel, E. Meusel, and B. Michel, "Constitutive Behaviour of Lead-Free Solders vs. Lead-Containing Solders-Experiments on Bulk Specimens and Flip-Chip Joints," *Proceedings of the ECTC,* pp. 890-902, 2001.

[29] R. J. McCabe and M. E. Fine, "Athermal and Thermally Activated Plastic Flow in Low Melting Temperature Solders at Small Stresses," *Scripta Materialia,* vol. 39, no. 2, pp. 189-195, 1998.

[30] J. H. Lau, "Solder Joint Reliability of Flip Chip and Plastic Ball Grid Array Assemblies under Thermal, Mechanical, and Vibrational Conditions," *IEEE Transactions on Components, Packaging, and Manufacturing Technology, Part B,* vol. 19, no. 4, pp. 728-735, 1996.

[31] K. M. Ralls, Courtney, T. H., Wulff, J, *Introduction to Materials Science and Engineering*. Wiley & Sons, 1976.

[32] R. W. Hertzberg, R. P. Vinci, and J. L. Hertzberg, *Deformation and Fracture Mechanics of Engineering Materials*. Wiley New York, 1996.

[33] H. Ma and J. C. Suhling, "A Review of Mechanical Properties of Lead-Free Solders for Electronic Packaging," *Journal of Materials Science,* vol. 44, no. 5, pp. 1141-1158, 2009.

[34] J. H. Lau and Y.-H. Pao, *Solder Joint Reliability of* BGA*, CSP, Flip Chip, and Fine Pitch SMT Assemblies*, McGraw-Hill New York, 1997.

[35] R. W. Evans and B. Wilshire, "Creep of Metals and Alloys," 1985.

[36] M. F. Ashby, "A First Report on Deformation-Mechanism Maps," *Acta Metallurgica,* vol. 20, no. 7, pp. 887-897, 1972.

[37] J. Weertman, "Steady-State Creep through Dislocation Climb," *Journal of Applied Physics,* vol. 28, p. 362, 1957.

[38] R. L. Coble, “A Model for Boundary Diffusion Controlled Creep in Polycrystalline Materials,” *Journal of Applied Physics,* vol. 34, p. 1679, 1963.

[39] C. Herring, “Diffusional Viscosity of a Polycrystalline Solid,” *Journal of Applied Physics,* vol. 21, pp. 437-445, 1950.

[40] A. C. Fischer-Cripps, *Nanoindentation*, Third ed. Springer, 2011.

[41] P. McCluskey, R. Grzybowski, and T. Podlesak, “High Temperature Electronics,” CRC Press, 1997.

[42] S. Ganesan and M. Pecht, *Lead-Free Electronics*. John Wiley and Sons, 2006.

[43] R. W. Johnson, J. L. Evans, P. Jacobsen, J. R. Thompson, and M. Christopher, “The Changing Automotive Environment: High-Temperature Electronics,” *IEEE Transactions on Electronics Packaging Manufacturing,* vol. 27, no. 3, pp. 164-176, 2004.

[44] M. Hattori, “Needs and Applications of High-Temperature Lsis for Automotive Electronic Systems,” *Proceedings of the International Conference on High Temperature Electronics,* pp. 37-43, 1999.

[45] B. Parmentier, O. Vermesan, and L. Beneteau, “Design of High Temperature Electronics for Well Logging Applications,” *Proceedings of the International Conference on High Temperature Electronics,* 2003.

[46] H. Ma, J. C. Suhling, P. Lall, and M. J. Bozack, “Reliability of the Aging Lead Free Solder Joint,” *Proceedings of ECTC,* pp. 849-864, 2006.

[47] H. Ma, J. C. Suhling, Y. Zhang, P. Lall, and M. J. Bozack, “The Influence of Elevated Temperature Aging on Reliability of Lead Free Solder Joints,” *Proceedings of ECTC,* pp. 653-668, 2007.

[48] Y., Zhang., Z., Cai., J. C. Suhling, P. Lall, and M. J. Bozack, "The Effects of Aging Temperature on SAC Solder Joint Material Behavior and Reliability," *Proceedings of ECTC*, pp. 99-112, 2008.

[49] I. E. Anderson and J. L. Harringa, "Elevated Temperature Aging of Solder Joints Based on Sn-Ag-Cu: Effects on Joint Microstructure and Shear Strength," *Journal of Electronic Materials,* vol. 33, no. 12, pp. 1485-1496, 2004.

[50] I. E. Anderson, J. W. Walleser, J. L. Harringa, F. Laabs, and A. Kracher, "Nucleation Control and Thermal Aging Resistanceof near-Eutectic Sn-Ag-Cu-X Solder Jointsby Alloy Design," *Journal of Electronic Materials,* vol. 38, no. 12, pp. 2770-2779, 2009.

[51] Z. Cai, Y. Zhang, J. C. Suhling, P. Lall, R. W. Johnson, and M. J. Bozack, "Reduction of Lead Free Solder Aging Effects Using Doped SAC Alloys," *Proceedings of ECTC,* pp. 1493-1511, 2010.

[52] S. Choi, T. R. Bieler, J. P. Lucas, and K. N. Subramanian, "Characterization of the Growth of Intermetallic Interfacial Layers of Sn-Ag and Sn-Pb Eutectic Solders and Their Composite Solders on Cu Substrate During Isothermal Long-Term Aging," *Journal of Electronic Materials,* vol. 28, no. 11, pp. 1209-1215, 1999.

[53] C. M. Chuang, T. S. Lui, and L. H. Chen, "Effect of Aluminum Addition on Tensile Properties of Naturally Aged Sn-9Zn Eutectic Solder," *Journal of Materials Science,* vol. 37, no. 1, pp. 191-195, 2002.

[54] R. Darveaux, "Shear Deformation of Lead Free Solder Joints," *Proceedings of ECTC,* pp. 882-893, 2005.

[55] R. Darveaux and K. Banerji, "Fatigue Analysis of Flip Chip Assemblies Using Thermal Stress Simulations and a Coffin-Manson Relation," *Proceedings of ECTC,* pp. 797-805, 1991.

[56] Y. Ding, C. Wang, Y. Tian, and M. Li, "Influence of Aging Treatment on Deformation Behavior of 96.5Sn3.5Ag Lead-Free Solder Alloy During in Situ Tensile Tests," *Journal of Alloys and Compounds,* vol. 428, no. 1, pp. 274-285, 2007.

[57] I. Dutta, D. Pan, R. A. Marks, and S. G. Jadhav, "Effect of Thermo-Mechanically Induced Microstructural Coarsening on the Evolution of Creep Response of SnAg-Based Microelectronic Solders," *Materials Science and Engineering: A,* vol. 410-411, pp. 48-52, 2005.

[58] T.-C. Hsuan and K.-L. Lin, "Effects of Aging Treatment on Mechanical Properties and Microstructure of Sn–8.5Zn–0.5Ag–0.01Al–0.1Ga Solder," *Materials Science and Engineering: A,* vol. 456, no. 1, pp. 202-209, 2007.

[59] K.-S. Kim, C.-H. Yu, and J.-M. Yang, "Aging Treatment Characteristics of Solder Bump Joint for High Reliability Optical Module," *Thin Solid Films,* vol. 462-463, pp. 402-407, 2004.

[60] B. Lampe, "Room Temperature Aging Properties of Some Solder Alloys," *Welding Journal,* vol. 55, no. 10, pp. 330-340, 1976.

[61] X. Luhua, J. H. L. Pang, K. H. Prakash, and T. H. Low, "Isothermal and Thermal Cycling Aging on IMC Growth Rate in Lead-Free and Lead-Based Solder Interface," *IEEE Transactions on Components and Packaging Technologies,* vol. 28, no. 3, pp. 408-414, 2005.

[62] A. S. Medvedev, “Aging of Tin-Lead Solders and Joints Soldered by Them,” *Metallovedenie I Obrabotka Metallov,* vol. 7, pp. 16-23, 1956.

[63] K. Mysore, D. Chan, D. Bhate, G. Subbarayan, I. Dutta, V. Gupta, J. Zhao, and D. Edwards, “Aging-Informed Behavior of Sn3.8Ag0.7Cu Solder Alloys,” *Proceedings of ITherm,* pp. 870-875, 2008.

[64] J. H. L. Pang, T. H. Low, B. S. Xiong, X. Luhua, and C. C. Neo, “Thermal Cycling Aging Effects on Sn–Ag–Cu Solder Joint Microstructure, IMC and Strength,” *Thin Solid Films,* vol. 462-463, pp. 370-375, 2004.

[65] S. Wiese and K. J. Wolter, “Creep of Thermally Aged SnAgCu-Solder Joints,” *Microelectronics Reliability,* vol. 47, no. 2, pp. 223-232, 2007.

[66] Q. Xiao, H. J. Bailey, and W. D. Armstrong, “Aging Effects on Microstructure and Tensile Property of Sn3.9Ag0.6Cu Solder Alloy,” *Journal of Electronic Packaging,* vol. 126, no. 2, pp. 208-212, 2004.

[67] J.-W. Yoon, C.-B. Lee, and S.-B. Jung, “Growth of an Intermetallic Compound Layer with Sn-3.5Ag-5Bi on Cu and Ni-P/Cu During Aging Treatment,” *Journal of Electronic Materials,* vol. 32, no. 11, pp. 1195-1202, 2003.

[68] Y. Zhang, “The Effects of Aging on the Mechanical Behavior of Lead Free and Mixed Formulation Solder Alloys,” PhD, Mechanical Engineering, Auburn University, Auburn, AL, 2010.

[69] Y. Zhang, Z. Cai, J. C. Suhling, P. Lall, and M. J. Bozack, “The Effects of SAC Alloy Composition on Aging Resistance and Reliability,” *Proceedings of ECTC,* pp. 370-389, 2009.

[70] S. L. Allen, M. R. Notis, R. R. Chromik, and R. P. Vinci, "Microstructural Evolution in Lead-Free Solder Alloys: Part I. Cast Sn–Ag–Cu Eutectic," *Journal of Materials Research,* vol. 19, no. 5, pp. 1417-1424, 2004.

[71] A. Bansal, T. Lee, K. Liu, and J. Xue, "Effects of Isothermal Aging and in-Situ Current Stress on the Reliability of Lead-Free Solder Joints," *Proceedings of ECTC,* pp. 1529-1535, 2010.

[72] S. Chavali, Y. Singh, P. Kumar, G. Subbarayan, I. Dutta, and D. R. Edwards, "Aging Aware Constitutive Models for SnAgCu Solder Alloys," *Proceedings of ECTC,* pp. 701-705, 2011.

[73] W. M. Chen, P. McCloskey, and S. C. O'Mathuna, "Isothermal Aging Effects on the Microstructure and Solder Bump Shear Strength of Eutectic Sn37Pb and Sn3.5Ag Solders," *Microelectronics Reliability,* vol. 46, no. 5, pp. 896-904, 2006.

[74] R. Gagliano, "Shear Testing of Solder Joints: The Effect of Various Parameters on the Maximum Shear Stress of Eutectic Tin-Lead Solder," *Advanced Materials for the 21st Century: Proceedings of Julia R. Weertman Symposium,* pp. 107-116, 1999.

[75] M. Hasnine, M. Mustafa, J. C. Suhling, B. C. Prorok, M. J. Bozack, and P. Lall, "Characterization of Aging Effects in Lead Free Solder Joints Using Nanoindentation," *Peoceedings of ECTC,* pp. 166-178, 2013.

[76] S. W. R. Lee, Y.-K. Tsui, X. Hunag, and E. C. C. Yan, "Effects of Room Temperature Storage Time on the Shear Strength of PBGA Solder Balls," *International Mechanical Engineering Congress and Exposition*, pp. 259-262, 2002.

[77] Y. Miyazawa and T. Ariga, "Influences of Aging Treatment on Microstructure and Hardness of Sn-(Ag, Bi, Zn) Eutectic Solder Alloys," *Materials Transactions,* vol. 42, no. 5, pp. 776-782, 2001.

[78] M. Mustafa, Z. Cai, J. C. Suhling, and P. Lall, "The Effects of Aging on the Cyclic Stress-Strain Behavior and Hysteresis Loop Evolution of Lead Free Solders," *Proceedings of ECTC*, pp. 927-939, 2011.

[79] J. Wilde, A. R. Fix, and W. Nüchter, "Microstructural Changes of Lead-Free Solder Joints During Long-Term Ageing, Thermal Cycling and Vibration Fatigue," *Soldering & Surface Mount Technology*, vol. 20, no. 1, pp. 13-21, 2008.

[80] M. Motalab, M. Mustafa, J. C. Suhling, J. Zhang, J. Evans, M. J. Bozack, and P. Lall, "Correlation of Reliability Models Including Aging Effects with Thermal Cycling Reliability Data," *Proceedings of ECTC*, pp. 986-1004, 2013.

[81] J. Zhang, Z. Hai, S. Thirugnanasambandam, J. L. Evans, M. Bozack, R. Sesek, Y. Zhang, and J. C. Suhling, "Correlation of Aging Effects on Creep Rate and Reliability in Lead Free Solder Joints," *Journal of SMT,* vol. 25, no. 3, pp. 19-28, 2012.

[82] T. Lee and H. Ma, "Aging Impact on the Accelerated Thermal Cycling Performance of Lead-Free BGA Solder Joints in Various Stress Conditions," *Proceedings of ECTC*, pp. 477-482, 2012.

[83] L. Yin, M. Meilunas, B. Arfaei, L. Wentlent, and P. Borgesen, "Effect of Microstructure Evolution on Pb-Free Solder Joint Reliability in Thermomechanical Fatigue," *Proceedings of ECTC*, pp. 493-499, 2012.

[84] T. Zhang, J. Evans, C. Mitchell, Z. Z. Li, E. Crandall, a. J. Ridenour, and F. Xie, "Reliability of Lead-Free BGA with SnPb Solder Paste for Harsh Environments," *Proceedings of SMTA/CAVE Symposium on AIMS Harsh Environment Electronics*, 2009.

[85] B. Çal, "Lead-Free Soldering Risks and Reliability Problems in Space Electronics," 2019 3rd International Symposium on Multidisciplinary Studies and Innovative Technologies (ISMSIT), Ankara, Turkey, 2019, pp. 1-8.

[86] I. Szendiuch, C. Vasko and P. Cejtchaml, "Lead-free Solder Quality Investigation," 2*006 29th International Spring Seminar on Electronics Technology*, St. Marienthal, Germany, pp. 215-218, 2006.

[87] R. J. Coyle, P. P. Solan, A. J. Serafino, and S. A. Gahr, "The Influence of Room Temperature Aging on Ball Shear Strength and Microstructure of Area Array Solder Balls," *Proceedings of ECTC*, pp. 160-169, 2000.

[88] T.-K. Lee, H. Ma, K.-C. Liu, and J. Xue, "Impact of Isothermal Aging on Long-Term Reliability of Fine-Pitch Ball Grid Array Packages with Sn-Ag-Cu Solder Interconnects: Surface Finish Effects," *Journal of Electronic Materials,* vol. 39, no. 12, pp. 2564-2573, 2010.

[89] M. A. Whitmore, A. C. Chilton, and W. B. Hampshire, "Fatigue Failure in a Model SMD Joint," *Soldering & Surface Mount Technology,* vol. 1, no. 3, pp. 21-24, 1989.

[90] L. Ming, K. Y. Lee, D. R. Olsen, W. T. Chen, B. T. C. Tan, and S. Mhaisalkar, "Microstructure, Joint Strength and Failure Mechanisms of SnPb and Pb-Free Solders in BGA Packages," *IEEE Transactions on Electronics Packaging Manufacturing,* vol. 25, no. 3, pp. 185-192, 2002.

[91] J.-M. Koo and S.-B. Jung, "Effect of Displacement Rate on Ball Shear Properties for Sn–37Pb and Sn–3.5Ag BGA Solder Joints During Isothermal Aging," *Microelectronics Reliability,* vol. 47, no. 12, pp. 2169-2178, 2007.

[92] R. Darveaux, "Shear Deformation of Lead Free Solder Joints," *Proceedings of ECTC*, pp. 882-893, 2005.

[93] J. R. Oliver, J. Liu, and Z. Lai, "Effect of Thermal Ageing on the Shear Strength of Lead-Free Solder Joints," *Proceedings of the International Symposium on Advanced Packaging Materials Processes, Properties and Interfaces*, pp. 152-157, 2000.

[94] H. L. J. Pang, K. H. Tan, X. Q. Shi, and Z. P. Wang, "Microstructure and Intermetallic Growth Effects on Shear and Fatigue Strength of Solder Joints Subjected to Thermal Cycling Aging," *Materials Science and Engineering: A,* vol. 307, no. 1, pp. 42-50, 2001.

[95] T. Lee, B. Zhou, and T. R. Bieler, "Impact of Isothermal Aging and Sn Grain Orientation on the Long-Term Reliability of Wafer-Level Chip-Scale Package Sn–Ag–Cu Solder Interconnects," *IEEE Transactions on Components, Packaging and Manufacturing Technology,* vol. 2, no. 3, pp. 496-501, 2012.

[96] R. C. J. Smetana, P. Read, R. Popowich, D. Fleming, and T. Sack, "Variations in Thermal Cycling Response of Pb-Free Solder Due to Isothermal Preconditioning," *Proceedings of SMTA International Conference*, pp. 641-654, 2011.

[97] L. Anand, "Constitutive Equations for Hot-Working of Metals," *International Journal of Plasticity,* vol. 1, no. 3, pp. 213-231, 1985.

[98] S. B. Brown, K. H. Kim, and L. Anand, "An Internal Variable Constitutive Model for Hot Working of Metals," *International Journal of Plasticity,* vol. 5, no. 2, pp. 95-130, 1989.

[99] J.-P. Clech, "An Obstacle-Controlled Creep Model for Sn-Pb and Sn-Based Lead-Free Solders," *Proceedings of SMTA International Conference,* 2004.

[100] Y. Hong, P. Deane, P. Magill, and K. L. Murty, "Creep Deformation of 96.5Sn-3.5Ag Solder Joints in a Flip Chip Package," *Peoceedings of ECTC,* pp. 1136-1142, 1996.

[101] X. Q. Shi, Z. P. Wang, Q. J. Yang, and H. L. J. Pang, "Creep Behavior and Deformation Mechanism Map of Sn-Pb Eutectic Solder Alloy," *Journal of Engineering Materials and Technology,* vol. 125, no. 1, pp. 81-88, 2002.

[102] S. Wiese, M. Roellig, and K. Wolter, "Creep of Eutectic SnAgCu in Thermally Treated Solder Joints," *Proceedings of ECTC*, vol. 2, pp. 1272-1281, 2005.

[103] Q., Xiao, L., Nguyen, and W. D., Armstrong, "Aging and Creep Behavior of Sn3.9Ag0.6Cu Solder Alloy," *Proceedings of ECTC*, pp. 1325-1332, 2004.

[104] J. H. Lau, "Solder Joint Reliability of Flip Chip and Plastic Ball Grid Array Assemblies under Thermal, Mechanical, and Vibrational Conditions," *IEEE Transactions on Components, Packaging, and Manufacturing Technology: Part B,* vol. 19, no. 4, pp. 728-735, 1996.

[105] W. K. Jones, Y. Q. Liu, M. A. Zampino, and G. L. Gonzalez, "The at-Temperature Mechanical Properties of Lead-Tin Based Alloys," in *Microelectronic Interconnections and Assembly*, Springer Netherlands, pp. 53-58, 1998.

[106] Y. L. W. K. Jones, M. A. Zampino, G. Gonzalez, and M. Shah, "Design and Reliability of Solders and Solder Interconnections," *TMS Annual Meeting,* 1997.

[107] X. Q. Shi, W. Zhou, H. L. J. Pang, and Z. P. Wang, "Effect of Temperature and Strain Rate on Mechanical Properties of 63Sn/37Pb Solder Alloy," *Journal of Electronic Packaging,* vol. 121, no. 3, pp. 179-185, 1999.

[108] F. Lang, H. Tanaka, O. Munegata, T. Taguchi, and T. Narita, "The Effect of Strain Rate and Temperature on the Tensile Properties of Sn–3.5Ag Solder," *Materials Characterization,* vol. 54, no. 3, pp. 223-229, 2005.

[109] L. H. Dai and S.-W. R. Lee, "Characterization of Strain Rate-Dependent Behavior of 63sn-37Pb Solder Alloy," *Proceedings of InterPACK*, pp. 307-313, 2001.

[110] H. Nose, M. Sakane, Y. Tsukada, and H. Nishimura, "Temperature and Strain Rate Effects on Tensile Strength and Inelastic Constitutive Relationship of Sn-Pb Solders," *Journal of Electronic Packaging,* vol. 125, no. 1, pp. 59-66, 2003.

[111] W. J. Plumbridge and C. R. Gagg, "Effects of Strain Rate and Temperature on the Stress–Strain Response of Solder Alloys," *Journal of Materials Science: Materials in Electronics,* vol. 10, no. 5, pp. 461-468, 1999.

[112] J. H. L. Pang, B. S. Xiong, and F. X. Che, "Modeling Stress Strain Curves for Lead-Free 95.5Sn-3.8Ag-0.7Cu Solder," *Proceedings of Microelectronics and Microsystems,* pp. 449-453, 2004.

[113] J. G. Harper, L. A. Shepard, and J. E. Dorn, "Creep of Aluminum under Extremely Small Stresses," *Acta Metallurgica,* vol. 6, no. 7, pp. 509-518, 1958.

[114] F. Garofalo and D. B. Butrymowicz, "Fundamentals of Creep and Creep-Rupture in Metals," *Physics Today,* vol. 19, no. 5, pp. 100-102, 1966.

[115] L. Anand, "Constitutive Equations for the Rate-Dependent Deformation of Metals at Elevated Temperatures," *Journal of Engineering Materials and Technology,* vol. 104, no. 1, pp. 12-17, 1982.

[116] F. X. Che, H. L. J. Pang, W. H. Zhu, W. Sun, and A. Y. S. Sun, "Modeling Constitutive Model Effect on Reliability of Lead-Free Solder Joints," *Proceedings of Electronic Packaging Technology,* pp. 1-6, 2006.

[117] M. Pei and J. Qu, "Constitutive Modeling of Lead-Free Solders," *Proceedings of International Symposium on Advanced Packaging Materials: Processes, Properties and Interfaces,* pp. 45-49, 2005.

[118] K. Mysore, G. Subbarayan, V. Gupta, and R. Zhang, "Constitutive and Aging Behavior of Sn3.0Ag0.5Cu Solder Alloy," *IEEE Transactions on Electronics Packaging Manufacturing,* vol. 32, no. 4, pp. 221-232, 2009.

[119] M. Motalab, Z. Cai, J. C. Suhling, and P. Lall, "Determination of Anand Constants for SAC Solders Using Stress-Strain or Creep Data," *Proceedings of ITherm,* pp. 910-922, 2012.

[120] N. Bai, X. Chen, and H. Gao, "Simulation of Uniaxial Tensile Properties for Lead-Free Solders with Modified Anand Model," *Materials & Design,* vol. 30, no. 1, pp. 122-128, 2009.

[121] M. Amagai, M. Watanabe, M. Omiya, K. Kishimoto, and T. Shibuya, "Mechanical Characterization of Sn–Ag-Based Lead-Free Solders," *Microelectronics Reliability,* vol. 42, no. 6, pp. 951-966, 2002.

[122] Y. Kim, H. Noguchi, and M. Amagai, "Vibration Fatigue Reliability of BGA -IC Package with Pb-Free Solder and Pb–Sn Solder," *Microelectronics Reliability,* vol. 46, no. 2, pp. 459-466, 2006.

[123] M. L. Huang and L. Wang, "Effects of Cu, Bi, and in on Microstructure and Tensile Properties of Sn-Ag-X(Cu, Bi, in) Solders," *Metallurgical and Materials Transactions A,* vol. 36, no. 6, pp. 1439-1446, 2005.

[124] M. Matahir, L. Chin, K. Tan, and A. Olofinjana, "Mechanical Strength and Its Variability in Bi-Modified Sn-Ag-Cu Solder Alloy," *Journal of Achievement in Materials and Manufacturing Engineering,* vol. 46, pp. 50-56, 2011.

[125] R. S. Pandher, B. G. Lewis, R. Vangaveti, and B. Singh, "Drop Shock Reliability of Lead-Free Alloys - Effect of Micro-Additives," *Proceedings of ECTC*, pp. 669-676, 2007.

[126] Z. Zhenqing, W. Lei, X. Xiaoqiang, W. Qian, and L. Jaisung, "The Influence of Low Level Doping of Ni on the Microstructure and Reliability of SAC Solder Joint," *Proceedings of Electronic Packaging Technology & High Density Packaging,* pp. 1-5, 2008.

[127] I. d. Sousa, D. W. Henderson, L. Parry, S. K. Kang, and D. Shih, "The Influence of Low Level Doping on the Thermal Evolution of SAC Alloy Solder Joints with Cu Pad Structures," *Proceedings of ECTC*, pp. 1454-1461, 2006.

[128] J. H. Lee, S. Kumar, H. J. Kim, Y. W. Lee, and J. T. Moon, "High Thermo-Mechanical Fatigue and Drop Impact Resistant Ni-Bi Doped Lead Free Solder," *Proceedings of ECTC*, pp. 712-716, 2014.

[129] T. Yeung, H. Sze, K. Tan, J. Sandhu, C. Neo, and E. Law, "Material Characterization of a Novel Lead-Free Solder Material — SACQ," *Proceedings of ECTC*, pp. 518-522, 2014.

[130] L. Sun and L. Zhang, "Properties and Microstructures of Sn-Ag-Cu-X Lead-Free Solder Joints in Electronic Packaging," *Advances in Materials Science and Engineering,* vol. 2015, no. 639028, 2015.

[131] M. Sadiq, R. Pesci, and M. Cherkaoui, "Impact of Thermal Aging on the Microstructure Evolution and Mechanical Properties of Lanthanum-Doped Tin-Silver-Copper Lead-Free Solders," *Journal of Electronic Materials,* vol. 42, no. 3, pp. 492-501, 2013.

[132] H. Lee, Y. Chen, T. Hong, K. Shih, and C. Hsu, "Microstructural Evolution of Sn-3.5Ag Solder with Lanthanum Addition," *International Conference on Electronic Packaging Technology & High Density Packaging,* pp. 617-622, 2009.

[133] H. Hao, Y. Shi, Z. Xia, Y. Lei, and F. Guo, "Microstructure Evolution of SnAgCu Lead-Free Solders under High Temperature Aging," *Journal of Electronic Materials,* vol. 37, no. 1, pp. 2-8, 2008.

[134] D. Witkin, "Influence of Microstructure on Mechanical Behavior of Bi-Containing Pb-Free Solders," *Proceedings of IPC APEX EXPO Conference and Exhibition,* vol. 1, pp. 540-560, 2013.

[135] A. Delhaise, D. Perovic, and P. Snugovsky, "The Effects of Bi and Aging on the Microstructure and Mechanical Properties of Sn-Rich Alloys," *Proceedings of Soldering and Reliability,* 2015.

[136] R. R. Chromik, R. P. Vinci, S. L. Allen, and M. R. Notis, "Measuring the Mechanical Properties of Pb-Free Solder and Sn-Based Intermetallics by Nanoindentation," *JOM,* vol. 55, no. 6, pp. 66-69, 2003.

[137] X. Deng, N. Chawla, K. K. Chawla, and M. Koopman, "Deformation Behavior of (Cu, Ag)–Sn Intermetallics by Nanoindentation," *Acta Materialia,* vol. 52, no. 14, pp. 4291-4303, 2004.

[138] F. Gao, H. Nishikawa, T. Takemoto, and J. Qu, "Mechanical Properties Versus Temperature Relation of Individual Phases in Sn–3.0Ag–0.5Cu Lead-Free Solder Alloy," *Microelectronics Reliability,* vol. 49, no. 3, pp. 296-302, 2009.

[139] Y. D. Han, H. Y. Jing, S. M. L. Nai, L. Y. Xu, C. M. Tan, and J. Wei, "Temperature Dependence of Creep and Hardness of Sn-Ag-Cu Lead-Free Solder," *Journal of Electronic Materials,* vol. 39, no. 2, pp. 223-229, 2010.

[140] M. Hasnine, J. C. Suhling, B. C. Prorok, M. J. Bozack, and P. Lall, "Exploration of Aging Induced Evolution of Solder Joints Using Nanoindentation and Microdiffraction," *Peoceedings of ECTC,* pp. 379-394, 2014.

[141] M. Hasnine, J. C. Suhling, B. C. Prorok, M. J. Bozack, and P. Lall, "Nanomechanical Characterization of SAC Solder Joints - Reduction of Aging Effects Using Microalloy Additions," *Peoceedings of ECTC,* pp. 1574-1585, 2015.

[142] M. Hasnine, J. C. Suhling, B. C. Prorok, M. J. Bozack, and P. Lall, "Anisotropic Mechanical Properties of SAC Solder Joints in Microelectronic Packaging and Prediction of Uniaxial Creep Using Nanoindentation Creep," *Experimental Mechanics,* vol. 57, no. 4, pp. 603-614, 2017.

[143] S. Lotfian, J. M. Molina-Aldareguia, K. E. Yazzie, J. Llorca, and N. Chawla, "Mechanical Characterization of Lead-Free Sn-Ag-Cu Solder Joints by High-Temperature Nanoindentation," *Journal of Electronic Materials,* vol. 42, no. 6, pp. 1085-1091, 2013.

[144] V. M. F. Marques, C. Johnston, and P. S. Grant, "Nanomechanical Characterization of Sn–Ag–Cu/Cu Joints—Part 1: Young's Modulus, Hardness and Deformation Mechanisms as a Function of Temperature," *Acta Materialia,* vol. 61, no. 7, pp. 2460-2470, 2013.

[145] V. M. F. Marques, B. Wunderle, C. Johnston, and P. S. Grant, “Nanomechanical Characterization of Sn–Ag–Cu/Cu Joints—Part 2: Nanoindentation Creep and Its Relationship with Uniaxial Creep as a Function of Temperature,” *Acta Materialia,* vol. 61, no. 7, pp. 2471-2480, 2013.

[146] H. Rhee, J. P. Lucas, and K. N. Subramanian, “Micromechanical Characterization of Thermomechanically Fatigued Lead-Free Solder Joints,” *Journal of Materials Science: Materials in Electronics,* vol. 13, no. 8, pp. 477-484, 2002.

[147] M. Sadiq, J.-S. Lecomte, and M. Cherkaoui, “Individual Phase Mechanical Properties at Different Temperatures of Sn–Ag–Cu Lead-Free Solders Incorporating Special Pileup Effects Using Nanoindentation,” *Journal of Electronic Packaging,* vol. 137, no. 3, pp. 031005-031005-5, 2015.

[148] Y. Sun, J. Liang, Z.-H. Xu, G. Wang, and X. Li, “Nanoindentation for Measuring Individual Phase Mechanical Properties of Lead Free Solder Alloy,” *Journal of Materials Science: Materials in Electronics,* vol. 19, no. 6, pp. 514-521, 2008.

[149] G. J. S. Chou, “Microstructure Evolution of Snpb and SnAg/Cu BGA Solder Joints During Thermal Aging,” *Proceedings of Advanced Packaging Materials Symposium*, pp. 39-46, 2002.

[150] R. L. J. M. Ubachs, P. J. G. Schreurs, and M. G. D. Geers, “Microstructure Evolution of Tin-Lead Solder,” *IEEE Transactions on Components and Packaging Technologies,* vol. 27, no. 4, pp. 635-642, 2004.

[151] U. Sahaym, B. Talebanpour, S. Seekins, I. Dutta, P. Kumar, and P. Borgesen, “Recrystallization and Ag_3Sn Particle Redistribution During Thermomechanical

Treatment of Bulk Sn–Ag–Cu Solder Alloys," *IEEE Transactions on Components, Packaging and Manufacturing Technology,* vol. 3, no. 11, pp. 1868-1875, 2013.

[152] M. Maleki, J. Cugnoni, and J. Botsis, "Isothermal Ageing of SnAgCu Solder Alloys: Three-Dimensional Morphometry Analysis of Microstructural Evolution and Its Effects on Mechanical Response," *Journal of Electronic Materials,* vol. 43, no. 4, pp. 1026-1042, 2014.

[153] A. U. Telang, T. R. Bieler, J. P. Lucas, K. N. Subramanian, L. P. Lehman, Y. Xing, and E. J. Cotts, "Grain-Boundary Character and Grain Growth in Bulk Tin and Bulk Lead-Free Solder Alloys," *Journal of Electronic Materials,* vol. 33, no. 12, pp. 1412-1423, 2004.

[154] P. Kumar, B. Talenbanpour, U. Sahaym, C. H. Wen, and I. Dutta, "Microstructural Evolution and Some Unusual Effects During Thermo-Mechanical Cycling of Sn-Ag-Cu Alloys," *Proceedings of ITherm*, pp. 880-887, 2012.

[155] P. Chauhan, S. Mukherjee, M. Osterman, A. Dasgupta, and M. Pecht, "Effect of Isothermal Aging on Microstructure and Creep Properties of SAC305 Solder: A Micromechanics Approach," *Proceedings of InterPACK*, pp. V001T07A009, 2013.

[156] W. Yang, R. W. Messler, and L. E. Felton, "Microstructure Evolution of Eutectic Sn-Ag Solder Joints," *Journal of Electronic Materials,* vol. 23, no. 8, pp. 765-772, 1994.

[157] C. Tz-Cheng, Z. Kejun, R. Stierman, D. Edwards, and K. Ano, "Effect of Thermal Aging on Board Level Drop Reliability for Pb-Free BGA Packages," *Proceedings of the 54th IEEE Electronic Components and Technology Conference*, vol. 2, pp. 1256-1262, 2004.

[158] S. Ahat, M. Sheng, and L. Luo, "Microstructure and Shear Strength Evolution of SnAg/Cu Surface Mount Solder Joint During Aging," *Journal of Electronic Materials,* vol. 30, no. 10, pp. 1317-1322, 2001.

[159] W. K. Choi and H. M. Lee, "Effect of Soldering and Aging Time on Interfacial Microstructure and Growth of Intermetallic Compounds between Sn-3.5Ag Solder Alloy and Cu Substrate," *Journal of Electronic Materials,* vol. 29, no. 10, pp. 1207-1213, 2000.

[160] A. M. Z. Akhtar, K. H. Wirda, I. S. R. Aisha, and I. Mahadzir, "Microstructure Evolution at the Solder Joint During Isothermal Aging," *Proceedings of International Electronics Manufacturing Technology Conference,* pp. 1-5, 2014.

[161] M. Berthou, P. Retailleau, H. Frémont, A. Guédon-Gracia, and C. Jéphos-Davennel, "Microstructure Evolution Observation for SAC Solder Joint: Comparison between Thermal Cycling and Thermal Storage," *Microelectronics Reliability,* vol. 49, no. 9, pp. 1267-1272, 2009.

[162] W. C., Oliver, and G. M., Pharr, "An Improved Technique for Determining Hardness and Elastic Modulus Using Load and Displacement Sensing Indentation Experiments," *Journal of Materials Research,* vol. 7, no. 6, pp. 1564-1583, 1992.

[163] D., Tabor, *The Hardness of Metals*, Oxford University Press, 2000.

[164] N., Chawla, "Thermomechanical Behavior of Environmentally Benign Pb-Free Solders," *International Materials Reviews*, Vol. 54(6), pp. 368-384, 2009.

[165] Yin, L., Wentlent, L., Yang, L., Arfaei, B., Oasaimeh, A., Borgesen, P., "Recrystallization and Precipitate Coarsening in Pb-Free Solder Joints During Thermomechanical Fatigue," *Journal of Electronic Materials*, Vol. 41, pp. 241-252, 2012.

[166] Hasan, S M K, Fahim, A., Suhling, J. C., Hamasha, Sa'd, Lall, P., "Effects of Thermal Cycling on the Mechanical and Microstructural Evolution of SAC305 Lead-Free Solder," *Proceedings of InterPACK,* Paper IPACK2*019*-6563, 2019.

[167] Hasan, S M K, Fahim, A., Suhling, J. C., Lall, P., “Evolution of Mechanical Behavior of Lead Free Solders Exposed to Thermal Cycling,” *Proceedings of ITherm*, pp. 1332-1341, 2019.

[168] A., Fahim, S. M. K., Hasan, J. C., Suhling, P., Lall, “Evaluation of the Creep Response of Lead Free Solder Materials Subjected to Thermal Cycling,” *Proceedings of InterPACK*, pp. 1-9, Anaheim, CA, October 27–29, 2020.

[169] A., Fahim, S. M. K., Hasan, J. C., Suhling, P., Lall, “Nanomechanical Characterization of Various Materials within PBGA Packages Subjected to Thermal Cycling Loading,” *Proceedings of ITherm*, Orlando, FL, pp. 1302-1310, 2020.

[170] U. Sahaym, B. Talebanpour, S. Seekins, I. Dutta, P. Kumar, and P. Borgesen, "Recrystallization and Ag_3Sn Particle Redistribution During Thermomechanical Treatment of Bulk Sn–Ag–Cu Solder Alloys," *IEEE Transactions on Components, Packaging and Manufacturing Technology,* vol. 3, no. 11, pp. 1868-1875, 2013.

[171] P. Borgesen, "Microstructurally Adaptive Constitutive Relations and Reliability Assessment Protocols for Lead Free Solder," in "*SERDP Project WP-1752 Final Report*," 2015.

[172] I. Dutta, "A Constitutive Model for Creep of Lead-Free Solders Undergoing Strain-Enhanced Microstructural Coarsening: A First Report," *Journal of Electronic Materials,* vol. 32, no. 4, pp. 201-207, 2003.

[173] I. Dutta, P. Kumar, and G. Subbarayan, "Microstructural Coarsening in Sn-Ag-Based Solders and Its Effects on Mechanical Properties," *JOM,* vol. 61, no. 6, pp. 29-38, 2009.

[174] P. Kumar, Z. Huang, S. C. Chavali, D. K. Chan, I. Dutta, G. Subbarayan, and V. Gupta, "Microstructurally Adaptive Model for Primary and Secondary Creep of Sn-Ag-Based

Solders," *IEEE Transactions on Components, Packaging and Manufacturing Technology,* vol. 2, no. 2, pp. 256-265, 2012.